

PROPYLENE SEPARATION FROM GASEOUS STREAMS BY PRESSURE SWING ADSORPTION

Ph.D. THESIS

by

SWAPNIL DIVEKAR



**DEPARTMENT OF PAPER TECHNOLOGY
INDIAN INSTITUTE OF TECHNOLOGY ROORKEE
ROORKEE - 247 667 (INDIA)
AUGUST, 2019**

PROPYLENE SEPARATION FROM GASEOUS STREAMS BY PRESSURE SWING ADSORPTION

A THESIS

*Submitted in partial fulfilment of the
requirements for the award of the degree*

of

DOCTOR OF PHILOSOPHY

in

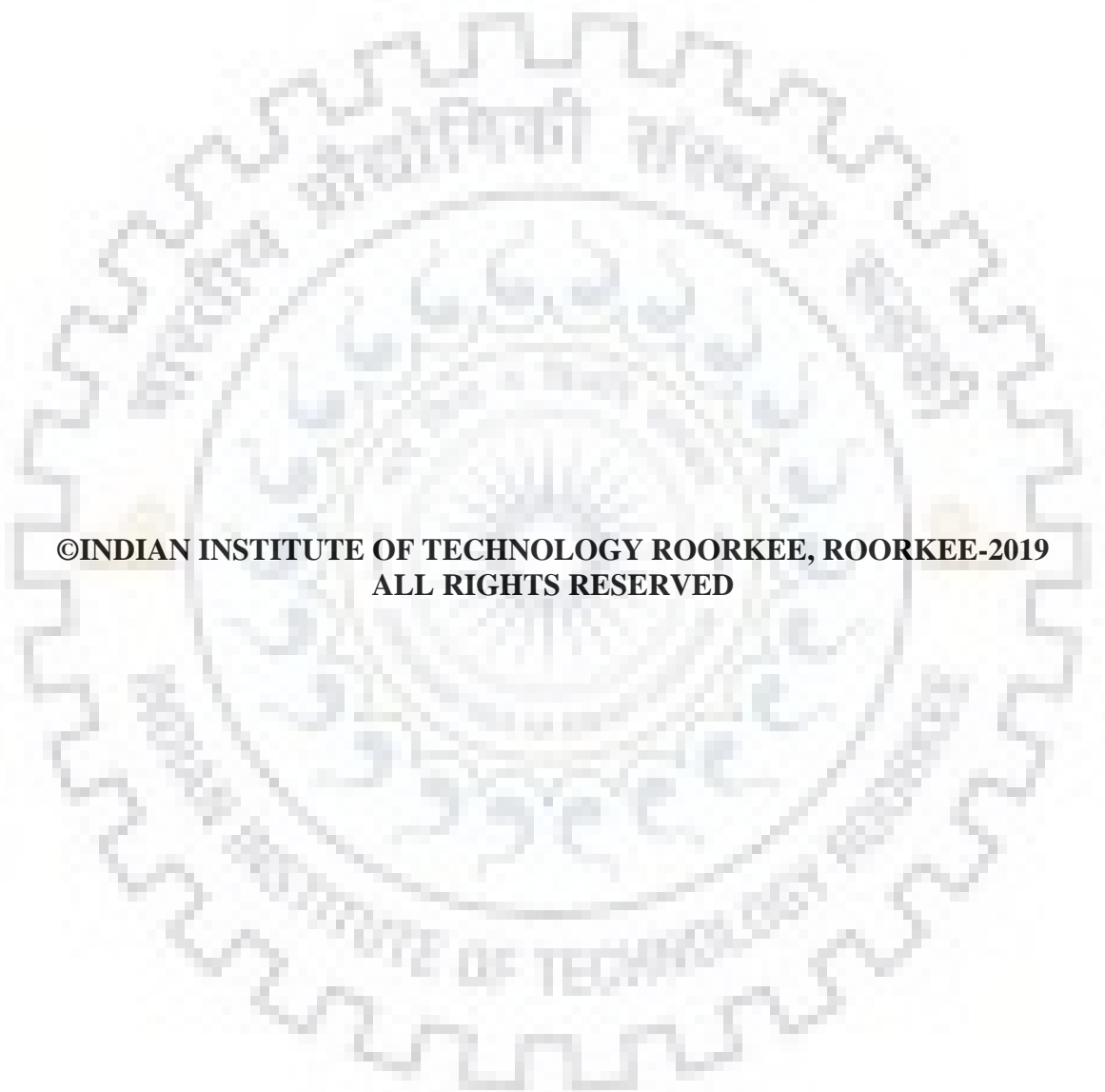
PAPER TECHNOLOGY

by

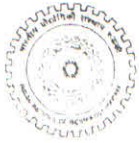
SWAPNIL DIVEKAR



**DEPARTMENT OF PAPER TECHNOLOGY
INDIAN INSTITUTE OF TECHNOLOGY ROORKEE
ROORKEE - 247 667 (INDIA)
AUGUST, 2019**



**©INDIAN INSTITUTE OF TECHNOLOGY ROORKEE, ROORKEE-2019
ALL RIGHTS RESERVED**



INDIAN INSTITUTE OF TECHNOLOGY ROORKEE

CANDIDATE'S DECLARATION

I hereby certify that the work presented in the thesis entitled "Propylene Separation from Gaseous Streams by Pressure Swing Adsorption" is my own work carried out during a period from December 2011 to August 2019 under the supervision of Dr. S. P. Singh, Professor, Department of Paper Technology, Indian Institute of Technology Roorkee, Roorkee and Dr. I. M. Mishra, Professor, Department of Chemical Engineering, Indian Institute of Technology (Indian School of Mines), Dhanbad and Dr. Anshu Nanoti, Chief Scientist, Separation Processes Division, CSIR- Indian Institute of Petroleum, Dehradun.

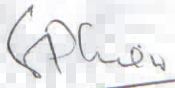
The matter presented in the thesis has not been submitted for the award of any other degree of this or any other Institute.

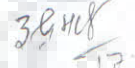

(Swapnil Divekar)


SUPERVISORS' DECLARATION

This is to certify that the above mentioned work is carried out under our supervision.

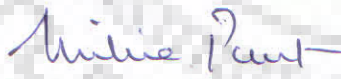
Dated: December 17, 2019


17.12.19
(S. P. Singh)


17.12.19
(I. M. Mishra)

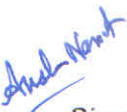



(Anshu Nanoti)


The Ph.D. Viva-Voce Examination of Swapnil Divekar, Research Scholar, has been held on December 17, 2019.


Chairperson, SRC


Signature of External Examiner

This is to certify that the student has made all the corrections in the thesis.




Signature of Supervisors
Dated: December 17, 2019


Head of the Department
Head of Department
Pulp and Paper Technology
IIT Roorkee, Saharanpur Campus
Saharanpur-247001

ABSTRACT

Propylene (or Propene) is the earliest raw material used for industrial-scale production of a petrochemical. It was used for the production of isopropanol over 60 years back. In modern petrochemical complexes, Propylene finds multiple applications for the production of various major petrochemical derivatives like polypropylene, acrylonitrile, cumene, etc. as well as value additions of fuel like gasoline to improve its octane rating.

Propylene has registered steady growth in terms of production volume and is the second largest petrochemical produced by volume. The importance of propylene as a feed stock is evident from its usage as a precursor to numerous petrochemicals. A concise summary of the propylene production process including basic principles, brief process description and details of the main process licensors are included in the introductory chapter. This chapter also gives a brief account of conventional propylene-propane separation techniques as well as the alternative approaches reported in the literature.

Despite being such an important petrochemical, propylene is mostly produced as a byproduct as it is generated in sufficient amounts in the production of ethylene by steam cracking and Fluid Catalytic Cracking (FCC) processes. Steam cracking and FCC accounts for 56 and 20% of the world's propylene production. The C₃ (Propane-Propylene) fraction from the off-gases of these units are separated in propylene and propane rich streams by distillation.

Separation of propylene and propane is a very energy intensive process in petroleum refineries and petrochemical industries, requiring large cryogenic distillation columns with 75-90 m height and 2-6 m diameter operating at a temperature of 240 K and a pressure of ~310 kPa with over 200 theoretical stages and a very high reflux ratio (R~10) due to low relative volatility of propane with respect to propylene. This separation becomes challenging because propylene and propane molecules have very similar properties e.g. Close boiling point (-42 and -47.6 °C), molecular weight (44 and 42 g/mol respectively), polarizability (6.29 and 6.26 10⁻²⁴ cm³), kinetic diameter (0.40 and 0.43 nm) respectively.

Propylene recovery is also desirable from the propane rich bottom product of propane-propylene splitter (distillation column). This product is used for fuel application and may contain 5-15% propylene. The recovery of propylene from this stream is desirable as propylene may cause problems of engine and injector deposits and also due regulatory

ABSTRACT

specifications on maximum propylene content in fuel grade propane in countries like USA. E.g., the maximum allowable propylene content in HD-5 and HD-10 grades of propane is 5 and 10% respectively in the USA.

Another instance of need for propylene recovery is from gas-phase polypropylene production units. Polymerization of propylene results in solid polymer product containing inter particle monomer. Before pelletization, the solid polymer phase is purged with nitrogen to recover the monomer. The propylene content of this product purge gas may reach up to 50%. Recovery and recycling of propylene is economically beneficial. There is a need for an economically viable method for recovering valuable olefin monomer from nitrogen purge gas and recovering nitrogen with satisfactory recovery and purity.

A number of alternative separation processes have been proposed including membrane separation using highly selective membranes, absorption, adsorption and its variants like adsorption-distillation hybrid systems and pressure swing adsorption (PSA) or Vacuum Swing Adsorption (VSA).

The overall objective of the present work is to pursue and describe the adsorptive studies on separation of propylene from propylene bearing streams by experimental Pressure Swing Adsorption (PSA) for binary mixtures arising from:

- (i) Steam Cracking of hydrocarbons (~50% propylene + balance propane)
- (ii) Fluid catalytic cracking (~75% propylene + balance propane)
- (iii) Propane-propylene splitter bottom (5-15% propylene + balance propane)
- (iv) Polypropylene reactor purge gas (10-50% propylene + balance Nitrogen)

The scope of experimental studies undertaken include:

- Comprehensive literature survey to identify the adsorbents, process operating conditions and PSA process configuration and to know the experimental results for benchmarking purpose
- To characterize and evaluate different adsorbents by:
 - Structural properties
 - Single component equilibrium isotherm data

ABSTRACT

- To develop an Ideal Adsorbed Solution Theory (IAST) based solver to predict the binary isotherm data and solver validation and
- To evaluate binary adsorption equilibrium data based on IAST solver
- To conduct experimental dynamic PSA studies to explore the applicability of recovery of propylene from above-identified feed streams

An exhaustive literature survey reveals that many adsorbents including metal organic frameworks (MOFs), zeolites, Na-ETS-10 and π - complexation adsorbents have been reported in the literature for propylene-propane separation. The Experimental adsorption data for propane-propylene binary adsorption is scantily available in open literature due to requirement of measurement set up, precise analytical facility and the considerable time taken in these measurements. The available experimental or predicted binary data for commercial zeolites (13X and 5A) from different manufacturers is limited to 100kPa pressure. Practical applications isotherm data for higher partial pressure will be required. A comprehensive evaluation of the applicability of these adsorbents as an adsorbent for PSA/VSA process on the basis of such scant data is difficult as the operating pressures of PSA/VSA process are higher than this pressure range.

Ideal Adsorbed Solution Theory (IAST) is a powerful tool to predict the performance of an adsorbent on the basis of competitive multicomponent adsorption prediction. An IAST based solver was developed and validated against the literature reported data for prediction of binary adsorption of propylene-propane and propylene-nitrogen mixtures. The binary adsorption data was predicted for a temperature and pressure range 303-423 K and 0-500 kPa. The IAST predicts high propylene selectivity over both propane and nitrogen.

Three adsorbents including laboratory synthesized adsorbent Na-ETS-10 and commercial adsorbents namely zeolite 13X (Z10-04), zeolite 5A (UOP) were tested for their applicability for selective propylene adsorption from propylene containing streams (propylene-propane and propylene-nitrogen mixture). The screening was conducted by equilibrium adsorption isotherm, and binary adsorption predicted based on the IAST theory. Among the commercial adsorbents, Zeolite 13 X showed the highest capacity for propylene adsorption and also the propylene-propane and propylene-nitrogen selectivity calculated on the basis IAST.

In the case of laboratory synthesized adsorbents Na-ETS-10, the results obtained over different batches of adsorbent was not consistent and reproducible. During initial attempts,

ABSTRACT

the adsorbent was co-formed with impurities of Quartz phase. The synthesis procedure was modified by different synthesis procedures reported in the literature and ultimately the synthesis procedure optimized to get consistent pure Na-ETS-10 phase formation. It was however felt that further scale-up of this adsorbent for adsorptive process development might itself take significant time.

The experimental data generated for propylene-propane and propylene-propane generated has been compared on the basis of key process performance indicators like purity, recovery and productivity of propylene with a single column six step VSA cycle. Effect of operating parameters like feed flow rate, adsorption temperature, adsorption pressure and adsorption time etc have been studied to identify favorable operating conditions.

The experimental results of this thesis suggest that propylene can be recovered in refinery grade purity from a mixture containing 15 mol % propylene in propane. This type of propylene recovery work from dilute streams has not been reported elsewhere. Simultaneous propylene and nitrogen recovery from polypropylene reactor purge gas which may contain up to 50% propylene was experimentally studied. A very high purity nitrogen product was recovered at recovery values of over 60 mol%. A preliminary economic analysis indicates that the recovery of high purity nitrogen presents attractive monetary benefits. The recovered propylene can also be used as a feed stock to alkylation process within refinery and petrochemical complex.

ACKNOWLEDGEMENTS

At the foremost, I am heartily grateful to the god almighty for bestowing me with the opportunity of learning and higher education. I owe it all to my mother, Mrs. Suniti Divekar. She taught me the value of education in life and without her support; I could not have achieved a thing in life.

I would like to express my sincere gratitude and thanks to my research supervisor Prof. S. P. Singh, Department of Paper Technology, Indian Institute of Technology, Roorkee, Saharanpur campus for his endless patience, encouragement and everlasting-support throughout the tenure of Ph.D. work and during writing of the thesis.

This thesis would not have seen the light of the day without the kind help and encouragement of my co-supervisor Dr. I. M. Mishra, Professor, Indian Institute Of Technology-ISM, Dhanbad (Formerly, Professor, Department of Chemical Engineering, IIT Roorkee) for his interest and encouragement during my PhD work.

I am indebted to my co-supervisor Dr. Anshu Nanoti, Chief Scientist, CSIR-Indian Institute of Petroleum, Dehradun. She has guided me in the field of adsorptive separation from scratch. My experience of working with her as a younger colleague and student has been a great learning curve. I sincerely appreciate her patience, expert guidance, encouragement, ever-lasting support and supervision throughout my thesis work and professional career. I also wish to convey my gratitude to Dr. S. M. Nanoti (Formerly, Chief Scientist, CSIR-IIP, Dehradun) for providing motivation and ideas for problem-solving.

I cannot adequately express my thankfulness towards the members of my Student and Department Research Committees (SRC & DRC) Dr. S. C. Sharma, Dr. Chhaya Sharma, Dr. V. C. Srivastava (Department of Chemical Engineering, IIT, Roorkee) and Dr. Millie Pant for their support and help to complete the Ph.D. work. I also express my sincere gratitude to all the faculty members of the IIT Roorkee (Saharanpur campus) for their kind help and support.

I gratefully acknowledge the kind help from my fellow research scholar Mr. Avinash and Mr. Pande during my PhD Work.

I would like to take this opportunity to put my heartfelt gratitude to my colleagues Dr. Soumen Dasgupta, Dr. Aarti, Ms. Pushpa Gupta, Ms. Rekha Chauhan, Mr. Sanjay Kumar,

ACKNOWLEDGEMENTS

Mr. Sandeep Singh, Ms. Deepika Dangi, Dr. Sandeep Saran for their immense help and kind assistance in carrying out the present research work.

I wish to express my sincere thanks to my friends and colleagues Mr. Mukesh Poddar, Dr. D V Naik, Mr. Mrityunjay Shukla, Dr. Sunil Kumar, Dr. S S Ray for their most valuable help and support. I gratefully acknowledge valuable support and encouragement from Dr. M. O. Garg (formerly Director, CSIR-IIP) and Dr. Anjan Ray (Director, CSIR-IIP).

I would like to express my sincere love and affection to my brother Harshal Divekar, sister-in-law Dhanashree and my adorable niece and nephew; Tanvi and Amogh. I am deeply grateful to my parents-in-law Mrs. Kavita Dindulkar, Mr. Vijay Dindulkar and my brother-in-law Vipul for their active interest regarding the progress of my work.

This thesis would not have been possible without the silent and resolute support of my wife Niketa. I thank her from the bottom of my heart for her patience, support and unconditional love. I also thank my daughter Anura, the eternal cheer-leader in my life, for her understanding, innocent inquiries and her belief in me.

Finally, I would like to thank everybody who contributed to the successful realization of this thesis and wish to express my apology for not mentioning them all by name.

SWAPNIL DIVEKAR

CONTENTS

CANDIDATE'S DECLARATION	I
ABSTRACT	II
ACKNOWLEDGEMENTS	VI
CONTENTS	VIII
LIST OF FIGURES	XIII
LIST OF TABLES	XX
NOMENCLATURE	XXI
CHAPTER-1 PROPYLENE: PROPERTIES, PRODUCTION, APPLICATIONS AND CHALLENGES IN ITS SEPARATION	1
1.1 INTRODUCTION	1
1.2 PROPERTIES OF PROPYLENE	2
1.3 PRODUCTION OF PROPYLENE	3
1.3.1 Steam cracking of gaseous and liquid hydrocarbons	3
1.3.2 Production of propylene by Fluid Catalytic Cracking(FCC)	6
1.3.3 On-purpose production of propylene	8
1.4 USAGE OF PROPYLENE	10
1.4.1 Thermal usage	10
1.4.2 Motor gasoline usage	10
1.4.3 Chemical usage	11
1.5 SEPARATION OF PROPYLENE FROM PROPYLENE BEARING STREAMS	12
1.5.1 Propylene separation reactor off-gases from polymerisation	12
1.5.2 Propylene recovery from bottom product of propane-propylene splitter	12
1.5.3 Propylene separation from off-gases of steam cracking and FCC units	12
1.6 OUTLINE OF THE THESIS	13

CONTENTS

CHAPTER-2 THEORY AND LITERATURE SURVEY	15
2.1 INTRODUCTION	15
2.2 COMMERCIAL ADSORBENTS	16
2.2.1 Activated carbon	16
2.2.2 Zeolites	17
2.2.3 Carbon molecular sieves (CMS)	17
2.2.4 Other adsorbents	17
2.3 ADSORPTION EQUILIBRIUM ISOTHERM OF SINGLE GAS	18
2.3.1 IUPAC classification of isotherms	18
2.3.2 Type of isotherms from a process point of view	19
2.4 ADSORPTION EQUILIBRIUM ISOTHERM MODELS	20
2.4.1 Langmuir model	22
2.4.2 Freundlich model	22
2.4.3 Sips model	23
2.4.4 Dual Site Langmuir (DSL) model	23
2.5 PREDICTION OF MULTI-COMPONENT ADSORPTION EQUILIBRIUM	24
2.5.1 Ideal Adsorbed Solution Theory (IAST)	25
2.5.2 Solution of IAST equations	27
2.6 BREAKTHROUGH CURVES	28
2.6.1 The length of the unused bed (LUNB)	30
2.6.2 Usable length	30
2.7 MEANS OF REGENERATION OF THE ADSORBENT	31
2.7.1 By reducing the partial pressure of the adsorbate	31
2.7.2 By increasing the temperature by purging the bed	32

CONTENTS

2.7.3	By purging the adsorbent with an inert gas	32
2.7.4	By displacement purge with a purge gas (with less adsorbed gas)	32
2.8	PRESSURE SWING ADSORPTION	34
2.8.1	Significance of different steps	35
2.8.2	PSA performance indicators	36
2.9	PROPYLENE SEPARATION FROM GASEOUS STREAMS BY PRESSURE SWING ADSORPTION: LITERATURE SURVEY	37
2.10	CURRENT RESEARCH GAPS	43
2.11	OBJECTIVES OF THE THESIS	44
CHAPTER-3	SYNTHESIS, CHARACTERIZATION AND SCREENING OF POTENTIAL ADSORBENTS	45
3.1	SYNTHESIS OF Na-ETS-10 ADSORBENT	45
3.2	SOURCES OF COMMERCIAL ADSORBENTS STUDIED	46
3.3	CHARACTERIZATION OF ADSORBENTS	46
3.3.1	BET Surface Area and Pore Size Analysis	46
3.3.2	X-Ray Diffraction (XRD) Studies of Synthesized Adsorbents	46
3.4	ADSORPTION EQUILIBRIUM ISOTHERMS MEASUREMENTS	46
3.5	ADSORBATES	48
3.6	ISOTHERM DATA REGRESSION	48
3.7	RESULTS AND DISCUSSION	48
3.7.1	Laboratory synthesis and characterization of Na-ETS-10	48
3.7.2	Characterization of commercial adsorbents	52
3.7.3	Isotherm measurements and data regression	52
3.7.4	Data regression and curve fitting	58
3.8	BINARY ADSORPTION ISOTHERM PREDICTION BY IAST MODEL	62

CONTENTS

3.8.1	Validation of IAST model solver	62
3.8.2	Prediction of Binary adsorption data based experimental single component data by IAST model	69
3.9	CONCLUSION	82
CHAPTER-4 PROPYLENE SEPARATION BY PRESSURE SWING ADSORPTION		83
4.1	DESCRIPTION OF EXPERIMENTAL SETUP AND EXPERIMENTAL PROCEDURE	83
4.1.1	Single Column Pressure/ Vacuum Swing Adsorption (PVSA) Microadsorber Unit	83
4.1.2	Analysis of gas streams	86
4.1.3	Breakthrough (BT) experiments	87
4.1.4	PVSA experimental studies	90
4.2	RESULTS AND DISCUSSIONS	92
4.2.1	Binary breakthrough curve analysis	92
4.2.2	Future work	102
4.2.3	PVSA Studies	104
4.3	PROPYLENE-NITROGEN SEPARATION: ECONOMIC ANALYSIS	125
4.4	CONCLUSION	127
CHAPTER-5 CONCLUSIONS AND RECOMMENDATIONS		129
5.1	CONCLUSION	129
5.1.1	Synthesis, characterisation and screening of potential adsorbents	129
5.1.2	Propylene separation by pressure swing adsorption	130
5.2	RECOMMENDATIONS	132

CONTENTS

BIBLIOGRAPHY	133
PUBLICATIONS FROM THE THESIS	151
ANNEXURE-A: PROPERTIES OF PROPYLENE	152



LIST OF FIGURES

Figure 1.1	Distribution of global demand of different types of plastics	1
Figure 1.2	Historical global propylene demand/ capacity data trend and forecast up to year 2024	2
Figure 1.3	Simplified block diagram of a steam cracking plant	5
Figure 1.4	Schematic diagram of Fluid Catalytic Cracking (FCC) process	7
Figure 1.5	Schematic diagram of propane dehydrogenation reactor	8
Figure 2.1	IUPAC classification of equilibrium adsorption isotherms	19
Figure 2.2	Different shapes of isotherm curves	20
Figure 2.3	Graphical representation of the breakthrough curve	29
Figure 2.4	Schematic illustration of regeneration by reducing pressure and increasing temperature	31
Figure 3.1	Schematic diagram of IGA-001 gravimetric microbalance	47
Figure 3.2	Photograph of the IGA-001 gravimetric microbalance for single component Isotherm measurement	48
Figure 3.3	X-Ray diffraction pattern of Na-ETS-10 (First Batch)	49
Figure 3.4	X-Ray diffraction pattern of laboratory synthesized Na-ETS-10	50
Figure 3.5	Comparison of the X-Ray diffraction patterns of laboratory synthesized Na-ETS-10 (First batch and finally optimized recipe)	51
Figure 3.6	(a) Propylene and (b) propane isotherm on Z10-04 (Zeochem) at different temperatures (●: 298 K, ■: 323 K, ◆: 343 K, ▲: 373 K, ×: 423 K, Solid lines: DSL fit)	53

LIST OF FIGURES

- Figure 3.7** (a) Propylene and (b) propane isotherm on Zeolite 5A (UOP) at different temperatures (●: 298 K, ■: 323 K, ◆: 343 K, ▲: 373 K, ×: 423 K, solid lines: DSL Fit) **54**
- Figure 3.8** (a) Propylene and (b) propane isotherm on Na-ETS-10 at different temperatures (●: 298 K, ■: 323 K, ◆: 343 K, ▲: 373 K, ×: 423 K, Solid lines: DSL Fit) **55**
- Figure 3.9** Experimental isotherms and the respective DSL fits for nitrogen on Z10-04 (●: 273 K, ■: 303 K, ◆: 333 K, Solid lines: DSL fit) **56**
- Figure 3.10** Literature reported Nitrogen isotherms on Zeolite 5A (Mofarahi and Sayyedi, 2009) (●: 273 K, ■: 303 K, ▲ : 333 K, Solid lines: DSL fit) **57**
- Figure 3.11** Experimental isotherms and DSL fits for Nitrogen on Na-ETS-10 (●: 298 K, ■: 323 K, ▲ : 343 K, Solid lines: DSL fit) **57**
- Figure 3.12** Experimental Isotherms and respective Langmuir, Sips, DSL fits for (a) propylene and (b) propane on Z10-04 at 298 K (◆: Experimental data, — —: Langmuir Fit,: Sips Fit, Solid line: DSL fit) **58**
- Figure 3.13** Absolute Relative Error (ARE) in Pure component Isotherm data **63**
- Figure 3.14** Comparison of IAST-DSL and EL model **64**
- Figure 3.15** Methane-Ethane binary Isotherm on Silicalite zeolite at 300 K and 350 kPa (◆: Methane Experimental data, ▲: Ethane Experimental data, Solid lines: IAST Prediction in conjunction with DSL) **65**
- Figure 3.16** Ethane-Ethylene binary Isotherm data on Na-ETS-10 at (a) 280 K and 150 kPa and (b) 280K and 500 kPa (◆: Ethane Experimental Solid lines: IAST Prediction in conjunction with DSL) **66**
- Figure 3.17** Propylene Uptake from Equimolar Propylene Propane Mixture at (a) 358 K and (b) 404 on Zeolite 13X (◆: Expt. Data, ■: IAST Prediction by Miltenberg Et al., 2008, Solid lines: IAST Prediction in Conjunction with DSL) **68**

LIST OF FIGURES

- Figure 3.18** Comparison of Selectivity Predicted by Miltenberg et al., 2008 and IAST Predicted Selectivity in conjunction with DSL model (◆: 318 K, ▲: 358 K, ×: 404 K, Solid lines: IAST prediction with DSL) **69**
- Figure 3.19** Binary Equilibrium Uptake predicted by IAST for Z10-04 for Feed-1 and Feed-2 (●: 298 K, ■: 323 K, ◆: 343 K, ▲: 373 K, ×: 423 K) **71**
- Figure 3.20** Predicted IAST selectivity of propylene over propane predicted for Z10-04 for Feed-1 and Feed-2 (Symbol Description- ●: 298 K, ■: 323 K, ◆: 343 K, ▲: 373 K, ×: 423 K) **73**
- Figure 3.21** Predicted IAST Binary uptake of propylene over nitrogen predicted for Z10-04 for Feed-3 and Feed-4 (Symbol Description- ●: 303, ■: 323 K, ◆: 343 K,) **74**
- Figure 3.22** Predicted IAST selectivity of propylene over nitrogen predicted for Z10-04 for Feed-3 and Feed-4 (Symbol Description- ●: 303, ■: 323 K, ◆: 343 K,) **75**
- Figure 3.23** Binary Equilibrium Uptake predicted by IAST for Zeolite 5A (UOP) for Feed-1 and Feed-2 (Symbols- ●: 298 K, ■: 323 K, ◆: 343 K, ▲: 373 K, ×: 423 K) **76**
- Figure 3.24** Predicted IAST selectivity of propylene over propane predicted for Zeolite 5A for Feed-1 and Feed-2 (●: 298 K, ■: 323 K, ◆: 343 K, ▲: 373 K, ×: 423 K) **77**
- Figure 3.25** Predicted IAST Binary uptake of propylene over nitrogen predicted for Z10-04 for Feed-3 and Feed-4 (●: 303, ■: 323 K, ▲: 343 K) **78**
- Figure 3.26** Predicted IAST Binary Selectivity of propylene over nitrogen predicted for Zeolite 5A for Feed-3 and Feed-4 (Symbol Description- ●: 303, ■: 323 K, ▲: 343 K,) **79**
- Figure 3.27** Binary Equilibrium Uptake predicted by IAST for Na-ETS-10 for Feed-1 and Feed-2 (Symbols- ●: 298 K, ■: 323 K, ◆: 343 K, ▲: 373 K, ×: 423 K) **80**

LIST OF FIGURES

Figure 3.28	Predicted IAST selectivity of propylene over propane predicted for Na-ETS-10 for Feed-1 and Feed-2 (Symbol Description- ●: 298 K, ■: 323 K, ◆: 343 K, ▲: 373 K, ×: 423 K)	81
Figure 4.1	Photograph of the single column Pressure/ Vacuum Swing Adsorption (PVSA) micro-adsorber unit	84
Figure 4.2	The schematic of the single column pressure/ vacuum swing adsorption (PVSA) micro-adsorber unit	85
Figure 4.3	The photograph of the GQA mass spectrometer	87
Figure 4.4	Propylene breakthrough curve with temperatures as a parameters (Pressure: 500 kPa, feed rate: $400 \times 10^{-3} \text{ dm}^3/\text{min}$, feed composition: 12 mol% propylene in propane)	93
Figure 4.5	Propylene breakthrough curve with temperatures as a parameters (Pressure: 500 kPa, feed rate: $400 \times 10^{-3} \text{ dm}^3/\text{min}$, feed composition: 50 mol% propylene in propane)	94
Figure 4.6	Effect of propylene concentration in feed on BT capacity at different temperatures (Pressure: 500 kPa, feed rate: $400 \times 10^{-3} \text{ dm}^3/\text{min}$, ◆: 12% propylene in feed, ■: 50% propylene in feed)	94
Figure 4.7	Effect of propylene concentration in feed on the BT time at different temperatures (Pressure: 500 kPa, feed rate: $400 \times 10^{-3} \text{ dm}^3/\text{min}$, ◆: 12% propylene in feed, ■: 50% propylene in feed)	95
Figure 4.8	Effect of adsorption pressure on the breakthrough curves (Temperature: 303 K, Feed rate: $400 \times 10^{-3} \text{ dm}^3/\text{min}$, feed composition: 50 mol% propylene in propane)	96
Figure 4.9	Effect of adsorption pressure on the breakthrough time (Temperature: 303 K, Feed rate: $400 \times 10^{-3} \text{ dm}^3/\text{min}$, feed composition: 50 mol% propylene in propane)	97
Figure 4.10	Effect of feed flow on the breakthrough curves (Temperature: 303 K, Pressure; 500 kPa, feed composition: 50 mol% propylene in propane)	98

LIST OF FIGURES

- Figure 4.11** Effect of feed flow on the breakthrough capacity (Temperature: 303 K and pressure: 500 kPa, feed composition: 50 mol% propylene in propane) **98**
- Figure 4.12** Effect of adsorption pressure on the breakthrough curves (Temperature: 303 K, Feed rate: $400 \times 10^{-3} \text{ dm}^3/\text{min}$, feed composition: 75 mol% propylene in propane) **99**
- Figure 4.13** Propylene breakthrough curve at different temperatures (Pressure: 500 kPa, Feed rate: $400 \times 10^{-3} \text{ dm}^3/\text{min}$, feed composition: 50 mol% propylene in propane) **100**
- Figure 4.14** Breakthrough profile of propylene in the feed gas (Temperature: 373 K, Feed rate: $400 \times 10^{-3} \text{ dm}^3/\text{min}$, feed composition: 10 mol% propylene in nitrogen) **101**
- Figure 4.15** Effect of pressure on the Propylene breakthrough capacity (Temperature: 373 K, Feed rate: $400 \times 10^{-3} \text{ dm}^3/\text{min}$, feed composition: 10 mol% propylene in nitrogen) **101**
- Figure 4.16** Effect of temperature on the propylene (a) BT time and (b) capacity (Pressure: 500 kPa, Feed rate: $400 \times 10^{-3} \text{ dm}^3/\text{min}$, feed composition: 10 mol% propylene in nitrogen) **102**
- Figure 4.17** Effect of feed time on propylene purity and recovery (Pressure: 500 kPa, Temperature: 303 K, feed rate: $400 \times 10^{-3} \text{ dm}^3/\text{min}$, ◆: propylene purity, ■: propylene recovery) **108**
- Figure 4.18** Effect of Adsorption Temperature on Propylene Purity and Recovery Feed Containing 12% Propylene in Propane (adsorption pressure: 500 kPa, adsorption time: 60% of BT Time, feed rate: $400 \times 10^{-3} \text{ dm}^3/\text{min}$, ◆: propylene purity, ■: propylene recovery) **109**
- Figure 4.19** Effect of adsorption Pressure on propylene purity and recovery (Temperature: 303 K, adsorption time: 60% of BT Time, feed rate: $400 \times 10^{-3} \text{ dm}^3/\text{min}$, ◆: propylene purity, ■: propylene recovery) **104**

LIST OF FIGURES

- Figure 4.20** Effect of adsorption time on propylene productivity (Adsorption pressure: 500 kPa, temperature; 303 K, feed rate: $400 \times 10^{-3} \text{ dm}^3/\text{min}$) **111**
- Figure 4.21** Effect of adsorption temperature on propylene productivity (Adsorption pressure: 500 kPa, adsorption time: 60% of BT Time, feed rate: $400 \times 10^{-3} \text{ dm}^3/\text{min}$) **111**
- Figure 4.22** Effect of adsorption Pressure on propylene productivity (Adsorption temperature: 303 K, adsorption time: 60% of BT Time, feed rate: $400 \times 10^{-3} \text{ dm}^3/\text{min}$) **112**
- Figure 4.23** Effect of adsorption time on specific power requirement (Adsorption pressure: 500 kPa, adsorption time: 60% of BT Time, feed rate: $400 \times 10^{-3} \text{ dm}^3/\text{min}$) **113**
- Figure 4.24** Effect of Adsorption Temperature on Power requirement for Feed Containing 12% Propylene in Propane at 500 kPa adsorption pressure and adsorption time equivalent to 60% of BT Time **114**
- Figure 4.25** Effect of adsorption Pressure on propylene productivity at 303 and adsorption time equivalent to 60% of BT Time & $400 \times 10^{-3} \text{ dm}^3/\text{min}$ feed rate **114**
- Figure 4.26** Effect of adsorption time on propylene purity and recovery from a feed containing 50% propylene in propane (Adsorption pressure: 500 kPa, temperature: 303 K, feed rate: $400 \times 10^{-3} \text{ dm}^3/\text{min}$, ♦: propylene purity, ■: propylene recovery) **115**
- Figure 4.27** Effect of adsorption time on propylene productivity from a feed containing 50% propylene in propane at adsorption pressure and temperature of 500 kPa and 303 K **116**
- Figure 4.28** Effect of adsorption temperature on propylene purity and recovery with a feed containing 50% propylene in propane (Adsorption pressure: 500 kPa, adsorption time: 100% of BT time, feed rate: $400 \times 10^{-3} \text{ dm}^3/\text{min}$, ♦: propylene purity, ■: propylene recovery) **117**

LIST OF FIGURES

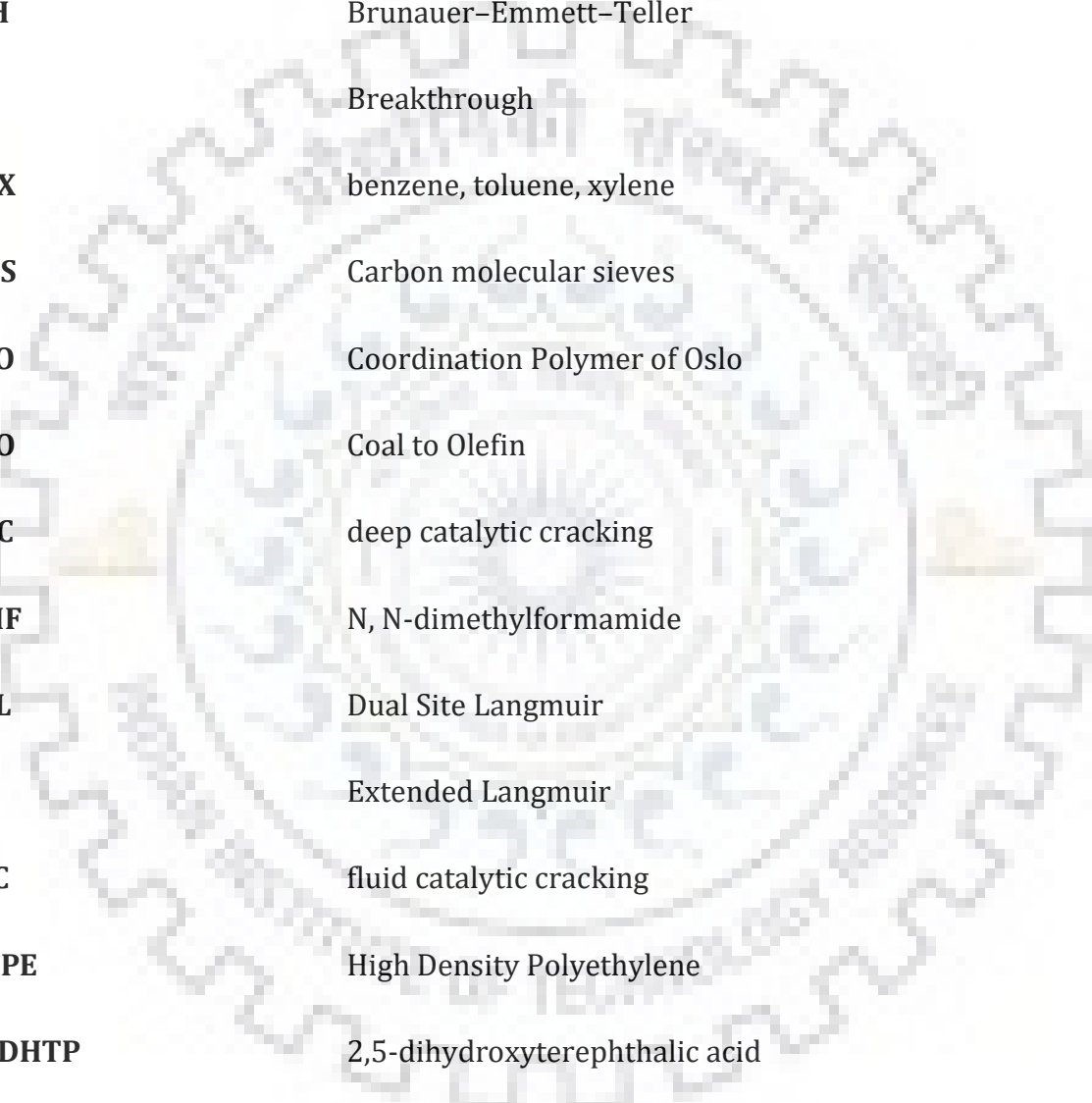
- Figure 4.29** Effect of adsorption temperature on propylene productivity with a feed containing 50% propylene in propane at 500 kPa adsorption pressure and feed time equivalent to 100% BT time **118**
- Figure 4.30** Effect of adsorption time on specific power consumption from a feed containing 50% propylene in propane at adsorption pressure and temperature of 500 kPa and 303 K **118**
- Figure 4.31** Effect of adsorption temperature on product purities and (Adsorption pressure: 200 kPa, adsorption time: 40% of BT time, feed rate: $400 \times 10^{-3} \text{ dm}^3/\text{min}$) **121**
- Figure 4.32** Productivity of (a) Nitrogen and (b) propylene at 2 bar adsorption pressure and adsorption time equal to 40% of BT time **122**
- Figure 4.33** Effect of adsorption time on product purities and recoveries at 500 kPa adsorption pressure and adsorption time equal to 40% of BT time, 303 K adsorption temperature (feed rate: $400 \times 10^{-3} \text{ dm}^3/\text{min}$) **122**
- Figure 4.34** Effect of adsorption pressure on product purities and recoveries at 303 K temperature and adsorption time equal to 40% of BT time **123**
- Figure 4.35** Productivity of (a) nitrogen and (b) propylene at at 303 K temperature and adsorption time equal to 40% of BT time (10% propylene in fee) **124**
- Figure 4.36** Effect of adsorption time on product purities and recoveries at 200 kPa adsorption pressure and adsorption time equal to 40% of BT time (20% propylene in feed , feed rate: $400 \times 10^{-3} \text{ dm}^3/\text{min}$) **125**

LIST OF TABLES

Table 1.1	Product yields from steam cracking of different hydrocarbons	6
Table 1.2	Comparison of commercial propane dehydrogenation processes	9
Table 2.1	Comparison of different means of regeneration	33
Table 3.1	Comparison of literature reported characteristic XRD pattern with laboratory synthesized Na-ETS-10	49
Table 3.2	The surface and structural properties of commercial adsorbents	52
Table 3.3	The DSL isotherm fitting parameters for propylene and propane	60
Table 3.4	The DSL isotherm fitting parameters for propylene nitrogen isotherm on different adsorbents	61
Table 3.5	Composition of the binary mixture for IAST predictions	70
Table 4.1	Process parametric values used in the experimental breakthrough studies with propylene-propane binary feed using Z10-04 adsorbent	89
Table 4.2	Process parametric values used in the experimental breakthrough studies with propylene-nitrogen binary feed using Z10-04 adsorbent	89
Table 4.3	PVSA Recipe Studies	91
Table 4.4	The PVSA steps and the respective inputs and outputs	92
Table 4.5	The P_H and P_L values used for power calculation	107
Table 4.6	Preliminary economical benefit calculations of recovery of nitrogen and propylene by PVSA process	126

NOMENCLATURE

ABBREVIATIONS



ABS	Acrylonitrile-butadiene-styrene
AC	Activated carbons
ASA	Acrylate-styrene-acrylonitrile
BJH	Brunauer–Emmett–Teller
BT	Breakthrough
BTX	benzene, toluene, xylene
CMS	Carbon molecular sieves
CPO	Coordination Polymer of Oslo
CTO	Coal to Olefin
DCC	deep catalytic cracking
DMF	N, N-dimethylformamide
DSL	Dual Site Langmuir
EL	Extended Langmuir
FCC	fluid catalytic cracking
HDPE	High Density Polyethylene
H2DHTP	2,5-dihydroxyterephthalic acid
IAST	Ideal Adsorbed Solution Theory
IUPAC	International Union of Pure and Applied Chemistry

NOMENCLATURE

LDPE	Low Density Polyethylene
LLDPE	Linear Low Density Polyethylene
MMTPA	Million metric ton per annum
MOFS	metal organic frameworks
MTO	Methanol to Olefin
MTP	Methanol to propylene
NA-ETS-10	Sodium Derivative of Engelhard Titano-silicates
P	Pressure
PA	Polyamides
PC	Polycarbonate
PET	Polyethylene terephthalate
P/E	propylene to ethylene ratio
PP	Polypropylene
PS	Polystyrene
PSA	pressure swing adsorption
PSD	pore size distribution
PUR	Polyurathane
PVC	Polyvinyl chloride
PVSA	Pressure/ Vacuum Swing Adsorption
RAST	Real Adsorbed Solution Theory

NOMENCLATURE

SAN	Styrene-acrylonitrile
SMR	Steam Methane Reformer
SSE	Sum of squared error
TCT	Thermodynamic Consistency Test
VSA	Vacuum Swing Adsorption
XRD	X-Ray Diffraction



NOMENCLATURE

NOTATIONS

A	=	Surface area of adsorbent per unit mass ($\text{m}^2 \text{g}^{-1}$)
b	=	Langmuir affinity parameter at temperature T (kPa^{-1})
b^∞	=	Langmuir Affinity Parameter (kPa^{-1})
P	=	Pressure (kPa)
P^0	=	Hypothetical equilibrium pressure for pure component "i" corresponding to spreading pressure π
q	=	Adsorbed Phase Concentration At Pressure P (mmol g^{-1})
q_0	=	Saturation Adsorption Capacity (mmol g^{-1})
R_g	=	Universal Gas Constant ($8.314 \text{ J mol}^{-1} \text{ K}^{-1}$)
t	=	time (sec)
T	=	Temperature (K)
V	=	Total volume of stream
x, X	=	Adsorbed phase mol fraction
y, Y	=	Gas phase mol fraction
Greek Letters:		
γ	=	Ration of specific heats (1.4)
η	=	Efficiency of compressor/ vacuum pump drive (80%)
π	=	Spreading pressure (N m^{-1})
$-\Delta H$	=	Heat of exothermic adsorption (kJ mol^{-1})

Subscript:

1, 2	=	Adsorption site type as per DSL
i	=	Component number
H	=	High
L	=	Low

CHAPTER-1 PROPYLENE: PROPERTIES, PRODUCTION, APPLICATIONS AND CHALLENGES IN ITS SEPARATION

1.1 INTRODUCTION

Propylene (or Propene) is the earliest raw material used for industrial-scale production of a petrochemical (Eisele and Killpack, 2012). It was used for the production of isopropanol over 60 years back. In modern petrochemical complexes, propylene finds multiple applications for the production of various major petrochemical derivatives such as polypropylene (PP), acrylonitrile, cumene, etc. as well as for the value additions to gasoline to improve its octane rating.

Propylene is the second largest petrochemical by volume of production and demand after ethylene. The demand and production of both ethylene and propylene is largely driven by their application of production of their polymer derivatives, i.e., polypropylene (PP) and polyethylene (PE), respectively. The distribution of global demand for different plastics is given in **Figure 1.1** (PEMRG, 2016).

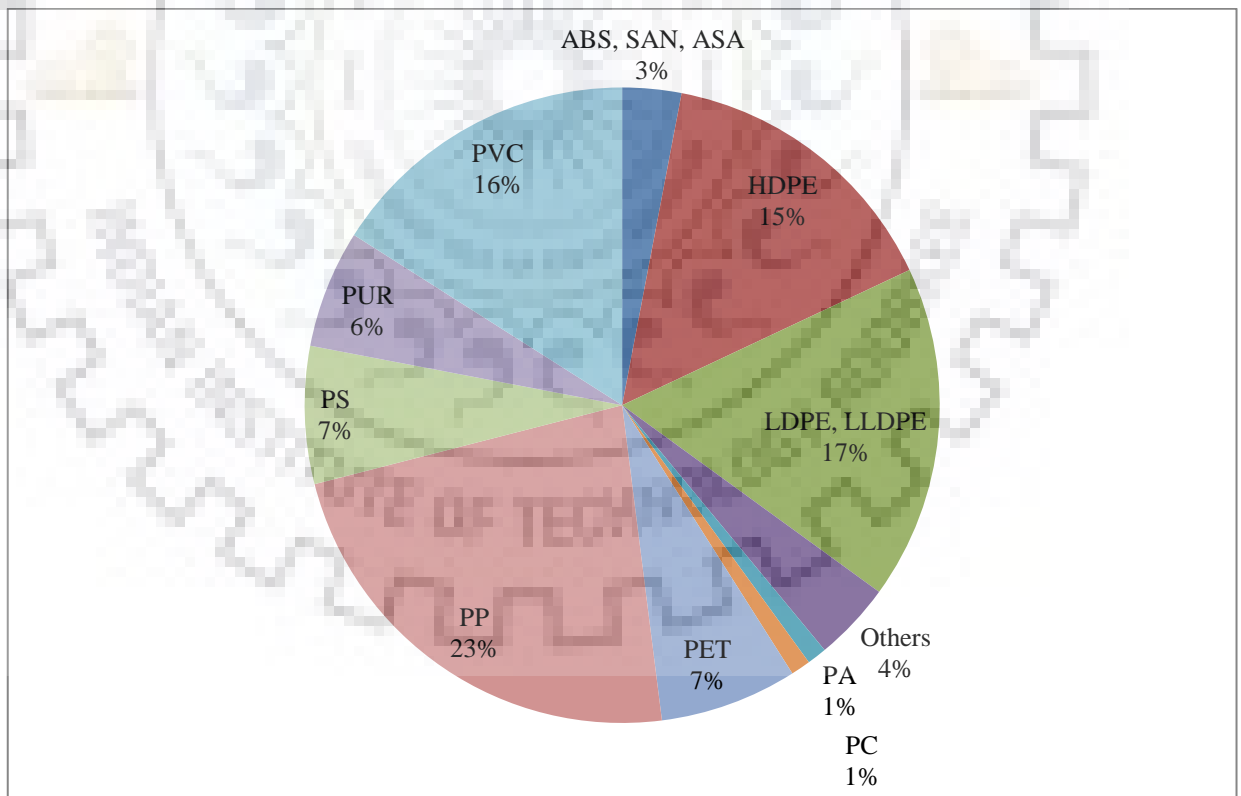


Figure 1.1 Distribution of global demand for different types of plastics

It can be seen that the different derivatives of polyethylene (PE) dominate the scenario with a

Chapter-1

combined demand of 32% of the total demand followed by PP with a 23% share. **Figure 1.2** shows the historical global demand/ capacity data trend and forecast up to year 2024.

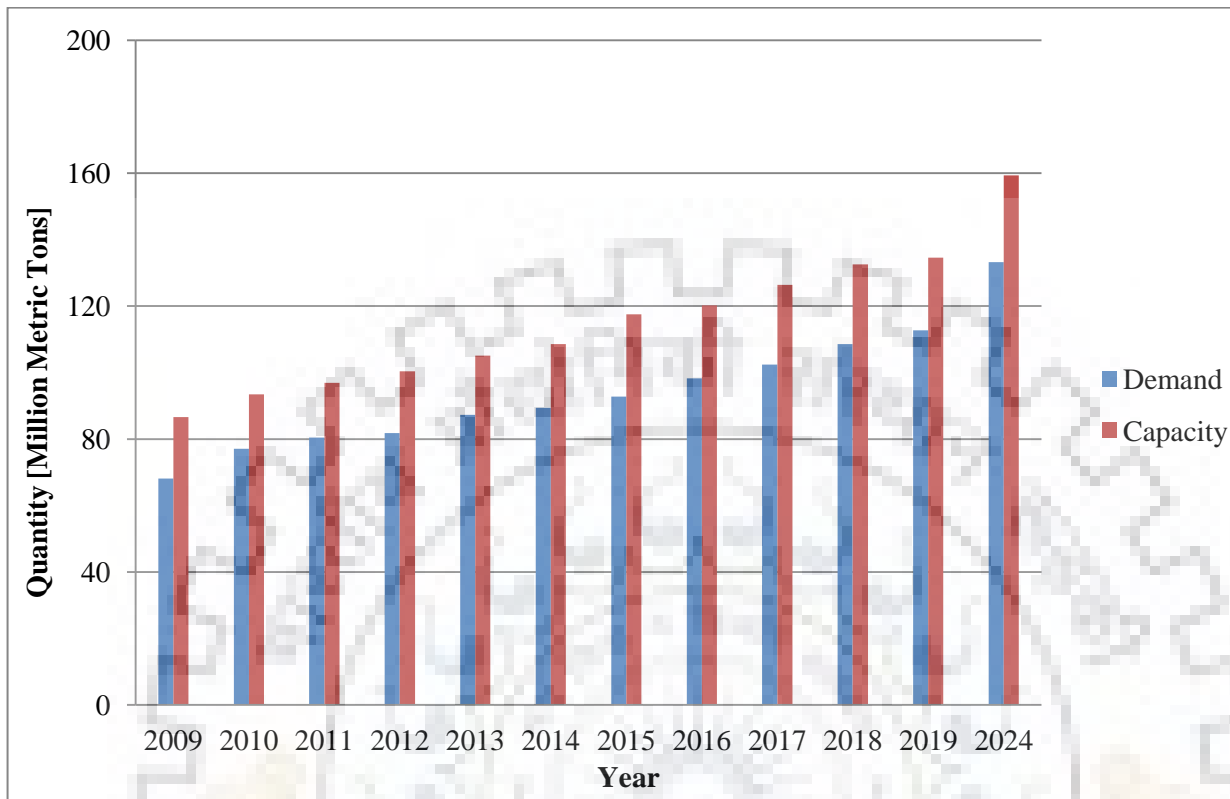


Figure 1.2 Historical global propylene demand/ capacity data trend and forecast up to the year 2024

The current world propylene production capacity is 130 MMTPA, which is forecasted to reach 160 MMTPA by 2024 (Wattanakarunwong, 2015). The current global propylene demand is 105 MMTPA, with an average growth of 4 MMT/ year for over a decade.

1.2 PROPERTIES OF PROPYLENE

Propylene is a gas at normal temperature and pressure, but it is denser than air. It is flammable and explosion with explosive limits in air being 2% (v/v) lower Explosion Limit (LEL) and 11.1 (v/v) Higher Explosion Limit (HEL). The most important properties of propylene are given in **Annexure-A**.

Propylene undergoes many chemical reactions that are typical to an olefin. The reactivity of the double bond dominates the chemical property of the propylene molecule. The presence of this double bond allows many chemical reactions including polymerisation, addition, oxidation, chlorination, hydroformylation, metathesis, etc. making propylene a significant building block

Chapter-1

for industrial chemicals with a variety of applications.

Propylene is classified in the following three grades, on the basis of its purity (Aitani, 2007):

- **Refinery-grade propylene:** (50–70% pure propylene in propane)
- **Chemical-grade propylene:** (92-95% pure propylene in propane)
- **Polymer-grade propylene:** (99.5-99.8% pure propylene in propane)

1.3 PRODUCTION OF PROPYLENE

Despite being such an important petrochemical, the majority of propylene is produced as a byproduct. It is generated in sufficient amounts in the production of ethylene by steam cracking and some refinery processes. Steam cracking accounts for 56% of the world's propylene production (Kuah et al., 2018). Propylene is also mainly produced in refinery and petrochemical complexes by the steam cracker and refinery fluid catalytic cracking (FCC) units. “On Purpose” generation of propylene is also achieved by various other technologies. The various routes for propylene production are briefly described in the following subsections:

1.3.1 Steam cracking of gaseous and liquid hydrocarbons

The steam cracking process of hydrocarbons, commercialised in the 1950s, is the major route for industrial production of light olefins such as ethylene and propylene. The global steam crackers capacity has grown continuously due to the increased demand for commodity polymers (polyethylene and polypropylene in particular) and other derivatives. Gaseous and liquid hydrocarbons such as ethane, LPG, and naphtha are the main feedstocks.

The main reaction involved in steam cracking reactions is the breaking of bonds in hydrocarbon chains, and hence a large amount of energy is required for the reaction to occur. Being an endothermic reaction high temperature and lower pressure operation is essential. To reduce the partial pressure of the reacting hydrocarbons, steam is added to the reaction mixture and to also reduce the carbon deposits formed by the pyrolysis of feedstocks. The long-chain hydrocarbons, which crack faster than the shorter carbon chain compounds, require lower cracking temperatures.

Figure 1.3 shows a simplified block diagram of a steam cracking plant. Typically steam cracker has many pyrolysis furnaces for cracking under the presence of steam. The cracked

Chapter-1

gaseous products are cooled and fed to the demethanizer for the removal of hydrogen and methane. The effluent is further treated to get rid of acetylene and ethylene in the ethylene fractionators. The bottom fraction is separated into ethane, and C_3^+ cut in the deethanizer. The C_3^+ cut is further treated to recover propylene and other olefins. Common operating conditions of ethane steam cracker are 750–800 °C temperature, 1–1.2 atm pressure, and steam/ethane ratio of 0.5.

Lower residence time and higher steam dilution are required for liquid feeds compared to the gaseous feeds. Typical conditions for naphtha cracking are 800 °C temperature, 1 atm pressure, steam/hydrocarbon ratio of 0.6–0.8, and a residence time of 0.35 s. Liquid feedstocks produce a broad range of essential petrochemicals co-products, including aromatics such as benzene, toluene, xylene (BTX).

In the cracking furnaces, the achievable propylene to ethylene (P/E) ratio is limited to a value of about 0.65, because the total olefin yield decreases at higher ratios (Aitani, 2007).



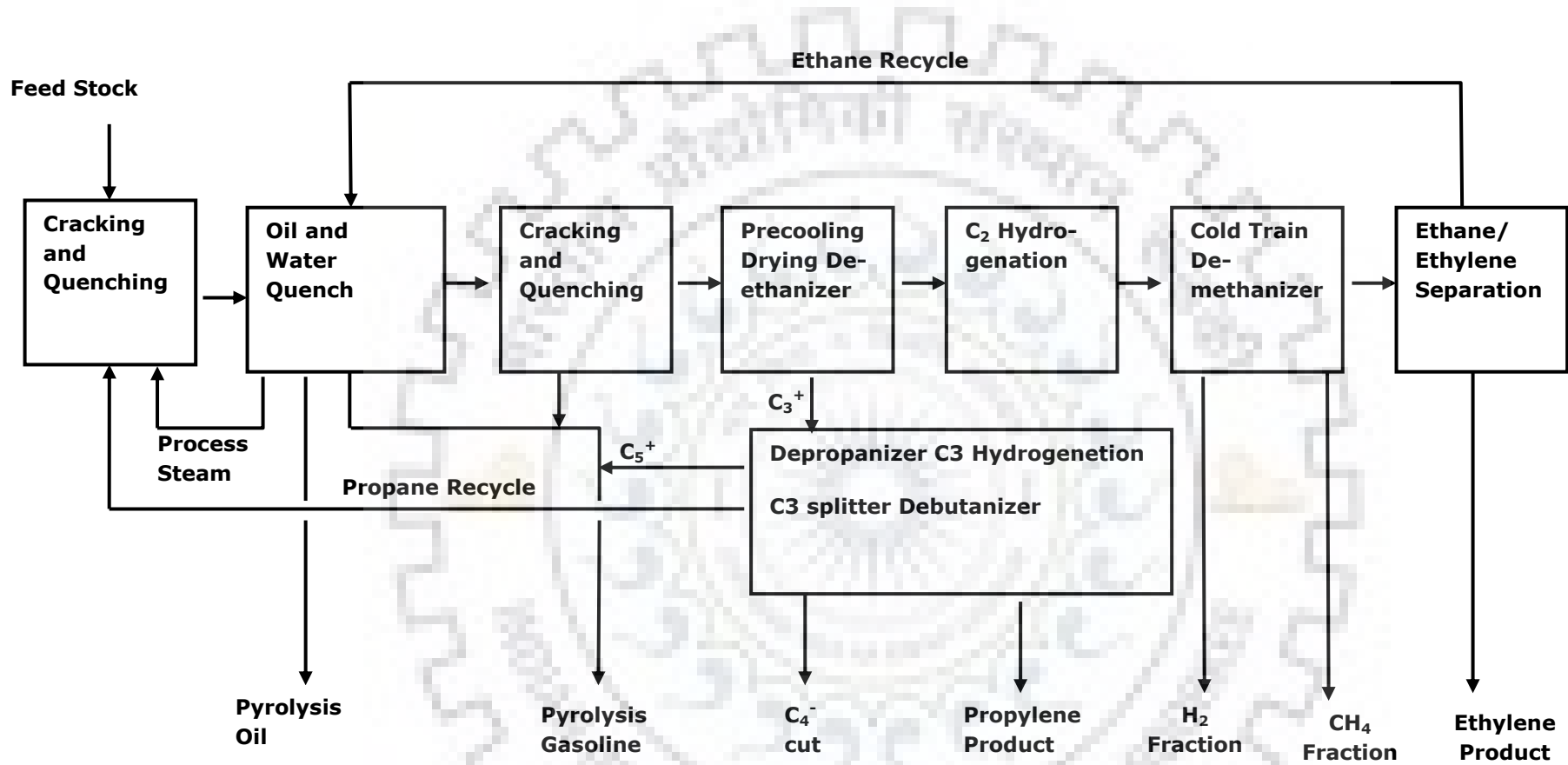


Figure 1.3 Simplified block diagram of a steam cracking plant

Chapter-1

Table 1.1 summarises the purity and other specifications for propylene production from steam cracking with different feeds (Houdek et al., 2001).

Table 1.1 Product yields from steam cracking of different hydrocarbons

Purity yield (wt. %)	Gaseous Feed			Liquid	
	Ethane	Propane	Butane	Naphtha	Gas Oil
H ₂ and Methane	13	28	24	26	23
Ethylene	80	45	37	30	25
Propylene	1.11	14	16.4	14.1	14.4
Butadiene	1.4	2	2	4.5	5
Mixed butenes	1.6	1	6.4	8	6
C5+	1.6	9	12.6	18.5	32

1.3.2 Production of propylene by Fluid Catalytic Cracking (FCC)

FCC converts heavy oil feedstocks such as residues, vacuum gas oil, deasphalted oil into lighter products that are mainly olefinic for light fractions and strongly aromatic for heavy fractions. Fluid catalytic cracking units account for about 97% of propylene produced at the refineries as a co-product of gasoline. Delayed cokers and visbreakers produce the remaining 3%. FCC is the most important refining process (Aitani, 2007).

The main components of the FCC plant are feed injection system, the reactor (riser), stripper, fractionators, and regenerator. The primary conversion reactor is used to facilitate catalyst and heat transfer between the reactor and the regenerator. Cracking reactions occurring in the reactor are endothermic; the heat required is obtained by the controlled burning of the coke deposited on the catalyst in the regenerator section. In general, all cracking reactions produce a considerable amount of olefins. **Figure 1.4** shows the schematic diagram of the FCC process.

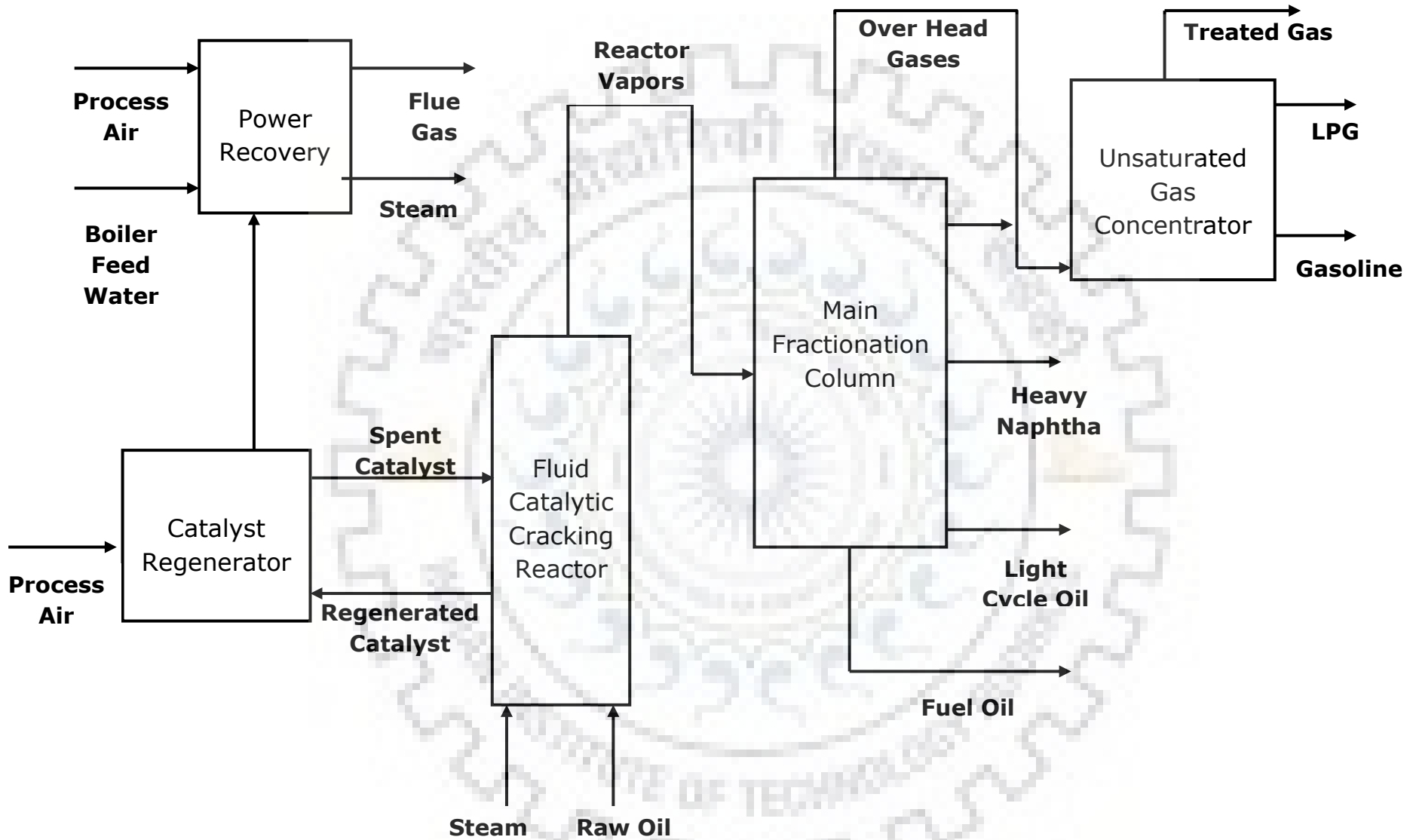


Figure 1.4 Schematic diagram of Fluid Catalytic Cracking (FCC) process

Annexure-A: Properties of propylene

1.3.3 On-purpose production of propylene

Propylene is produced as a co-product of steam cracking and FCC processes. However, recently, some processes called ‘on-purpose propylene production’ processes have been commercialised, wherein the sole purpose is to produce propylene only (Jasper and El-Halwagi, 2015; Thinnis, 2010). These processes use alternate feedstocks such as propane, methanol, coal, etc. which are cheaper or available in abundance in the market. Development of ‘on-purpose’ propylene production processes have changed the propylene market outlook in the last decade, and these processes now account for ~20% of the global propylene production (Alvarado, 2017)

1.3.3.1 Dehydrogenation of propane

Propane dehydrogenation is equilibrium based endothermic process. The process is operated at high temperatures and relatively low pressures to attain good conversion of propane. The schematic diagram of propane dehydrogenation process is given in **Figure 1.5**:

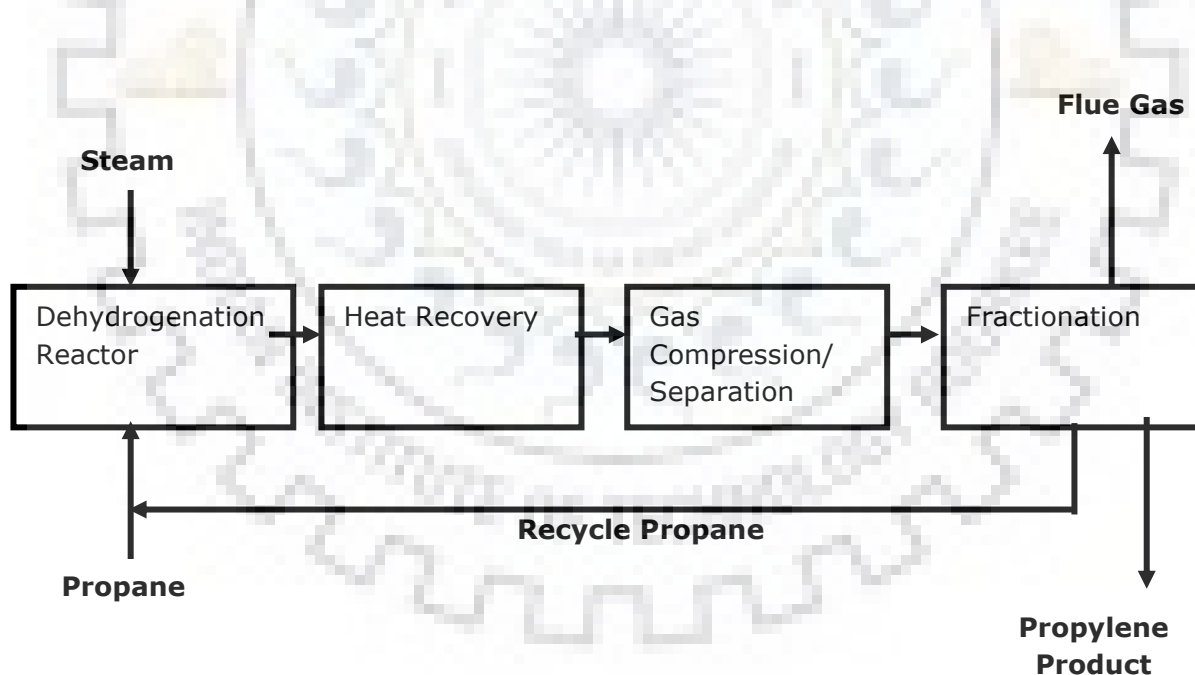


Figure 1.5 Schematic diagram of propane dehydrogenation reactor

A comparison of industrial propane dehydrogenation processes is presented in **Table 1.2** below (Bartholomew and Farrauto, 2005):

Annexure-A: Properties of propylene

Table 1.2 Comparison of commercial propane dehydrogenation processes

Process	Licensor	Reactor type	Catalyst	Reaction conditions
Catofin	Lummus-Houdry	Fixed bed	Cr ₂ O ₃ / Al ₂ O ₃	560-620 °C, >0.5 atm
FBD-3	Snamprogetti-Yarsintez	Fluidized bed	Cr ₂ O ₃ / Al ₂ O ₃	540-590 °C, 1 atm
Oleflex	UOP	Moving bed	Pt/ Al ₂ O ₃	550-650 °C, >1 atm
PDH	Linde-BASF-Statoil	Fixed bed	Cr ₂ O ₃ / Al ₂ O ₃	590 °C, >1 atm
STAR	Kropp Uhde	Fixed bed	Pt/Sn/Zn/ Al ₂ O ₃	500 °C, 3.5 atm

1.3.3.2 Olefin metathesis

Propylene is produced from ethylene and butenes by metathesis reaction, which employs a transition-metal catalyst. Two simultaneous equilibrium reactions namely metathesis and isomerisation take place. The metathesis reaction transforms the carbon-carbon double bonds and rearranges carbon-carbon double bonds that are formed at or near room temperature even in aqueous media from starting materials. As olefin metathesis is a reversible reaction, propylene can be produced from both ethylene and butene-2.

1.3.3.3 Methanol to propylene (MTP) process

During the last ten years ‘Methanol to Olefin’ (MTO) technology has become a significant end-use of methanol. In the year 2010 (total demand 49.3 MMTPA methanol), there was no significant consumption of methanol in MTO processes, whereas by 2015 (total demand 95.2 MMTPA methanol) MTO process consumes 18% of global methanol production (Alvarado, 2016). The global methanol industry has been driven by the MTO process in the recent past, and the trend is expected to continue beyond 2026 (Alvarado, 2017).

Annexure-A: Properties of propylene

1.3.3.4 Other novel processes

Among the other notable propylene production processes are ‘Coal to Olefin’ (CTO), olefin inter-conversion and deep catalytic cracking (DCC), etc.

1.4 USAGE OF PROPYLENE

The applications of propylene can be divided into the following categories:

1.4.1 Thermal usage

The main use of refinery-grade propylene is blending in LPG for heat/ power generation (Pure propylene has a calorific value of 45.8 kJ/kg) or as an additive to motor gasoline for enhancement of octane number. Refinery-grade propylene is also used as feedstocks in some chemical synthesis (e.g., of cumene or isopropanol).

1.4.2 Motor gasoline usage

The dimerisation of propylene is also used extensively to enhance the octane rating of gasoline via, i.e., the formation of polygasoline or alkylation.

1.4.2.1 Dimerization

The dimerisation of refinery-grade propylene takes place catalytically at high temperature and pressure in the presence of a catalyst (Comito et al., 2017; Munshieva, 2001) such as phosphoric acid to produce polygasoline. Polygasoline contains dimers, trimers, and tetramers of propylene. Polygasoline is used as a blendstock in motor gasoline. Dimer product has a low vapour pressure and high blending octane rating of 89.

1.4.2.2 Alkylation

An acid-catalysed reaction between propylene (or other light olefins) and isobutane yields a highly branched higher alkane (2,3-dimethyl pentane in the case of propylene) of low vapour pressure and high octane rating (Albright and Li, 1970; Oden and Burch, 1949). The reaction catalyst is either hydrofluoric acid, which gives octane ratings of 90 – 92, or sulfuric acid, which gives octane ratings of 88 – 91. The catalyst selection depends on feedstocks, process conditions, and octane rating (Chapin et al., 1985).

Annexure-A: Properties of propylene

1.4.3 Chemical usage

The main chemical products obtained from propylene are polypropylene, acrylonitrile, oxo alcohols, propylene oxide, cumene, and propylene oligomers, etc.

1.4.3.1 Polypropylene

Polypropylene is the second-largest bulk polymer produced. Polypropylene has desirable qualities such as high melting point, good rigidity, good chemical, and abrasion resistance but suffers from poor thermal and abrasion resistance. Propylene is polymerised in a liquid or gas phase by the Ziegler-Natta catalyst.

1.4.3.2 2-propanol

2-Propanol (or isopropanol) is produced by the hydration of chemical-grade propylene either in the presence of sulfuric acid or directly as vapour phase reaction in the presence of a catalyst at 180-270 °C (Eisele and Killpack, 2012). 2-Propanol is used extensively as a solvent in paint, cosmetics, and pharmaceuticals.

1.4.3.3 Cumene

Benzene is alkylated by refinery-grade propylene to produce 1-methylethylbenzene (cumene) in the presence of a phosphoric acid catalyst. Cumene can also be further oxidised to cumene hydroperoxide, phenol, and acetone are the decomposition products of cumene hydroperoxide.

1.4.3.4 Propylene oxide

Propylene (polymer grade) is converted into the ether propylene oxide either by hydrochlorination/epoxidation or by reaction with an organic hydroperoxide. Propylene oxide is used in the production of poly(propylene glycols), propanolamines, and intermediates such as polyether polyols.

1.4.3.5 Acrylonitrile

Acrylonitrile is produced by catalytic oxidation of chemical-grade propylene in the presence of ammonia. Among the industrial processes, the Sohio process is most

Annexure-A: Properties of propylene

significant. Here a stoichiometric mixture of propylene, ammonia, and oxygen is reacted over a catalyst at 400-500 °C (Ginsberg, 1996).

1.5 SEPARATION OF PROPYLENE FROM PROPYLENE BEARING STREAMS

1.5.1 Propylene separation from polymerisation reactor off-gases

The polymerisation of lighter olefins such as ethylene and propylene results in solid polymer product containing inter particle monomer. Before pelletization, the solid polymer phase is purged with nitrogen to recover the monomer. The purging step yields a nitrogen-rich gaseous stream containing unreacted monomer, some alkanes, and co-monomers such as 1-butene, 1-hexene. The hydrocarbon content of this product purge gas may reach up to 50%, most of which is ethylene or propylene. Hence, there is a need for an economically viable method for recovering valuable olefin monomer from nitrogen purge gas and recovering nitrogen with satisfactory recovery and purity.

1.5.2 Propylene recovery from the bottom product of propane-propylene splitter

Propylene recovery is also desirable from the bottom product of propane-propylene splitter (distillation column), which may contain 5-15% propylene. The propane rich bottom product is used for fuel application. However, the recovery of propylene from this stream becomes necessary to meet the regulatory specifications on maximum propylene content in fuel grade propane. E.g., the maximum allowable propylene content in HD-5 and HD-10 grades of propane is 5 and 10%, respectively, in the USA. High-value propylene (USD 900-1200/ton) in fuel is not desired. Propane contains substantial amounts of propylene. The Propylene in fuel grade propane is also undesirable as it may polymerise during storage, fuel lines, or vaporisers, causing plugging by gum formation (Bryan, 2004) cause problems of engine and injector deposits.

1.5.3 Propylene separation from off-gases of stream cracking and FCC units

The separation of propylene from propane is carried out conventionally by distillation. Industries use different variants of distillation technology, which include a single column, two-column and heat pump processes (Eisele and Killpack, 2012).

Separation of propylene and propane is a very energy-intensive process (Moulijn et al., 2013) due to their close boiling points and low relative volatility. It requires large

Annexure-A: Properties of propylene

cryogenic distillation columns with 75-90 m height and 2-6 m diameter with over 200 theoretical stages and a very high reflux ratio ($R \sim 10$). The distillation columns operate at a temperature range of 243 K-327 K and a pressure of ~ 310 kPa (Bryan, 2004; Da Silva and Rodrigues, 2001a; Grande et al., 2003b; Keller et al., 1992; Rege et al., 1998).

Many alternative separation processes have been proposed, including highly selective membranes (Swaidan et al., 2015), absorption (Chen et al., 2013) and adsorption (Ruthven and Reyes, 2007). Other alternative processes such as adsorption-distillation hybrid systems (Ghosh et al., 1993; Kumar et al., 1992) and pressure swing adsorption (PSA) or vacuum swing adsorption (VSA) are being developed (Da Silva and Rodrigues, 2001b; Grande et al., 2010a; Grande and Rodrigues, 2005; Khalighi et al., 2013a; Plaza et al., 2012; Rege et al., 1998).

1.6 OUTLINE OF THE THESIS

The thesis is organised into five chapters. **Chapter-1** highlights the importance of propylene as a feedstock in the refinery and petrochemical industries, including the usages of propylene. A concise summary of the propylene production process including basic principles, brief process description and details of the leading process licensors have also been presented in this chapter.

Chapter-2 summarises the underlying fundamental principles of adsorption as applied in the present work. This chapter also presents a comprehensive survey of the literature, published in last thirty years, on different techniques for the separation of propylene from the propylene-propane mixtures arising from:

- Steam Cracking of hydrocarbons,
- Fluid catalytic cracking,
- Propane-propylene splitter bottom, and
- Polypropylene reactor purge gas

The literature review is used to identify different adsorbents based on their adsorption capacity, the heat of adsorption and the salient process performance indicators such as product purity, product recovery and process productivity. This chapter also gives a brief account of conventional propylene-propane separation techniques as well as the

Annexure-A: Properties of propylene

alternative approaches reported in the literature. Based on the literature survey attempts were made to identify and highlight the research gaps in the literature for adsorptive separation of propylene. The objectives of the thesis have been defined on the basis of the above analysis.

Chapter-3 presents the experimental studies carried out for the screening of a suitable adsorbent for selective propylene adsorption. Three adsorbents, namely titano-silicate type molecular sieve Na-ETS-10 and commercial adsorbents such as aluminosilicate zeolite 13 X (Zeochem), and Zeolite 5A (UOP), were used. The adsorbents have been characterised by X-Ray diffraction patterns and specific surface area. Single component adsorption isotherms for propylene, propane, and nitrogen on these adsorbents were measured in the pressure range of 0 to 300 kPa, and in the temperature range of 273 to 423 K. The experimental data have been fitted by non-linear regression to well-known adsorption isotherm models [Langmuir, Sips and Dual Site Langmuir (DSL)].

An MS Excel-based solver was developed for the prediction of binary competitive adsorption following Ideal Adsorbed Solution Theory (IAST). The thermodynamic consistency test was used to test the validity of the IAST model for binary adsorption of propylene and propane. The IAST solver was also validated against the literature reported multi-component adsorption data.

On the basis of the validated IAST model, binary propylene-propane and propylene-nitrogen adsorption equilibrium data have been predicted for different feed compositions. Finally, adsorbent zeolite 13X was chosen for further studies on the basis of its high propylene adsorption capacity, and also selectivity for propylene over nitrogen.

Chapter-4 presents the experimental studies on the adsorptive separation of propylene using the Pressure/ vacuum swing adsorption (PVSA) cycle results generated with Zeolite 13X. The PVSA cycle performance is analysed by the process performance indicators of product purity, product recovery, and process productivity, etc. **Chapter-5** presents the summary and overall conclusions based on the work carried out in this thesis.

CHAPTER-2 THEORY AND LITERATURE SURVEY

2.1 INTRODUCTION

Adsorption is a surface phenomenon wherein a molecule (adsorbate) from a bulk phase (gas/liquid) is spontaneously attracted to the surface of a solid, called adsorbent (or sorbent). The adsorption of a molecule on an adsorbent surface is characterised by the release of a finite amount of energy due to a reduction in potential energy due to interaction with the atoms/molecules on the surface of the adsorbent, which is called heat of adsorption (Ruthven et al., 1993). Physical adsorption involves the liberation of heat between 10 and 40 kJ/mol of heat which is close to values associated with heats of liquefaction of gases (R. Yang, 1987; Yang, 2003). Chemical adsorption or chemisorption involves sharing or exchange of electrons between adsorbate and adsorbent and heat released during chemisorptions is 50-500 kJ/mol.

The continuous contact of adsorbate with adsorbent surface leads to saturation or adsorption equilibrium. At this point, the removal of an adsorbed molecule is necessary from the adsorbent. The removal of an adsorbed molecule from an adsorbent surface is called desorption. Hence to make the adsorption process continuous, the adsorbent is used in a cyclic manner of adsorption and desorption.

The interaction between adsorbate and adsorbent mainly include molecular forces such as the permanent dipole, induced dipole, and quadruple electrostatic effects, commonly known as van der Waal's forces. Both short-range (repulsive) and long-range (attractive) forces between adsorbate and adsorbent become balanced when adsorption occurs. The adsorption of an adsorbate depends upon the temperature and pressure (or concentration) of adsorbate in the bulk phase. Specifically, the adsorption is favoured at low temperature and high pressure.

According to the porous adsorbents can be classified into three distinct categories by the pore size ranges (Everett, 1972):

Micropores: $<2 \text{ nm}$ ($<20 \text{ \AA}$)

Mesopores $2\text{--}50 \text{ nm}$ ($20\text{--}50 \text{ \AA}$)

Macropores ($>50 \text{ nm}$) ($> 500 \text{ \AA}$)

Practically all the industrial relevant adsorbents are predominantly microporous. The estimation of the pore size distribution (PSD) for the microspore is essential for the characterisation of

Chapter-2

sorbents. Out of numerous existing methods, three prominent ones are Kelvin equation (and the BJH method), Horváth–Kawazoe approach (Horváth and Kawazoe, 1983), and the integral equation approach (Jaroniec et al., 1991; Stoeckli, 1990, 1977).

The extent and strength of interaction of different species on an adsorbent surface differ due to the nature of both adsorbent and adsorbates. Therefore one type of adsorbate molecule is adsorbed preferentially as compared to others. The preferential adsorption of one species over another qualifies the adsorption process suitable as a separation technique.

2.2 COMMERCIAL ADSORBENTS

Adsorbents are solids with a porous structure and preferably have a large surface area per unit weight, which is called specific surface area having a large surface area per unit mass. Many classes of adsorbents have been used commercially for diverse applications, e.g., bulk gas and liquid separation, gas and liquid purification etc. Few notable examples of adsorbents and their usages are:

2.2.1 Activated carbon

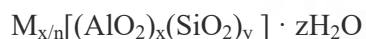
Activated carbons (AC) have been manufactured and used commercially since the nineteenth century (Cheripally et al., 2013; Yang, 2003). Activated carbons are manufactured from naturally occurring sources of such as wood, coconut shells, peat, anthracite, and bituminous coals, etc. Their manufacturing mainly involves the development of desired pore size distribution by carbonisation at lower temperatures (400-500 °C) to remove volatile matters. This step is followed by the ‘activation’ step to develop the pore structure and enhance the specific surface area, which is achieved by physical or chemical oxidising agents. For physical activation, super-heated steam or carbon dioxide are used. Examples of few chemical activation/oxidizing agents are phosphoric acid, zinc chloride, potassium sulfide and potassium carbonate.

Activated carbons are used in H₂ purification from Steam Methane Reformer (SMR) off-gas, hydrocarbon/vent streams (Bagreev et al., 2005; Seredych and Bandosz, 2010; Yu et al., 2013), air pollutant removal, water purification, heavy metal removal and organic/ inorganic contaminant removal (Chatterjee et al., 2018; Kapur and Mondal, 2013; Maiti et al., 2007; Mohan et al., 2008, 2002; Mohan and Karthikeyan, 1997; Mondal, 2009, 2010; Mukherjee and De, 2016; Narayan et al., 2016; Purkait et al., 2005b, 2005a) etc.

Chapter-2

2.2.2 Zeolites

Zeolite is a versatile class of crystalline adsorbents characterised by unimodal pore size distribution. Their primary building blocks are tetrahedra of silicon and aluminium oxides, SiO_4 and AlO_4 . The general composition of zeolite is:



where x and y are integers with y/x equal to or greater than 1, n is the charge of cation M (Na^+ , K^+ , Ca^{2+} , etc) and z is the number of water molecules in each unit cell.

Over 800 crystalline structures of zeolites are possible, and less than 200 of them have been found in natural deposits or synthesised in laboratories around the world (Thompson, 1998).

The industrial uses of zeolites include air separation (nitrogen selective), hydrocarbon removal/separation (Mofarahi and Salehi, 2012) from vent stream, liquid phase *p*-xylene/*o*-xylene separation, glucose/ fructose separation etc.

2.2.3 Carbon molecular sieves (CMS)

CMS is also derived from carbon-rich precursors and are characterised by a very narrow micropore size distribution (PSD). A detailed account of the preparation procedure of CMS has been compiled by Spencer (1967), Cabrera et al. (1993) and Armor (1994). The general procedure includes carbonisation, activation of precursors followed by carbon deposition (Yang, 2003).

As the CMS has a narrow PSD, separation of adsorbates on the basis of their size or diffusivity (molecular sieving) can be achieved with CMS. E.g., the bulk application of CMS is air separation because the ratio of the diffusivity ratio of O_2/N_2 is close to 30 (Chen et al., 1994). The difference in diffusivity arises as only oxygen (kinetic diameter 3.46 Å) enters the pore of CMS, excluding nitrogen (kinetic diameter 3.64 Å) from getting adsorbed which is produced in high purity in adsorption step.

2.2.4 Other adsorbents

Other classes of industrially important adsorbents include silica(Manu et al., 2009) gel, activated alumina, clay (Joshi et al., 2009; Patel et al., 2006; Pawar et al., 2009; Pires et al., 2008; Taylor et al., 2010) etc. which find applications in gas drying, hydrocarbon adsorption,

etc. Iler (Iler, 1979) has described many preparation methods of silica gel. Activated alumina is commercially prepared exclusively by thermal dehydration or activation of aluminum trihydrate, $\text{Al}(\text{OH})_3$ or gibbsite (Chatterjee and De, 2014; R. Yang, 1987). New classes of adsorbent such as Metal-Organic Frameworks (MOFs) (Chowdhury et al., 2009; Karmakar et al., 2019; Mishra et al., 2012), Zeolitic Imidazolate Frameworks (ZIFs), etc have also attracted the scientific community's attention due to their unique and tunable properties.

2.3 ADSORPTION EQUILIBRIUM ISOTHERM OF SINGLE GAS

Adsorption equilibrium isotherm quantifies the specific amount of adsorption of an adsorbate against concentration/ pressure of adsorbate in bulk/ gas phase at a constant temperature.

For a given gas-solid pair, the amount adsorbed (q) at equilibrium is described as:

$$q=f(P,T)$$

where q (volume, weight or moles adsorbed/g of adsorbent) may be expressed as a function of pressure and temperature. Then at a fixed temperature, q is only a function of P , which is called an adsorption isotherm.

It may be noted that the theory of the adsorption presented in this chapter is presented from the point of view of the adsorption of gases. However, most of the principles apply to adsorption of liquids as well.

2.3.1 IUPAC classification of isotherms

The IUPAC classification of adsorption isotherms is given in **Figure 2.1**.

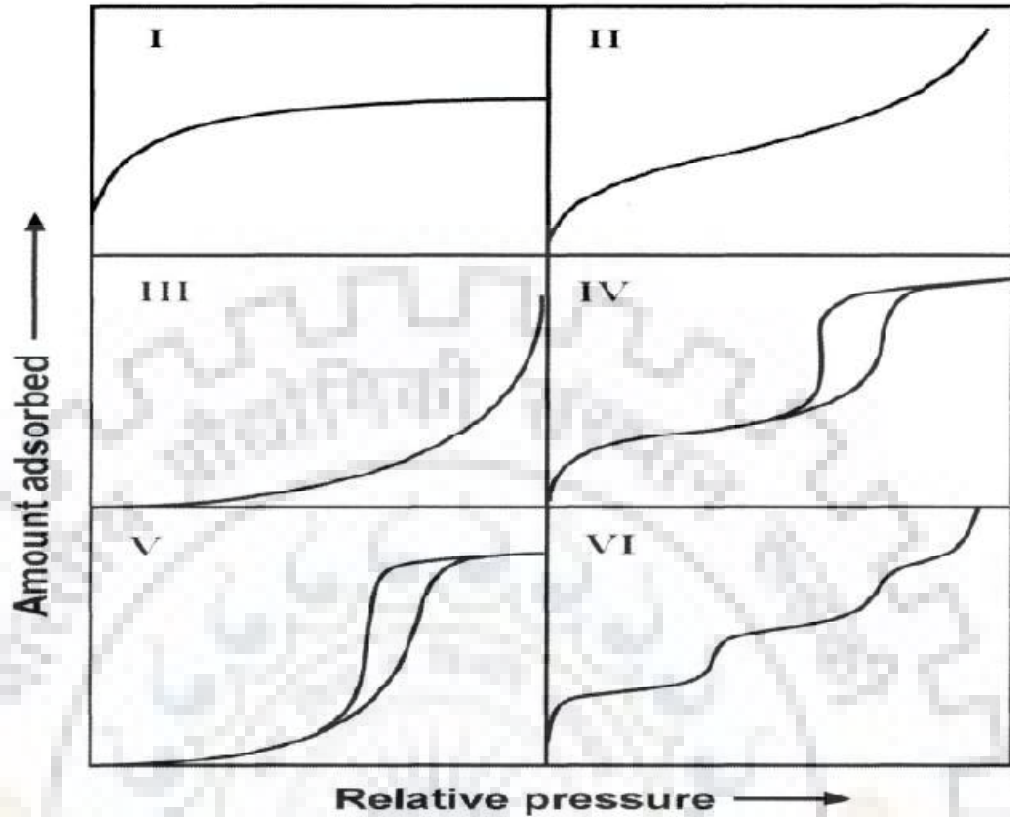


Figure 2.1 IUPAC classification of equilibrium adsorption isotherms

Depending on the predominant pore sizes, the following types of adsorbents show different isotherm behaviour: (Type I); nonporous or macroporous (Type II, III, VI) and mesoporous (types IV and V) isotherm behaviour (Lowell et al., 2004).

Type I isotherm, which is a characteristic of microporous materials, approaches a limiting value. Types II and III describe adsorption on macroporous adsorbents with strong and weak adsorbate-adsorbent interactions respectively (Sing, 1994). Types IV and V represent mono- and multilayer adsorption plus capillary condensation in mesoporous materials. Type VI illustrates that the adsorption isotherms can have one or more steps (Adamson, 1976) due to adsorption in multiple layers at higher pressure.

2.3.2 Type of isotherms from a process point of view

The shape of the curve is very significant factors for the design of adsorption process. From a process point of view, adsorption isotherms can be classified in different categories. A

graphical description of the different shapes of isotherm encountered is given in **Figure 2.2** below:

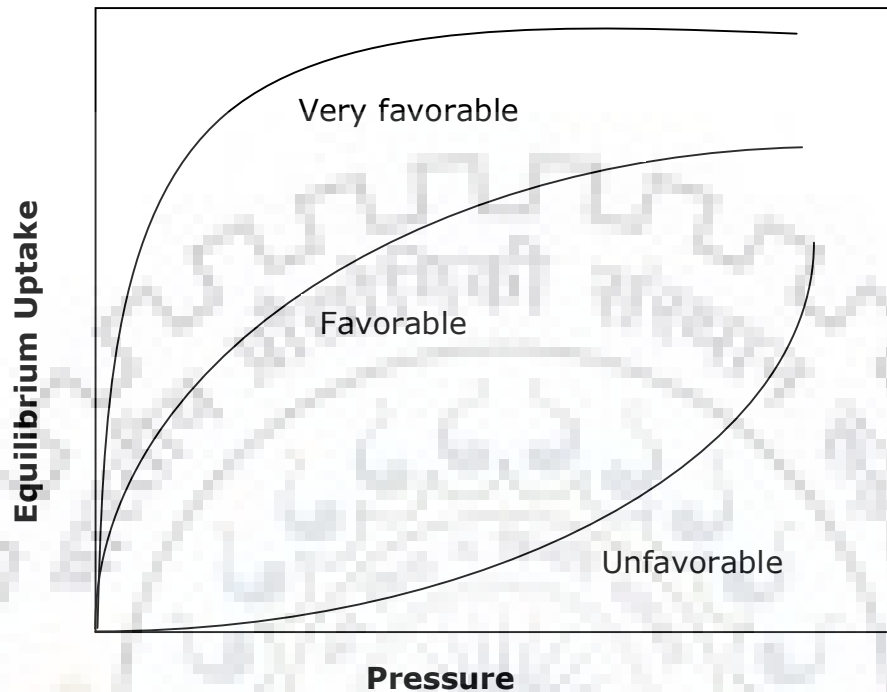


Figure 2.2 Different shapes of isotherm curves

"Favorable" isotherms permit higher solid loadings at lower pressure. These tend to start steeply and level out. The initial slope of "very favourable" isotherms is very high, which means that more quantity is adsorbed at a very low pressure as compared to even "favourable" isotherms. "Unfavorable" isotherms are relatively flat at lower pressure values. The relationship between pressure and equilibrium uptake is linear in case of the "linear" type of isotherm indicating the ease of regenerability.

2.4 ADSORPTION EQUILIBRIUM ISOTHERM MODELS

The adsorption isotherm model is a mathematical correlation between pressure (or concentration) of adsorbate in gas (or bulk) phase and the amount adsorbed on the surface of adsorbent at a constant temperature. The isotherm data is the most basic and vital source of information on the quantity and nature of the adsorption process. Therefore a thorough understanding and interpretation of adsorption isotherms are of utmost importance for the development of an adsorption based system (Ayawei et al., 2017).

Chapter-2

A number of theoretical and empirical isotherm mathematical models e.g. Langmuir (Langmuir, 1916; Zito et al., 2015), Freundlich (Freundlich, 1931), Sips (Langmuir-Freundlich) (Sips, 1948), Dual Site Langmuir (DSL) (Mathias et al., 1996; Tang et al., 2016), Toth (Campo et al., 2013; Lamia et al., 2008), Brunauer–Emmett–Teller (BET) (Brunauer et al., 1938; Munshieva, 2001), Redlich–Peterson (Redlich and Peterson, 1959), Dubinin–Radushkevich (Hutson and Yang, 1997), Temkin (Ayawei et al., 2017; Vijayaraghavan et al., 2006), etc. have been formulated to represent the experimental isotherm data.

The most widely used isotherm models are the Langmuir, Sips, and DSL isotherm equation, etc. The Langmuir model is thermodynamically consistent with the well defined physical significance of its parameters. It follows Henry's law at low pressures. The model is particularly applicable to homogeneous surfaces and describes the adsorption isotherms at low pressure accurately. However, at higher pressure, this model does not predict the adsorption equilibrium accurately because of non-ideality creeping in.

The Sips model is an empirical three-parameter isotherm. Sips model is a combination of Langmuir and Freundlich isotherm models. The surface heterogeneity is accounted for in the Sips model with an exponential parameter; therefore the Freundlich model's limitation of increased adsorbate concentration predicted at higher pressure is avoided. The Sips model reduces to Langmuir form when the exponential term is unity.

The DSL model, which is an extension of the Langmuir model, is also a thermodynamically consistent model and has been used widely to describe adsorbate-adsorbent interaction, especially when the adsorbent surface exhibits heterogeneous nature. Langmuir, Sips and DSL models were initially chosen for correlating the isotherm data as these models are easy to implement in the IAST algorithm and an analytical solution for the spreading pressure can be readily obtained using these models.

The Langmuir, Sips, and DSL isotherms models were chosen to be tested for their applicability to fit the isotherm data generated and also to know the surface heterogeneity. Another reason for choosing these models is that their mathematical form makes it easy to implement in the IAST model as an analytical solution to the integral calculating the reduced spreading pressure can be obtained for these models (Equation 2.12 described later in this chapter). The models are described in details as follows:

Chapter-2

2.4.1 Langmuir model

The Langmuir adsorption model is the most commonly used model. It is a thermodynamically consistent model with a solid theoretical foundation. The following assumptions are inherent to the Langmuir adsorption isotherm model:

- All the adsorption sites are equivalent.
- The total number of adsorption sites depends on the surface area of the adsorbent.
- The adsorbed molecules cannot interact laterally.
- Adsorption occurs only in a single layer of adsorbed molecules. The molecules of adsorbate do not deposit on the other adsorbed molecules of adsorbate on the free surface of the adsorbent.

The mathematical form of Langmuir isotherm is given by:

$$q = \frac{q_0 b P}{1 + b P}$$

Equation 2.1

Where, q is the amount adsorbed (mmol g^{-1}), P is the partial pressure of the gas (kPa) in the gas phase. q_0 (mmol g^{-1}) is called the monolayer saturation adsorption capacity of the adsorbent and b (kPa^{-1}) represents the Langmuir affinity parameter.

The parameter b has an Arrhenius like temperature dependence given by:

$$b = b^\infty \exp(-\Delta H/RT)$$

Equation 2.2

Where b^∞ (kPa^{-1}) is temperature independent affinity parameter, $-\Delta H$ is the heat of adsorption, R is universal gas constant ($8.314 \text{ J K}^{-1} \text{ mol}^{-1}$), T (K) is the temperature.

2.4.2 Freundlich model

The Freundlich equation was originally proposed as an empirical equation. It may be however derived on a theoretical basis as well (Do, 1998). The equation has the following form:

$$q = K P^{1/n}$$

Equation 2.3

K and n are Freundlich model constants and are temperature dependent.

2.4.3 Sips model

In the case of the Freundlich model, the continuing increase in the adsorbed amount with an increase in pressure (concentration) is predicted which is often not the case in experimental observation. Therefore, it limits the use of the Freundlich model to certain pressure range up to which the Freundlich model can be applied.

Sips (Sips, 1948) overcame this limitation by proposing a model based on both Langmuir and Freundlich models (Do, 1998). The mathematical expression of the Sips model is:

$$q = \frac{q_o(bP)^{1/n}}{1 + (bP)^{1/n}}$$

Equation 2.4

A close comparison between Langmuir and Sips model reveals a difference is the additional parameter 'n' in the Sips equation. If n=1, the Sips model reverts to the Langmuir model which is applicable for ideal surfaces. Hence the parameter n is supposed to be the parameter characterising the system heterogeneity. The system heterogeneity could stem from the solid or the adsorbate or a combination of both. The parameter n is usually higher than unity, and therefore the larger is this parameter, the more heterogeneous is the system.

2.4.4 Dual Site Langmuir (DSL) model

The DSL model again is derived from the Langmuir model. The DSL model assumes that there are two types of adsorption sites available at the surface of the adsorbent and that the surface heterogeneity is taken in to account with this assumption.

The DSL model is represented by the following equations:

$$q = \frac{q_{o1}b_1P}{1 + b_1P} + \frac{q_{o2}b_2P}{1 + b_2P}$$

Equation 2.5

$$b_1 = b_1^\infty \exp\left(\frac{-\Delta H_1}{RT}\right)$$

Equation 2.6

$$b_2 = b_2^\infty \exp\left(\frac{-\Delta H_2}{RT}\right)$$

Equation 2.7

Here subscript 1 and 2 represent two types of adsorbent sites.

DSL model has been used extensively in the modeling of adsorption isotherms (Mason et al., 2011; Mathias et al., 1996; Rosson et al., 2007; Tang et al., 2016)

2.5 PREDICTION OF MULTI-COMPONENT ADSORPTION EQUILIBRIUM

Most of the adsorption-based separation processes involve simultaneous adsorption of two or more adsorbates. Therefore an understanding of adsorption equilibrium involving competitive adsorption between molecules of different adsorbates is needed for design purpose. In the case of adsorption of gas mixtures at a given temperature and pressure, a complete specification of the system is described by the total amount adsorbed and the compositions of both the gas and the adsorbed phase. In a binary mixture (of component 1 and 2), as in the case of vapour-liquid equilibrium, relative volatility (α) has been defined as:

$$\alpha = \frac{\left(\frac{Y_1}{X_1}\right)}{\left(\frac{Y_2}{X_2}\right)}$$

Equation 2.8

In the adsorption system, the selectivity is defined as:

$$S = \frac{\left(\frac{X_1}{Y_1}\right)}{\left(\frac{X_2}{Y_2}\right)}$$

Equation 2.9

Chapter-2

However, experimental multi-component adsorption equilibrium data is scantily available in the open literature (Calleja et al., 1994; Costa et al., 1991; Maghsoudi, 2015) due to the requirement of measurement set up (Dickey et al., 2012), precise analytical facility and the considerable time taken in these measurements (Sievers and Mersmann, 1994; Wu et al., 2007). Many empirical and thermodynamic approaches have been proposed for the prediction of multi-component adsorption data. The theories for prediction of the adsorption of gaseous mixtures can be classified into the following groups:

- (a) Extensions of pure gas equations
- (b) Ideal Adsorbed Solution Theory (IAST)
- (c) Real Adsorbed Solution Theory (RAST)
- (d) Extensions of the Polanyi Potential Theory
- (e) Empirical methods

An overall analysis of these approaches has been detailed by Do (Do, 1998) and detailed theory is not presented here for all the cases.

Ideal adsorbed solution theory (IAST) (Malek and Farooq, 1996; Myers and Prausnitz, 1965; Weston et al., 2014; Yun et al., 1999) is a useful and versatile tool reported in literature to predict the adsorption of multi-component mixtures on an adsorbent on the basis of single-component adsorption equilibrium isotherms. IAST is a thermodynamically derived model based on the assumption that the adsorbed phase is ideal and is not constrained by the assumption of equal saturation capacities of the adsorbates. The theoretical basis of the IAST method is given below:

2.5.1 Ideal Adsorbed Solution Theory (IAST)

The IAST is prolifically used for predicting mixed gas adsorption from pure component isotherms. The adsorbed mixture is assumed to be a two-dimensional phase. From the Gibbs isotherm, one can calculate a spreading pressure for each component based on its pure component isotherm. The underlying assumption of the IAST is that the spreading pressures are equal for all components at multi-component equilibrium conditions. The mathematical basis of IAST is given below (Do, 1998; Myers and Prausnitz, 1965) :

Chapter-2

For an ideal adsorption system involving N components, the analogous Raoult's law may be written as:

$$P y_i = P_i = x_i P_i^0(\pi) \quad \text{for } i = 1, 2, \dots, N \quad \text{Equation 2.10}$$

and

$$\sum_{i=1}^N x_i = 1 \quad \text{Equation 2.11}$$

where x and y are the mol fraction of i^{th} component in the adsorbed and gas-phase respectively and $P_i^0(\pi)$ is the hypothetical pressure of the i^{th} pure component that gives the same spreading pressure on the surface, as per the following equation:

$$z = \frac{\pi A}{RT} = \int_0^P \frac{q}{P} dP \quad \text{Equation 2.12}$$

where q is represented by any isotherm model in terms of pressure P and z is called the reduced spreading pressure. It is to be noted that the **Equation 2.12** is applicable for pure gases only. Activation coefficients of unity are assumed for all components in the adsorbed phase since the spreading pressure of the individual components is equal. For a binary mixture, **Equation 2.12** can be written as:

$$\int_0^{P_1^0} \frac{q_1}{P_1} dP_1 = \int_0^{P_2^0} \frac{q_2}{P_2} dP_2 = \dots = \int_0^{P_N^0} \frac{q_N}{P_N} dP_N \quad \text{Equation 2.13}$$

Applying Raoult's law,

$$P Y_1 = P_1^0 X_1 \quad \text{Equation 2.14}$$

$$P Y_2 = P_2^0 X_2 = P_2^0 (1 - X_1) \quad \text{Equation 2.15}$$

Where, P_i^0 is the equilibrium vapour pressure for the i^{th} component at the spreading pressure, π , and the same temperature as that of the adsorbed mixture components. **Equations 2.11** to **Equation 2.13** are used to define the adsorbed phase. On calculating P_1^0 , P_2^0 and X_1 , the adsorbed phase concentration of component 1 and 2 and the total adsorbed phase concentration are calculated using **Equations 2.16** to **Equation 2.18**.

Chapter-2

$$\frac{1}{q_t} = \frac{X_1}{q_1(P_1^0)} + \frac{X_2}{q_2(P_2^0)} \quad \text{Equation 2.16}$$

$$q_1 = q_t X_1 \quad \text{Equation 2.17}$$

$$q_2 = q_t X_2 \quad \text{Equation 2.18}$$

Selectivity of component 1 over component 2 is defined as

$$\alpha_{1/2} = \frac{(X_1/Y_1)}{(X_2/Y_2)} \quad \text{Equation 2.9}$$

The IAST is thermodynamically consistent and exact at the limit of zero Pressure (Valenzuela and Myers, 1989). The accuracy of the IAST calculations depends on how well the single component data are fitted, especially in the low-pressure region as well as at high-pressure region where the pure hypothetical pressure lies. An error in these regions, in particular, the low-pressure region, can cause a significant error in the multi-component calculations.

The spreading pressure is the negative of the surface potential. In an N component system, for a given total pressure (P) and the mole fraction in the gas phase, **Equation 2.10** and **Equation 2.11** provides N+1 equations, and **Equation 2.13** gives N equations, a total of 2N+1 equations. With this set of 2N+1 equations, there are 2N+1 unknowns.

- N values of mole fractions in the adsorbed phase (X)
- One value of the spreading pressure, and
- N values of the spreading pressure of the pure component, P° ,

The solutions methodology for IAST is described in the next section.

2.5.2 Solution of IAST equations

An analytical solution of the equations given in the previous section is not possible. Therefore these equations need to be solved numerically. Although the **Equation 2.13** for spreading pressure can be integrated analytically, the inverse of the hypothetical pure component pressure versus spreading pressure is not generally available in an analytical form with the exception of the Langmuir, Freundlich, Sips and DSL isotherms.

The numerical solution is easily achieved with standard numerical tools, such as the Newton-Raphson method for the solution of algebraic equations and the quadrature method for the evaluation of integrals. An algorithm for solving the equilibrium problem is given in the literature when the gas phase conditions (P, y) are given (Do, 1998; Myers and Valenzuela, 1986).

2.6 BREAKTHROUGH CURVES

Unlike the distillation and liquid-liquid extraction process, which are steady-state processes, adsorption is a transient process. Hence the amount of gases adsorbed within a bed is a function of both on time and location within the adsorber column. The term breakthrough curves refer to “the response of an initially clean bed (i.e., free of adsorbate) to an influent of constant (i.e., time-independent) composition” (R. Yang, 1987). Considering the time dependence, as a feed mixture of gases enters the adsorber, it comes in contact with a few finite layers of the absorbent. As the concentration wave moves through the bed, most of the mass transfer is occurring in a fairly small region called the mass transfer zone (MTZ). Adsorbates start adsorbing on the surface of adsorbent within these layers, saturating some of the available sites. As the feed continues, the adsorbent layers near the entrance get saturated, and the feed penetrates farther into the bed. Thus the MTZ shifts towards the other end of the bed as time progresses. The product emerging from the bed initially is free from a strongly adsorbed component of the feed until the bulk of the bed becomes saturated. The “*breakthrough point*” occurs when the concentration of the fluid is leaving the bed spikes as unadsorbed solute begins to emerge.



Figure 2.3 Graphical representation of the breakthrough curve

Figure 2.3 depicts a typical breakthrough (BT) curve. At the start of adsorption (t_0), a feed containing an initial concentration of more adsorbed component (C_0) enters the adsorber bed. The adsorption starts at the entrance of the bed ($L=0$). At time $t=t_1$, the MTZ has progressed further towards the exit of the bed ($L=L$), and a part of the bed is saturated (no net mass transfer occurs). As the adsorption continues at time $t=t_3$, the more adsorbed component appears at the exit streams. This time is called the breakthrough time t_b . If the feed is allowed to enter the bed after this time, the bed will be eventually saturated with adsorbates, and no clear separation will occur. At this point (t_e), the exit concentration becomes equal to feed concentration.

Chapter-2

The breakthrough time and shape of the curve provide much insight into the performance of the adsorbent under the operating conditions prevailing during the breakthrough curve generation. The time required for a bed to become totally saturated is obtained by integrating till saturation time. The usable capacity of the bed is given by the area above the breakthrough curve up to the breakthrough time. The usable capacity is represented by

$$t_u = \int_0^{t_b} \left(\frac{C_t}{C_o} \right) dt \quad \text{Equation 2.17}$$

The total stoichiometric capacity of the bed up to saturation is given by:

$$t_T = \int_0^{t_e} \left(\frac{C_t}{C_o} \right) dt \quad \text{Equation 2.18}$$

2.6.1 The length of the unused bed (LUNB)

Length of unused Bed (LUNB) method was the first short-cut method to design or scale-up of a fixed bed process. The LUNB, which represents the distance that is not saturated at the breakthrough time.

It can be calculated as:

$$LUNB = L \left(1 - \frac{t_u}{t_T} \right) \quad \text{Equation 2.19}$$

The MTZ moves across the bed unchanged; therefore for a given feed velocity the length of MTZ and LUNB does not change. Therefore the bed utilisation improves with an increase in bed length as LUNB becomes a smaller fraction of total bed length

2.6.2 Usable length of the bed (LUB)

$$LUB = L \left(\frac{t_u}{t_T} \right) \quad \text{Equation 2.20}$$

The total bed length is obtained by as:

$$\text{Total Length} = LUB + LUNB \quad \text{Equation 2.21}$$

2.7 MEANS OF REGENERATION OF THE ADSORBENT

Adsorbent regeneration (removal of adsorbed molecules from the surface of the adsorbent or reducing the equilibrium adsorbed amount) can be achieved by following methods in an industrial process:

2.7.1 By reducing the partial pressure of the adsorbate

The adsorption process is favoured at high pressure and low temperature. In a typical pressure swing adsorption process the strongly adsorbed component of feed is adsorbed during the high-pressure adsorption step. The adsorbed components can be recovered (counter-current to feed) by reducing the pressure of the adsorber vessel by connecting the feed end to atmospheric pressure.

When the pressure is reduced by the application of vacuum, the process is called “Pressure/Vacuum Swing Adsorption” (PVSA or simply VSA) which is a particular case of PSA. The duration of the cycle time is short, often in minutes. The regeneration of the adsorber bed by the reduction in pressure can be easily understood in **Figure 2.4**.

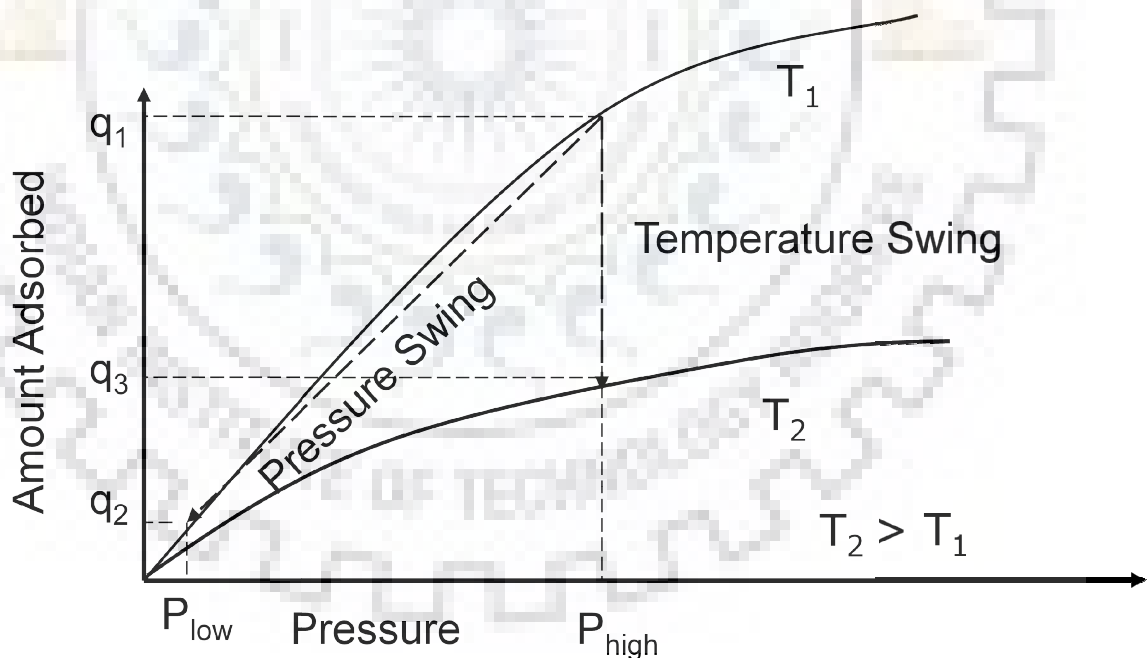


Figure 2.4 Schematic illustration of regeneration by reducing pressure and increasing temperature

Chapter-2

When adsorption pressure is reduced from P_{High} to P_{low} , the adsorbent's equilibrium uptake capacity decreases from q_1 to q_2 . The difference ' $q_1 - q_2$ ' is called the working capacity of the adsorbent between pressure P_{High} and P_{low} .

2.7.2 By increasing the temperature by purging the bed

An increase in temperature decreases the quantity adsorbed at any given partial pressure of the adsorbate in the gas phase. Hence, increasing the temperature from T_1 to T_2 will decrease the equilibrium loading from q_1 to q_3 (Thomas and Crittenden, 1998). Similarly, for this process, the working adsorbent capacity is ' $q_1 - q_3$ '. A change in temperature is achieved by passing a hot stream which could be a part of pre-heated adsorption product, steam or inert gas. The hot stream is also necessary to drive the desorbed gases out of the adsorber bed.

This process finds a practical approach in a process called Temperature Swing Adsorption (TSA) (Ntiamoah et al., 2016). Because heating is a slow and often rate-limiting step, the length of each cycle usually ranges from several hours to over a day. This cycle is used only for purification purposes.

2.7.3 By purging the adsorbent with an inert gas

The inert gas removes adsorbed molecules without changing the temperature or pressure. However, after the inert gas occupies all the voids space in the adsorber bed after the inert purge. The inert gas contaminates the less adsorbed component product during the next adsorption step.

2.7.4 By displacement purge with a purge gas (with less adsorbed gas)

This step is different from inert purge in the sense that a gas or vapour that adsorbs about as strongly as the adsorbate is used as the purge gas. Regeneration is achieved both by reducing the partial pressure of strongly adsorbed gas and also by the competitive adsorption of the displacement medium.

The different means of regeneration of adsorbents are compared in **Table 2.1** (Ruthven, 1984; Thomas and Crittenden, 1998).

Reducing the partial pressure (PSA/ VSA)	Excellent for weakly adsorbed species Rapid cycles The less adsorbed component can be produced in high purity	Mechanical energy is required Very low pressure may be required for strongly bonded species Regeneration product (desorbate) obtained at low purity
Increasing the temperature (TSA)	Good for strongly adsorbed species Desorbate obtained at high purity Thermal energy cheaper than mechanical energy	Long cycle time Thermal ageing of adsorbent
Purging the adsorbent with an inert gas	Essentially constant temperature and pressure	Only for weakly adsorbed species Not used when the desorbate needs to be recovered
Displacement purge with a purge gas	Good for strongly adsorbed species Thermal ageing of the adsorbent can be avoided	As the desorbate is purge gas, another separation step may be needed

2.8 PRESSURE SWING ADSORPTION

In pressure swing adsorption (PSA) the regeneration of adsorption adsorbent is carried out by reducing the pressure of the absorber column and/or passing the bed with a gaseous stream. Therefore, the PSA process works between two different points defined on the equilibrium isotherm as illustrated in **Figure 2.4**.

The commercial examples of PSA based process include heatless dryer for a drying hydrogen purification from steam methane reforming (SMR) (Cen and Yang, 1985; Kumar, 1990; Malek and Farooq, 1998; Park et al., 2000; Sircar, 1979), air separation for nitrogen and oxygen production (Berlin, 1966; Ruthven et al., 1986; Skarstrom, 1960). The PSA system is very versatile and adaptable for separation of gaseous streams involving a different kind of gases owing to the choice of adsorption and variable range of operating pressure and temperature.

In addition to the above commercial processes, PSA has garnered wide research attention for development of processes for CO₂ to capture from flue gases (Aarti et al., 2011; Dasgupta et al., 2015, 2009), propane-propylene separation, ethane-ethylene separation (Pires et al., 2014b, 2014a; Saini et al., 2010; Sivakumar and Rao, 2006), propylene nitrogen separation (Da Silva and Rodrigues, 2001a; Liu et al., 2015; Miltenburg et al., 2006; van Miltenburg et al., 2008), biogas purification (Arya et al., 2015; Jiang et al., 2018; Kapoor and Yang, 1989; Pires et al., 2008) etc.

Skarstrom patented the first and most basic PSA cycle. It consists of four steps namely pressurisation with feed, adsorption, blowdown to atmospheric pressure and purge with adsorption product (Skarstrom, 1960)

Typical PSA cycle necessary consists of two parts, i.e. adsorption and regeneration. In the first part, the gaseous mixture is separated at high pressure by allowing the feed mixture to pass through an adsorbent bed. In this step, highly absorbed gaseous species is retained in the absorber column, and the least adsorbed species are obtained in high purity. In the second part, the adsorbed components are removed from the adsorbent bed by reducing the pressure and/or purging the bed with a gaseous stream. In a PSA process, these two parts can be divided into many steps to achieve the design specifications such as high purity and/or high recovery of more or less adsorbed components.

Chapter-2

2.8.1 Significance of different steps

Any PSA cycle follows a combination of following necessary steps:

2.8.1.1 Pressurization

In this step, the column is pressurised with the feed from feed end or less adsorbed component. This step enriches the product end of the adsorber with less strongly adsorbed species.

2.8.1.2 High pressure feed (adsorption step)

This step is carried out at the highest pressure of the process. The purpose of this step is to obtain less adsorbed component at high pressure.

In a particular variation, the pressure is gradually decreased to enhance the recovery of the less adsorbed component, but the product is delivered at low pressure.

2.8.1.3 Depressurization or Blowdown (co-current or counter-current to the feed)

In counter-current blowdown step, the pressure of the column is reduced by letting the high-pressure column from the feed end. This step is used when the less adsorbed component is required at high purity as it prevents the contamination of the product and with more strongly adsorbed species.

The co-current blowdown, which is generally followed by the counter-current blowdown, is used when the more adsorbed component is required at high purity. It can also help in increasing the recovery of the less adsorbed component.

2.8.1.4 Desorption at low pressure

The desorption step is carried out by lowering the pressure by:

- Counter-current desorption with product purge. However, the overall recovery is reduced if the Purge is carried out at moderate pressure as it reduces the loss in the recovery of the less adsorbed component.

or

- Counter-current desorption with external Purge. It is possible to enhance the recovery and at the same time get the less adsorbed component in high purity.

or

- **Evacuation.** The step allows the production of both the less and more adsorbed component in high purity. It is advantageous over purge with the product when the heat of adsorption is very high and the column is not completely desorbed only by blowdown. When the regeneration is carried out under vacuum, the process is called vacuum swing adsorption (VSA)

2.8.1.5 Pressure equalisation

A continuous PSA process essentially operates with two or more absorber column undergoing the same sequence of PSA cycle steps in tandem. In pressure equalisation step (Ntiamoah et al., 2015), two adsorber beds at high and low pressures are connected through either their respective feed and product end. This step helps to conserve energy.

2.8.1.6 Rinse

In the rinse step, the adsorber is rinsed, co-current to the feed, with the highly adsorbed component of the feed after high-pressure adsorption. This step improves the purity of more adsorbed component when other components are also adsorbed in significant amount along with the highly adsorbed component.

2.8.2 PSA performance indicators

The following key indicators are used to evaluate the performance of a PSA or VSA process:

2.8.2.1 Product purity

The product purity is the average purity (or mole fraction) of the desired component in the product. It may be noted that the product may mean weakly adsorbed component (adsorption product), strongly adsorbed component (desorption/ evacuation product) or both depending upon the nature of feed and process objectives. It is commonly reported in mol% or weight%.

2.8.2.2 Product recovery

The product recovery is the ratio of the quantity of the desired component in the respective product to the quantity of that component in the feed. Once again the recovery may pertain to either or both of the products as in case of product recovery. The exact expression of the

product recovery will depend upon the steps involved in a PSA/VSA cycle. It is commonly reported in mol% or weight%.

2.8.2.3 Process productivity

The process productivity implies the normalised rate of production of the desired component. In other words, productivity is the rate of production of the desired component per unit weight/volume of adsorbent. The most common units for reporting the productivity are $\text{mol}(\text{product})\text{-kg}^{-1}(\text{adsorbent})\text{h}^{-1}$, $\text{liter}(\text{product})\text{-liter}(\text{adsorbent})^{-1}\text{h}^{-1}$ etc.

2.9 PROPYLENE SEPARATION FROM GASEOUS STREAMS BY PRESSURE SWING ADSORPTION: LITERATURE SURVEY

A number of alternative separation processes have been proposed including membrane separation using highly selective membranes (Swaidan et al., 2015), absorption (Chen et al., 2013), adsorption (Ruthven and Reyes, 2007) and its variants such as adsorption-distillation hybrid systems (Ghosh et al., 1993; Kumar et al., 1992) and pressure swing adsorption (PSA) or vacuum swing adsorption (VSA) (Da Silva and Rodrigues, 2001b; Grande et al., 2010a; Grande and Rodrigues, 2005; Khalighi et al., 2013a; Plaza et al., 2012; Rege et al., 1998).

Many adsorbents have been reported in the literature for propylene-propane separation including metal-organic frameworks (MOFs). MOFs are a novel class of materials synthesised by binding organic long-chain linkers with polyvalent metal ions, which makes their properties tunable (Mallick et al., 2012).

MOFs have been extensively investigated for adsorptive separation such as CO_2 adsorption (Bakken et al., 2011; Chowdhury et al., 2009; Dasgupta et al., 2015; Dietzel et al., 2008; Grande et al., 2017; Masala et al., 2017; Mishra et al., 2014; Schell et al., 2012), H_2/CO_2 separation (Chandrasekhar et al., 2013; Mallick et al., 2010), methane storage (He et al., 2014; Sun and Webley, 2010; Tagliabue et al., 2011) etc. MOFs including Cu-BTC (Chowdhury et al., 2009; Plaza et al., 2012) and CPO-27 (Luna-Triguero et al., 2017) have been reported. Plaza et al. (Plaza et al., 2012) have described experimental breakthrough data at 150 kPa and 373 K and simulation results of a five-step PSA cycle have been reported. The simulation results indicate that polymer grade propylene can be produced with a productivity value of $0.6 \text{ mol kg}^{-1}\text{h}^{-1}$. A separation factor of 2.2–2.3 was observed from the propane/ propylene binary breakthrough curves.

Chapter-2

Azahara et al. (Luna-Triguero et al., 2017) conducted Monte Carlo simulations by Grand-Canonical Monte Carlo simulations to study adsorption mechanisms of the saturated/unsaturated hydrocarbon mixtures on CPO-27 MOF with different metal cations, at 318 K and 353 K. They computed the adsorption isotherms, and from these the adsorption selectivity which was compared To IAST model. Fe-based MOF-74 is reported to be the best option for both ethane/ethylene and propane/propylene separation applications.

The earliest report on propane-propylene separation includes the work of Jarven and Fair (Jarvelin and Fair, 1993). They reported a pilot-scale breakthrough study with equimolar propane-propylene mixture diluted with nitrogen at 269 kPa pressure and 296 K temperature. A high degree of separation was reported with a highly diluted system.

Rege et al. (Rege et al., 1998) studied the separation of an equimolar mixture of propane and propylene with Ag^+ dispersed silica gel and zeolite 4A. A four-step VSA process (pressurisation with Feed, high-pressure adsorption, high-pressure purge with the product, low-pressure counter-current blowdown) is reported. The remarkable process performance results are:

- For AgNO_3 -Silica (343 K): Propylene purity (mol%): 97.6-99.1, Propylene recovery (mol%): 18.1- 43.6, Productivity (mmol/h/kg): 15.5-52.1
- For Zeolite 4A (373 K): Propylene purity (mol%): 99.0-99.9, Propylene recovery (mol%): 8.0- 27.3, Productivity (mmol/h/kg): 15.5-52.1

Da Silva and Rodrigues (Da Silva and Rodrigues, 1999) compared the separation performance of Zeolite 13X (equilibrium separation) and zeolite 4A (kinetic separation) by adsorption isotherm and diffusivity data. It is interesting to see that zeolite 13X show very little difference in the adsorption capacities for propylene and propane. For example the adsorption isotherm capacity for zeolite 13 X at 100 KPa, 303 are; (Propylene: 2.7 mmol/g, Propane: 2.3 mmol/g). However, there is marked the difference in the adsorption equilibrium capacities for zeolite 4A owing to the exclusion of propane by the narrow pores of zeolite 4A. Adsorption isotherm capacities for zeolite 4A at 100 KPa, 303 are/(Propylene: 1.9 mmol/g, Propane: 0.1 mmol/g). The pore diffusivity, molecular diffusivity and Knudsen diffusivity values for both propane and propylene in the temperature range of 393-473 K are of the same order of magnitude confirming the equilibrium based separation.

Chapter-2

Da Silva and Rodrigues (Da Silva and Rodrigues, 2001a), tested zeolite 13X for separation of equimolar mixture of propylene/propane (diluted with nitrogen) in a single column five-step VSA cycle (pressurization with feed, high-pressure adsorption, high-pressure purge with propylene product, co-current blowdown; and countercurrent vacuum blowdown) over temperature and pressure range of 393-423 K and 110-500 kPa respectively. The best results reported show propylene purity of 98%, recovery of 19%, and productivity of 0.785 mol/kg/ h.

Process performance for separation of an equimolar mixture of propylene/ propane (diluted with nitrogen) on zeolite 4A is also reported by Da Silva and Rodrigues (Da Silva and Rodrigues, 2001b). VSA cycle used was similar to their earlier report (Da Silva and Rodrigues, 2001a). Zeolite 4A is reported to produce a propylene-rich product of similar purity (97 mol% relative to the propylene/propane mixture, with 4.4% of nitrogen) but at slightly improved recovery (26 mol%) and productivity 1.03 mol/kg/ h.

Choudary et al. (Chao et al., 1998; Choudary et al., 2002) reported olefin/ paraffin separation with Ag- impregnated clay adsorbent. The VSA steps included high-pressure adsorption, high-pressure rinse with the product, evacuation to low pressure, re-pressurisation with propane gas and/or rinse gas from the bed undergoing product rinse step.

VSA results for separation of an ethane-ethylene mixture (Ethylene: 83.1%; Ethane: 16.8% Impurities: Balance) are reported. The very high heat of adsorption of propylene on adsorbent (~60kJ/mol) reported, making the application of high vacuum (6 kPa) is required. Ethylene purity of 99.8 % Ethylene recovery of 85.0% has been reported. VSA separation data for propane-propylene was not reported in this paper.

Grande et al. (Carlos A. Grande et al., 2005; Grande and Rodrigues, 2004), demonstrated the application of a commercial carbon molecular sieve with a single column five-step VSA process (pressurisation, feed, rinse, intermediate depressurisation, and countercurrent blowdown) by computer simulation. From the nature of the breakthrough curve, it was concluded that the separation of propane and propylene would be challenging to perform in a PSA unit using this adsorbent. They have reported single component and binary adsorption isotherm data at 373 K and in the pressure range of 0-300 kPa. For an equimolar mixture of propylene and propane at 373 K, propane purity and recovery of 83 and 84 mol% is reported experimentally.

Chapter-2

Another alumino-silica based silver impregnated adsorbent for propylene-propane separation has been reported by Ko et al., 2006. Propylene and propane isotherm data at 298 K and in the pressure range of 0-490 kPa is reported. From the analysis of the data, the propylene adsorption capacity of AgNO₃/aluminosilica was 2.3 mmol/g, and the selectivity of propylene over propane was 3.1 at 298 K and 294 kPa. The heat of adsorption of propylene is very high (up to 52 kJ/mol) which implies that in a dynamic VSA process with very low evacuation pressure will be required to desorb the propylene from the adsorbent completely.

Sodium Derivative of Engelhard Titano-silicates (Na-ETS-10) (Chowdhury et al., 2012; Kuznicki, 1987; Prasanth et al., 2009), is a member of the family of molecular sieve type of materials. It has been found to be suitable for catalysis (Das et al., 1996; Waghmode et al., 2001; Xu et al., 2001), adsorptive separation (Al-Baghli and Loughlin, 2005; Anson et al., 2008; Garcia et al., 2008; Shi et al., 2011, 2010) and ion-exchange (L Lv et al., 2004; Zhao et al., 2003).

The Na-ETS-10 has been reported to be synthesised through various precursors and routes (Ferreira et al., 1998; Kim et al., 2000; L. Lv et al., 2004). Na-ETS-10 or (ETS-10) is a mixed octahedral/tetrahedral titanium silicate with a kinetic pore diameter of 8 Å, which is large enough to allow species such as C₃H₈, C₃H₆, CO₂, CH₄, etc. inside the framework. The separation efficiency of Na-ETS-10 thus will depend upon the equilibrium competitive adsorption of these species on the surface of ETS-10.

Tiscornia et al., (Tiscornia et al., 2007) have reported propane and propylene isotherm data on a laboratory synthesised silver-impregnated Na-ETS-10 adsorbent. The experimental data is reported for a temperature of 311 K and up to 20 kPa only. Binary propane-propylene adsorption data on a faujasite (13X) is reported by Miltenburg (van Miltenburg et al., 2008) at 318, 358 and 408 K with a partial pressure of the two components between 0.8–54 kPa. The binary adsorption data is reported to be accurately predicted by IAST. A comprehensive evaluation of the applicability of this adsorbent for PSA/VSA process from such scant data is difficult as the operating pressures of the PSA/VSA process are higher than this pressure range.

Grande et al. (Grande et al., 2010a) modified a commercial Zeolite 13X by exchanging extra-framework Na⁺ ions with Li⁺. The experimental isotherm shows, a slight loss in capacity at 323 K. The heat of adsorption for propylene and propane was 61.4 and 58.4 kJ/mol which is very high indicating very strong interaction with adsorbent and difficulty in the regeneration of adsorbent.

Chapter-2

Grande et al. (Grande et al., 2010b) described a two-stage VSA scheme for the production of polymer-grade propylene with Zeolite 4A. The first stage is designed to increase the purity of propylene while the second stage served to enhance the overall recovery of propylene. The process simulation predicts a propylene purity of 99.6% and a propylene recovery of 67%. The recovery value is higher than the previously reported literature data (Da Silva and Rodrigues, 2001b; Rege et al., 1998).

More recently, the applicability of Cu-BTC MOF has been tested by simulation of a five-step VSA cycle (Plaza et al., 2012). The highest propylene specific adsorption capacity known up to date for a shaped material (up to 8 mol kg⁻¹ of dry adsorbent at 323 K is reported here. The simulation results indicate that For the cycle carried out (simulation results) a propylene purity of 99.8% was attained (above polymer grade specifications) with the productivity of 0.6 mol kg⁻¹h⁻¹. However, the propylene recovery was low (15 mol %).

Khalighi et al. (Khalighi et al., 2014, 2013a) introduced pure silica chabazite (SiCHA) for kinetic separation of propylene and propane. A simple four-step pressure vacuum swing adsorption (PVSA) cycle has been proposed and simulated to obtain two high purity products from a propylene/propane mixture using a new kinetically selective adsorbent, silica chabazite (SiCHA). The cycle, involving pressurisation, high-pressure adsorption, forward rinse, and reverse evacuation, can satisfactorily separate two industrially relevant feed mixtures of 50/50 and 85/15 propylene/propane into 99 mol % propylene and 90 mol % propane.

Most recently Kuah et al. (Kuah et al., 2018) simulated a seven-step VSA cycle (feed pressurisation, high-pressure adsorption, co-current depressurising pressure equalisation, co-current rinse, counter-current evacuation, co-current pressurising pressure equalisation, and co-current rinse reflux) based on Zeolite 4A. A comparative cost calculation concludes that the minimum total cost (propylene recovery by VSA) is US\$20.86 per ton of propylene, compared to US\$41.07 per ton of propylene (propylene recovery by C₃ splitter).

There are only a few literature reports on the propylene recovery from polypropylene reactor off-gas. Ribeiro et al. (Ribeiro et al., 2013) reported a PSA process for recovering only nitrogen or recovering both nitrogen and propylene using MOF MIL-100(Fe). They simulated the experimental propylene breakthrough curves of a gas mixture containing propylene (30 mol%) and nitrogen (70 mol%). The experimental breakthrough curves were simulated using a mathematical model. The fitting parameters derived from the breakthrough simulations were used to simulate the PSA process. For the recovery of nitrogen only a cycle five steps:

Chapter-2

adsorption, co-current depressurisation, blowdown, purge and pressurisation with part of nitrogen product was used. Similarly, for the recovery of both nitrogen and propylene was achieved by a cycle with six steps including adsorption, co-current depressurisation, rinse with the propylene-rich product, blowdown, purge with nitrogen product and pressurisation with part of nitrogen product. For the nitrogen recovery (first cycle) nitrogen purity and recovery of 99.9% and 81.5% are reported respectively with adsorbent productivity was $0.08 \text{ kg N}_2/\text{kg}_{\text{ads}}/\text{h}$. For the simultaneous recovery of nitrogen and propylene, purities obtained were respectively 99.9% for nitrogen and 97.9% for propylene with nitrogen and propylene recovery of 97.4% and 87.6% respectively. The adsorbent productivity was $0.20 \text{ kgN}_2/\text{kg}_{\text{ads}}/\text{h}$ and $0.07 \text{ kgC}_3\text{H}_6/\text{kg}_{\text{ads}}/\text{h}$.

In continuation of the above work, Narin et al. (Narin et al., 2014) simulated an industrial scale PSA plant with feed throughput of 60000 SLPM at 343 K and 100 kPa (70% nitrogen and 30% propylene) using the same parameters reported by Ribeiro et al. (Ribeiro et al., 2013). For the nitrogen recovery by the 2-column, 5-step PSA (pressurisation, adsorption, co-current depressurisation, blowdown, and purge) process nitrogen with 95.4% purity and 85.2% recovery was reported. The adsorbent productivity was $6.0 \text{ mol N}_2/\text{kg}_{\text{adsorbent}}/\text{h}$. It may be noted that the purity and recovery values are similar to bench scale PSA simulations ((Ribeiro et al., 2013), however, the nitrogen productivity is significantly higher of industrial-scale PSA simulations. The authors have not deliberated on the possible cause of increased productivity. For simultaneous recovery of nitrogen and propylene, the additional rinse step necessitates the addition of another column to the process. Here, nitrogen and propylene purity of 96.2% and 97.6% respectively are predicted by simulations. The nitrogen and propylene productivity and propylene productivities predictions for the commercial scale simulations are 4.61 and 1.83 mol product/kg_{adsorbent}/h, which are again higher than corresponding bench-scale simulations (Ribeiro et al., 2013).

Zwilling et al. (Zwilling et al., 2003) have patented a 4-bed, eight-step PSA process for recovery of ethylene and nitrogen from polypropylene reactor off-gas containing 30 mol% propylene balance nitrogen. The steps used in the PSA cycle are adsorption, pressure equalisation (depressurising), idle, provide purge, blowdown, purge, pressure equalisation (re-pressurizing) and product re-pressurisation. The computer simulation results indicate that the nitrogen is obtained at ~100% purity and 65.4% recovery. The propylene is enriched from 30% in the feed to 55% in a propylene-rich product which is recycled back to the propylene recovery

unit. The overall propylene recovery obtained is 99.9%. The process operates at an adsorption pressure of 1960 kPa and 283 K. The adsorbent used is silica gel and/or activated alumina.

2.10 CURRENT RESEARCH GAPS

A survey of literature data on propylene-propane separation for over the last twenty-five years has been presented above. A close analysis of these literature reports reveals that there are still many aspects which have not been studied comprehensively. On the basis of analysis of the data following the main research gaps are identified:

- There is a dearth of literature reports experimental data for binary isotherm of propane-propylene on different zeolites. A few reports for adsorbents such as MOF-74 or ETS-10 are available but for a very low range pressure and temperature
- The Binary adsorption data for propane-propylene needs to be generated for commercial adsorbents as well for their evaluation
- The applicability of IAST for prediction of binary propylene-propane adsorption data has not been studied in details
- Commercial adsorbents of similar type (say zeolites), have different adsorption capacities for propane and propylene under same conditions (Da Silva and Rodrigues, 1999; Grande et al., 2003a) owing to differences in formulation and amount of binder used for pelletizing (Divekar et al., 2016)

Therefore evaluation for similar adsorbents from various commercial sources is necessary

- Recovery of propylene from the dilute mixture in propane, e.g. C₃ splitter column bottom stream has not been reported
- Experimental PSA data on the recovery of propylene and nitrogen from polypropylene unit purge gas, which may contain up to 50% propylene in nitrogen is scant. Most of the available reports are based on MOFs, silica gel and activated alumina.

2.11 OBJECTIVES OF THE THESIS

The overall objective of the present work is to prepare an effective separation techniques for propylene from propylene bearing streams such as adsorptive Pressure Swing Adsorption (PSA) or Vacuum Swing Adsorption (VSA) (Webley et al., 2017). The following simulated feed mixtures are proposed to be used:

- (i) Steam cracking of hydrocarbons (~50% propylene + balance propane);
- (ii) Fluid catalytic cracking (~75% propylene + balance propane) ;
- (iii) Propane-propylene splitter bottom (5-15% propylene + balance propane);
- (iv) Polypropylene reactor purge gas (10-30% propylene + balance nitrogen).

To achieve the overall objective of the thesis the following scope of work was envisaged:

- Comprehensive literature survey to identify the adsorbents, process operating conditions and PSA process configuration and to know the experimental results for benchmarking purpose;
- To characterise and evaluate different adsorbents by:
 - structural properties, and
 - single component equilibrium isotherm data;
- To develop an Ideal Adsorbed Solution Theory (IAST) based solver to predict the binary isotherm data and solver validation;
- To evaluate binary adsorption equilibrium data based on IAST solver;
- To conduct experimental dynamic PSA studies to explore the applicability of recovery of propylene from above-identified feed streams.

CHAPTER-3 SYNTHESIS, CHARACTERIZATION AND SCREENING OF POTENTIAL ADSORBENTS

3.1 SYNTHESIS OF Na-ETS-10 ADSORBENT

As discussed in **chapter-2 (section 2.9)**, Na-ETS-10 has been reported to be selective (Al-Baghli and Loughlin, 2005; Shi et al., 2011, 2010) for C₂H₄ over C₂H₆. Therefore an attempt is made to synthesize this material in our laboratory and use this synthesized material for the separation of Propylene from Propane.

Na-ETS-10 was synthesized following the methodology proposed by Shi et al., 2011. This synthesis involved a thorough mixing of 50 g of sodium silicate (28.8% SiO₂, 9.14% Na₂O), 3.2 g of sodium hydroxide (97% NaOH), 3.8 g of KF. (Anhydrous), 4 g of HCl (1 M) and 16.3 g of TiCl₃ solution, all sources from Fisher. The mixture was stirred in a blender for one h at an rpm of 200 and then reacted in a 200 × 10⁻³ dm³ sealed autoclave) at 488 K for 64 h. The resultant solid was washed with a copious amount of de-ionized water and dried at 523 K for 12 h.”

The synthesis of Na-ETS-10 in pure form was by using the above procedure as modified with a slight modification of the procedure described by Lv et al., 2004. As per the procedure given in this paper, “Mixture A was prepared by dissolving sodium silicate solution (27wt% SiO₂, 8wt% Na₂O, and 65wt% H₂O, Aldrich), NaOH, and KOH (in examination of the effects of Na⁺, K⁺, and F⁻ on the crystallization of ETS-10, NaCl, KCl, and KF were added in mixture A) in de-ionized water under stirring for 10 min. Mixture B was prepared by dissolving a titanium source, namely either TiCl₃ (15wt% TiCl₃ in 20wt% HCl solution, Merck), or TiF₄ (Aldrich), or (NH₄)₂F₆Ti (Aldrich), or P25 (76wt% anatase and 24wt% rutile, Degussa), or a commercial titanium dioxide (designed as TiO₂, Fisher chemical), in de-ionized water under stirring for 10min. Subsequently the two mixtures were combined under stirring for 30 min to obtain a slurry gel. The gel was then transferred into a Teflon-lined autoclave and placed in an oven at either 200 or 230 °C. After a given period, the solids were recovered by filtration, washed with de-ionized water, and dried at 100 °C)”. In the synthesis work for this thesis TiO₂ was used as the source of titanium, the pH of the reaction mixtures was adjusted to 11.2 (instead of recommended value of 10.5) and aging time of 72 h was used.

3.2 SOURCES OF COMMERCIAL ADSORBENTS STUDIED

The Zeolite 5A pellets and Zeolite 13 X beads (trade name Z10-04) were obtained from UOP (USA) and Zeochem (USA), respectively and used as procured with no zeolite phase analysis carried out using X-Ray Diffraction (XRD) technique.

3.3 CHARACTERIZATION OF ADSORBENTS

3.3.1 BET Surface Area and Pore Size Analysis

The BET surface area and pore volume of the adsorbents were measured using a Micromeritics TriStar analyzer with high purity nitrogen used as the probe adsorbate. Before N₂ adsorption measurement at 77 K, the zeolite and Na-ETS-10 adsorbents were degassed for 12 h at 623 K under a dynamic vacuum.

3.3.2 X-Ray Diffraction (XRD) Studies of Synthesized Adsorbents

The crystalline structures of as-synthesized adsorbents were examined by powder X-ray diffraction (XRD) using a Bruker D8 Advance diffractometer operated with Cu K α radiation of 0.15418 nm wavelength at 40 kV and 40 mA.

3.4 ADSORPTION EQUILIBRIUM ISOTHERMS MEASUREMENTS

Single component adsorption equilibrium isotherms of Propane, Propylene, and Nitrogen were measured in a Hiden IGA-002 (Hiden Isochema, UK) gravimetric microbalance at 298, 323, 343, 373 and 423 K temperature and up to 300 kPa pressure for the three adsorbents. About 150 mg of each adsorbent was loaded in the adsorption cell, and the adsorbent was activated *in situ* at a suitable temperature under ultra vacuum ($< 10^{-6}$ mbar) condition for 6 hours before each isotherm measurement. The least count of IGA-002 is 1 μ g.

The adsorbent sample was suspended to the balance in an SS sample holder and sealed in SS 316 sample cell (chamber). For *in-situ* sample activation, the sample cell was heated with a furnace to the desired temperature. A diaphragm vacuum pump and a turbo molecular pump were used to apply ultra-high vacuum ($< 10^{-6}$ mbar) to degas the sample until the balance showed a constant weight.

For adsorption analysis, the sample cell was held at a constant temperature using a furnace or a jacketed water bath. A high-pressure gas cylinder was used to supply the gas, and the isotherm measurement was carried out at the predetermined pressure point. Two computer-controlled

Chapter-3

valves control the pressure. The gas, for which isotherm was to be measured, was introduced in the adsorption cell at predetermined pressure steps. As the pressure increases, the gas is adsorbed on the surface of the adsorbent, and the increase in weight of the adsorbent is measured by the gravimetric balance. The gas uptake was measured gravimetrically after allowing sufficient time for attaining equilibrium at each fixed pressure. The adsorption isotherm unit is automated and requires very little manual intervention. **Figure 3.1** and **Figure 3.2** present the schematic diagram and picture of the IGA-001 instrument, respectively:

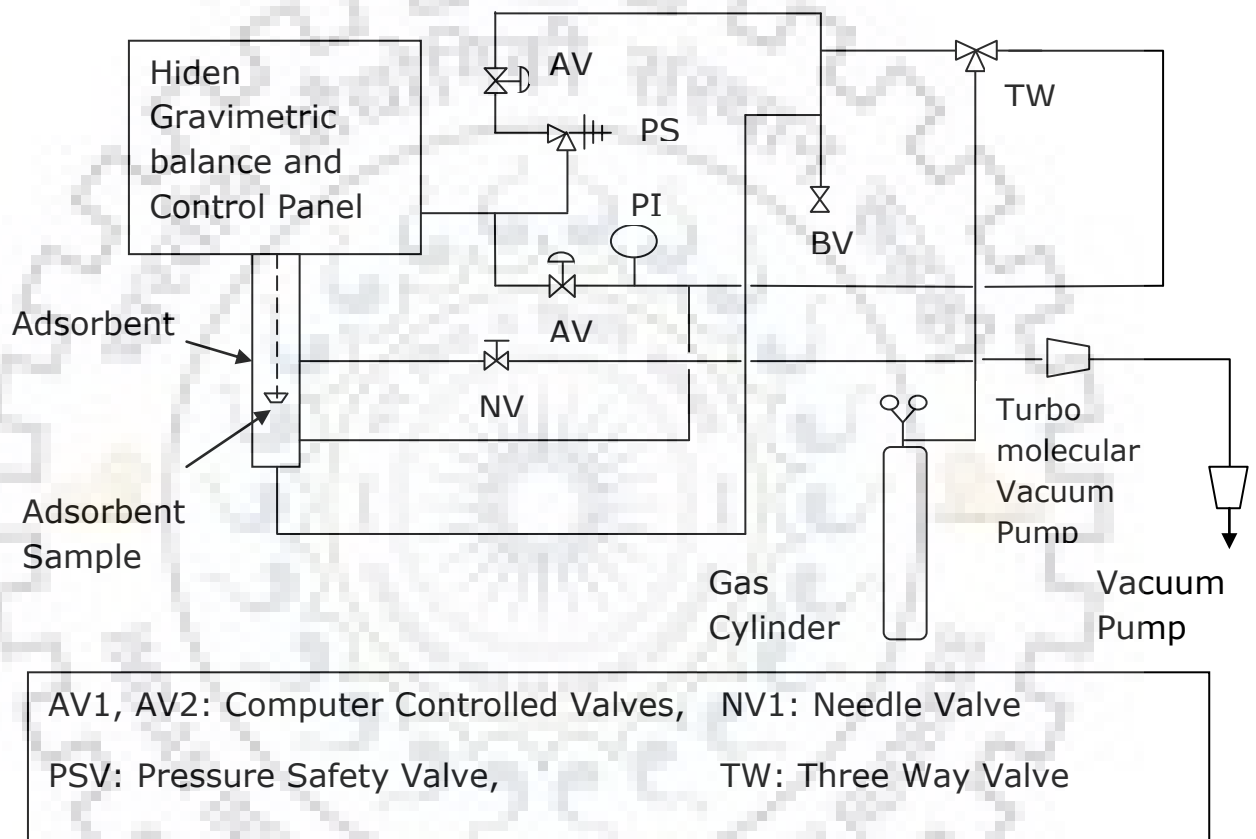


Figure 3.1 Schematic diagram of IGA-001 gravimetric microbalance



Figure 3.2 Photograph of the IGA-001 gravimetric microbalance for single component Isotherm measurement

3.5 ADSORBATES

The gaseous adsorbates, i.e., propane, propylene, and nitrogen (>99.9% Purity), were supplied by M/s Sigma Gases and Services, India.

3.6 ISOTHERM DATA REGRESSION

Langmuir, Sips and DSL isotherm equations were initially fitted to the experimental data. The sum of squared error (SSE) was minimized by fitting the experimental isotherm data to these models with the 'solver' add-in function in MS Excel. The default Newton's (Quasi-Newton) method was used for minimizing SSE. The minima of objective functions (SSE) were found by simultaneously varying the fitting parameters.

3.7 RESULTS AND DISCUSSION

3.7.1 Laboratory synthesis and characterization of Na-ETS-10

The XRD pattern of a crystalline material is obtained to ascertain the formation of the desired phase and also to determine the presence of any undesired impurity formed during the synthesis. The XRD pattern of Na-ETS-10 is presented in **Figure 3.3**.

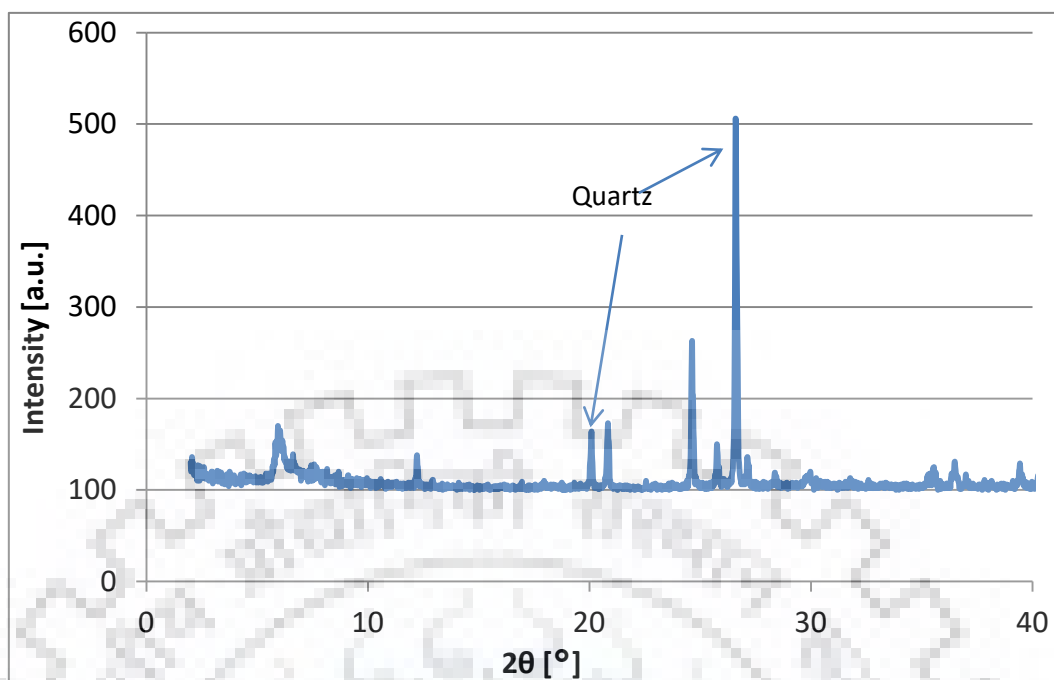


Figure 3.3 X-ray diffraction pattern of Na-ETS-10 (First Batch)

The XRD peaks are compared with those reported in the literature (Kuznicki, 1987) characteristic peaks are shown in **Table 3.1**:

Table 3.1 Comparison of literature reported characteristic XRD pattern with laboratory synthesized Na-ETS-10

Literature D-spacing (Å)	Experimental D-spacing (Å)
14.7± 3.5	14.69
7.2 ±0.15	7.23
4.41 ±0.1	4.41
3.60± 0.05	3.60
3.28 ±0.05	3.28

It was, however, noted that Na-ETS-10 showed two distinct peaks. These peaks indicate the formation of quartz impurities (Su and Zhao, 2006). These peaks are highlighted in **Figure 3.3**. Two more batches of Na-ETS-10 were prepared so as to reduce/ eliminate the formation of quartz phase. However, in both the attempts, ETS-10 materials were not formed and the XRD patterns of resulted materials are compared with the first batch in **Figure 3.4**.

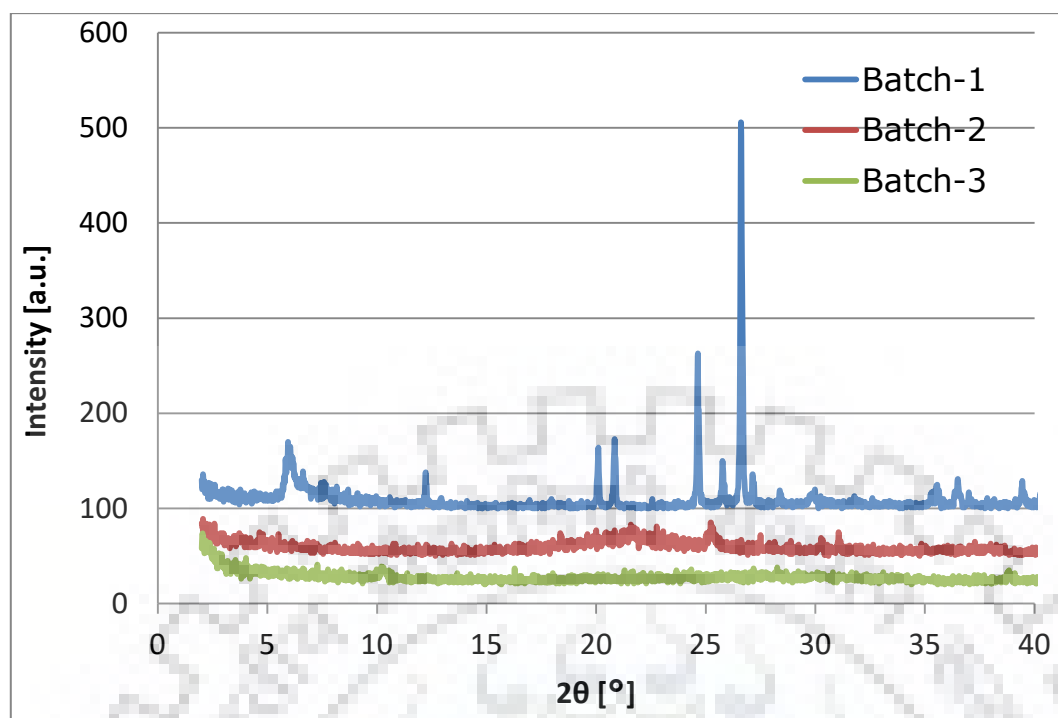


Figure 3.4 X-ray diffraction pattern of laboratory synthesized Na-ETS-10

A thorough literature study conducted to understand the factors affecting the formation of Na-ETS-10 adsorbent reveals that a number of parameters such as the source of titanium ion, composition of sodium silicate solution (i.e., $\text{Na}_2\text{O}:\text{SiO}_2$) ratio, pH, the presence of seed crystal, etc. are critical to the formation of ETS-10 structure. In the present case, the composition of the sodium silicate solution was disturbed to the precipitation of the Na_2O phase, and it was deemed to be the most probable reason for the non-repetition of the results.

As discussed in Section 3.1.1, Pure Na-ETS-10 material was prepared using the method suggested by L. Lv et al., 2004. The XRD patterns of Na-ETS-10 (first batch) and the optimized recipe is compared in **Figure 3.5**.

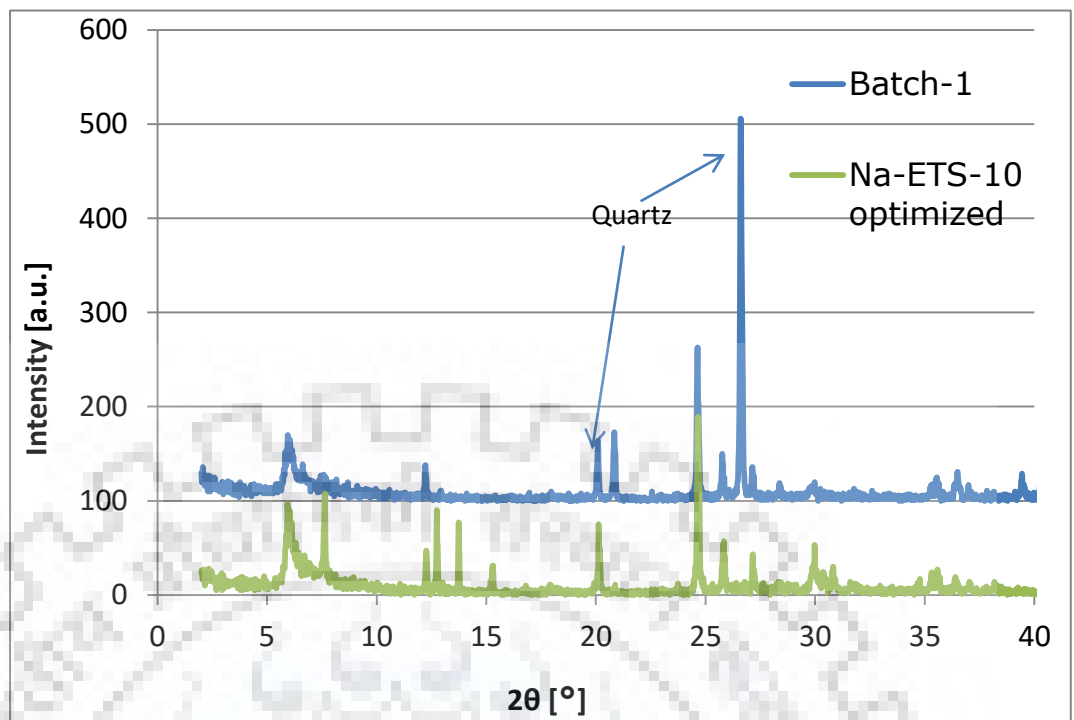


Figure 3.5 Comparison of the X-Ray diffraction patterns of laboratory synthesized Na-ETS-10 (First batch and finally optimized recipe)

As shown in **Figure 3.5**, the Na-ETS-10 prepared under optimal conditions does not contain any quartz impurity.

3.7.2 Characterization of commercial adsorbents

The surface and structural properties of the commercial adsorbents studied are given in **Table 3.2**:

Table 3.2 The surface and structural properties of commercial adsorbents

Adsorbent	Form	Particle Size (mm)	Specific Surface Area (m ² /g)	Pore Volume (cm ³ /g)	Bulk Density (g/cm ³)
Zeolite 5A (UOP)	Pellet	1.6	383	0.24	0.70 ^a
Z10-04 (Zeochem)	Sphere	2.0	516	0.35	0.67 ^a
Na-ETS-10 (lab synthesized)	Powder	-	278	0.18	0.89 ^b

^a As reported by the manufacturer; ^b Experimentally determined data

The surface and structural properties of the three adsorbent lies within the literature reported range for these materials.

3.7.3 Isotherm measurements and data regression

Pure component isotherm data

The experimental isotherm data for propane and propylene conform to type I isotherm for all the three adsorbents. Type I isotherms are characteristic for monolayer adsorption inside the pores of these microporous adsorbents when the pore size of the adsorbent does not exceed a few adsorbate molecular diameters (Lowell and Shields, 1984). At the higher pressure, all the adsorption sites available are occupied by the adsorbed molecule resulting in a plateau in the isotherm curve and hence, no appreciable adsorption is recorded at higher pressure. This conclusion is well supported by fitting of this set of experimental data to different isotherm models. The curve fitting and data regression are discussed in **Section 3.7.4** in detail.

Figures 3.6 to Figure 3.8 show the experimentally measured isotherms for propane and propylene for all the adsorbents along with the best-fit DSL isotherm equation curves. The goodness of fit in terms of Sum of Squared Error (SSE) is summarized in **Table 3.3** and **Table 3.4** for the three adsorbents.

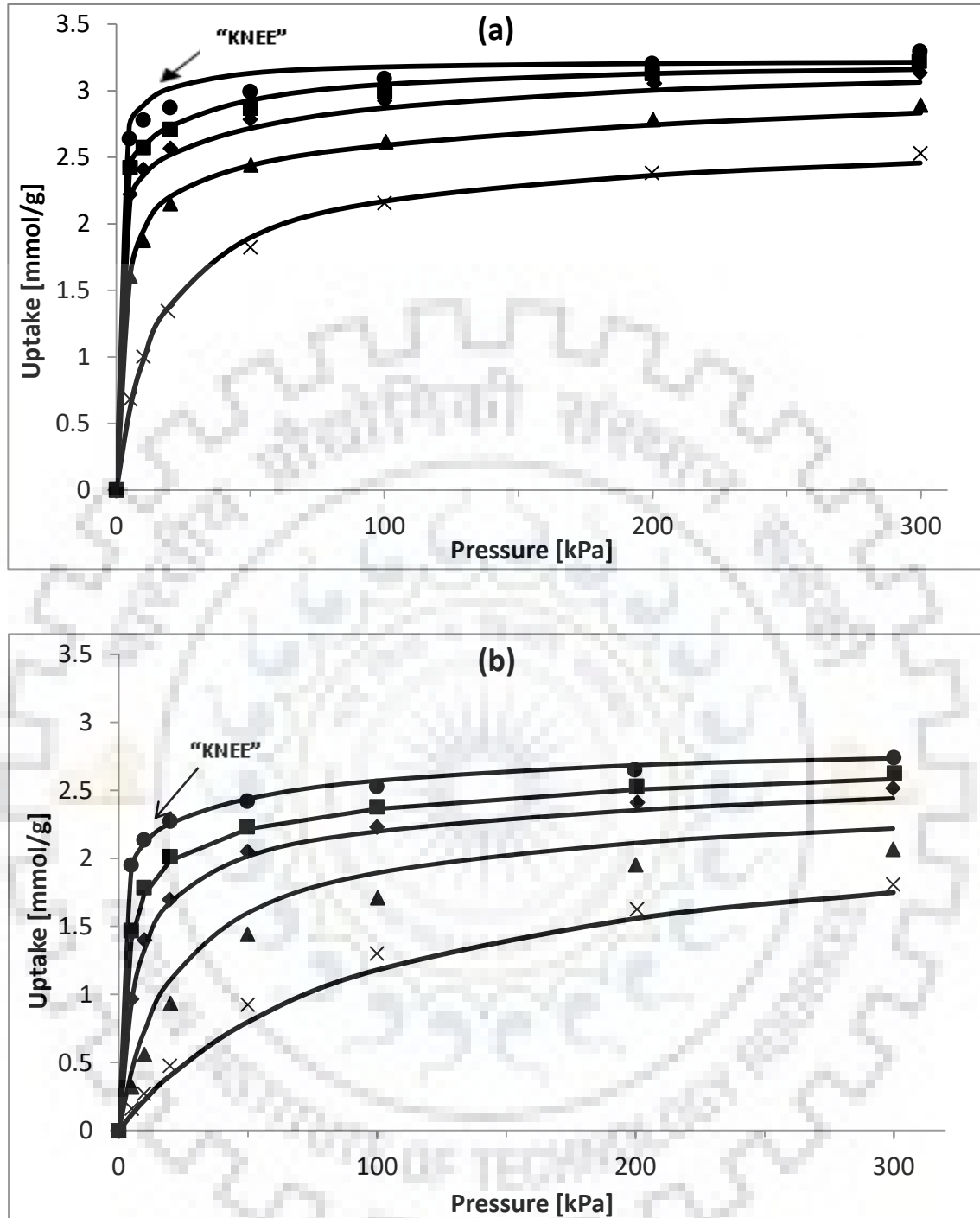


Figure 3.6 (a) Propylene and (b) propane isotherm on Z10-04 (Zeochem) at different temperatures (●: 298 K, ■: 323 K, ◆: 343 K, ▲: 373 K, ×: 423 K, Solid lines: DSL fit)

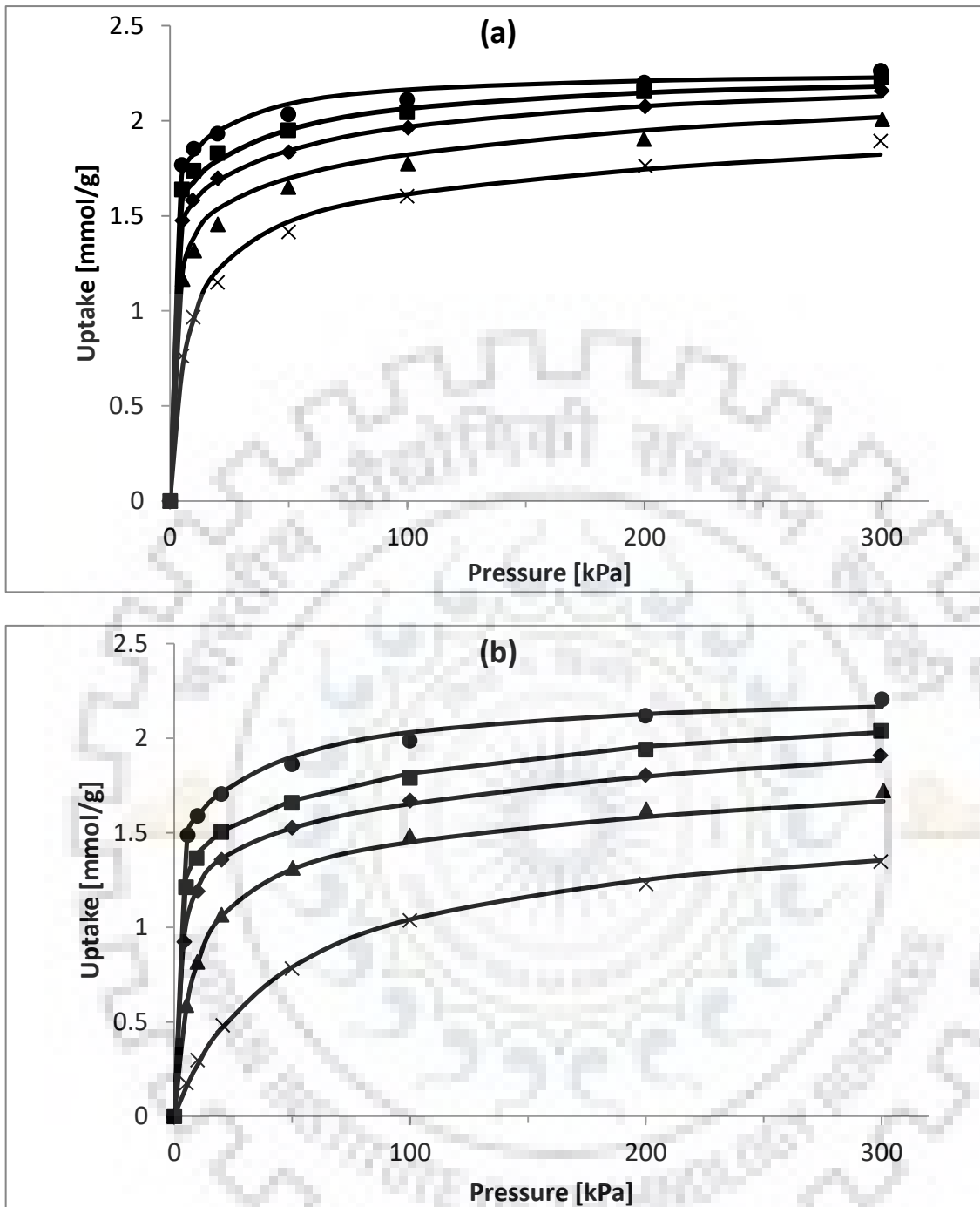


Figure 3.7 (a) Propylene and (b) propane isotherm on Zeolite 5A (UOP) at different temperatures (●: 298 K, ■: 323 K, ◆: 343 K, ▲: 373 K, ×: 423 K, solid lines: DSL Fit)

It can be seen that for both propane and propylene, the slope of the adsorption isotherms is very steep up to the “knee” region. The “knee” of adsorption isotherm is shown in **Figure 3.7**. Above this pressure region, the equilibrium uptake is practically constant.

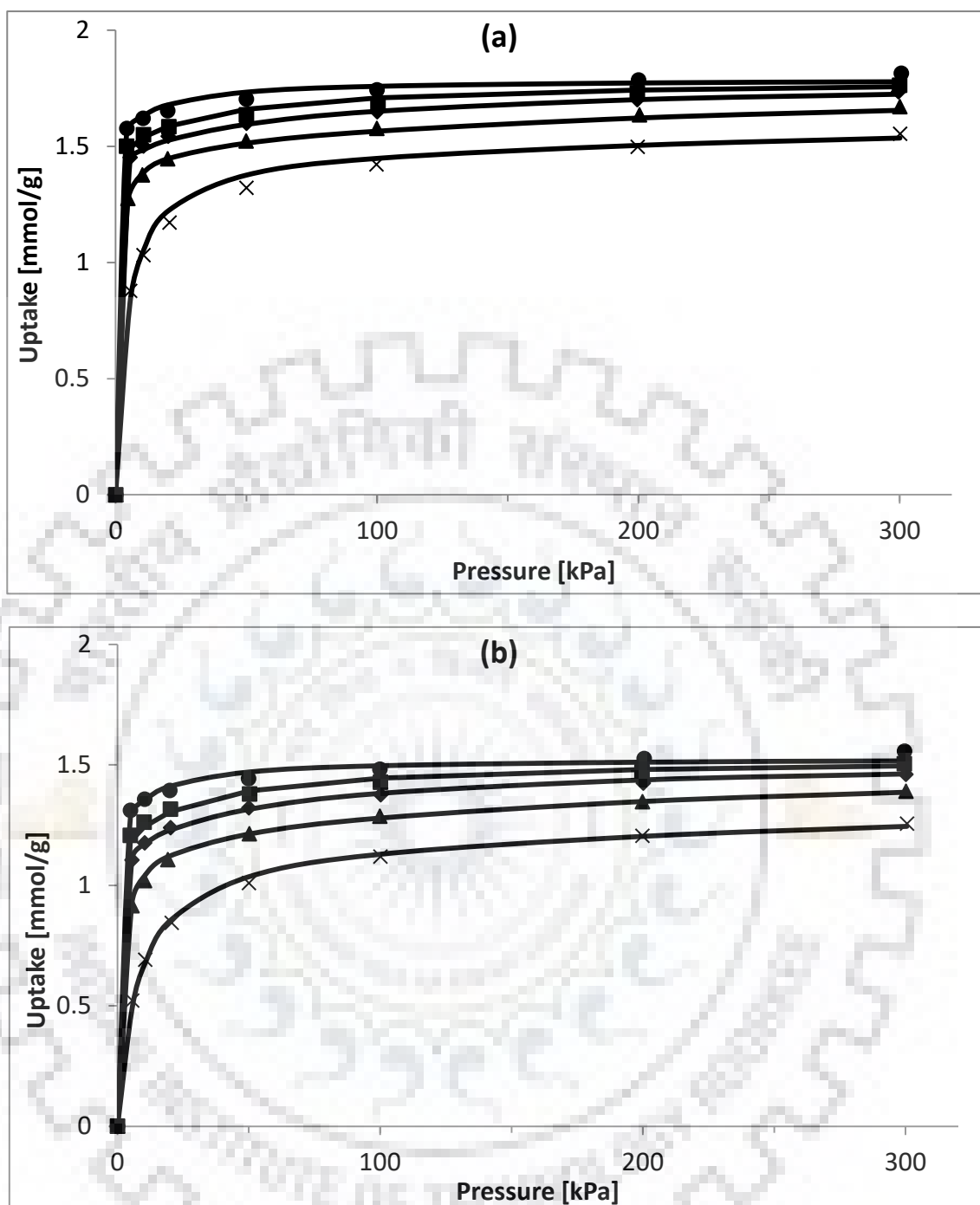


Figure 3.8 (a) Propylene and (b) propane isotherm on Na-ETS-10 at different temperatures (●: 298 K, ■: 323 K, ◆: 343 K, ▲: 373 K, ×: 423 K, Solid lines: DSL Fit)

Single component experimental isotherm data of propylene and propane has been reported by Da Silva and Rodrigues (1999) for another commercial 13X Zeolite (CECA). The equilibrium uptake values for the Z10-04 (Zeochem) reported here are higher than the data reported for CECA Zeolite. The equilibrium uptake values of propylene on Z10-04 at 100 kPa and 323, 343, 373 and 423 K are 3.0, 2.9, 2.6 and 2.5 mmol/g respectively whereas corresponding values (Da

Chapter-3

Silva and Rodrigues, 1999) for Zeolite 13X (CECA) are 2.5, 2.4, 2.2 and 1.7 mmol/g respectively. Similarly, the propylene uptake on commercial Zeolite 5A pellets reported by Grande et al., 2002 at 100 kPa and 343, 373, 423 K is ~ 2.3, 2.1 and 1.6 mol/kg. In comparison, the corresponding values reported in this study are 1.97, 1.82 and 1.61 mol/kg. The propane equilibrium uptake reported by Grande et al. (Grande et al., 2002) at 100 kPa and 343, 373, 423 K is ~ 2.2, 1.8 and 1.2 mmol/g, whereas corresponding values obtained in this study are 1.67, 1.48 and 1.03 mol/kg. It suggests that the type and amount of binder in a commercial zeolite adsorbent can affect its isotherm capacity.

Nitrogen isotherms on the Z10-04, Zeolite 5A and Na-ETS-10, are presented below in **Figure 3.9**, **Figure 3.10**, and **Figure 3.11** respectively. The data for Z10-04 and Na-TS-10 is experimentally measured in this study. The corresponding data of Zeolite 5A has been used from literature (Mofarahi and Sayyedi, 2009).

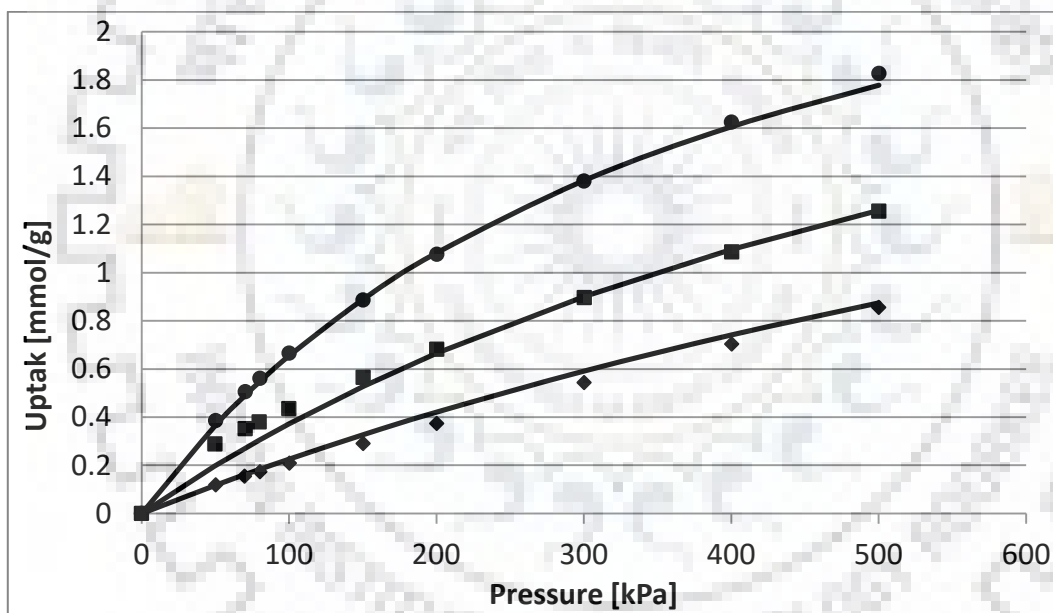


Figure 3.9 Experimental isotherms and the respective DSL fits for nitrogen on Z10-04 (●: 273 K, ■: 303 K, ◆: 333 K, Solid lines: DSL fit)

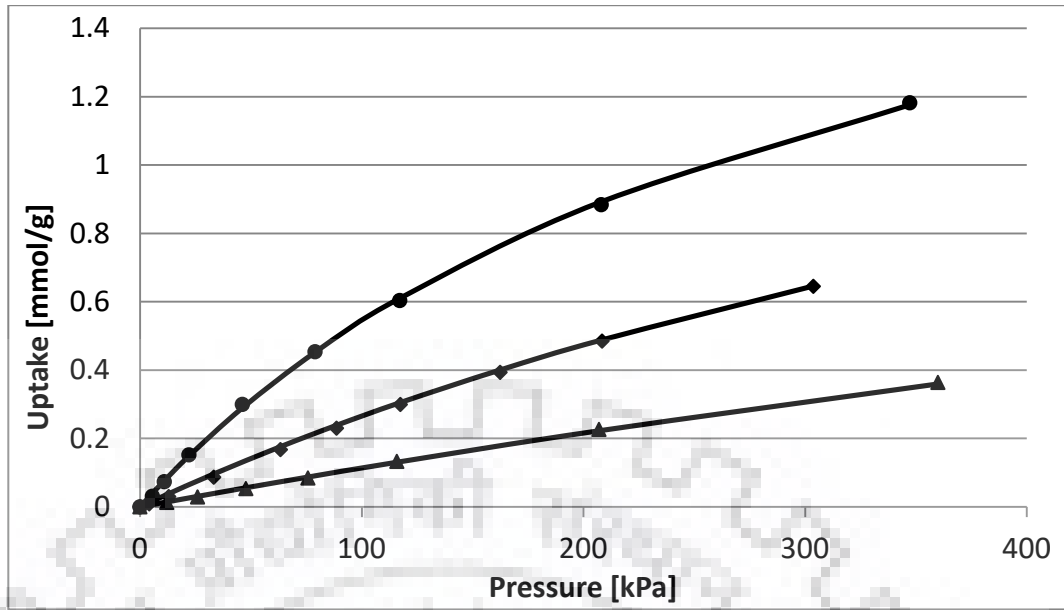


Figure 3.10 Literature reported Nitrogen isotherms on Zeolite 5A (Mofarahi and Sayyedi, 2009) (●: 273 K, ■: 303 K, ▲ : 333 K, Solid lines: DSL fit)

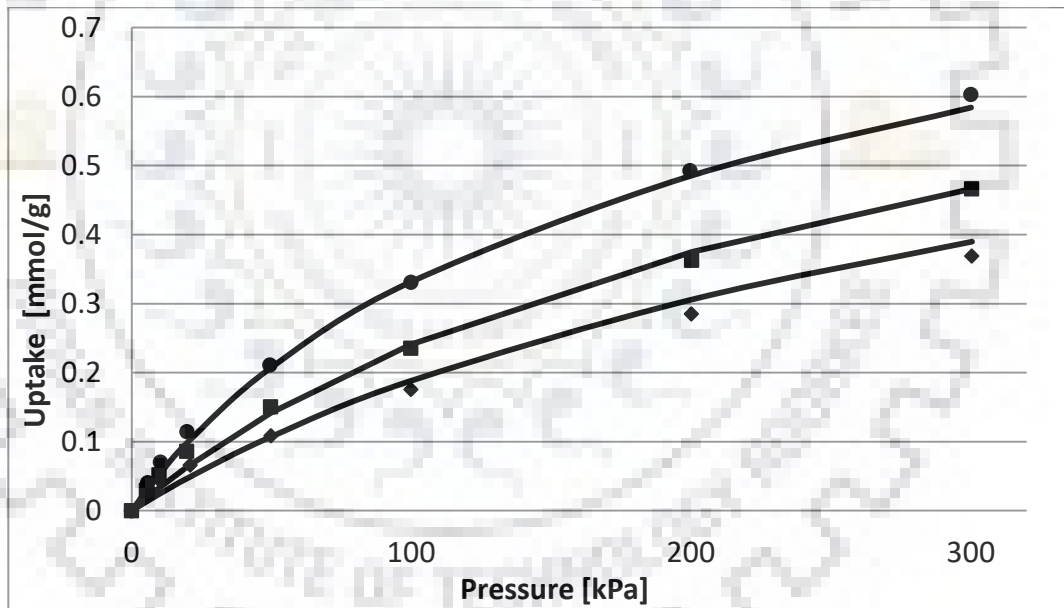


Figure 3.11 Experimental isotherms and DSL fits for Nitrogen on Na-ETS-10 (●: 298 K, ■: 323 K, ▲ : 343 K, Solid lines: DSL fit)

3.7.4 Data regression and curve-fitting

A comparison of the accuracy of Langmuir, Sips and DSL model fits against the experimental data for Z10-04 at 298 K with propylene and propane is shown in **Figure 3.12**. Although the comparison is made for only Z10-04 at 298 K, the single component experimental isotherm data for propane and propylene on all three adsorbents at five temperatures, however, could be best correlated by the DSL model.

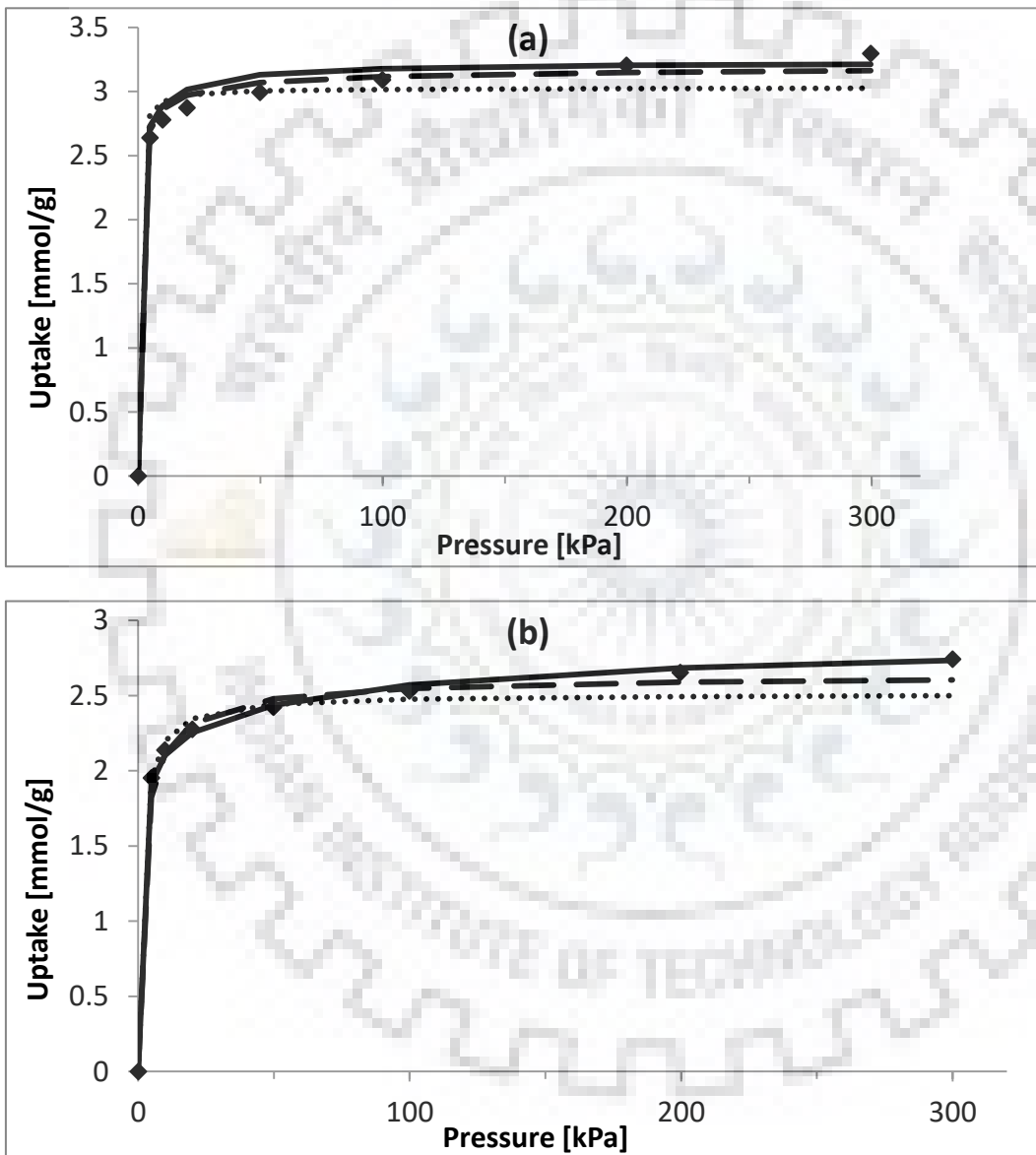


Figure 3.12 Experimental Isotherms and respective Langmuir, Sips, DSL fits for (a) propylene and (b) propane on Z10-04 at 298 K (♦: Experimental data, : — —: Langmuir Fit,:Sips Fit, Solid line: DSL fit)

Chapter-3

The DSL model predicts the single component isotherm data with reasonable accuracy over the temperature and pressure range studied. The DSL fitting parameters are presented in **Table 3.3**. The extent of deviation in isotherm prediction from experimental data is also tabulated as a total sum of error squared (SSE) obtained during the data regression.

Similarly, the isotherm data regression results for Z10—04, Zeolite 5A and Na-ETS-10 are presented in **Table 3.4**.



Chapter-3

Table 3.3 The DSL isotherm fitting parameters for propylene and propane

Parameter	Z10-04 (Zeochem)		Zeolite 5A (UOP)		Na-ETS-10	
	Propylene	Propane	Propylene	Propane	Propylene	Propane
q_{01} (mmol g ⁻¹)	0.78	0.67	1.60	1.45	1.48	1.17
q_{02} (mmol g ⁻¹)	2.45	2.20	0.66	0.81	0.31	0.36
b_1^∞ (kPa ⁻¹)	1.83×10^{-09}	3.27×10^{-08}	8.28×10^{-06}	7.95×10^{-08}	9.68×10^{-07}	6.32×10^{-07}
b_2^∞ (kPa ⁻¹)	1.80×10^{-07}	1.70×10^{-07}	8.13×10^{-07}	1.91×10^{-08}	3.08×10^{-08}	4.00×10^{-08}
$-\Delta H_1$ (kJ mol ⁻¹)	44.9	32.1	34.3	44.2	43.5	43.0
$-\Delta H_2$ (kJ mol ⁻¹)	45.0	39.0	27.6	35.0	37.0	36.7
SSE (mmol/g) ²	0.14	0.27	0.07	0.02	0.02	0.01

Chapter-3

Table 3.4 The DSL isotherm fitting parameters for propylene nitrogen isotherm on different adsorbents

Parameter	Z10-04 (Zeochem)		Zeolite 5A		Na-ETS-10	
	Propylene	Nitrogen	Propylene	Nitrogen	Propylene	Nitrogen
q_{01} (mmol g ⁻¹)	0.78	1.13	1.60	2.25	1.48	0.51
q_{02} (mmol g ⁻¹)	2.45	1.17	0.66	3.09	0.31	0.75
b_1^∞ (kPa ⁻¹)	1.83×10^{-09}	6.04×10^{-07}	8.28×10^{-06}	1.00×10^{-08}	9.68×10^{-07}	2.33×10^{-06}
b_2^∞ (kPa ⁻¹)	1.80×10^{-07}	3.33×10^{-07}	8.13×10^{-07}	2.99×10^{-06}	3.08×10^{-08}	1.746×10^{-05}
$-\Delta H_1$ (kJ mol ⁻¹)	44.9	20.0	34.3	14.9	43.5	15.6
$-\Delta H_2$ (kJ mol ⁻¹)	45.0	20.0	27.6	15.4	37.0	15.6
SSE (mmol/g) ²	0.14	8.46×10^{-04}	0.07	3.84×10^{-02}	0.02	4.67×10^{-03}

It can be concluded from **Figure 3.6 to Figure 3.11** and **Table 3.3** and **Table 3.4** that the DSL model is adequate and accurate to represent the adsorption isotherm data of propane, propylene, and nitrogen on the three adsorbents under investigation.

3.8 BINARY ADSORPTION ISOTHERM PREDICTION BY IAST MODEL

3.8.1 Validation of IAST model solver

IAST is a thermodynamically consistent model and has been widely reported in the literature to predict the multi-component isotherm data by single component isotherm only. Myers and Prausnitz, 1965 in their seminal paper (Myers and Prausnitz, 1965), have also reported particularly that for engineering applications, IAST can be used for predicting mixed-gas adsorption equilibria, in the absence of mixture data. However, it may be noted that the accuracy of the models such as IAST and extended Langmuir depends upon the nature of adsorbate-adsorbent interaction; Therefore, before choosing the IAST model for prediction of the binary propylene-propane adsorption, the following tests were made:

(i) **Binary Data Consistency Test (BDCT) as proposed by Talu for IAST**

To enhance the confidence on the IAST predicted data, Talu (Talu, 1998) had proposed a BDCT to predict multi-component adsorption data, which states that the amount adsorbed from a binary mixture must approach the respective pure component isotherm value as the mole fraction of the respective component approaches unity and that the selectivity must approach the ratio of Henry's Law constants for pure components as the pressure approaches zero, regardless of the composition of the gas mixture.

The deviation between the pure component propane and propylene data, and IAST-DSL predicted pure component data was tested by using mol fraction of propylene or propane as the case may be, equal to zero as input in the binary IAST-DSL model. The (%) Absolute relative error is defined below. The results of the BDCT are shown in **Figure 3.13**.

$$\text{Absolute Relative Error (ARE)(\%)} = \frac{\text{Abs (Experimental value - IAST(DSL) Predicted value)}}{\text{Experimental Value}} \times 100$$

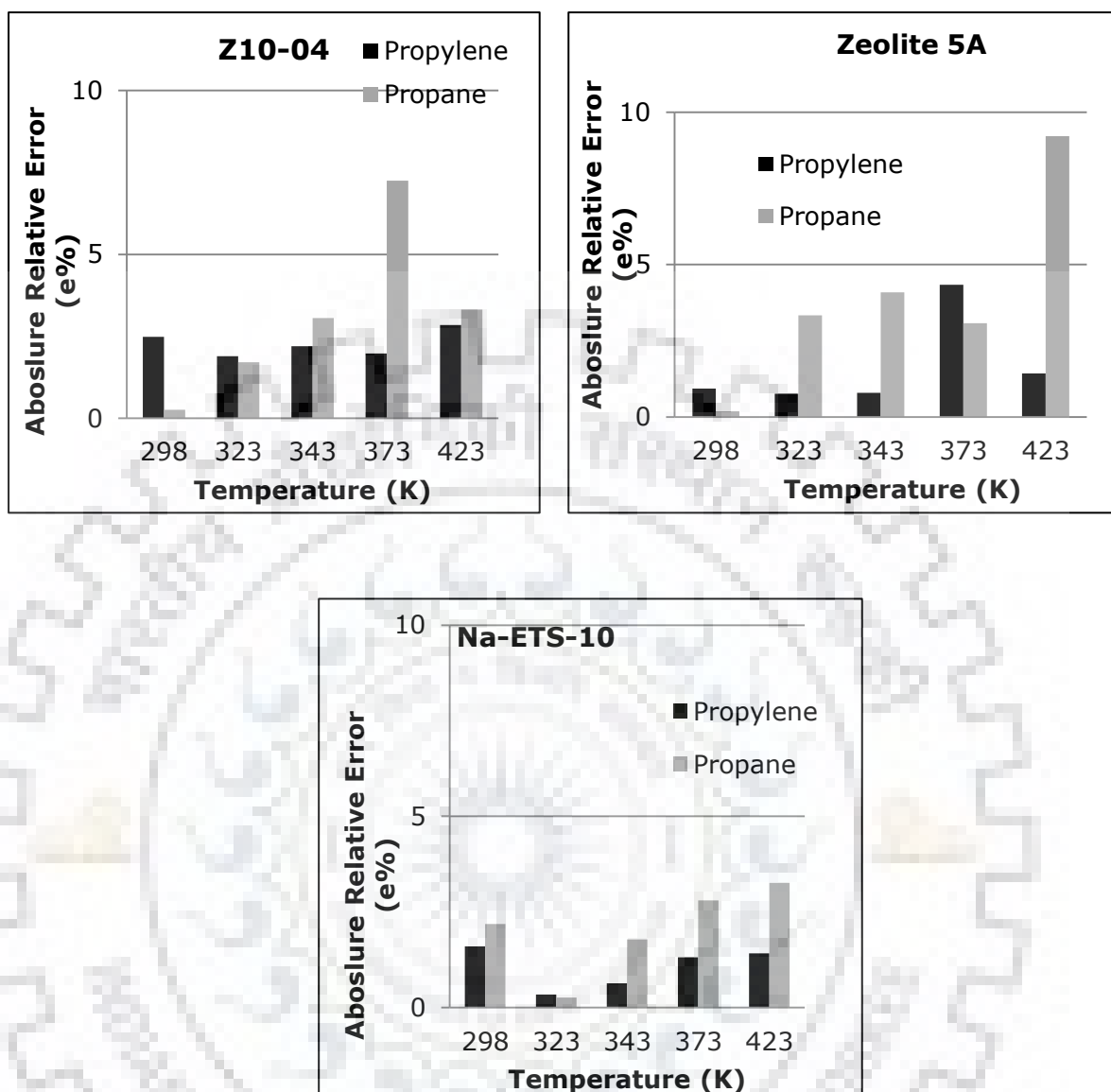


Figure 3.13 Absolute Relative Error (ARE) in Pure component Isotherm data

It can be noted from **Figure 3.13** that except for a couple of points, the experimental pure component data matches well (error < 3%) with the corresponding IAST-DSL predicted values obtained by putting gas phase mole fraction of the propane or propylene as zero.

The propane and propylene gases have very similar properties, e.g., close boiling point (-42 and -47.6 °C), molecular weight (44 and 42 g/mol respectively), polarizability (6.29 and 6.26×10^{-24} cm³) respectively. Propane has no dipole moment, whereas propylene has a dipole moment of 0.04 debye owing to the double bond. It can be assumed that the propylene and propane do not deviate significantly from the ideal state in a binary mixture under the temperature and pressure

range studied. The selective adsorption of propylene over propane on zeolites may be ascribed to the stronger interaction of the double bond of propylene with the adsorbent surface.

(ii) Comparison of IAST and Extended Langmuir Model (EL)

EL is an alternative approach to predict binary adsorption equilibrium (Khashimova et al., 2008). Like IAST, EL also does not require experimental binary data. Therefore, the accuracy of both these methods needs to be compared.

A comparison between the accuracy of multi-component adsorption prediction of IAST-DSL and EL model was made for data reported in the literature (Khashimova et al., 2008), as shown in **Figure 3.14**. It can be seen that for a zeolite-hydrocarbon system, i.e. binary methane-ethane adsorption on silicalite zeolite, the IAST-DSL model is superior to EL.

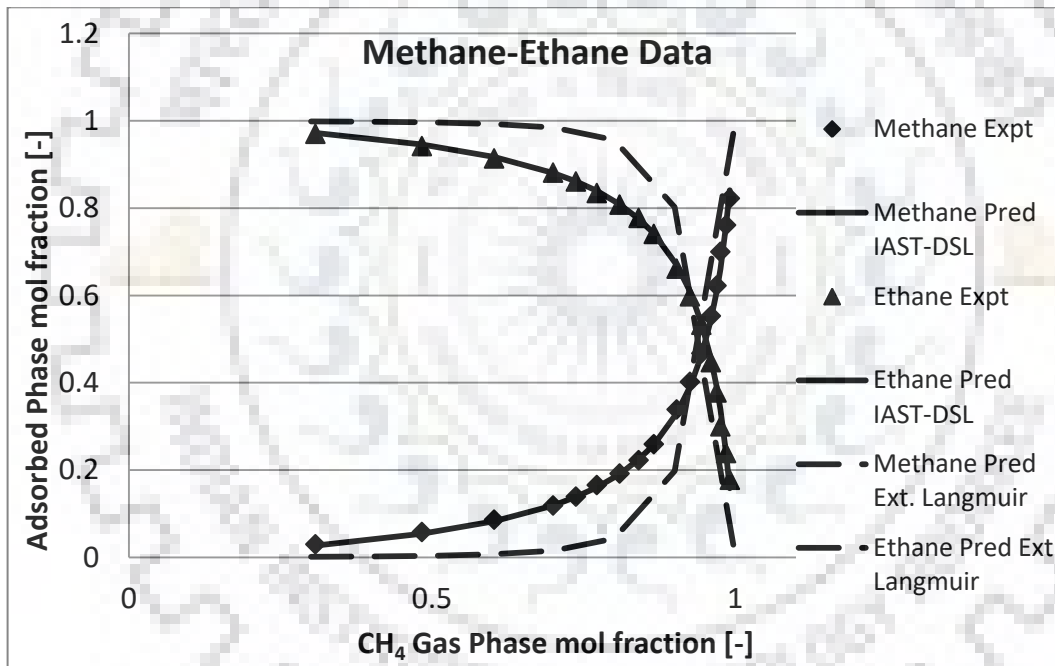


Figure 3. 14 Comparison of IAST-DSL and EL model

IAST solver model was tested rigorously against literature reported experimental multi-component isotherm data to test its accuracy. The single-component isotherm data reported in the literature was used to predict multi-component isotherm data for the same adsorbent reported in the literature. Some adsorbate-adsorbent systems based on zeolite-hydrocarbon isotherm data (Al-Baghli and Loughlin, 2006; Khashimova et al., 2008; van Miltenburg et al., 2008) were specifically chosen for the validation as these systems represent similarity of interactions between the zeolite and hydrocarbon isotherm presented in this thesis.

Chapter-3

Khashimova et al., 2008 have reported comprehensive single and binary experimental isotherm data of methane, ethane, propane, and butane on silicalite zeolite up to 1 MPa pressure and 275 to 350 K temperature range. Among the binary experimental data reported, the methane-ethane binary adsorption data at 300 K and 350 kPa (gas phase mol fraction vs. adsorbed phase mol fraction) are presented in **Figure 3.15**. It can be seen that the IAST solver can predict the binary isotherm with high accuracy.

It may be noted that the deviation from non-ideality may arise from two factors: mainly due to non-ideality on the adsorbent (lateral interaction of the adsorbed molecules). As the IAST model is based on the assumption that the bulk (gas) phase shows ideal gas behaviour; therefore the applicability of the IAST model for binary adsorption isotherm prediction and accuracy of the IAST model developed in this thesis was found to be valid when tested with the literature data.

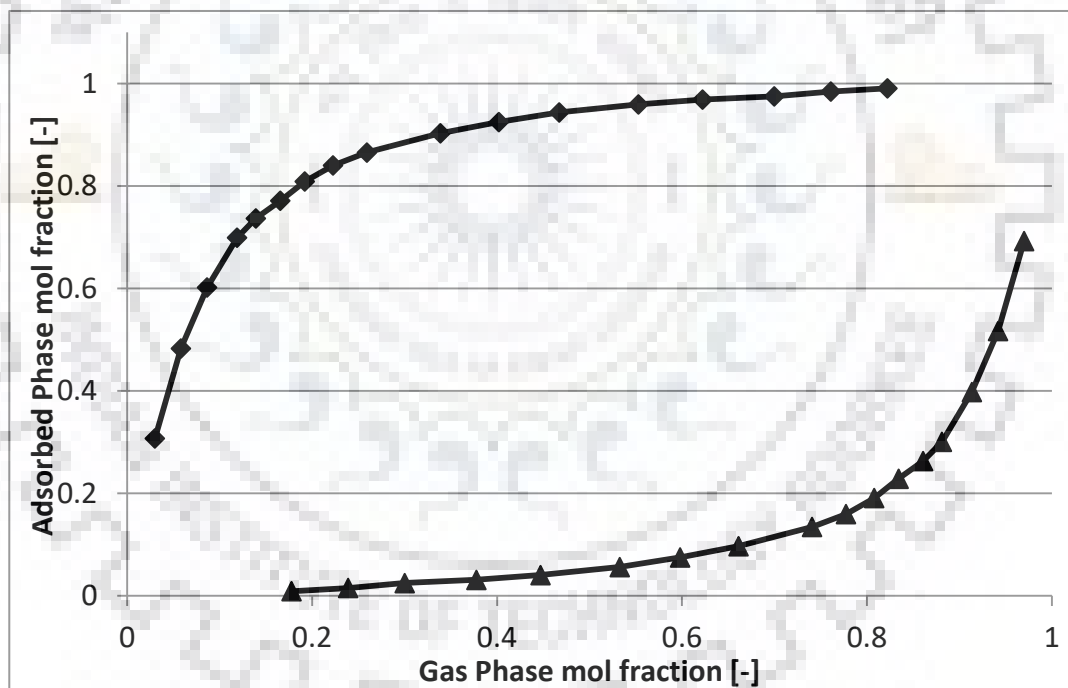


Figure 3.15 Methane-Ethane binary Isotherm on Silicalite zeolite at 300 K and 350 kPa (◆: Methane Experimental data, ▲: Ethane Experimental data, Solid lines: IAST Prediction in conjunction with DSL)

Single component and binary experimental isotherms for ethane and ethylene are reported by Al-Baghli and Loughlin, 2006 (Al-Baghli and Loughlin, 2006) at 280 K and 325 K temperatures and pressure of 350 kPa and 700 kPa on Na-ETS-10 zeolite. **Figure 3.15** indicates

Chapter-3

a close match between the literature reported experimental data and ethane-ethylene binary adsorption isotherm predicted as by the IAST solver. The methane-ethane binary adsorption isotherm data were predicted with much more accuracy with the IAST solver.

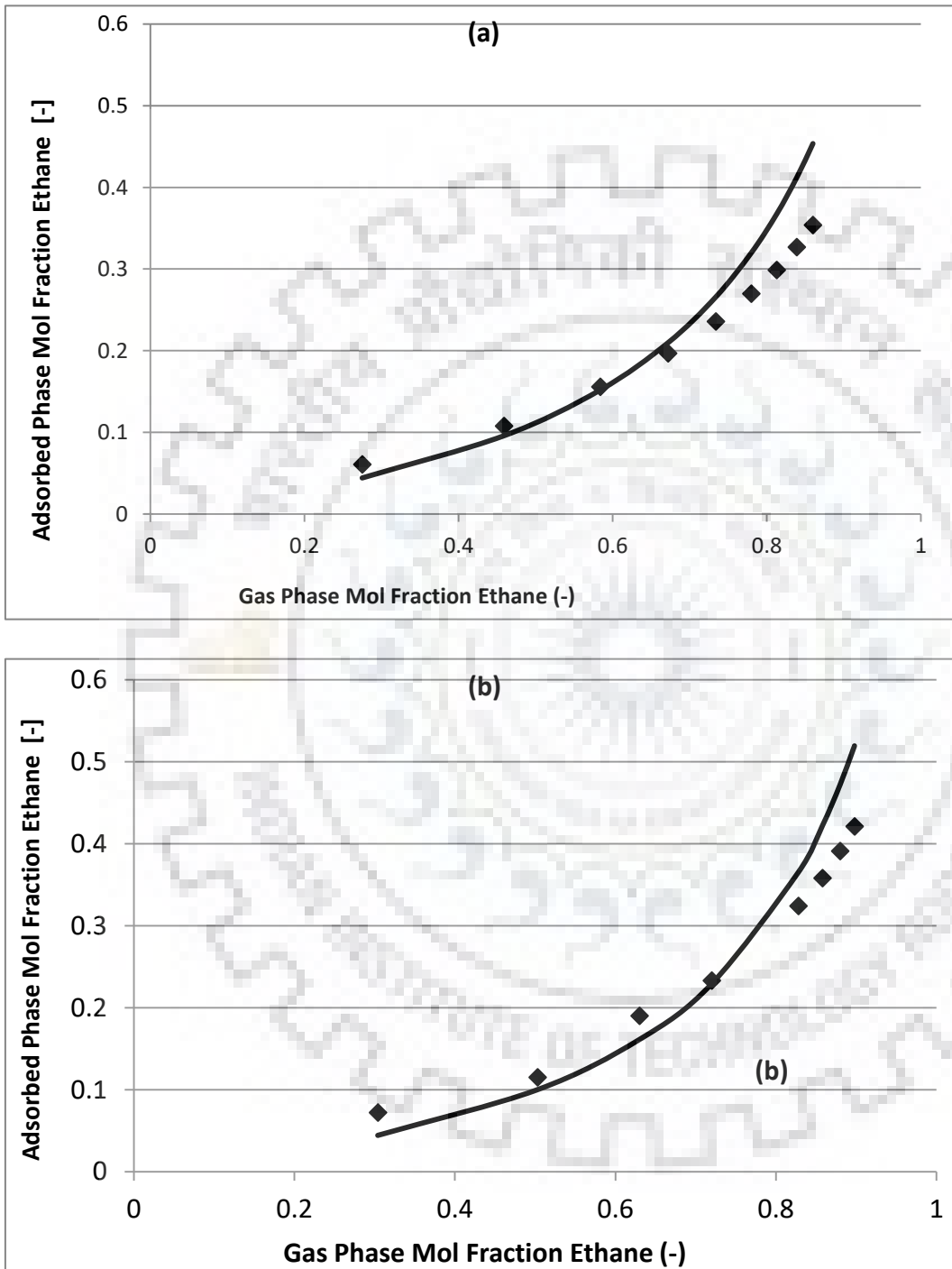


Figure 3.16 Ethane-Ethylene binary Isotherm data on Na-ETS-10 at (a) 280 K and 150 kPa and (b) 280K and 500 kPa (♦: Ethane Experimental Solid lines: IAST Prediction in conjunction with DSL)

Chapter-3

Propane-propylene binary experimental isotherm data (solid diamonds) on a lab synthesized 13X zeolite powder is reported for an equimolar mixture at 318, 358 and 408 K up to 100 kPa by Miltenberg et al., 2008 (van Miltenburg et al., 2008). The binary data prediction (solid squares) by Miltenberg et al., 2008 (van Miltenburg et al., 2008) is compared with our predictions (solid line) in **Figure 3.16**.



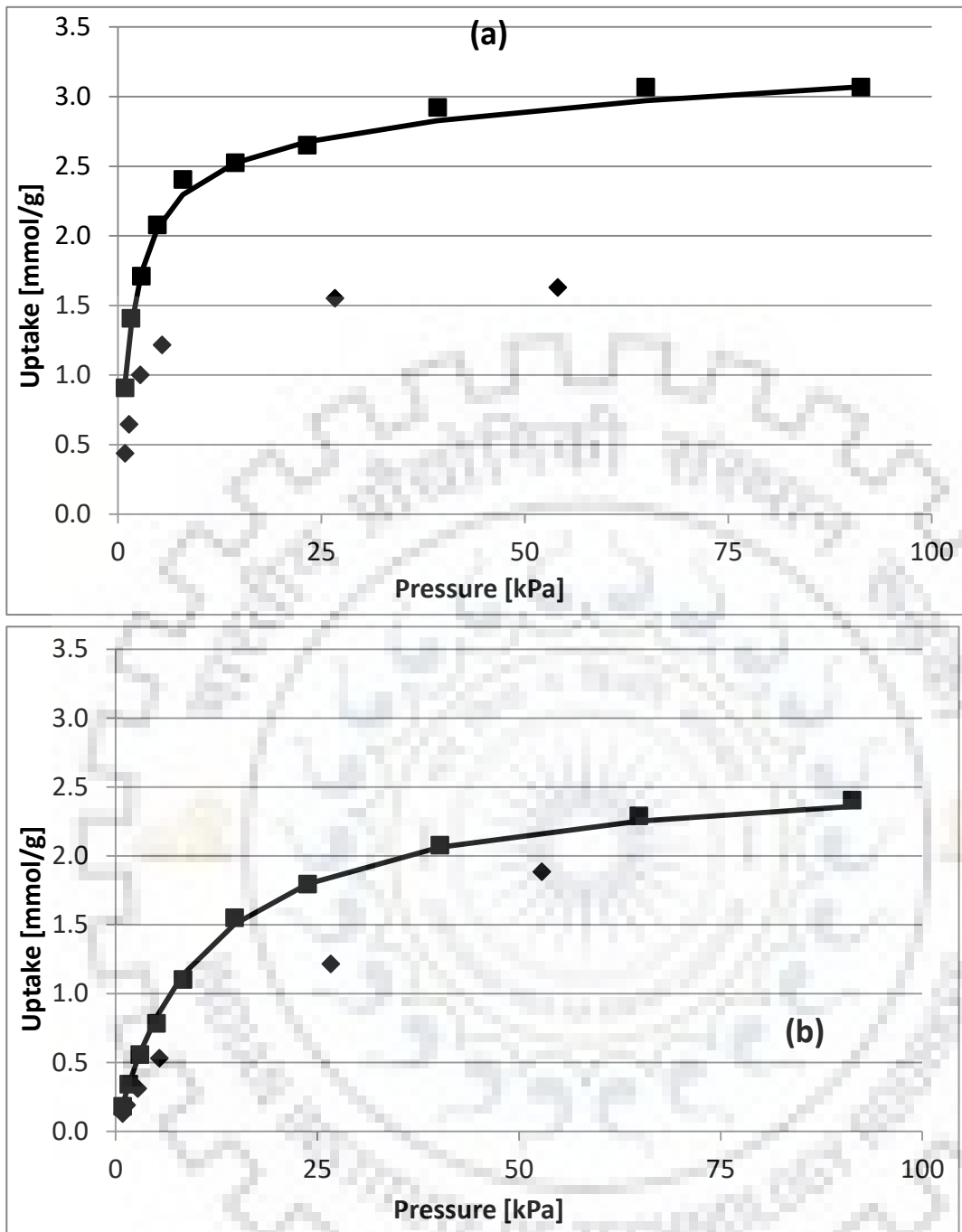


Figure 3.17 Propylene Uptake from Equimolar Propylene Propane Mixture at (a) 358 K and (b) 404 on Zeolite 13X (♦ : Expt. Data, ■: IAST Prediction by Miltenberg Et al., 2008, Solid lines: IAST Prediction in Conjunction with DSL)

Some deviation between the experimental binary uptake data and the IAST prediction is observed in results reported by Miltenberg et al., 2008 (van Miltenburg et al., 2008) probably due to inadequacy of the IAST solver or inaccuracy of the input parameters used by Miltenberget al.. The similarity in the trend of the data has been observed by the authors (van Miltenburg et al., 2008) but they have not given any specific justification for this mismatch in

Chapter-3

the numerical values. The binary uptake data predicted by our solver matches the corresponding prediction reported by Miltenberg et al. (van Miltenburg et al., 2008). The binary propylene to propane selectivity data (van Miltenburg et al., 2008) reported on Zeolite 13 X is compared with our IAST prediction at 318, 358 and 408 K up to 100 kPa in **Figure 3.17**. The trend of selectivity values predicted by Miltenberg Et al. (van Miltenburg et al., 2008) matches reasonably well with the binary selectivity predicted in this thesis . The difference in the numerical values may be due the fact these selectivity values are simply the ratio of uptakes of propylene and propane in the binary mixture (**Figure 3.18**) and there is a mismatch in the binary equilibrium values.

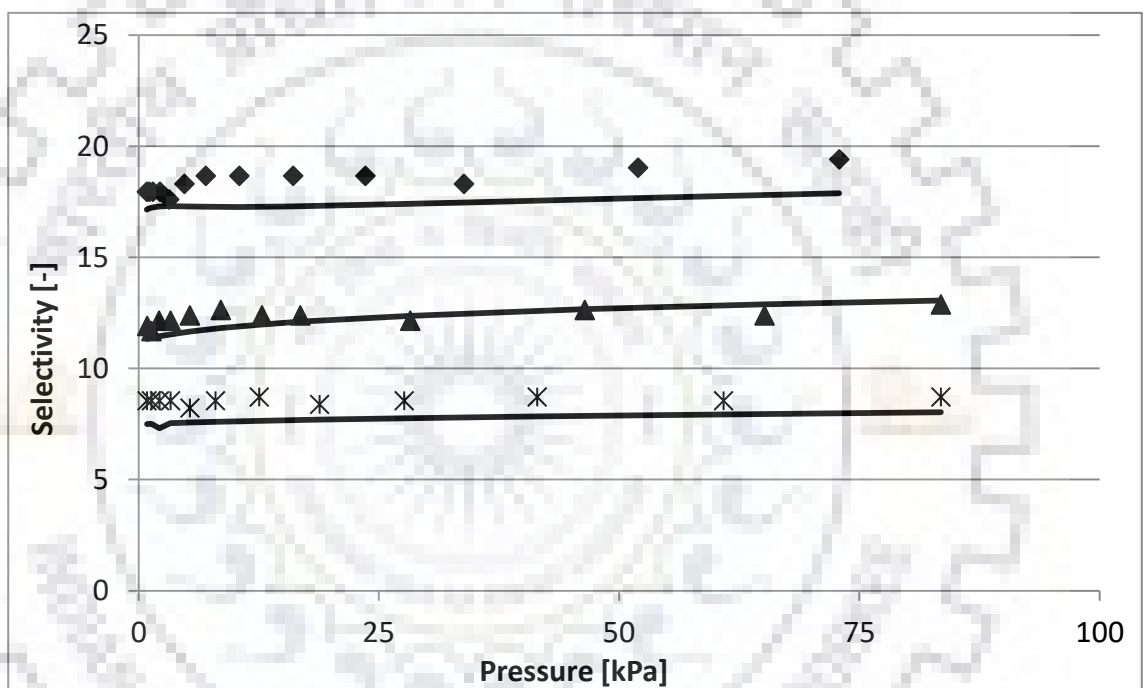


Figure 3. 18 Comparison of Selectivity Predicted by Miltenberg et al., 2008 and IAST Predicted Selectivity in conjunction with DSL model (♦: 318 K, ▲: 358 K, ×: 404 K, Solid lines: IAST prediction with DSL)

It is evident that the IAST solver and the algorithm employed here can closely predict the literature reported experimental binary isotherm data in terms of adsorbed phase mol fraction, uptake of individual components and binary selectivity.

3.8.2 Prediction of Binary adsorption data-based experimental single component data by IAST model

IAST selectivity of propylene over propane for two feed compositions up to 500 kPa total pressure was predicted using the validated IAST solver. This was done to test the applicability

Chapter-3

of these adsorbents for a PSA process to separate the propylene-propane mixture and predict favourable operating conditions. The first composition (**Feed-1**) consisting of equimolar propylene/propane mixture represents steam cracker off-gas and a second composition (**Feed-2**) used for selectivity prediction was 85% propylene and balance propane representing FCC off-gas. Similarly, the binary adsorption equilibrium data of Nitrogen and Propylene was predicted at two different feed composition, i.e., feed containing 10 and 20 mol% propylene in nitrogen which covers the typical composition of polypropylene reactor purge gas

The IAST binary adsorption has been predicted for compositions given in **Table 3.5**:

Table 3.5 Composition of the binary mixture for IAST predictions

	Composition (mol%)	Source
Feed-1	Propylene: 50 + Propane: 50	Steam cracker off gas
Feed-2	Propylene: 85 + Propane: 15	FCC off gas
Feed-3	Propylene: 20 + Nitrogen: 80	Polymerization Unit off gas
Feed-4	Propylene: 30 + Nitrogen: 70	Polymerization Unit off gas

3.8.2.1 IAST simulation results for Z10-04

The equilibrium adsorption amounts for Z10-04 predicted for **Feed-1** and **Feed-2** at different temperatures are given in **Figure 3.19**.

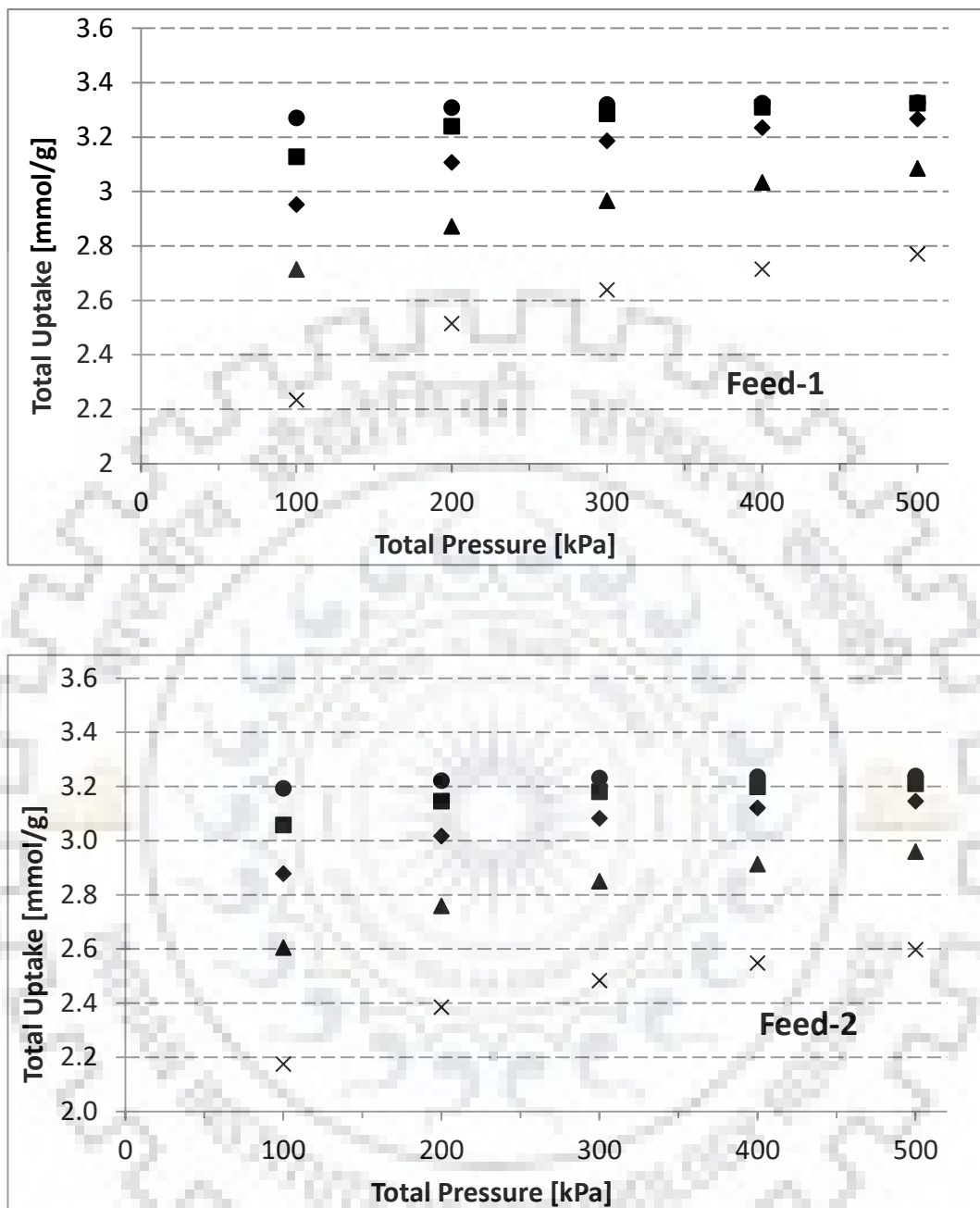


Figure 3. 19 Binary Equilibrium Uptake predicted by IAST for Z10-04 for Feed-1 and Feed-2 (●: 298 K, ■: 323 K, ◆: 343 K, ▲: 373 K, ×: 423 K)

For Z10-04, at low temperature, the binary equilibrium adsorbed amount does not change much with pressure. While at high temperature, the variation in uptake amount is significant with pressure. The observation can be attributed to the steep nature of single component isotherm of propane and propylene (**Figure 3.6**) at low temperatures, where the “knee” in isotherms are achieved at very low pressure.

Chapter-3

Very high propylene to propane selectivity is observed in simulated IAST results presented in **Figure 3.20**. The highest selectivity value of 26.9 is obtained with IAST for Feed-1 at 500 kPa and 298 K, whereas the corresponding value for Feed-2 is 28.6. However, there is not much difference in selectivity values at a given temperature and pressure for Feed-1 and Feed-2. It may be concluded here that for Z10-04 based PSA/VSA good separation can be achieved at a lower temperature and higher pressure.



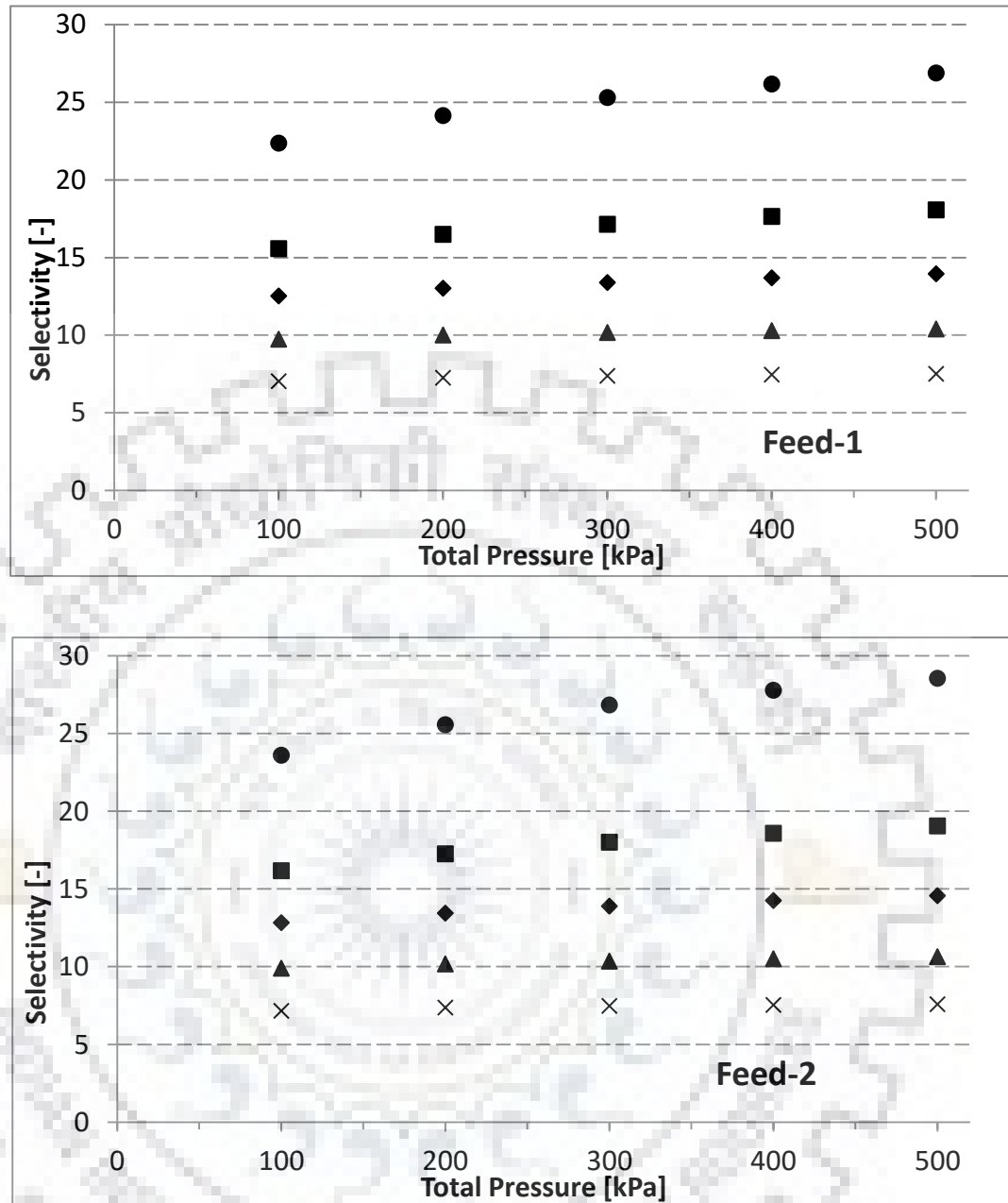


Figure 3.20 Predicted IAST selectivity of propylene over propane predicted for Z10-04 for Feed-1 and Feed-2 (Symbol Description- ●: 298 K, ■: 323 K, ◆: 343 K, ▲: 373 K, ×: 423 K)

Da Silva and Rodrigues (Da Silva and Rodrigues, 1999) studied the equilibrium and kinetics of propane and propylene adsorption on Zeolite 13X (CECA) between 373 K and 473 K. This temperature range was chosen to minimize the problems arising due to irreversibility of equilibrium isotherms, the steepness of the adsorption equilibrium isotherm and mass transfer resistance at lower temperature for Zeolite 13 X (CECA). No irreversible adsorption was observed in the case of propylene or propane in our study with Z10-04. Therefore a PSA or VSA process for propylene propane separation may also be operated at a lower temperature

Chapter-3

with Z10-04. However, the ultimate selection of process conditions is to be based on the conditions of feed, product purity desired, process productivity, etc.

The IAST binary adsorption prediction for propylene-nitrogen mixtures containing 20% (**Feed-3**) and 30 mol% (**Feed-4**) propylene in nitrogen on Zeolite 13 X (Z10-04) are presented below in **Figure 3.21** and **3.22** respectively

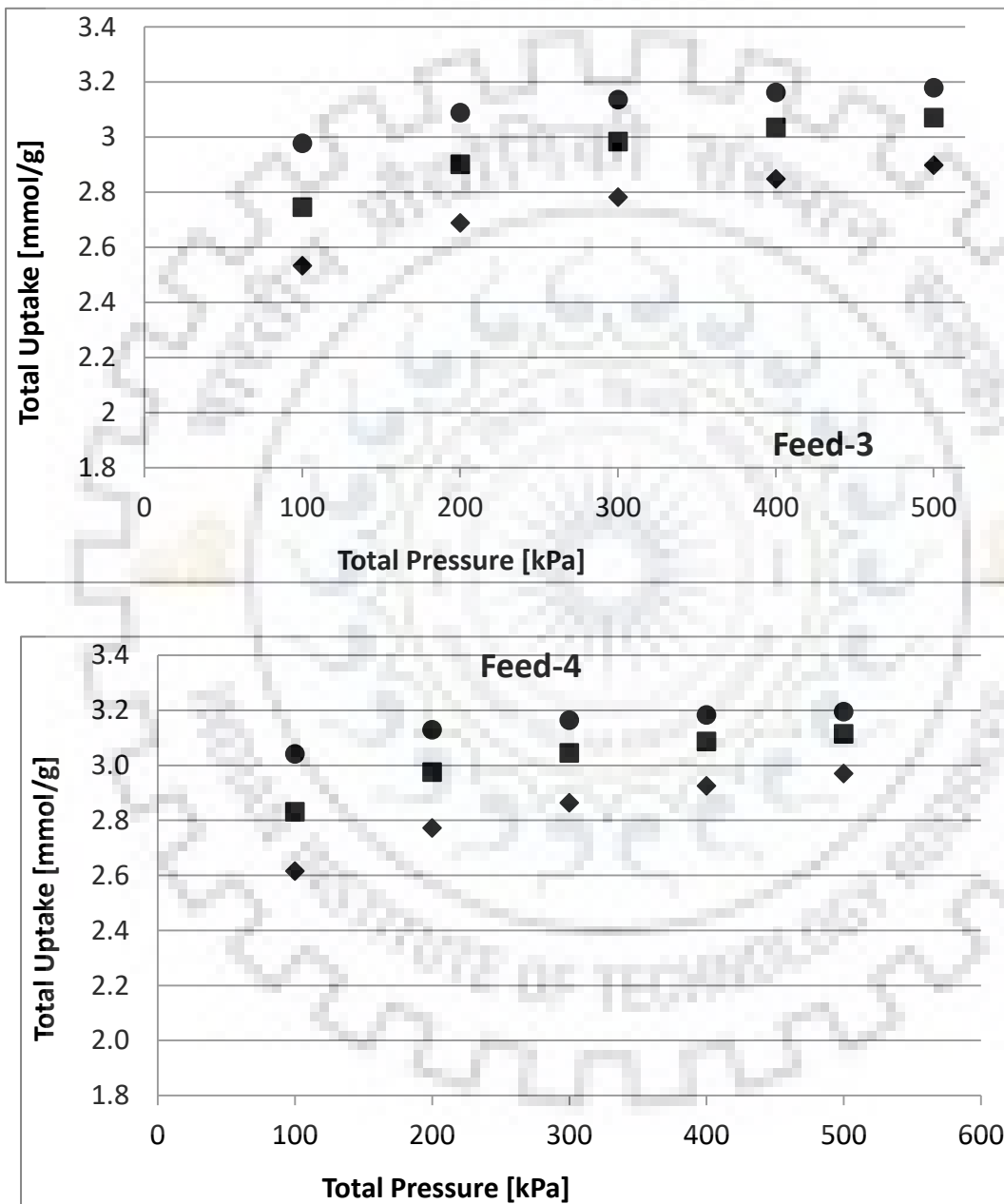


Figure 3.21 Predicted IAST Binary uptake of propylene over nitrogen predicted for Z10-04 for Feed-3 and Feed-4 (Symbol Description- ●: 303, ■: 323 K, ◆: 343 K,)

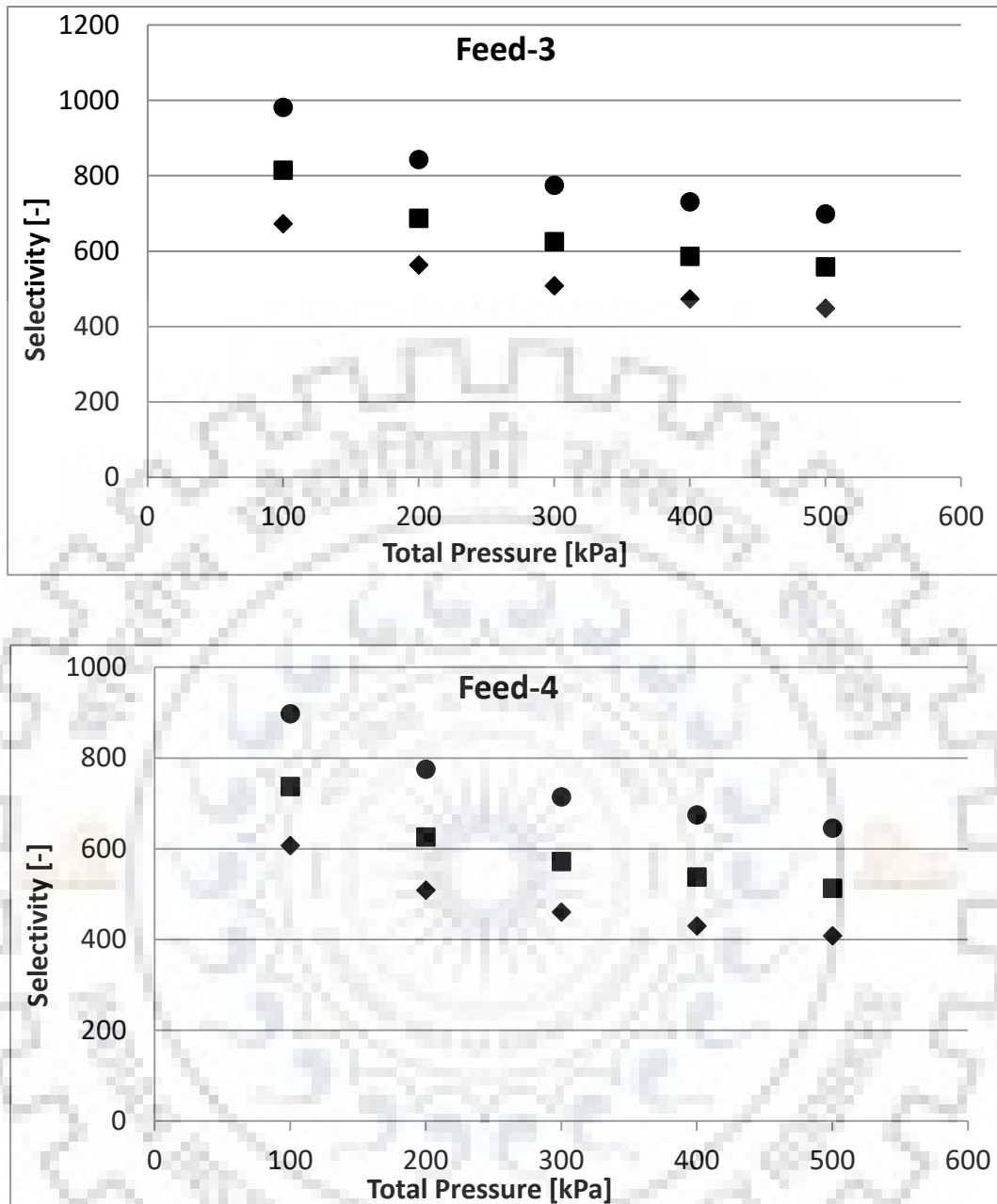


Figure 3.22 Predicted IAST selectivity of propylene over nitrogen predicted for Z10-04 for Feed-3 and Feed-4 (Symbol Description- ●: 303, ■: 323 K, ◆: 343 K,)

Similar to the propylene-propane binary mixtures, the binary adsorption uptake increases with pressure. On the contrary, the propylene- nitrogen adsorption selectivity of adsorbent decreases with pressure. This observation is attributed to the shape of pure component isotherm of propylene and nitrogen on Z10-04 (**Figure 3.6** and **Figure 3.9**). The propylene uptake is practically constant after 100 kPa pressure; however, the nitrogen uptake is increasing continuously in the pressure range studied. Therefore the ratio of equilibrium (equilibrium selectivity) decreases with pressure.

3.8.2.2 IAST simulation results for zeolite 5A (UOP)

The IAST results for Zeolite 5A (UOP) are given in **Figure 3.23** and **Figure 3.24**. There is no significant difference in the total adsorption amount predicted with IAST (**Figure 3.23**). It is worth noticing in **Table 3.4** that in the case of Zeolite 5A, the heat of adsorption obtained by fitting the isotherm data to the DSL model of propane is higher than propylene. It is also noticeable that the monolayer adsorption capacity q_0 is comparable for propane and propylene.

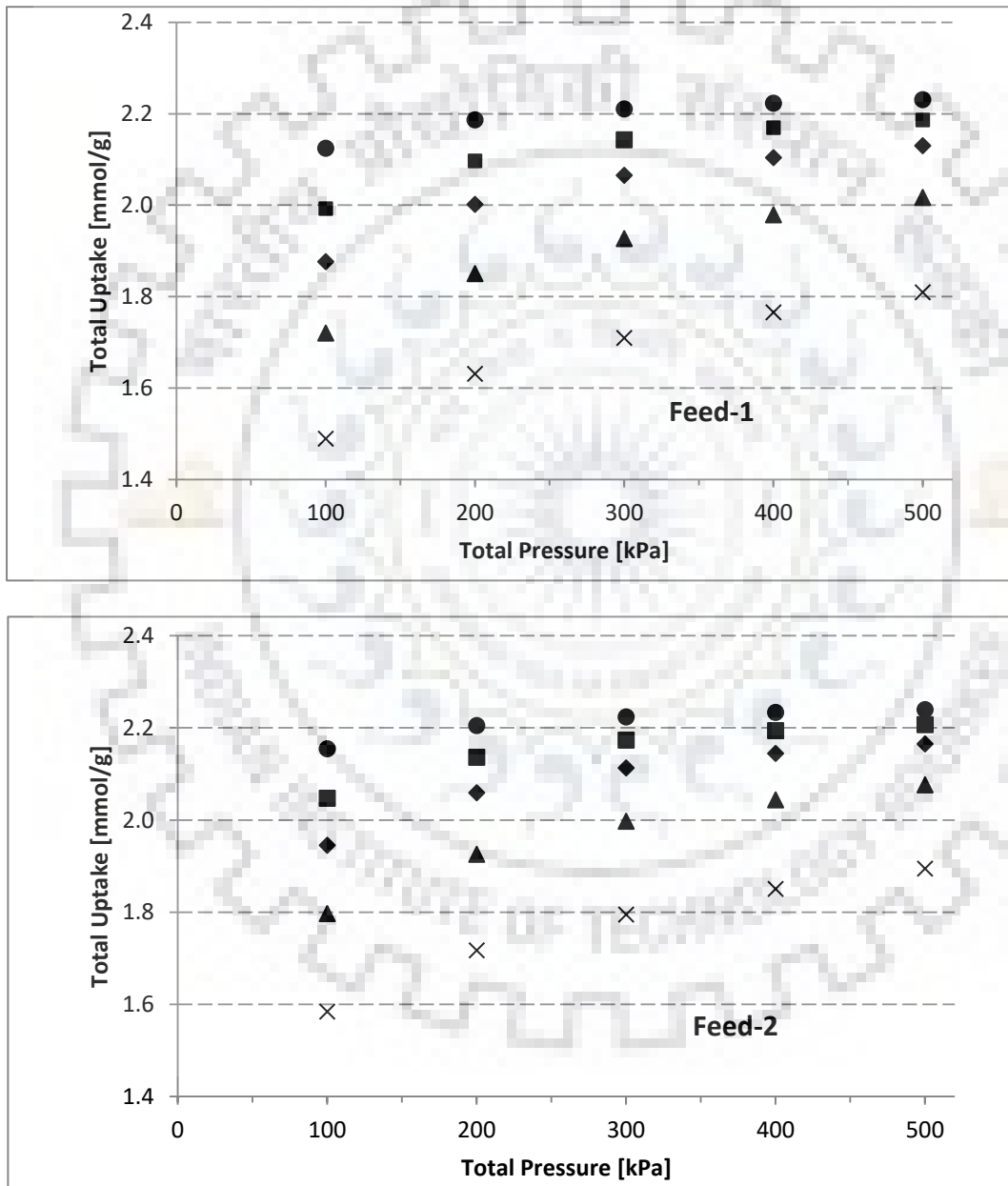


Figure 3.23 Binary Equilibrium Uptake predicted by IAST for Zeolite 5A (UOP) for Feed-1 and Feed-2 (Symbols- ●: 298 K, ■: 323 K, ◆: 343 K, ▲: 373 K, ×: 423 K)

Chapter-3

The higher heat of adsorption for propane indicates stronger binding of propane. A reverse trend in the IAST predicted selectivity for Zeolite 5A as compared to Z10-04 is observed concerning temperature and pressure, as given in **Figure 3.24**.

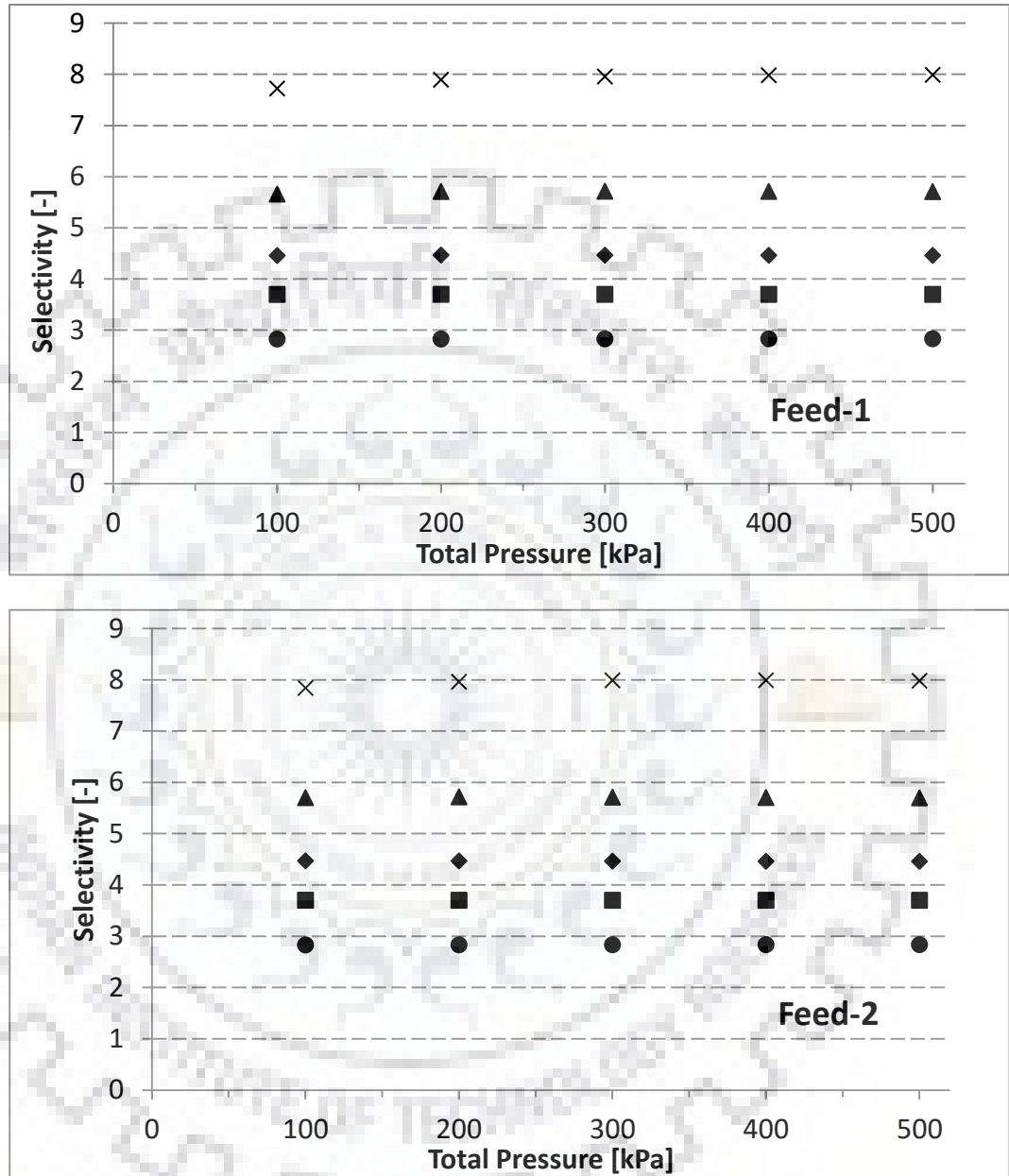


Figure 3.24 Predicted IAST selectivity of propylene over propane predicted for Zeolite 5A for Feed-1 and Feed-2 (●: 298 K, ■: 323 K, ◆: 343 K, ▲: 373 K, ×: 423 K)

In contrast to Z10-04, the IAST predicted selectivity for zeolite 5A at any given total pressure increases with temperature. With the increase in temperature, the equilibrium uptake of both propylene and propane decreases; however, the extent of decreases in propylene uptake is relatively lower than propane. Hence higher selectivity at high temperatures is observed.

Chapter-3

The average heats of adsorption for propylene and propane are 30 and 40 kJ/mol in case of Zeolite 5A. However, the heat of adsorption of propylene and propane on zeolite 13X are 45 and 35 kJ/mol. Grande et al. (2002)(Grande et al., 2002) have studied the adsorption of propane and propylene on Zeolite 5A in the crystal as well as pellet (Grace Davison) form. They fitted the adsorption equilibrium isotherm data to Toth isotherm model, and a similar trend of higher heat of adsorption of propane has been observed. Mofarahi et al. (2005)(Mofarahi et al., 2005) have also reported a higher heat of adsorption for propane over propylene fitting the isotherm data to GM isotherm model(von Gemmingen, 1993). It can also be inferred from **Figure 3.24** that the IAST selectivity of Zeolite 5A is almost independent of bulk phase concentration (**Feed-1** or **Feed-2**) and pressure under the temperature ranges studied.

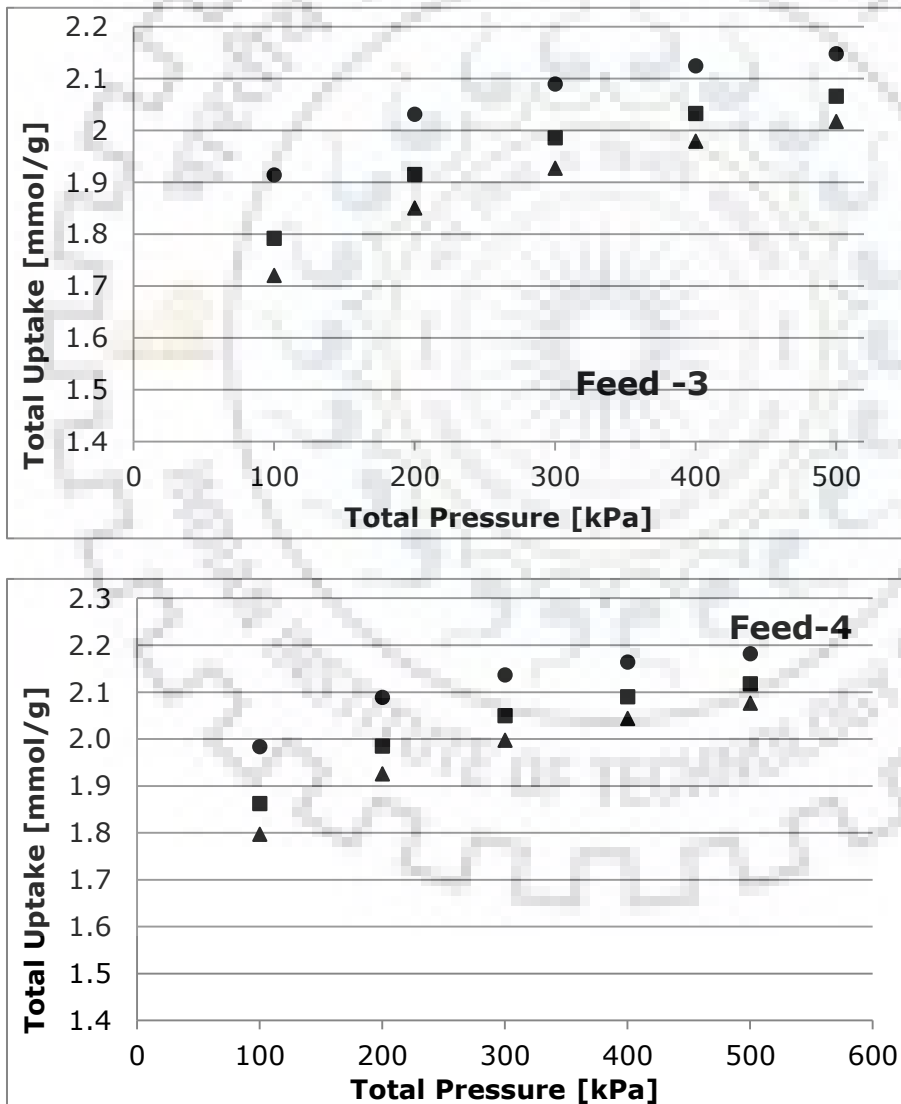


Figure 3. 25 Predicted IAST Binary uptake of propylene over nitrogen predicted for Zeolite 5A for Feed-3 and Feed-4 (●: 303, ■: 323 K, ▲: 343 K)

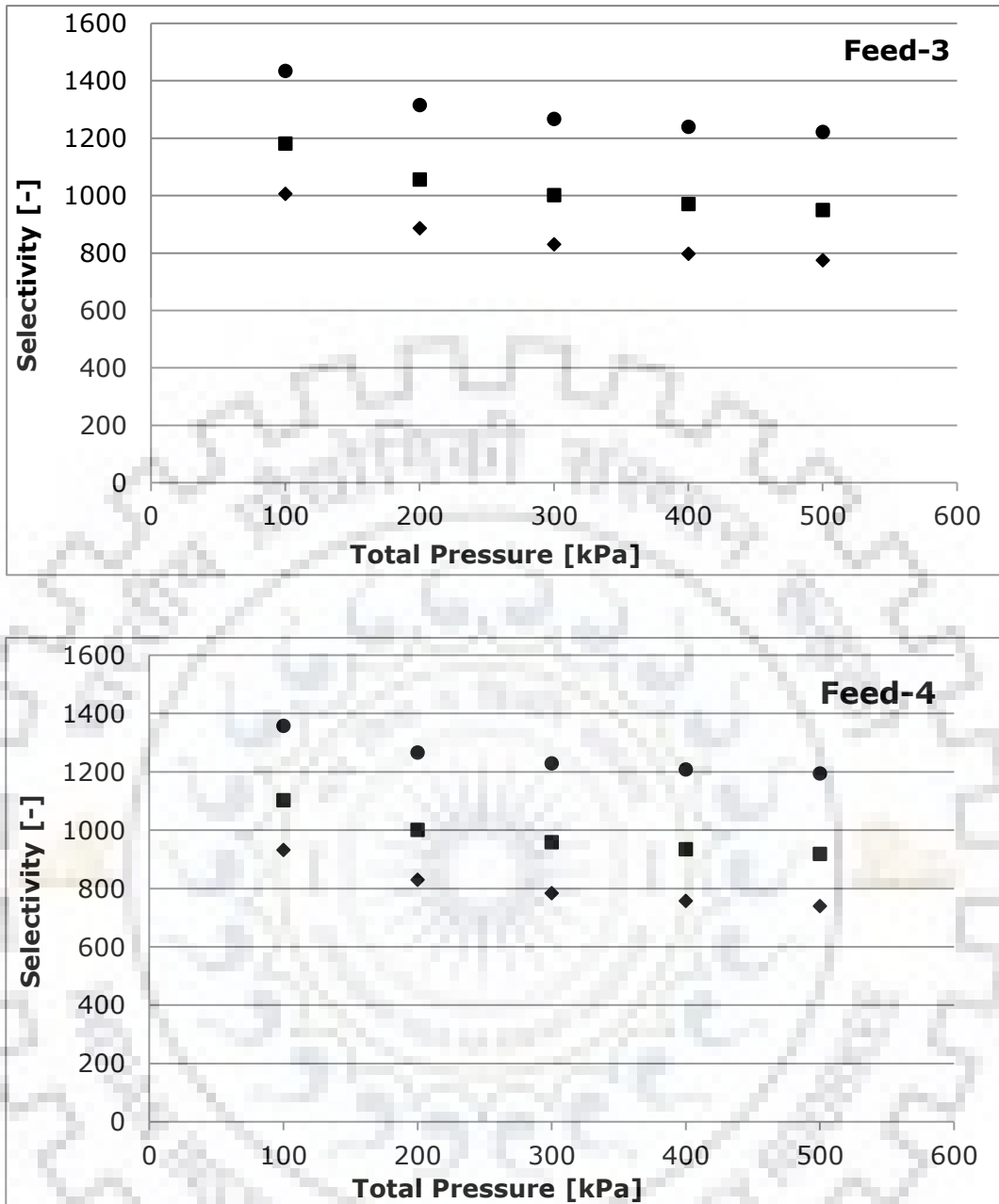


Figure 3. 26 Predicted IAST Binary Selectivity of propylene over nitrogen predicted for Zeolite 5A for Feed-3 and Feed-4 (Symbol Description- ●: 303, ■: 323 K, ▲: 343 K,)

The IAST results for Zeolite 5A exhibit the same trends as that of Zeolite due to the similarity of the shape of isotherms of both propylene and nitrogen in these adsorbents.

3.8.2.3 IAST Simulation Results for Na-ETS-10 (Lab synthesized)

In the case of laboratory synthesized Na-ETS-10, the equilibrium binary uptake is found to be lower as compared to corresponding Z10-04 and Zeolite 5A data (Figure 3.27). In the case of laboratory synthesized Na-ETS-10 adsorbent, the heat of adsorption of propane is comparable to that of propylene.

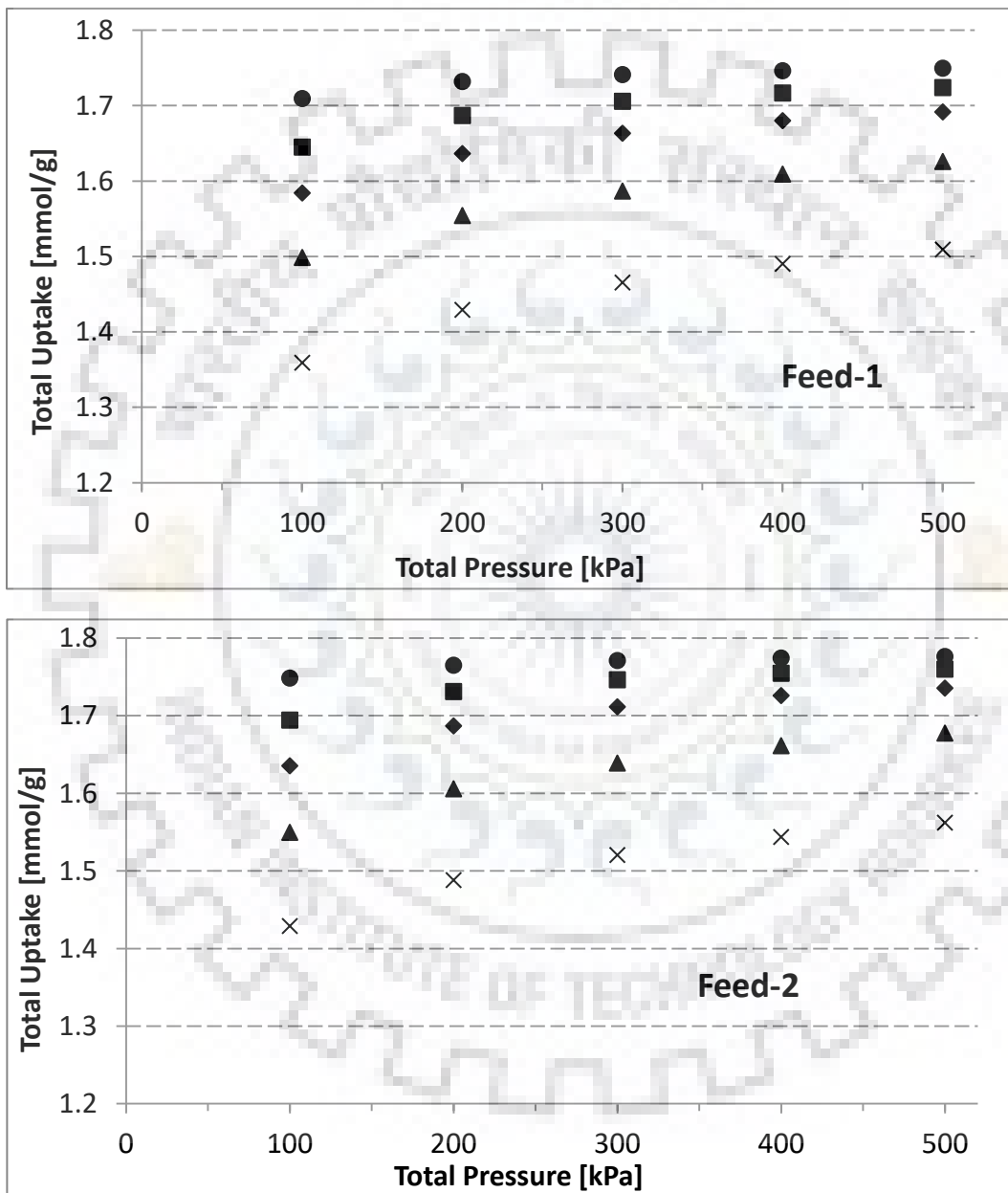


Figure 3.27 Binary Equilibrium Uptake predicted by IAST for Na-ETS-10 for Feed-1 and Feed-2 (Symbols- ●: 298 K, ■: 323 K, ◆: 343 K, ▲: 373 K, ×: 423 K)

IAST theory predicts a selectivity trend similar to Zeolite Z10-04 for Na-ETS-10 (Figure 3.28), where the selectivity at a lower temperature is higher for a given pressure. However, in

Chapter-3

contrast to Zeolite 5A, the selectivity values increase with pressure for a given temperature. It may be because the isotherm parameter q_0 for propylene and propane are comparable in the case of Zeolite 5A whereas in the case of Na-ETS-10 the q_0 for propylene is higher than for propane.

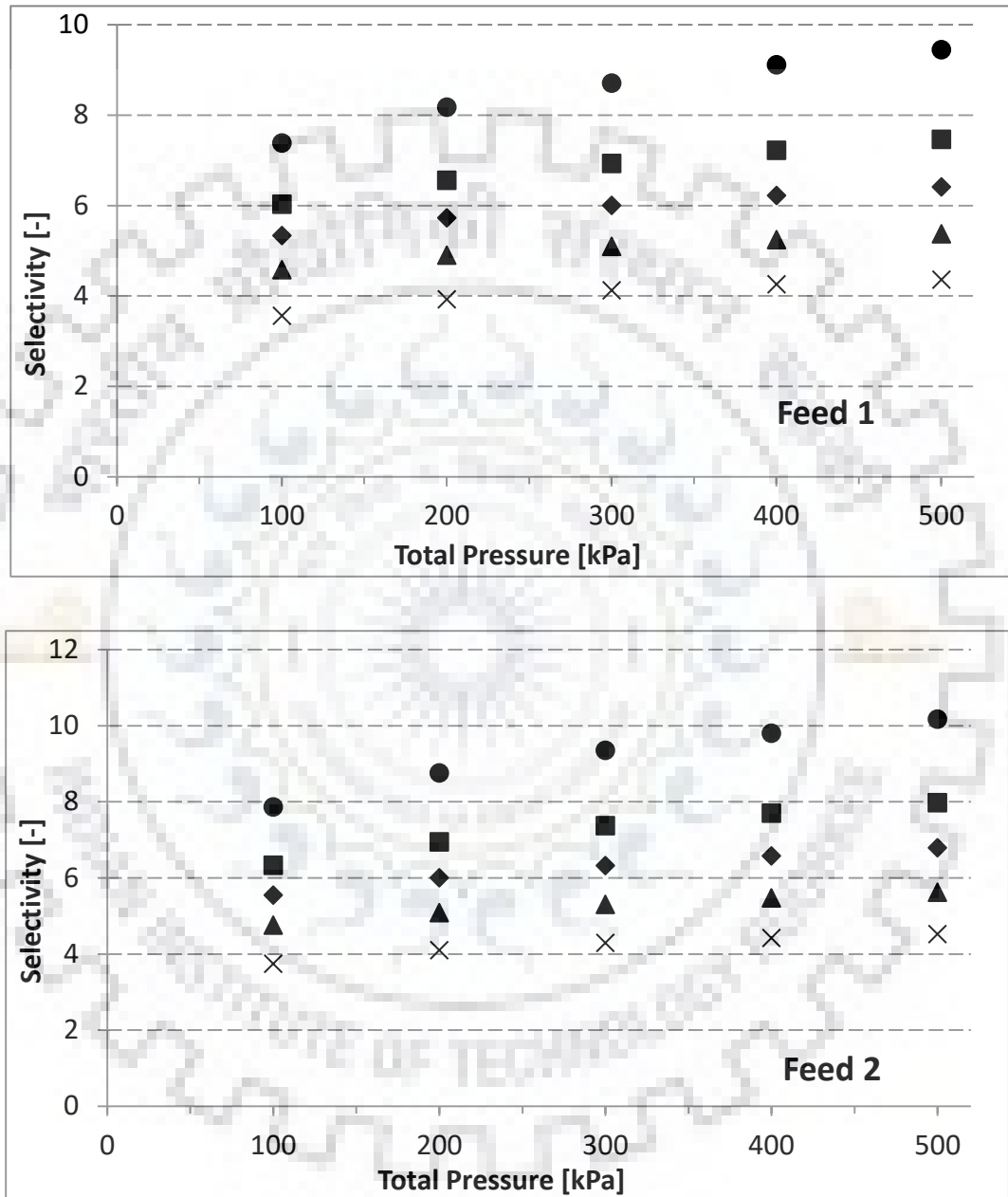


Figure 3.28 Predicted IAST selectivity of propylene over propane predicted for Na-ETS-10 for Feed-1 and Feed-2 (Symbol Description- ●: 298 K, ■: 323 K, ◆: 343 K, ▲: 373 K, ×: 423 K)

Annexure-A: Properties of propylene

3.9 CONCLUSION

Three adsorbents, including laboratory-synthesized adsorbent Na-ETS-10, and Commercial adsorbents, namely zeolite 13X (Z10-04), zeolite 5A (UOP) were tested for their applicability for selective propylene adsorption from propylene containing streams (propylene-propane and propylene-nitrogen mixture). The screening was conducted by equilibrium adsorption isotherm, and binary adsorption predicted based on the IAST theory.

In the case of laboratory synthesized adsorbents Na-ETS-10, the results obtained over different batches of adsorbent was not consistent and reproducible. During initial attempts, the adsorbent was co-formed with impurities of the Quartz phase. The synthesis procedure was modified by different synthesis procedures reported in the literature and ultimately, the synthesis procedure optimized to get consistent pure Na-ETS-10 phase formation. It was however felt that further scale-up of this adsorbent for adsorptive process development might itself take significant time.

Among the commercial adsorbents, Zeolite 13 X showed the highest capacity for propylene adsorption and also the propylene-propane and propylene-nitrogen selectivity calculated on the basis IAST. Further experiments for an adsorptive process for recovery of propylene from propylene bearing streams have been carried only with Zeolite 13 X (Z10-04, Zeochem).

CHAPTER-4 PROPYLENE SEPARATION BY PRESSURE SWING ADSORPTION

After thorough screening, a commercial Zeolite 13X, Z10-04 (Zeochem, USA) was selected for adsorptive separation of propylene from propylene bearing mixtures, by experimental single component equilibrium adsorption measurements and binary adsorption predictions based on IAST. The adsorption of propylene on various adsorbents studied is characterized by very high heat of adsorption (**Table 3.4, Chapter 3**). The heat of adsorption is the energy released by the adsorbate when it gets attached to the adsorbents surface. Heat release is preceded by the adsorption of the gas-phase on the surface to form a more orderly, quasi-liquid adsorbed phase with low energy. The high heat of adsorption is also indicative of strong interactions between adsorbed propylene molecule and the surface of the adsorbents.

4.1 DESCRIPTION OF EXPERIMENTAL SETUP AND EXPERIMENTAL PROCEDURE

4.1.1 Single Column Pressure/ Vacuum Swing Adsorption (PVSA) Microadsorber Unit

A Single Column Pressure/ Vacuum Swing Adsorption (PVSA) micro-adsorber unit (Dasgupta et al., 2015; Hanif et al., 2014) was used for dynamic experimental adsorption breakthrough curve measurements. The unit was modified to handle flammable gases under the relevant temperature and pressure conditions.

The photographic view and schematic diagram of the micro-adsorber unit are given respectively in **Figure 4.1** and **Figure 4.2** respectively:



Figure 4.1 — Photograph of the single column Pressure/ Vacuum Swing Adsorption (PVSA) micro-adsorber unit

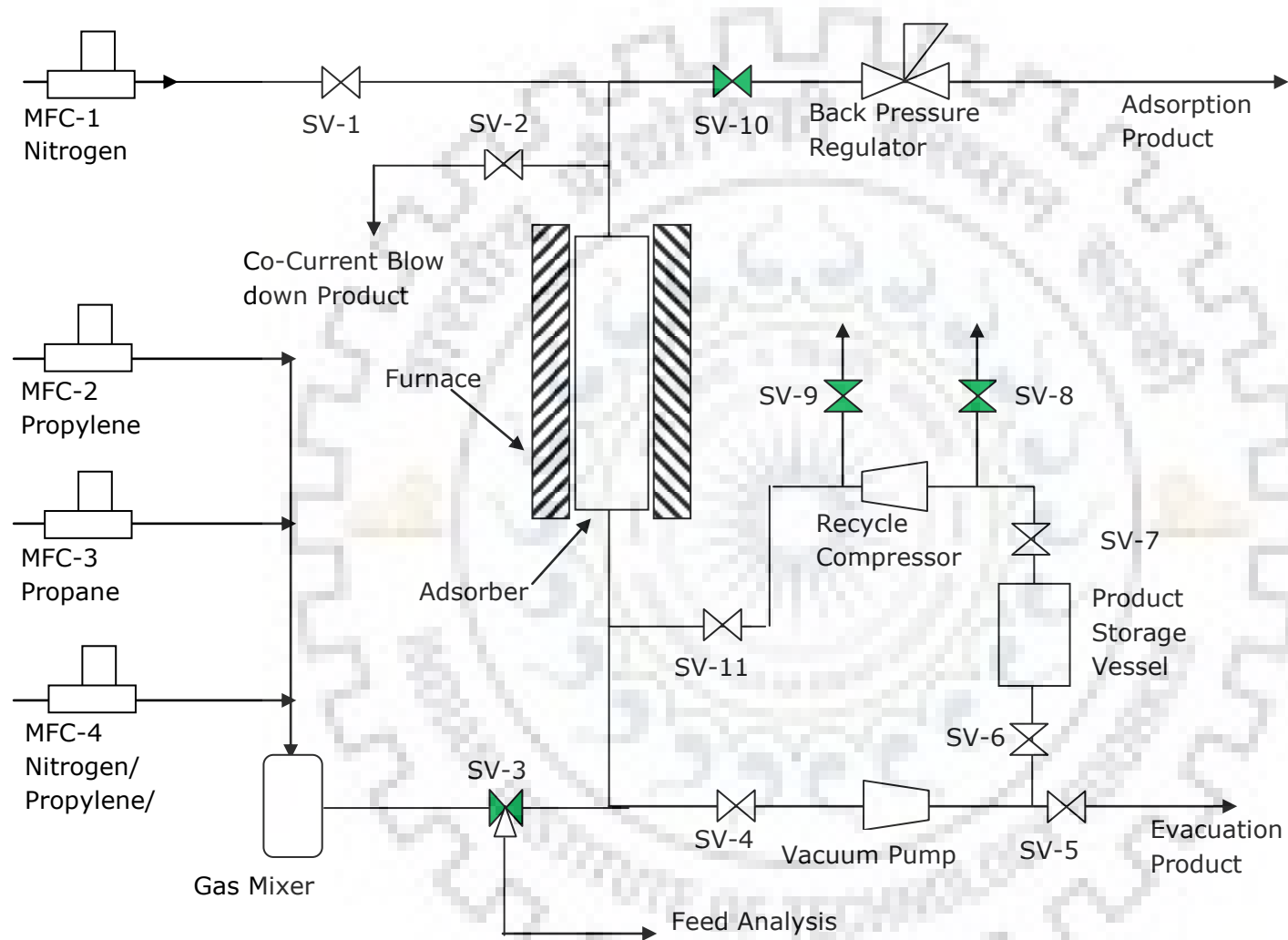


Figure 4.2 The schematic of the single column pressure/ vacuum swing adsorption (PVSA) micro-adsorber unit

Chapter-4

This micro-adsorber unit is a fully automated SCADA based single column PVSA unit. The unit consists of a SS 303 adsorber column with 11 mm internal diameter and 300 mm total height. The pressure rating of the adsorber column is 2000 kPa. The adsorber is placed inside a tubular furnace. The furnace controls the adsorber temperature at the desired set point. The feed mixtures of desired composition (propylene-propane & propylene-nitrogen) were simulated by setting the outputs of respective thermal mass flow controllers (Make: Brooks, Germany) at desired flow rates according to the total feed flow. The adsorbent bed was activated in-situ at 423 K under continuous flow of nitrogen ($0.1 \text{ dm}^3/\text{min}$) and dynamic vacuum ($<8 \text{ mbar}$).

A manual backpressure regulator (Make: Tescom, Germany) controls the downstream adsorber pressure during the adsorption step. The unit is equipped in multiple pneumatically actuated solenoid valves (SV), which allow gas the flow through them in ON position. The unit is also equipped with a flame-proof vacuum pump and a recycle compressor. The mass flow controllers for propane and propylene (full range: $0 - 0.5 \text{ dm}^3/\text{min}$) are used for preparing feed mixtures of the desired composition. A variation in the range of 1-2% in the composition of the feed streams was observed during the experimental runs. For higher variations, the set points of mass flow controllers were adjusted accordingly. During different steps of a PSA cycle, these SVs are switched 'ON' and 'OFF' as per predefined sequence called "Recipe." The recipe of the PVSA cycle studied is described later in this chapter (**Table 4.3**).

4.1.2 Analysis of gas streams

The real-time composition analysis of the simulated feed gas and the product streams of the PVSA process was performed by a quadrupole-based mass spectrometer model QGA (Qualitative gas analyser) procured from M/s Hiden Analytical, UK. The QGA analyser can detect and measure any gas up to 200 amu (Atomic mass unit) with a minimum detectable concentration limit of 100 ppb. Its response time to gas composition variation is 300 ms.

The analyser works on the principle of mass spectroscopy (Hoffmann and Stroobant, 2007). The mass spectrometer fragments the gas molecule under investigation into multiple positively charged ions by electron ionisation. These ions are separated in spectrometer according to their mass to charge ratio or m/z . Here 'm' stands for mass, and 'z' stands for charge number of ions. Each gas molecule has its characteristic mass spectra having multiple peaks at different (m/z) values. The characteristic peaks are used for the qualitative and quantitative determination of gaseous species in a gas mixture. The QGA was calibrated against pure and calibrated gas

Chapter-4

mixtures of appropriate gas under investigation. **Figure 4.3** displays a photograph of GQA mass spectrometer.

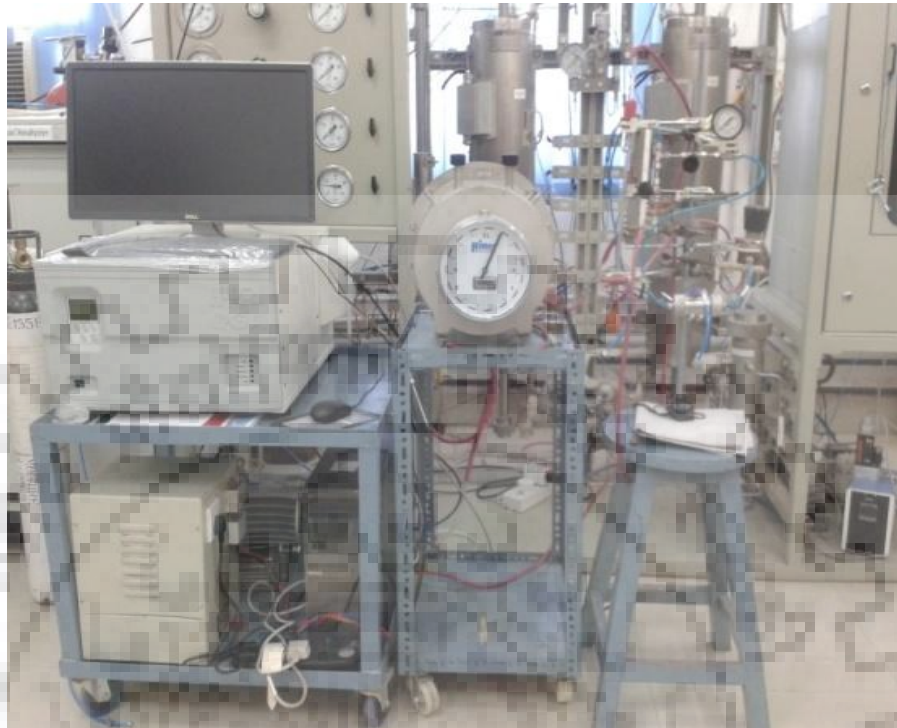


Figure 4.3 The photograph of the GQA mass spectrometer

4.1.3 Breakthrough (BT) experiments

The dynamic breakthrough studies under relevant process conditions for different feed mixtures over an adsorbent are essential for designing a PVSA cycle. 13g of Zeolite 13X was loaded in the adsorber up to a height of 90 mm. The adsorbent was activated *in-situ* at 623 K under nitrogen flow and vacuum to desorb any impurity. The column was evacuated to <10 kPa pressure to conduct breakthrough experiments. After a breakthrough experiment, the adsorber column was regenerated under nitrogen purge and vacuum till no propylene traces were found from the analysis of the purge gas. In a typical breakthrough experiment, the binary feed was introduced in the adsorber at a constant flow rate by opening the solenoid valves SV-3 and SV-10, and the pressure was regulated at the desired level by a back pressure regulator (BPR). The exit gas composition profile measured by QGA was recorded.

The experimental breakthrough curve generation is an essential aspect of adsorptive process development. The analysis of the breakthrough curve provides an insight to the dynamic adsorption in an adsorber column. The dynamic behavior of a fixed bed column is described in terms of this curve. The shape of this curve is determined by the shape of the equilibrium

isotherm and is influenced by the individual transport processes in the adsorber column. The most effective adsorptive separation performance can be obtained when the shape of the breakthrough curve is as sharp as possible. (Ahmed et al., 2010; R. T. Yang, 1987).

The dynamic breakthrough capacity of more adsorbed components can also be calculated from the breakthrough time, i.e. the time at which the more adsorbed component starts appearing at the outlet of adsorber or in other words 'breaks through' the adsorber. The breakthrough time reported in this thesis correspond to propylene content of 0.1% in the In this case, the breakthrough capacity is the amount of propylene adsorbed per unit weight of adsorbent until the breakthrough is observed.

4.1.3.1 Breakthrough experiments with propylene-propane binary feed

Column breakthrough studies for Propane/ Propylene separation for three mixture compositions with propylene content of 12, 50 and 75 mol% with balance propane representing propane/propylene splitter bottom stream, steam cracker and fluid catalytic cracker (FCC) off-gas, respectively on Zeolite 13X (Z10-04, Zeochem) under different pressures, temperatures and different feed flow rates were carried out. The process parametric values used in the experimental work studied during the breakthrough studies are given in **Table 4.1** below:

Chapter-4

Table 4.1 Process parametric values used in the experimental breakthrough studies with propylene-propane binary feed using Z10-04 adsorbent

Sl. No.	Parameter	Values
1.	Temperature, K	303, 323, 348, 373, 423
2.	Pressure, kPa _{abs}	200, 300, 400, 500
3.	Feed Flow rate, $\times \text{dm}^3/\text{min} (\times 10^3)$	200, 400, 600

4.1.3.2 Breakthrough experiments with propylene-nitrogen binary feed

Column breakthrough studies for propylene/ nitrogen separation from binary mixtures were carried out with a propylene mol% of 10, 20 and 30 and with balance nitrogen under different pressures, temperatures and different feed flow rate. These mixtures represent the polypropylene reactor purge gas. The process parameters studied during the PVSA studies are given in **Table 4.2** below:

Table 4.2 Process parametric values used in the experimental breakthrough studies with propylene-nitrogen binary feed using Z10-04 adsorbent

Sl. No.	Parameter	Values
1.	Temperature, K	303, 323, 348, 373
2.	Adsorption Pressure, kPa _{abs}	200, 300, 400, 500
3.	Evacuation pressure, kPa	10
4.	Feed Flow rate, $\text{dm}^3/\text{min} (\times 10^3)$	200, 400

One variable was changed at a time to understand the effect of individual parameters on process performance.

4.1.4 PVSA experimental studies

Most of the earlier PSA/PVSA based studies for separation of propylene and propane have employed steps such as pressurization with feed, high pressure adsorption, co-current depressurization (to intermediate pressure), purge with part of high purity propylene product, countercurrent blowdown, evacuation of column etc. (Da Silva and Rodrigues, 2001a; Grande et al., 2003a; Padin and Yang, 2000; Rege et al., 1998). A similar PVSA configuration was devised for single column micro-adsorber unit for the experimental studies in this thesis.

The PVSA cycle used in the experiments consisted of the following six steps: (i) Pressurization with Feed, (ii) High-pressure adsorption (iii) Co-current blow down (to atmospheric pressure) (iv) Co-current rinse with pure propylene (v) Evacuation (propylene product withdrawal), and (vi) Evacuation with propane/ nitrogen purge.

These steps were implemented in the micro-adsorber unit using pre-planned sequence of opening and closing of solenoid valves as per a “recipe.” The frequent closing at the opening of these valves in a particular manner at predefined intervals constitutes a PVSA “recipe.” The “recipe” of the PVSA cycle studied is given in **Table 4.3**. It may be noted that evacuation pressure was kept constant at 10 kPa, which was the lowest achievable pressure during the evacuation step. The effect of evacuation level was not studied. The six steps of the PVSA cycle are given in **Table 4.3**. Many cycles (at least 10) of this recipe were repeated in experiments up till a cyclic steady state was observed i.e. no cycle to cycle variation in the composition of different product streams was observed.

Chapter-4

Table 4.3 PVSA Recipe Studies

Sr. No.	Step Description	Solenoid Valve											Step timing (% of propylene breakthrough time)	
		SV-1	SV-2	SV-3	SV-4	SV-5	SV-6	SV-7	SV-8	SV-8	SV-9	SV-10		SV-11
1	Pressurization with Feed	OFF	OFF	ON	OFF	OFF	OFF	OFF	OFF	ON	ON	OFF	OFF	10-15
2	High-pressure adsorption	OFF	OFF	ON	OFF	OFF	OFF	OFF	OFF	ON	ON	ON	OFF	30-80
3	Co-current blow down (to atmospheric pressure)	OFF	ON	OFF	OFF	OFF	OFF	OFF	OFF	ON	ON	OFF	OFF	30 s
4	Co-current rinse with pure propylene	OFF	ON	OFF	OFF	OFF	OFF	ON	OFF	OFF	OFF	OFF	ON	20
5	Evacuation (propylene product withdrawal)	OFF	OFF	OFF	ON	ON	OFF	OFF	OFF	ON	ON	OFF	OFF	30-80
6	Evacuation with propane/nitrogen purge	ON	OFF	OFF	ON	OFF	OFF	OFF	OFF	ON	ON	OFF	OFF	10-15

- For step no. 4, pure propylene from the cylinder was used, and the amount of this propylene was subtracted from total propylene product, as in an industrial process high purity propylene product will be used in this step
- For regeneration step no. 6, the column was purged with the less adsorbed component of the feed (propane or nitrogen) fed through MFC-1. In the case of propylene/nitrogen separation, this amount of gas was subtracted from the nitrogen-rich product for productivity calculation

Table 4. 4 The PVSA steps and the respective inputs and outputs

Step	Input		Output Product
	Stream	Total Flow Set Point (dm ³ /min) (× 10 ³)	
Pressurization with Feed	Propylene + Propane/Nitrogen	200/400	
High pressure adsorption	Propylene + Propane/Nitrogen	200/400	Propane/ nitrogen Rich
Co-current blow down (to atmospheric pressure)	-		Propane/ nitrogen Rich
Co-current rinse with pure propylene	Propylene	100	Propane/ Nitrogen Rich
Evacuation (propylene product withdrawal)	-		Propylene Rich
Evacuation with propane/ nitrogen purge	Propane/ Nitrogen	200/400	Propylene Rich

4.2 RESULTS AND DISCUSSIONS

4.2.1 Binary breakthrough curve analysis

4.2.1.1 Propylene-propane binary feed

More than forty breakthrough curves were experimentally recorded to study the effect of variation of different parameters like temperature, pressure and feed flow rate as listed in **Table 4.1**. The breakthrough time obtained under a set of operating conditions forms the basis of PVSA process design to be operated under those conditions. The breakthrough time reported here correspond to a propylene content of 0.1 mol% in the adsorption product exiting the adsorbent bed during the breakthrough experiments for all feeds types. As this work is based exclusively on experimental PVSA studies only, BT time becomes most important to determine the PVSA cycle timing. Salient results of these experiments are discussed in the following paragraphs.

4.2.1.1.1 Feed containing 12 % propylene in propane

The effect of temperature on the breakthrough curve is illustrated in **Figure 4.4**.

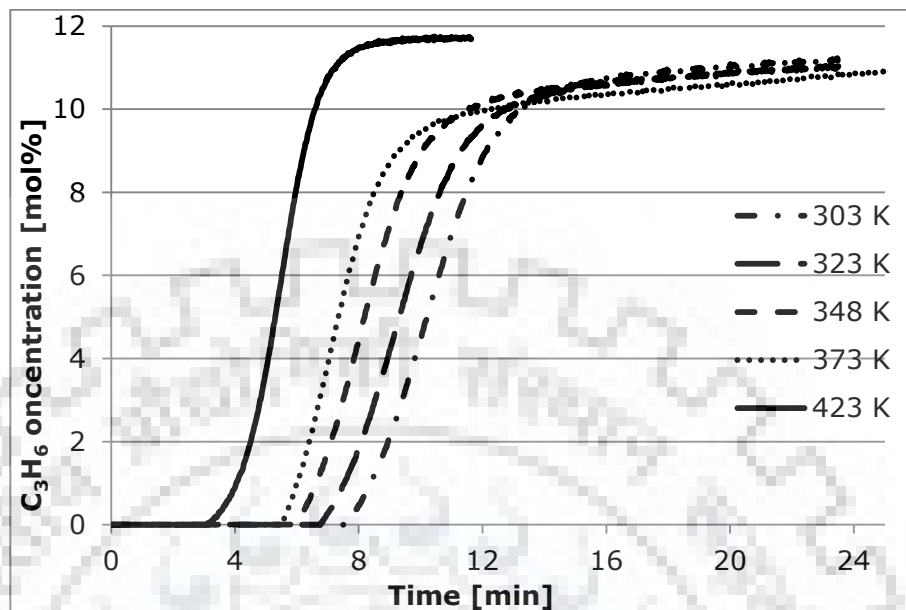


Figure 4.4 Propylene breakthrough curve with temperatures as a parameters (Pressure: 500 kPa, feed rate: $400 \times 10^{-3} \text{ dm}^3/\text{min}$, feed composition: 12 mol% propylene in propane)

The adsorption capacity of propylene is expected to decrease with an increase in temperature. Similar behavior is observed in **Figure 4.5** also.

The effect of feed composition on breakthrough time can be observed by comparing **Figure 4.4** with **Figure 4.5**, under the same operating conditions except the feed concentration, which is 50 mol% propylene in propane, in case of **Figure 4.5**. It is seen that with an increase of mole fraction of propylene in the feed, the breakthrough time decreases. This is expected as more amount of propylene is entering the adsorber column with an increase in propylene concentration (50 mol%) in the feed.

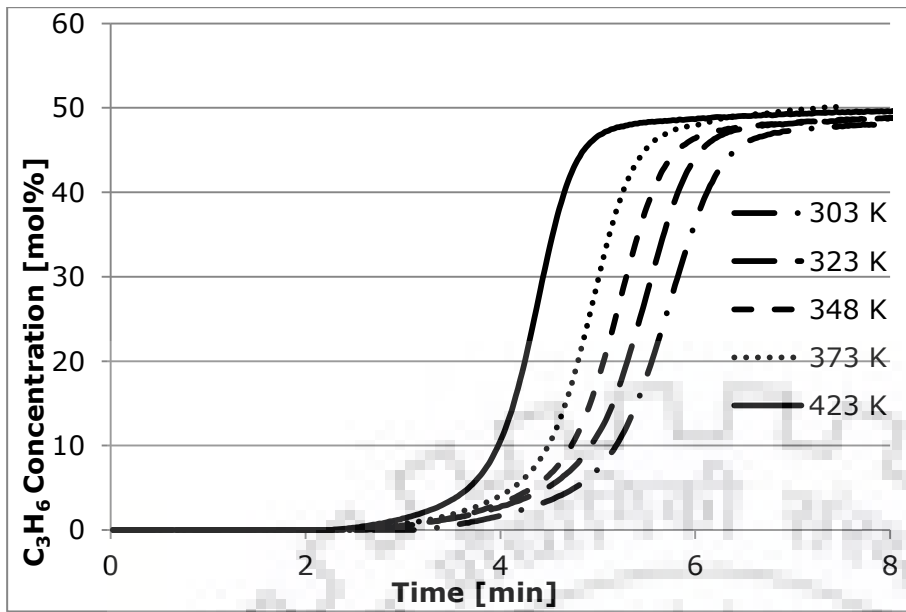


Figure 4.5 Propylene breakthrough curve with temperatures as a parameters (Pressure: 500 kPa, feed rate: $400 \times 10^{-3} \text{ dm}^3/\text{min}$, feed composition: 50 mol% propylene in propane)

The BT time and capacities of the Zeolite 13 X at different temperatures are compared in **Figure 4.6** and **Figure 4.7** respectively.

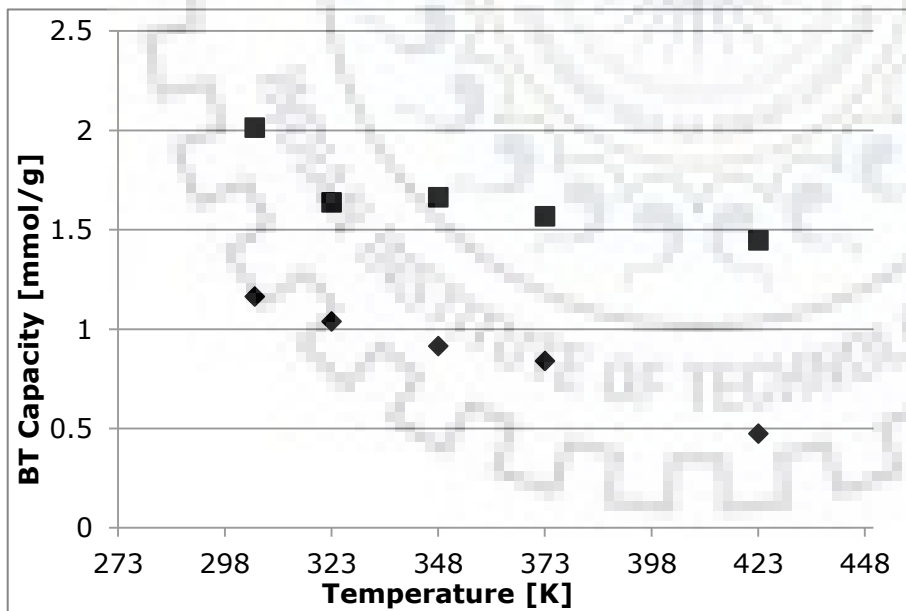


Figure 4.6 Effect of propylene concentration in feed on BT capacity at different temperatures (Pressure: 500 kPa, feed rate $400 \times 10^{-3} \text{ dm}^3/\text{min}$, \blacklozenge : 12% propylene in feed, \blacksquare : 50% propylene in feed)

Chapter-4

The BT capacities for both the feed streams decrease with an increase in temperature as expected. In an ideal breakthrough curve, the breakthrough curve is very steep, and the exit gas composition approaches the feed composition very rapidly after the breakthrough. In this case ideally, the Propylene BT capacity and equilibrium capacity should be very close to each other. The propylene equilibrium capacity at 303 K for propylene partial pressure of 60 kPa and 250 kPa (Corresponding to feeds with total pressure of 500 kPa in **Figure 4.7**) are ~3.0 and ~3.1mmol/g (**Figure 3.7**). However, the corresponding BT capacities are only 1.16 and 2.01 mmol/g. This implies that the propylene mass transfer zone is spread as indicated by BT curve with a low slope.

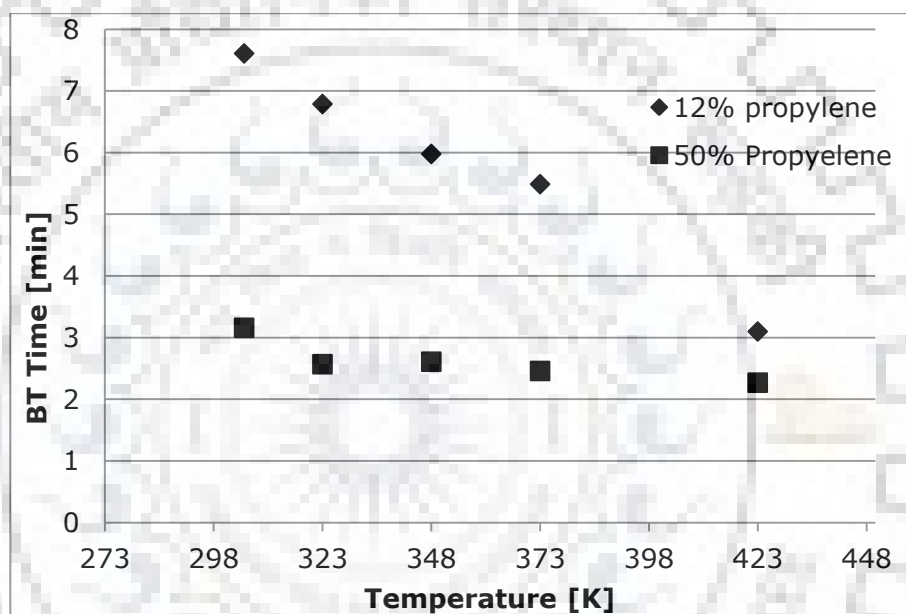


Figure 4.7 Effect of propylene concentration in feed on the BT time at different temperatures (Pressure: 500 kPa, feed rate $400 \times 10^{-3} \text{ dm}^3/\text{min}$, \blacklozenge : 12% propylene in feed, \blacksquare : 50% propylene in feed)

The effect of feed concentration on the BT time is more pronounced in the case of the feed containing 12% propylene. From the equilibrium isotherm of propylene on Zeolite 13X, it can be observed that the variation in equilibrium capacity with temperature is also more pronounced at lower propylene partial pressure. The theoretical notion that the nature of isotherm governs breakthrough behavior is found to be valid from the above analysis (R. T. Yang, 1987).

Effect of pressure on the breakthrough curves at 303 K with a total feed rate of $400 \times 10^{-3} \text{ dm}^3/\text{min}$ is shown in **Figure 4.8**.

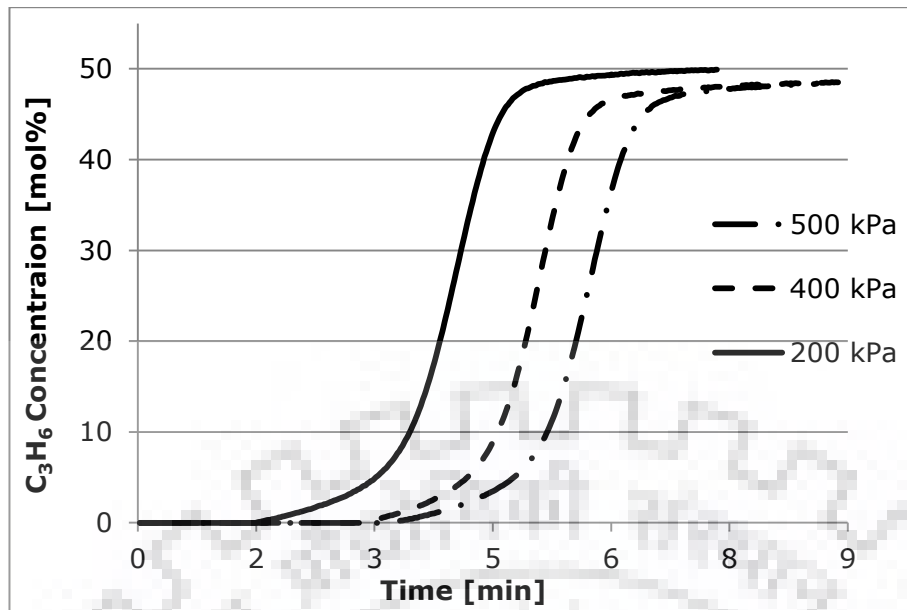


Figure 4.8 Effect of adsorption pressure on the breakthrough curves (Temperature: 303 K, Feed rate: $400 \times 10^{-3} \text{ dm}^3/\text{min}$, feed composition: 50 mol% propylene in propane)

From **Figure 4.8** it is evident that the increase in pressure leads to the shifting of the breakthrough curves with an increase in breakthrough capacity for Zeolite 13X. However, flatness of the curves remains almost the same. It may, however, be noted that the breakthrough time increase is not substantial.

4.2.1.1.2 Feed containing 50 % propylene in propane

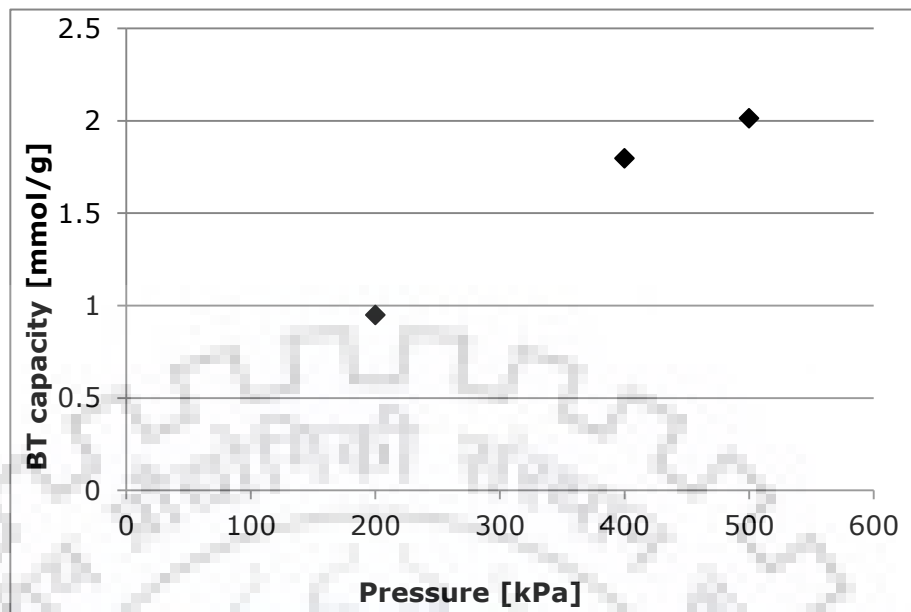


Figure 4.9 Effect of adsorption pressure on the breakthrough time (Temperature: 303 K, Feed rate: $400 \times 10^{-3} \text{ dm}^3/\text{min}$, feed composition: 50 mol% propylene in propane)

Figure 4.9 shows the effect of pressure on the BT capacity (mmol/g) of the adsorbent. Almost a linear increase in BT capacity is observed with an increase in pressure.

Figure 4.10 shows the effect of feed flow rate on breakthrough behavior. The breakthrough time is found to decrease with an increase in feed flow rate at 500 kPa pressure and 303 K temperature.

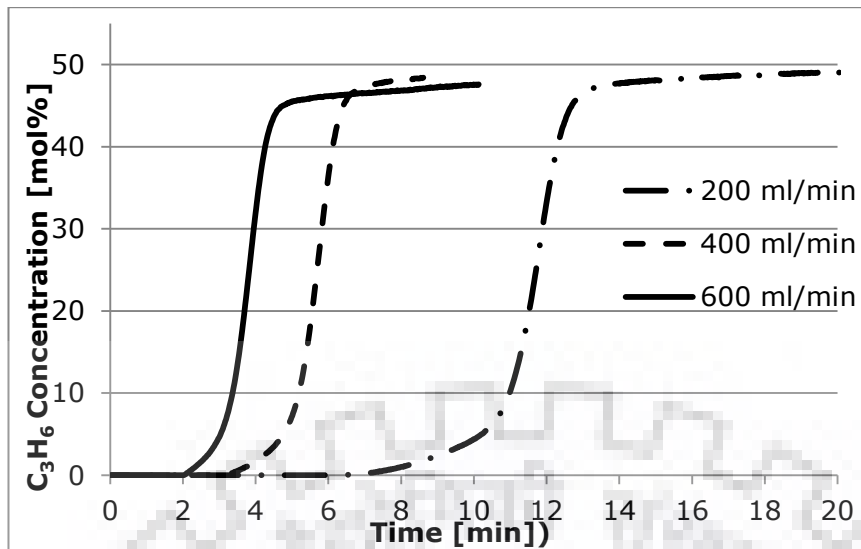


Figure 4.10 Effect of feed flow on the breakthrough curves (Temperature: 303 K, Pressure; 500 kPa, feed composition: 50 mol% propylene in propane)

Ideally, the breakthrough capacity should have no effect of feed flow rate. The total adsorbed amount at the constant temperature and pressure conditions should also remain constant.

However, the adsorption time required is much lower than the feed residence time in the adsorption cell, which adversely affects the breakthrough time. The breakthrough capacity is plotted against the flow rate in **Figure 4.11**:

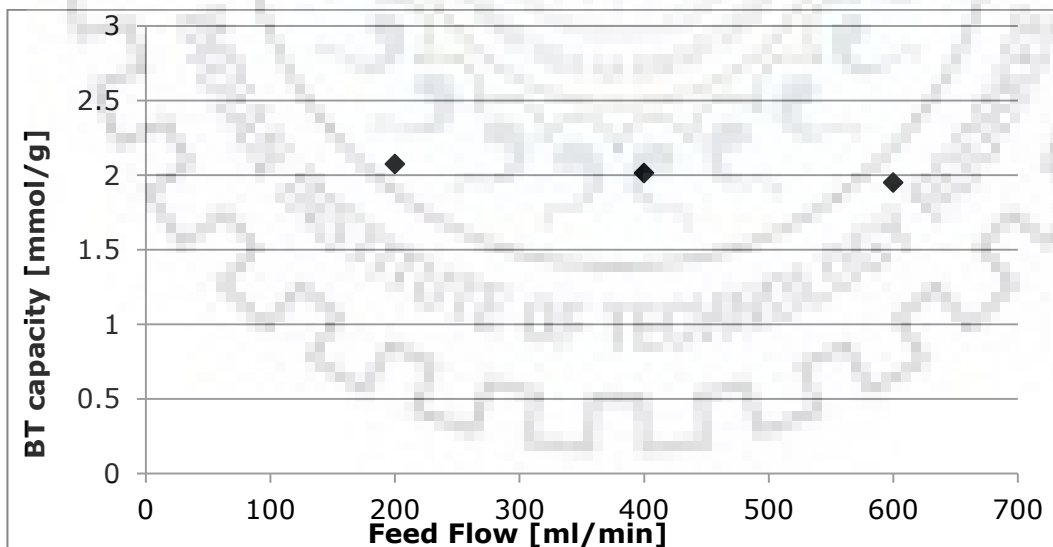


Figure 4.11 Effect of feed flow on the breakthrough capacity (Temperature: 303 K and pressure: 500 kPa, feed composition: 50 mol% propylene in propane)

However, if we look at the breakthrough capacity calculated by BT time, there appears to be albeit a marginal loss in the propylene BT capacity with an increase in the flow rate. Although

Chapter-4

the hydrodynamic residence time decreases drastically with an increase in the feed flow rate, the propylene BT capacity does not decrease appreciably. It can thus be concluded that with the introduction of the feed, the majority of propylene is adsorbed very rapidly and the approach to saturation of the bed is very slow. Similar trend is also observed from the adsorption isotherm data. It is pertinent to mention here that the literature is bereft of an extensive experimental parametric study on propylene-propane binary mixture breakthrough for Zeolite 13 X or any other adsorbent. (C. A. Grande et al., 2005; Grande et al., 2010a; Khalighi et al., 2013b; Miltenburg et al., 2006; Pan et al., 2012; Plaza et al., 2012).

4.2.1.1.3 Feed containing 75 % propylene in propane

This feed stream represents the propylene-propane mixture from FCC off-gas. The effect of pressure and temperature on breakthrough time (Breakthrough capacity) is shown in **Figure 4.12** to **Figure 4.13** respectively.

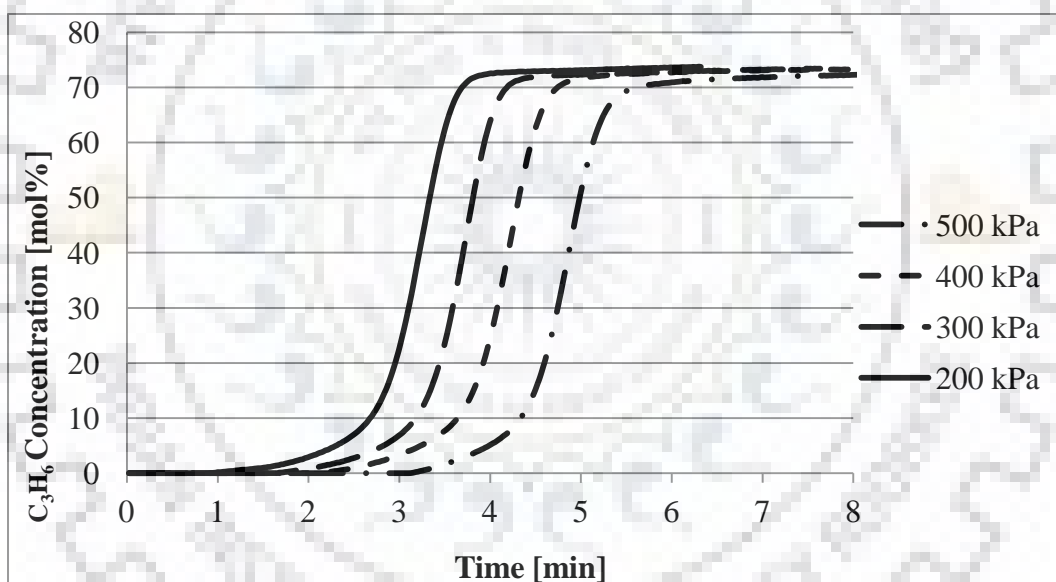


Figure 4.12 Effect of adsorption pressure on the breakthrough curves (Temperature: 303 K, Feed rate: $400 \times 10^{-3} \text{ dm}^3/\text{min}$, feed composition: 75 mol% propylene in propane)

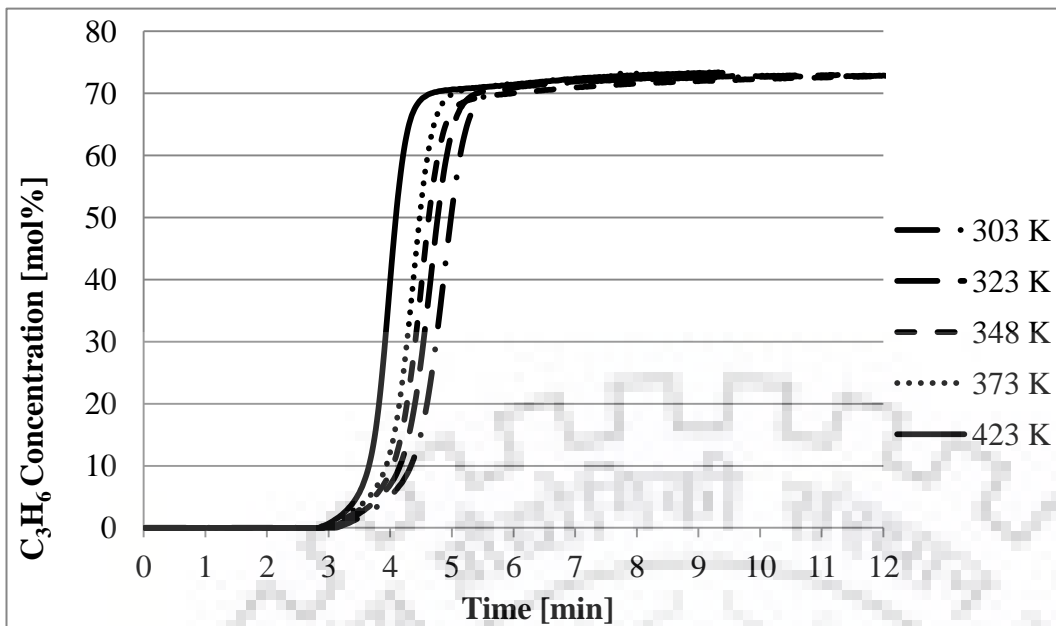


Figure 4.13 Propylene breakthrough curve at different temperatures (Pressure: 500 kPa, Feed rate: $400 \times 10^{-3} \text{ dm}^3/\text{min}$, feed composition: 50 mol% propylene in propane)

It is observed that the propylene BT time at 500 kPa (**Figure 4.13**) does not vary much with temperature; however the slope of the BT curves at different temperatures is markedly different. The BT curve is steepest at 423 K and the slope decreases with decreasing temperatures.

4.2.1.2 Propylene-nitrogen binary feed

The separation of propylene from nitrogen is another separation challenge, which is needed to be addressed. As discussed earlier, the propylene-nitrogen mixture separation is necessary for polypropylene manufacture, wherein the polymer product is purged with nitrogen to remove unreacted propylene. The propylene content of this purge gas is in the range of 10-50 mol%. Given the importance and price of both propylene and utility nitrogen, it is of utmost importance and necessity to recover the propylene and nitrogen, so as to make the whole process is economically viable.

In the following, we present the adsorption data for lean purge gas containing 10 mol% propylene in nitrogen on Zeolite 13X at 373 K with a feed rate of $400 \times 10^{-3} \text{ dm}^3/\text{min}$.

Figure 4.14 shows the typical breakthrough curve for propylene under varying pressure conditions.

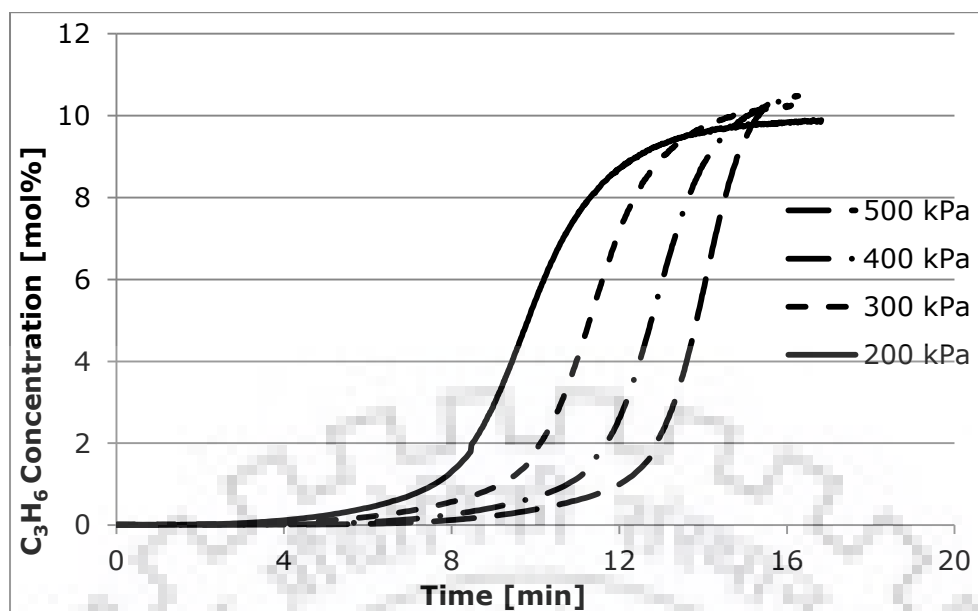


Figure 4.14 Breakthrough profile of propylene in the feed gas (Temperature: 373 K, Feed rate: $400 \times 10^{-3} \text{ dm}^3/\text{min}$, feed composition: 10 mol% propylene in nitrogen)

The BT time is found to shift as pressure increases. This trend is similar as was found for the propane-propylene mixtures. The plot of the corresponding BT capacity with pressure is shown in Figure 4.15.

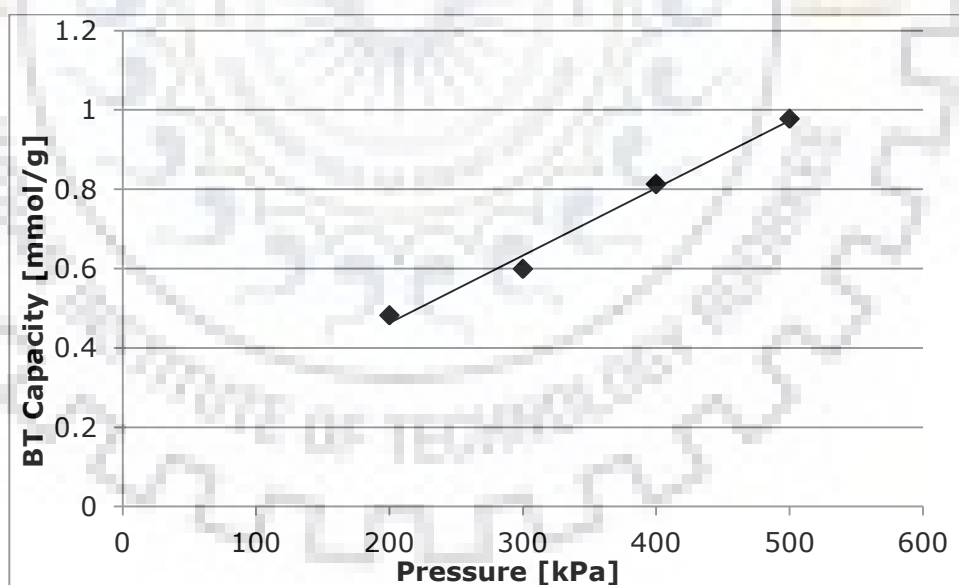


Figure 4.15 Effect of pressure on the Propylene breakthrough capacity (Temperature: 373 K, Feed rate: $400 \times 10^{-3} \text{ dm}^3/\text{min}$, feed composition: 10 mol% propylene in nitrogen)

The propylene equilibrium adsorption capacity at 50 kPa partial pressure on zeolite 13X at 373 K is found to be $\sim 2.4 \text{ mmol/g}$ (Figure 3.7), whereas the corresponding BT capacity for 10% propylene in nitrogen is 1.0 mmol/g . The effect of temperature on the propylene BT time and

Chapter-4

capacity is shown in **Figure 4.16**. It is found that the increase in temperature reduces the physical adsorption breakthrough capacity of Zeolite 13X from 1.3 mmol/g to 1.0 mmol/g for 10% propylene in nitrogen as the temperature increases from 298 K to 373 K. Similarly the breakthrough time decreases from 10.2 to 7.7 min as the temperature is increases from 298 K to 373 K

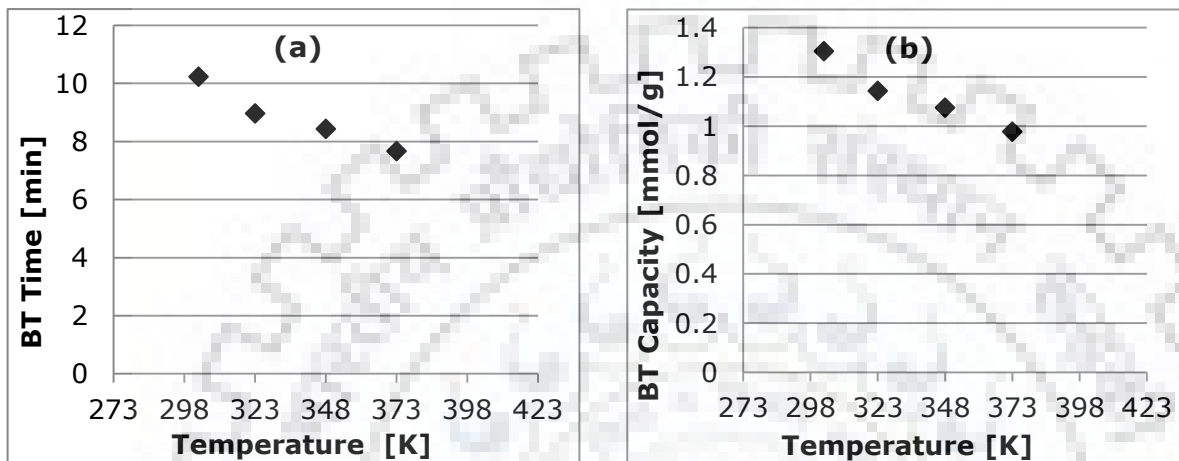


Figure 4.16 Effect of temperature on the propylene (a) BT time and (b) capacity (Pressure: 500 kPa, Feed rate: $400 \times 10^{-3} \text{ dm}^3/\text{min}$, feed composition: 10 mol% propylene in nitrogen)

4.2.2 Future work

A mathematical model was developed in the laboratory with a commercial process simulator (gPROMS, UK) (Arya et al., 2015) for simulation of breakthrough. As the breakthrough studies with propylene bearing gases were ongoing, the model was first applied to the simulation of CO_2 breakthrough from a simulated biogas mixture comprising 40 mol% CO_2 and the balance CH_4 . Four adsorbent namely Z10-04, K^+ ion exchanged Z10-04, and Carbon molecular sieve (CMS 3K) were used in the study. The mathematical model employed has the following assumptions:

- The axial dispersed plug flow model is used to describe the flow behavior.
- The total pressure remains constant.
- Adsorption equilibrium is represented by the Langmuir model.
- Mass transfer rate is governed by the linear driving force (LDF) model.

Chapter-4

- e) Gas and solid phases are at thermal equilibrium at a given location along the length of the adsorbent bed.
- f) The adsorption is considered to be isothermal with the heat loss from the bed being negligible.

The generalized equations for the model are discussed next:

The model consisted of partial equations governing the mass, heat and momentum balance within the adsorber column. These equations in the mathematical model were non-dimensionalized and solved numerically by finite element orthogonal collocation method (OCFEM) using the gPROMS software. The axial dimension was discretized into 50 segments with three internal collocation points in each element. The mass transfer coefficients of CO₂ and CH₄ were obtained by simulating the experimental breakthrough curve with mass transfer coefficients as the fitting parameter for the four adsorbents.

However, simulation of the breakthrough data of the present work has been taken up with the commercial Aspen Adsorption software. However, this work is under progress.

4.2.3 PVSA Studies

4.2.3.1 Propylene- propane separation

In the previous sections, it has been experimentally shown that the propylene BT capacity of Z10-04 is not affected by the feed flow rate at a given temperature and pressure (**Figure 4.14**). However, the propylene BT capacity linearly increases with pressure (**Figure 4.15**) and decrease with an increase in temperature.

The performance of the PVSA cycle was studied experimentally within the parametric boundary of breakthrough studies already performed. It is important to note that breakthrough data forms the primary basis of the PVSA cycle design as the distribution of the feed components within the adsorber bed will depend upon the extent (or time) to which the mass transfer front of the more adsorbed component has been allowed to propagate inside the adsorber column. This plays a crucial role in fixing the purity and recovery targets for a PVSA process.

A close look at the PVSA cycle reveals that as the propylene is selectively adsorbed from a mixture of propylene and propane. The high purity propylene can be obtained during the regeneration of the adsorber bed during the cycle, i.e. during the evacuation step and evacuation with propane purge step. Therefore, the propylene product purity and recovery can be defined in two ways:

- i. Method-1: Propylene recovered during the evacuation step; and
- ii. Method-2: Combined propylene recovered during both evacuation and evacuation with a propylene purge step.

It was observed that the average purity of both evacuation and evacuation with propane purge stream are similar and fall in the range of refinery-grade propylene. Therefore, the propylene product purity is weighted average purity of both these streams and similarly the propylene recovery also taken into account the combined amount of propylene obtained. The formula for propylene purity and recovery is given below:

Propylene purity (mol%)

$$= \left(\frac{\{V_{\text{Evac}} \times Y_{\text{Propylene in Evac product}}\} + \{V_{\text{Evac with Purge}} \times Y_{\text{Propylene in Evac with purge product}}\}}{[V_{\text{Evac}} + V_{\text{Evac with Purge}}]} \right) \times 100$$

Equation 4.1

Propylene recovery (mol%)

$$= \left(\frac{\{V_{\text{Evac product}} \times Y_{\text{Propylene in Evac Product}}\} + \{V_{\text{Evac with purge product}} \times Y_{\text{Propylene in Evac with purge Product}}\}}{\{F_{\text{Feed}} \times Y_{\text{Propylene in Feed}} \times t_{\text{Feed}}\} + \{F_{\text{Rinse}} \times Y_{\text{Propylene in Rinse}} \times t_{\text{Rinse step}}\}} \right) \times 100$$

Equation 4.2

Where V is given in 10^{-3} dm^3 ; y is given as mol fraction, F is given in $10^{-3} \text{ dm}^3/\text{min}$, t is given in min. The productivity of an adsorption process which denotes the hourly product throughput per unit weight of adsorbents is a key parameter for evaluation of an adsorptive process. A higher value of productivity means that the process can affect a higher amount of separation for given adsorbent weight. Productivity can be calculated by the following equation:

$$\text{Productivity} \left(\frac{\text{mol}}{\text{h.kg}} \right) = \frac{\{V_{\text{Evac product}} \times Y_{\text{Propylene in Evac Product}}\} + \{V_{\text{Evac with purge product}} \times Y_{\text{Propylene in Evac with purge Product}}\} - \{F_{\text{Rinse}} \times Y_{\text{Propylene in Rinse}} \times t_{\text{Rinse step}}\}}{\text{cycle time} \times \text{weight of adsorbent}}$$

Equation 4.3

where, the cycle time and adsorbent weight are given in h and kg respectively.

It may be noted here that the propylene flow during the rinse step is an external input here (supplied from a gas cylinder). It will be desirable to use a part of a propylene-rich product for a co-current rinse in an industrial process.

Chapter-4

Process Power Requirement

Specific power consumption i.e. amount of power expended per mol of the desired product is another important criterion for assessment of a PVSA process. A closer look at the PVSA cycle indicates that power is required during the following steps: Pressurization with Feed, High-pressure adsorption, Evacuation (propylene product withdrawal), Evacuation with propane purge.

With respect to the cycle studied in this work following assumption are made:

- The feed is available at 200 kPa (Khalighi et al., 2014), therefore compression energy is required when the adsorption pressure is greater than 200 kPa
- A part of propylene-rich evacuation product is stored at 150 kPa and used for co-current rinse step, hence co-current rinse step does not need power
- A part of propane rich adsorption product (available at adsorption pressure is used in evacuation with purge step)
- The feed compressor and vacuum pumps remain ON continuously even when their action is not required in the single column PVSA cycle. This is in congruence with the experimental setup and procedure

An important point can be made here with respect to the last assumption. Keeping the compressor and vacuum pump ON for the entire duration of the cycle invariably results in higher projected power requirement values for the single column PVSA cycle used in this study.

The total power consumed for these steps per cycle was calculated for the experimental data set as per the following equation:

$$\mathbf{Power (kW)} = \left(\frac{\gamma}{\gamma - 1}\right) R_g T_{feed} \left[\left(\frac{P_H}{P_L}\right)^{\left(\frac{\gamma-1}{\gamma}\right)} - 1 \right] \frac{B}{1000\eta}$$

Equation 4.4

Where, γ is ratio of specific heats of gas stream, R_g is the universal gas constant (8.314 J/K/mol), T_{feed} is the temperature of feed (K), P_L and P_H (kPa) are the suction and delivery pressure respectively, B is molar flow (mol/s) of the feed stream to be compressed/ evacuated, η is the efficiency of the compressor/ vacuum pump drive.

Chapter-4

The values used for power calculations are given below in **Table 4.5** below:

Table 4.5 The P_H and P_L values used for power calculation

Step	P_H (kPa)	P_L (kPa)
Feed Pressurization	200 – 500	200
Adsorption	200 – 500	200
Evacuation	150	10
Evacuation with purge	150	10

The results of the theoretical specific power calculations are discussed in detailed in the following sections.

4.2.3.1.1 Feed containing 12 % propylene in propane

- *Effect of key variables on the purity and recovery of propylene*

The effect of feed time (as % of BT time) on the purity and recovery of propylene product is given in **Figure 4.17**. The feed pressurization and adsorption steps durations were 85 and 15% of total feed time. For example, the propylene BT time at 500 kPa and 303 K is 480 s. The duration of the feed pressurization and adsorption steps was 170 and 214 s respectively.

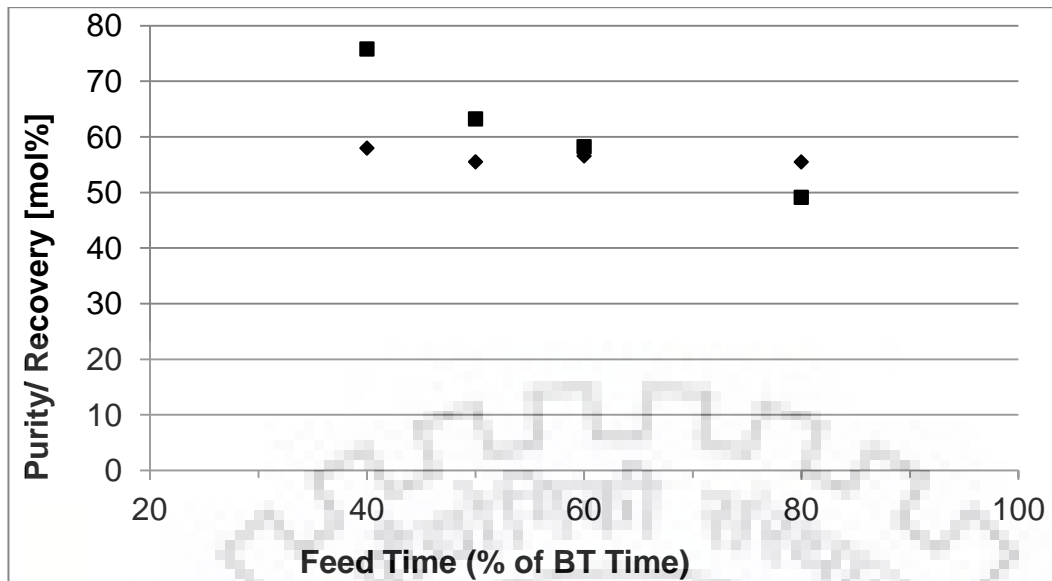


Figure 4.17 Effect of feed time on propylene purity and recovery (Pressure: 500 kPa, Temperature: 303 K, feed rate $400 \times 10^{-3} \text{ dm}^3/\text{min}$, ◆: propylene purity, ■: propylene recovery)

It can be seen from **Figure 4.17** that propylene recovery decreases with an increase in feed time (with evacuation time kept constant). This observation can be attributed to the fact that the adsorption mass transfer zone of the propylene advances further along the adsorption bed with time and the adsorbed propylene is not being recovered fully by evacuation.

The purity of propylene is observed to be almost independent of adsorption time as mass transfer zone of propylene is progresses rapidly towards the exit of the reactor; the bed is getting saturated with propylene.

The effect of adsorption temperature on the performance of the PVSA process is given below in **Figure 4.18**.

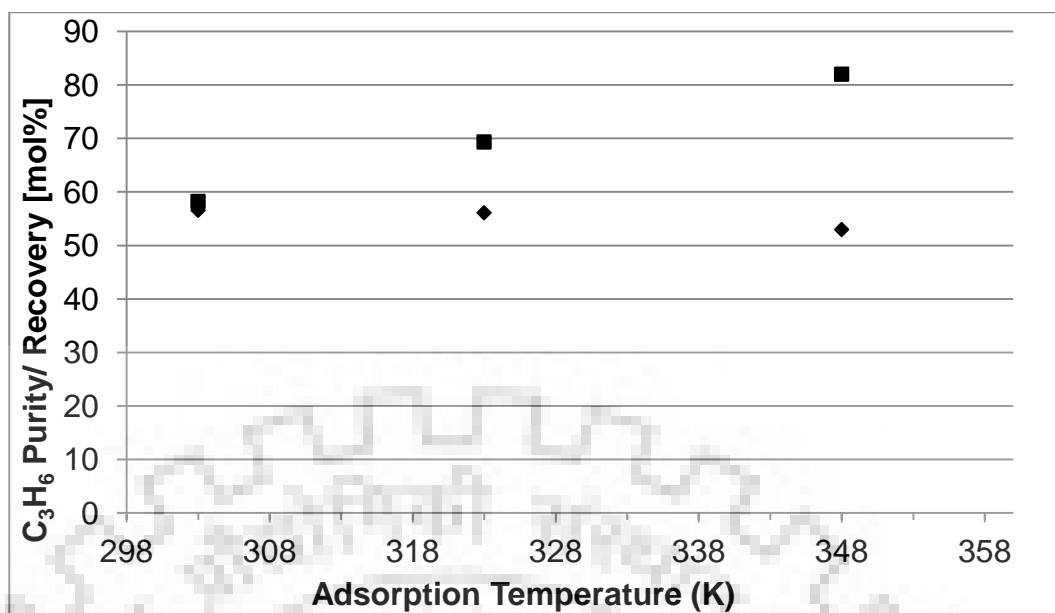


Figure 4.18 Effect of Adsorption Temperature on Propylene Purity and Recovery Feed Containing 12% Propylene in Propane (adsorption pressure: 500 kPa, adsorption time: 60% of BT Time, feed rate: $400 \times 10^{-3} \text{ dm}^3/\text{min}$, \blacklozenge : propylene purity, \blacksquare : propylene recovery)

The recovery of propylene increases with a rise in temperature, as at higher temperature propylene is weakly adsorbed, and during evacuation step, this adsorbed propylene desorbs readily. The purity of propylene decreases with temperature as at high temperature the adsorption capacity of the adsorbent for propylene decreases, which leads to loss of adsorption selectivity of propylene over propane on the adsorbent. This observation is in agreement with our binary equilibrium selectivity studies with Ideal Adsorbed Solution Theory (IAST) (Chapter-3, Section 3.8).

Adsorption pressure is an important parameter in the design of a PVSA process. An increase in the adsorption pressure increases the adsorption of the propylene up to 300-400 kPa and there is very little increase in propylene equilibrium uptake between 300 and 500 kPa. It is also noted that the selectivity of propylene over propane also increases with an increase in pressure at temperature above 343 K, the selectivity does not improve appreciably with temperature below 343 K (Figure 3.21). Therefore, we observe an increase in propylene purity up to from 300 to 400 kPa and then a slight loss is observed in propylene purity. The slight decrease in the propylene purity may occur due to higher increase in equilibrium capacity of propane between 400 and 500 kPa as compared to propylene. This prediction is supported by the experimental data on the effect of pressure on propylene purity as given in Figure 4.19.

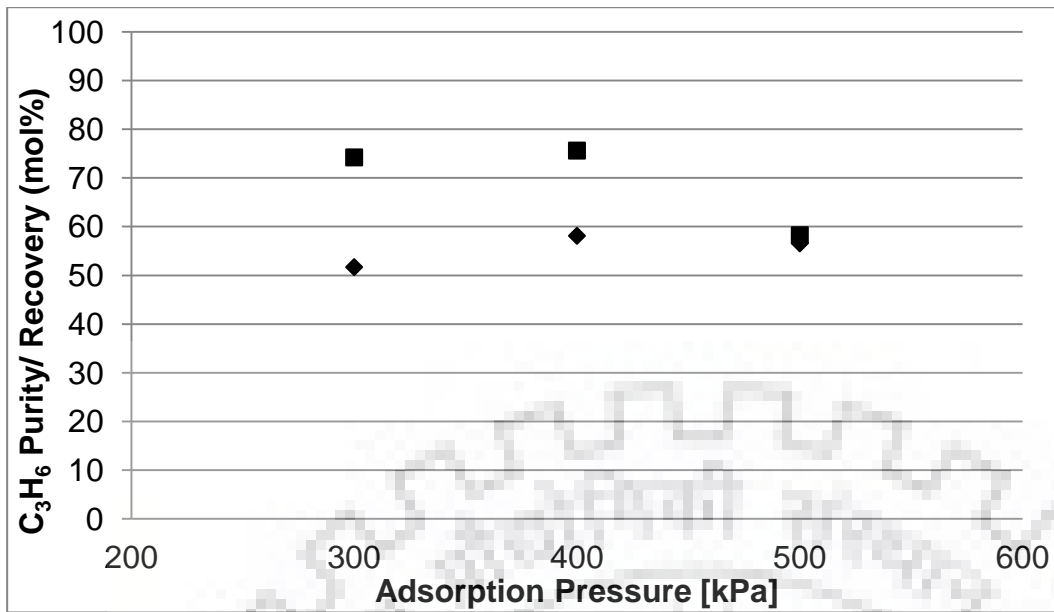


Figure 4.19 Effect of adsorption Pressure on propylene purity and recovery (Temperature: 303 K, adsorption time: 60% of BT Time, feed rate: $400 \times 10^{-3} \text{ dm}^3/\text{min}$, \blacklozenge : propylene purity, \blacksquare : propylene recovery)

- *Effect of key variables on the process propylene productivity*

The effect of key variables such as adsorption time, temperature and pressure on process productivity is shown in Figure 4.20 Figure 4.22. The productivity values decrease with an increase in adsorption time as at higher adsorption time the bed is saturated to a large extent because of the strong bonding of Zeolite 13X with propylene adsorbent cannot be regenerated to the same extent during short period of the regeneration steps. The productivity values predictably increase with temperature of adsorption as higher temperature loosely bound propylene is easier to be removed by evacuation. Highest productivity of 2.6 mol/h/kg is obtained at 500 kPa and 348 K. These productivity values could not be benchmarked by the literature reported data as to best of our knowledge; no literature report has addressed the recovery of propylene from a dilute stream containing 10-12% propylene in propane. However, these values fall into acceptable levels of productivity of PSA processes (Campo et al., 2013; Da Silva and Rodrigues, 2001a).

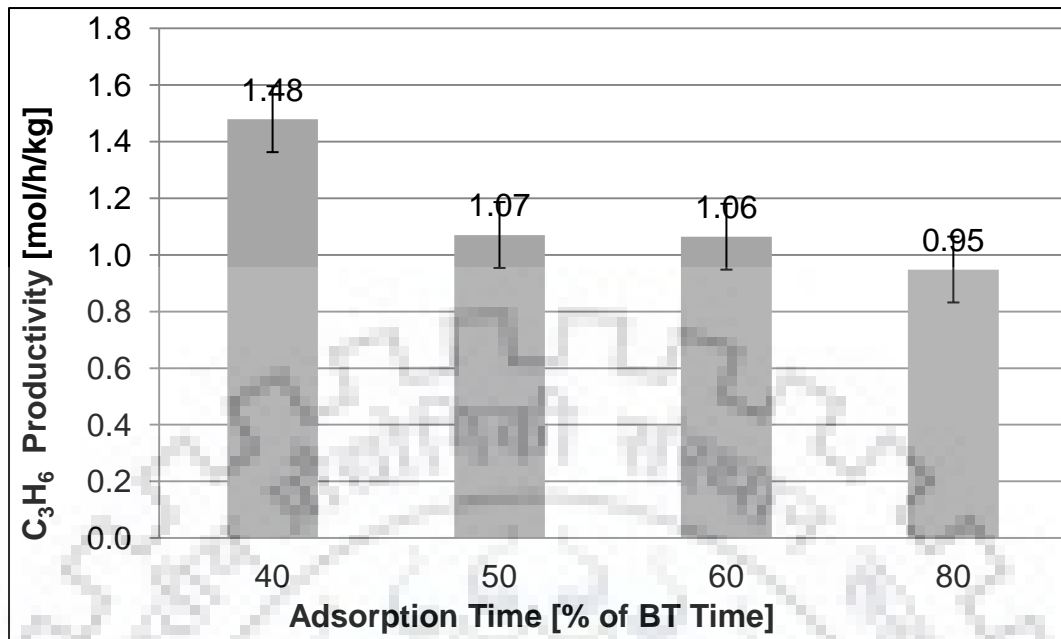


Figure 4.20 Effect of adsorption time on propylene productivity (Adsorption pressure: 500 kPa, temperature; 303 K, feed rate: $400 \times 10^{-3} \text{ dm}^3/\text{min}$)

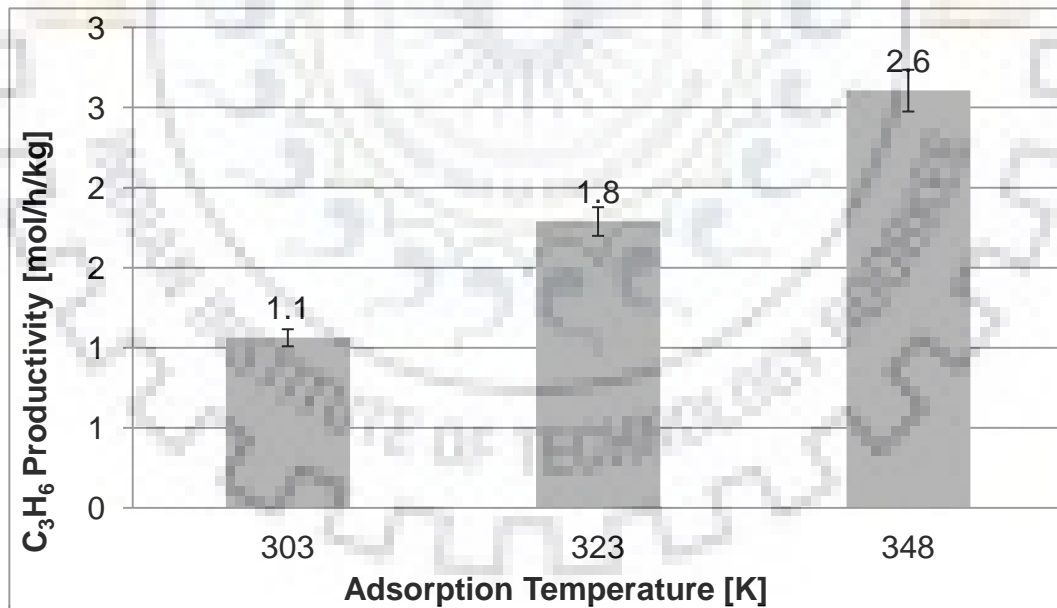


Figure 4.21 Effect of adsorption temperature on propylene productivity (Adsorption pressure: 500 kPa, adsorption time: 60% of BT Time, feed rate: $400 \times 10^{-3} \text{ dm}^3$)

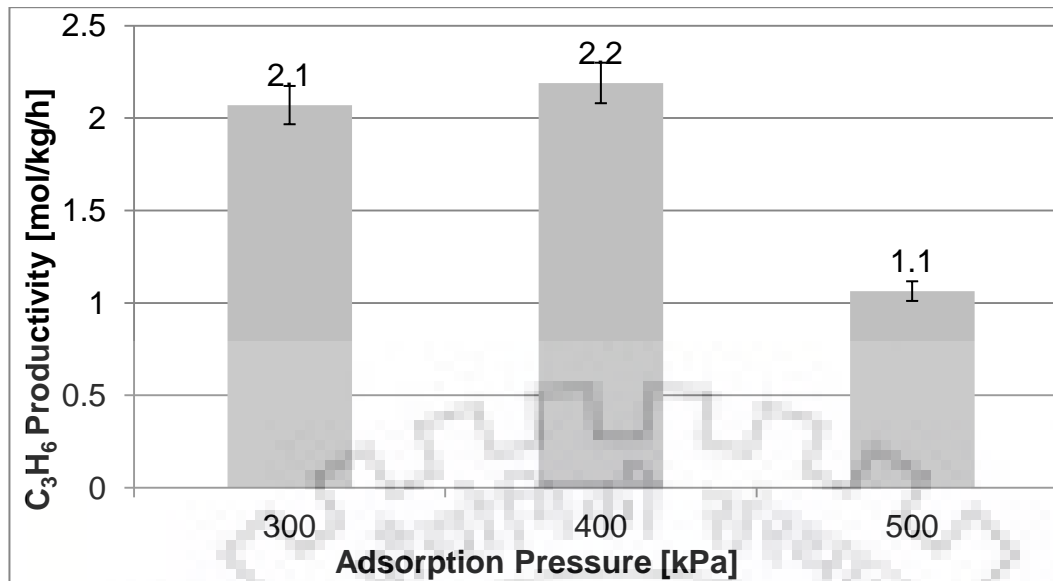


Figure 4.22 Effect of adsorption Pressure on propylene productivity (Adsorption temperature: 303 K, adsorption time: 60% of BT Time, feed rate: $400 \times 10^{-3} \text{ dm}^3/\text{min}$)

It is concluded that the PVSA process studies in this thesis are suitable to recovery very low-value propylene stream containing ~12% propylene to refinery grade propylene. The immediate implication of this finding is that the refinery-grade propylene can be used as feed-stock for the alkylation process or it can be recycled back to C₃ splitter to enhance the overall propylene production.

- *Effect of key variables on the specific power consumption*

Figure 4.23 to **Figure 4.25** show the effect of adsorption time, adsorption temperature and pressure on the specific power consumption for a dilute feed containing 12% propylene in propane. It may be noted that these values are expected to decrease in the multicolumn deployment of the PVSA cycle.

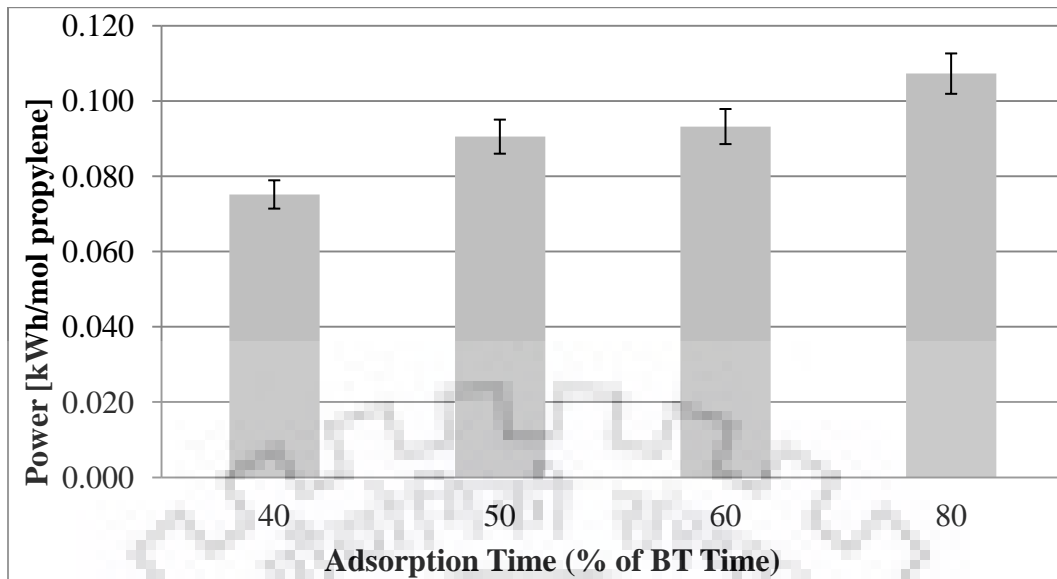


Figure 4.23 Effect of adsorption time on specific power requirement (Adsorption pressure: 500 kPa, temperature 303 K, feed rate: $400 \times 10^{-3} \text{ dm}^3/\text{min}$)

The specific power requirement data of experimental/ simulated PSA or VSA data for propylene/propane separation with propylene-lean streams of such concentration is not available in published literature. For this reason, it is difficult to compare or benchmark this data with available literature reports. The effect of adsorption temperature on power requirement is given in **Figure 4.25**:

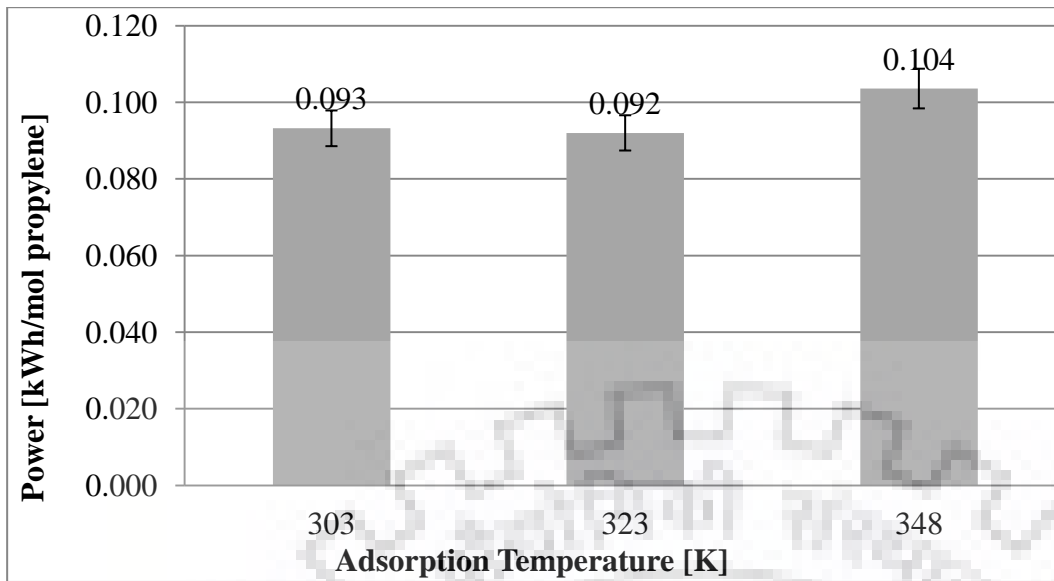


Figure 4.24 Effect of Adsorption Temperature on Power requirement for Feed Containing 12% Propylene in Propane at 500 kPa adsorption pressure and adsorption time equivalent to 60% of BT Time

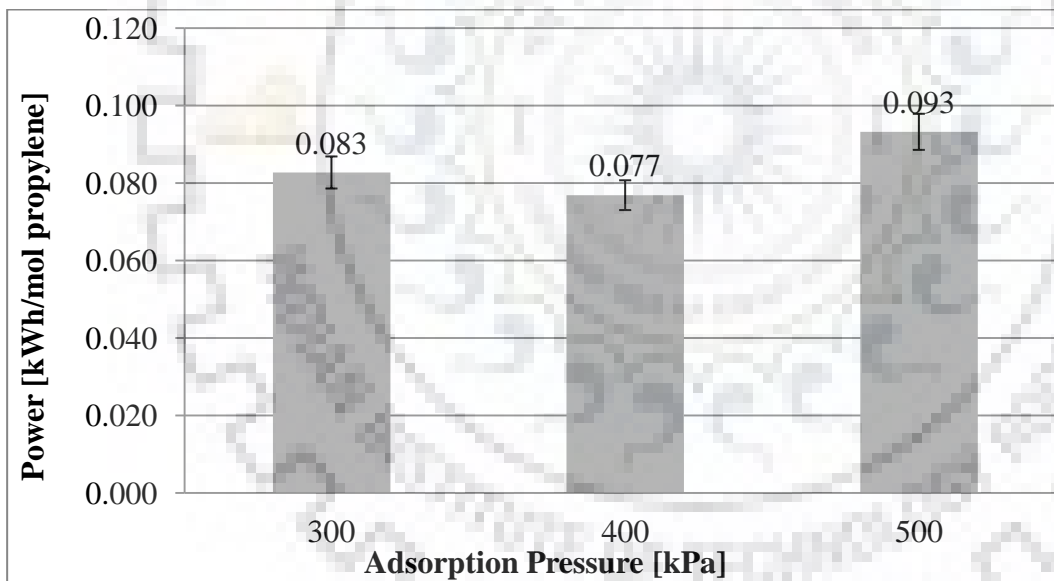


Figure 4.25 Effect of adsorption Pressure on propylene productivity at 303 and adsorption time equivalent to 60% of BT Time & $400 \times 10^{-3} \text{ dm}^3/\text{min}$ feed rate

In case of **Figure 4.24** and **Figure 4.25**, no particular trend can be observed.

4.2.3.1.2 Feed containing 50 % propylene in propane

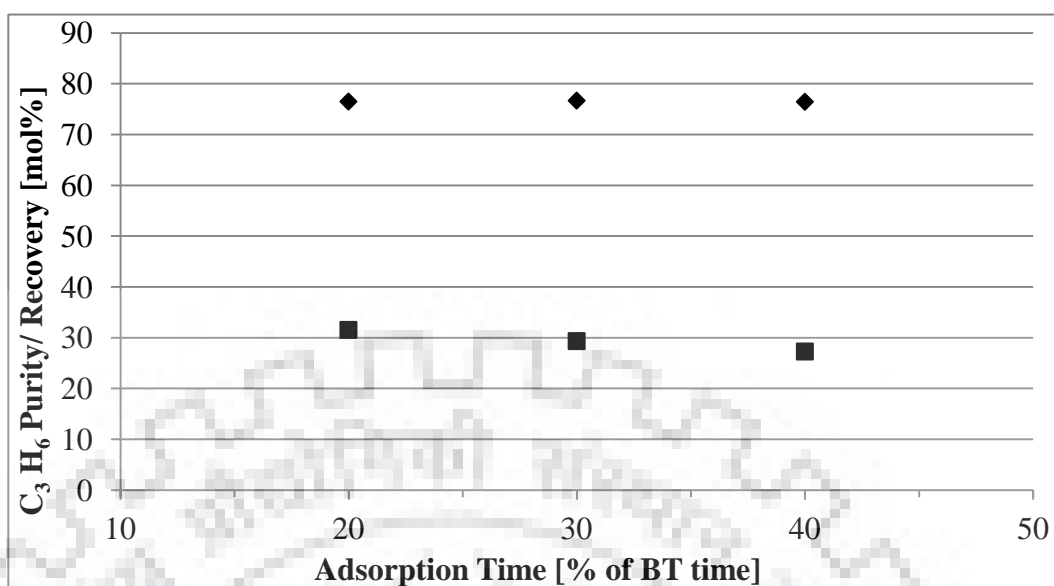


Figure 4.26 – Effect of adsorption time on propylene purity and recovery from a feed containing 50% propylene in propane (Adsorption pressure: 500 kPa, temperature: 303 K, feed rate: $400 \times 10^{-3} \text{ dm}^3/\text{min}$, ◆: propylene purity, ■: propylene recovery)

As seen in **Figure 4.26**, for feed containing 50% Propylene (Hydrocracker off-gas), the recovery of propylene decreases as also observed in **Figure 4.18** (for the feed mixture containing 12% propylene). The recovery of propylene with 50% propylene in the feed is in the range of 27-32%. This data matches with literature reported data (Da Silva and Rodrigues, 2001a). Da Silva and Rodrigues have reported a propylene recovery of 19 mol% at a productivity value of 0.785 mol/kg/h for a feed containing 50% propylene in propane, albeit at a purity of 98 mol%. Low propylene recoveries can be attributed to very strong adsorption of propylene at lower temperatures. The purity of propylene seems to be independent of adsorption time as mass transfer zone of propylene is progresses rapidly towards the exit of the reactor.

The corresponding productivity values of these experiments are given in **Figure 4.27**. Productivity is a function of recovery and follows the same trend, Higher values from the literature reported data could be attributed to higher propylene recovery values obtained (**Figure 4.27**) and higher propylene adsorption capacity of Zeochem 13X as compared to the 13X adsorbent used by Da Silva and Rodrigues (Da Silva and Rodrigues, 2001a)

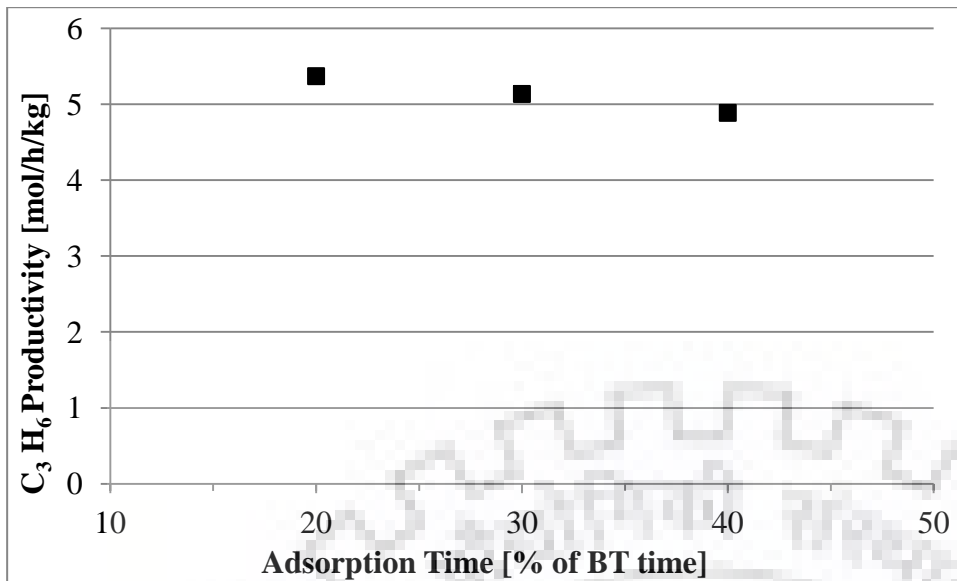


Figure 4.27 Effect of adsorption time on propylene productivity from a feed containing 50% propylene in propane at adsorption pressure and temperature of 500 kPa and 303 K

The experimental results for propylene recovery from an equimolar mixture in propane were largely similar to the literature reported data

An important observation can be made from **Figure 4.28** which shows the effect of adsorption temperature on propylene purity and recovery at 500 kPa adsorption pressure and total feed time equivalent to 100% of BT Time. In these experiments, no product was withdrawn as adsorption product i.e. the column was pressurized with feed for entire feed duration and propane rich product was withdrawn only during co-current blowdown step. These experiments were conducted with presumption that the recovery of propylene could be increased if propylene is not allowed to exit the column at all in propane rich product. While the propylene purity obtained in regeneration steps remains in the range of 70-76 mol%, the recovery of propylene increases with an increase in adsorption temperature. This trend may have arisen due to the fact that at higher temperature adsorbed propylene is relatively weakly adsorbed on the adsorbent and hence is recovered to a larger extent.

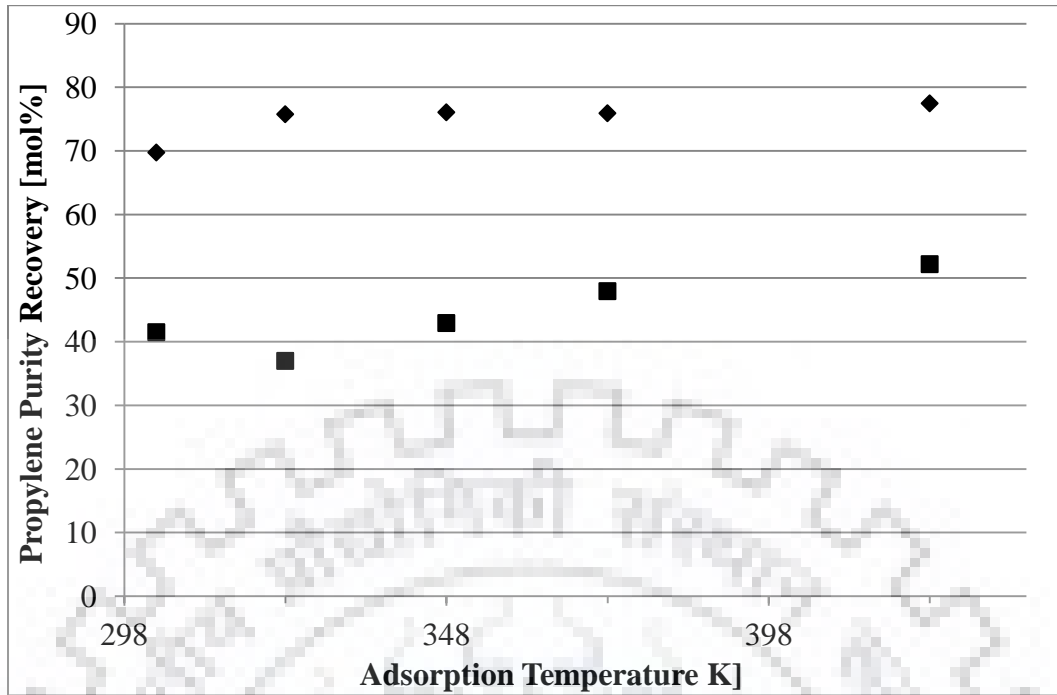


Figure 4.28 Effect of adsorption temperature on propylene purity and recovery with a feed containing 50% propylene in propane (Adsorption pressure: 500 kPa, adsorption time: 100% of BT time, feed rate: $400 \times 10^{-3} \text{ dm}^3/\text{min}$, ◆: propylene purity, ■: propylene recovery)

This reasoning is supported by the corresponding trend of productivity values as given in **Figure 4.29**:

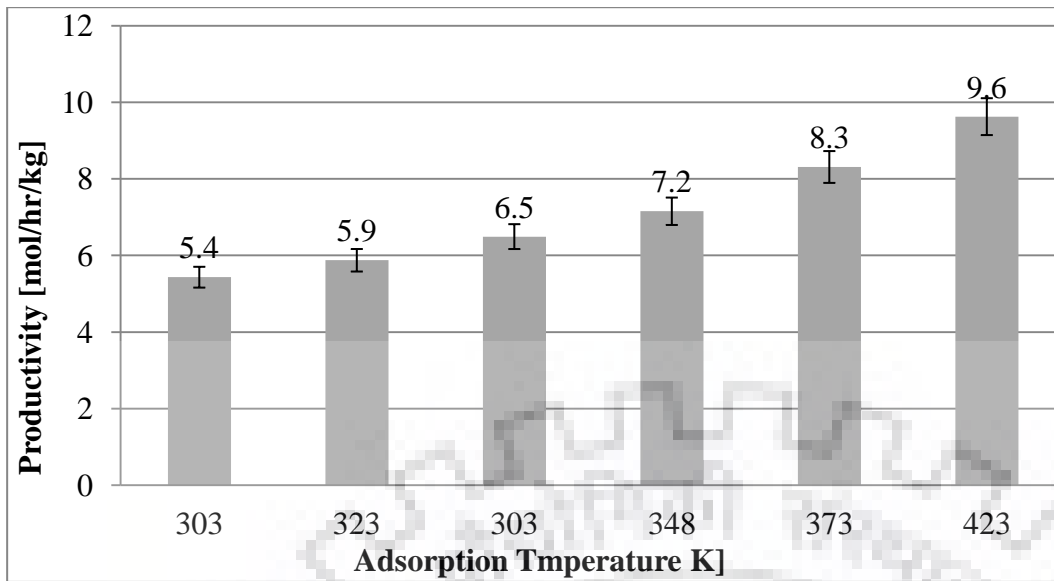


Figure 4.29 Effect of adsorption temperature on propylene productivity with a feed containing 50% propylene in propane at 500 kPa adsorption pressure and feed time equivalent to 100% BT time

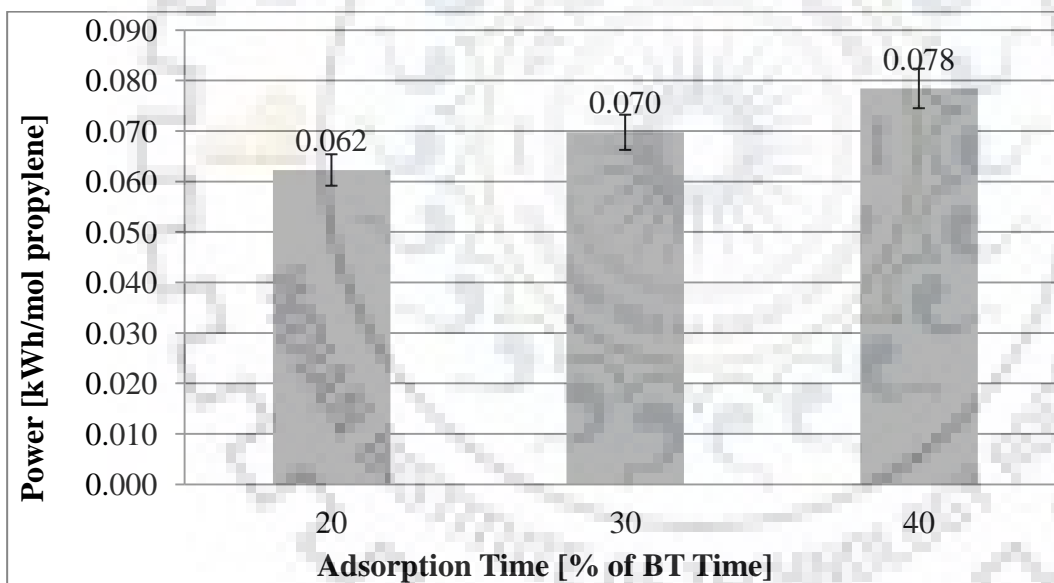


Figure 4.30 Effect of adsorption time on specific power consumption from a feed containing 50% propylene in propane at adsorption pressure and temperature of 500 kPa and 303 K

Due to increase in the amount of gas being compressed, as expected the specific power consumption increases with an increase in Adsorption (and regeneration time) in **Figure 4.30**.

4.2.3.1.3 Feed containing 75% propylene in propane

The PVSA based experimental results for propane and propylene obtained with 12 and 50% propylene in propane indicate that propylene binds very strongly to Zeochem 13 X zeolite and

Chapter-4

the adsorbent will be most suitable for propylene-lean streams. This is also the explanation behind the high heat of adsorption and equilibrium propylene loading for Zeochem 13X as compared to other 13X materials reported in literature. Few experiments were carried out at high adsorption temperature considering the ease of regeneration observed for high temperature. However, the propylene could be upgraded only up to 88.5% purity with ~ 40% recovery.

It may be concluded that due to high adsorption equilibrium capacity and heat of adsorption of both propylene and propane Zeochem zeolite 13X has been found to be most suitable for recovery of propylene from propylene –lean (12 % Propylene in propane) wherein up to 75% purity was obtained at 40% recovery.

4.2.3.2 Propylene-nitrogen separation

The average purity of the nitrogen-rich adsorption product obtained was calculated as per the following equation:

Nitrogen purity (mol%)

$$= \left(\frac{\left[\begin{aligned} &V_{\text{Adsorption product (ml)}} \times Y_{\text{N2 Adsorption Product (mol\%)}} \right\} + \\ &\left\{ V_{\text{Blowdown product (ml)}} \times Y_{\text{N2 Blowdown Product (mol\%)}} \right\} + \\ &\left\{ V_{\text{Rinse product (ml)}} \times Y_{\text{N2 Rinse Product (mol\%)}} \right\} \end{aligned} \right]}{\left[\begin{aligned} &V_{\text{Adsorption product (ml)}} + V_{\text{Blowdown product (ml)}} + \\ &V_{\text{Rinse product (ml)}} \end{aligned} \right]} \right) \times 100$$

Equation 4.5

$$\left[\begin{aligned} &V_{\text{ Adsorption product}} \times Y_{\text{N2 Adsorption Product}} \right\} \\ &+ \\ &\left\{ V_{\text{ Blowdown product}} \times Y_{\text{N2 Blowdown Product}} \right\} \\ &+ \\ &V_{\text{ Rinse product}} \times Y_{\text{N2 Rinse Product}} \end{aligned} \right]$$

$$\text{Nitrogen recovery} = \frac{\left[\begin{aligned} &F_{\text{Feed}} \times t_{\text{feed}} \times Y_{\text{N2 in Feed}} \right\} \\ &+ \\ &F_{\text{Evacuarion with purge}} \times t_{\text{Evac with purge}} \end{aligned} \right]}{\left[\begin{aligned} &F_{\text{Feed}} \times t_{\text{feed}} \times Y_{\text{N2 in Feed}} \right\} \\ &+ \\ &F_{\text{Evacuarion with purge}} \times t_{\text{Evac with purge}} \end{aligned} \right]} \times 100$$

Equation 4.6

$$\text{Nitrogen Productivity} \left(\frac{\text{mol}}{\text{h} - \text{kg}} \right) = \left(\frac{\left\{ \left[\begin{aligned} & \{V_{\text{Adsorption product}} \times Y_{\text{N2 Adsorption Product}} \} + \\ & \{V_{\text{Blowdown product}} \times Y_{\text{N2 Blowdown Product}} \} + \\ & V_{\text{Rinse product}} \times Y_{\text{N2 Rinse Product (mol)}} - \\ & \{F_{\text{Purge}} \times t_{\text{Purge}} \times Y_{\text{N2 Purge}} \} \end{aligned} \right\}}{\left[\text{cycle time} \times \text{weight of adsorbent} \right]} \right) \times 100$$

Equation 4.7

There are very few literature reports on the development of adsorption based process for recovery of propylene and nitrogen from polypropylene reactor purge gas. (Narin et al., 2014; Ribeiro et al., 2013; Zwilling et al., 2003). These reports deal with theoretical modeling of PSA based plants for recovery of both propylene and nitrogen.

An inherent advantage with adsorptive separation of propylene and nitrogen (as compared to propylene and propane) is that both these molecule have vastly different properties and interaction with the adsorbent surface. Due to the dipole moment of the propylene molecule, the propylene molecule is strongly adsorbed on the zeolite surface. The strong adsorption is also evident by the heat of adsorption of these molecules on Zeolite 13X surface. (Table 3.5, Chapter 3)

By the above consideration, it may be possible to recovery both propylene and nitrogen in high purity. In the context of the PVSA cycle studied here, it is possible to obtain nitrogen in high purity in three steps: adsorption, co-current blow-down and concurrent rinse with propylene. High purity propylene is again obtained in the following two regeneration steps: evacuation and evacuation with a nitrogen purge.

4.2.3.2.1 Feed containing 10 % propylene in nitrogen

The effect of adsorption temperature on the process key process performance indicator such as, i.e. purity and recovery of propylene and nitrogen is shown in Figure 4.31 for a feed mixture containing 10% propylene in nitrogen.

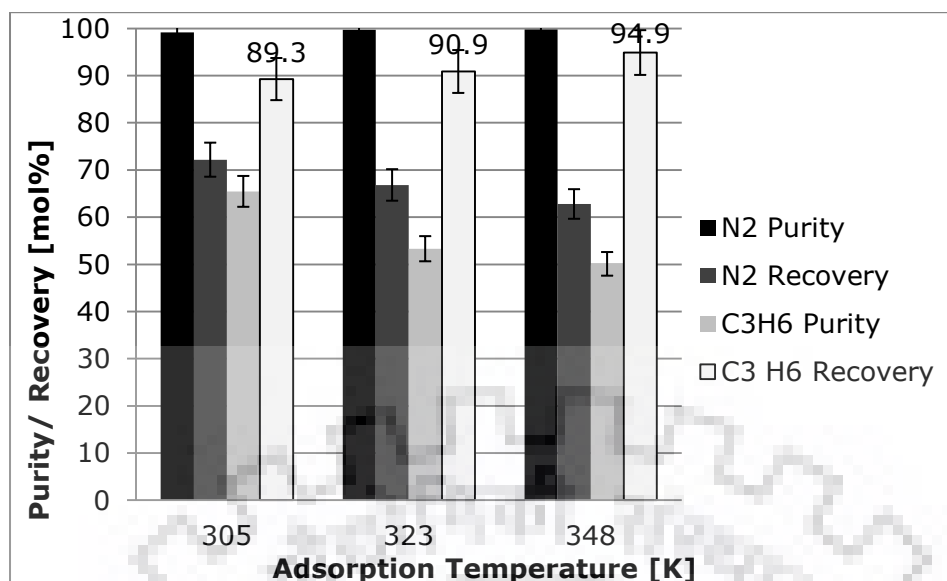


Figure 4.31 Effect of adsorption temperature on product purities and (Adsorption pressure: 200 kPa, adsorption time: 40% of BT time, feed rate $400 \times 10^{-3} \text{ dm}^3/\text{min}$)

It can be observed that the purity of nitrogen is independent in the temperature range as propylene strongly binds to the adsorbent surface and does not exit the adsorber column during the adsorption step. Therefore very high purity nitrogen is obtained. The trend in nitrogen recovery is unexpected. However it may be seen that the purity of propylene decreases with temperature. Due to the reduced adsorption capacity of propylene at high temperatures, the part of propylene is going in the pure nitrogen stream, and as the concentration of propylene is very low, it does not affect the purity of nitrogen produced by a large extent, but noticeable drop in nitrogen purity is observed. The nitrogen product at this purity can be recycled to be used again as purge gas in the polymerization reactor. Propylene can also be purified from 10 mol to >50 mol%, making it suitable as alkylation plant feed stock

The propylene and nitrogen productivities of the process are shown in **Figure 4.32**.

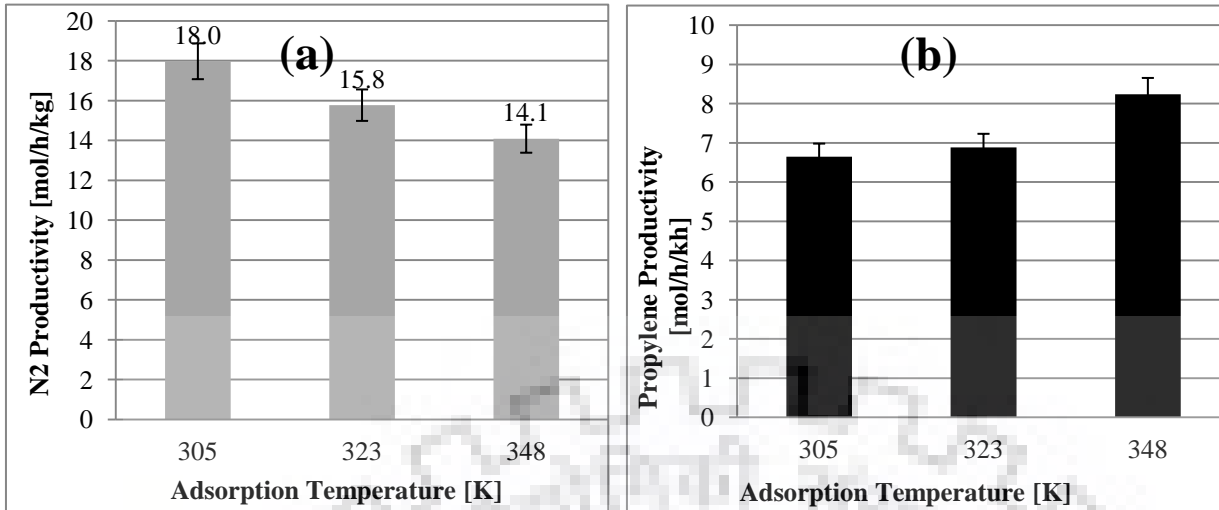


Figure 4.32 Productivity of (a) Nitrogen and (b) propylene at 2 bar adsorption pressure and adsorption time equal to 40% of BT time

The effect of adsorption time on the process purity and recovery is given in **Figure 4.33**:

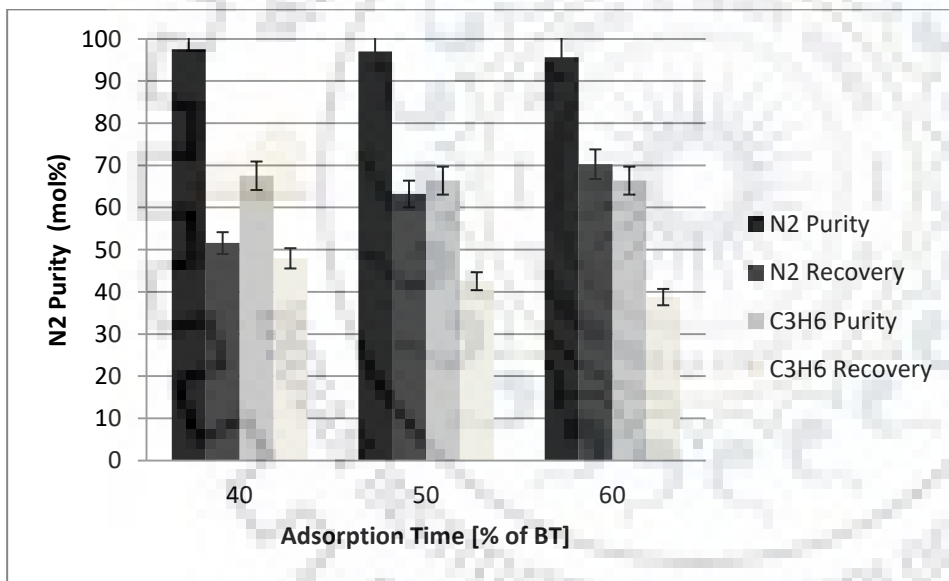


Figure 4.33 Effect of adsorption time on product purities and recoveries at 500 kPa adsorption pressure and adsorption time equal to 40% of BT time, 303 K adsorption temperature (feed rate $400 \times 10^{-3} \text{ dm}^3/\text{min}$)

As the adsorption time increases the propylene mass transfer from move towards the product end of the bed and some propylene slips or breaks out of the adsorbent bed. It can be seen by slight decrease in nitrogen purity in **Figure 4.33**. However, the recovery of nitrogen naturally increases. The adsorption time does not have the same effect on propylene purity trend, which remains unchanged, due to and stronger adsorption of propylene on zeolite 13X. The further

Chapter-4

progression of propylene mass transfer from with adsorption time also results in lower propylene recovery at high adsorption time.

In case of feed containing 10% propylene the nitrogen can be obtained with purity of > 99% making it suitable for recycling to purge the un-reacted monomer from the polypropylene reactor.

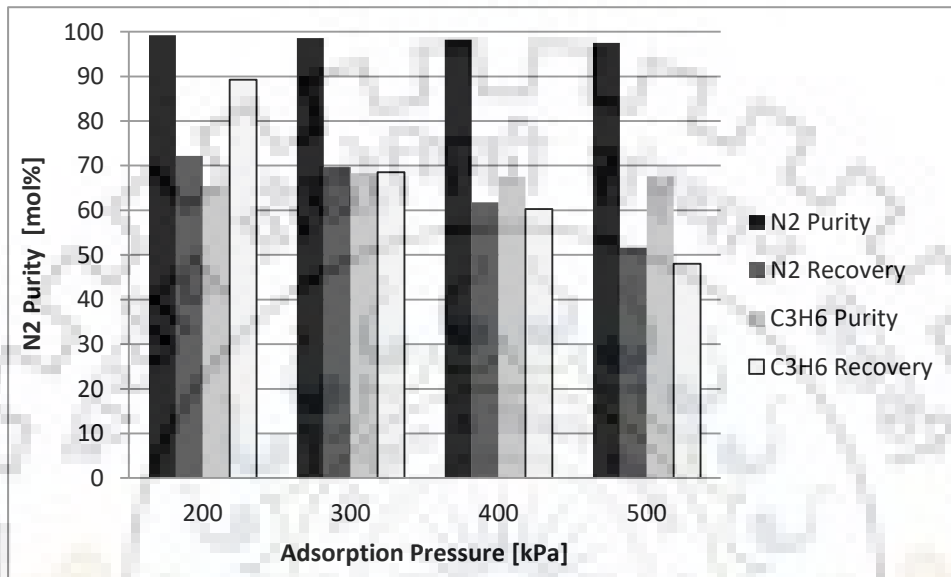


Figure 4.34 Effect of adsorption pressure on product purities and recoveries at 303 K temperature and adsorption time equal to 40% of BT time

The productivity of propylene and nitrogen is given in **Figure 4.35**:

As the adsorption pressure increases the adsorber columns is increasing gets saturated with propylene, a part of propylene is vented to nitrogen-rich product and slightly decreases its purity. The purity of the propylene product is largely constant.

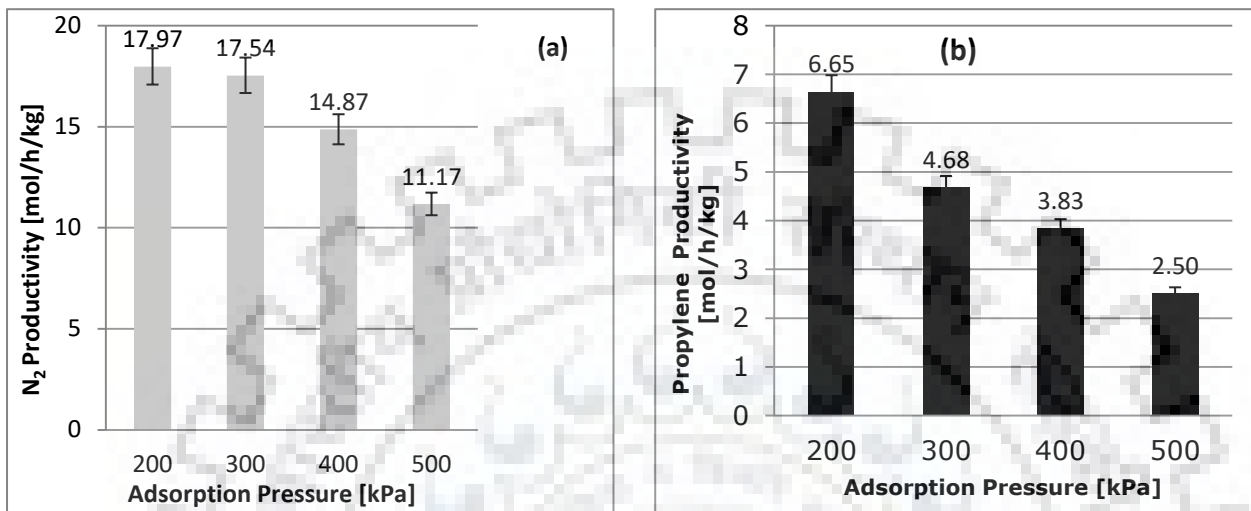


Figure 4.35 Productivity of (a) nitrogen and (b) propylene at 303 K temperature and adsorption time equal to 40% of BT time (10% propylene in fee)

Ribeiro et al. have reported the theoretical simulation results of a PVSA process (Ribeiro et al., 2013) using MIL-Fe(100) adsorbent. They report nitrogen and propylene productivity values of 0.20 kg N₂/kg_{ads}/h (7.1 mol/kg/h) and 0.07 kg_{C₃H₆}/kg_{ads}/h (1.67 mol/kg/h). Although a direct comparison of experimental results of this thesis and simulation results given in literature will not be fair, it could be concluded that the experimental results presented here are comparable (or better) than literature reported data.

4.2.3.2.2 Feed containing 20 % propylene in nitrogen

As the propylene content of polypropylene reactor purge stream can go as high as 50 mol%. The effect of feed composition was also checked with feed containing higher propylene content in Figure 3.36.

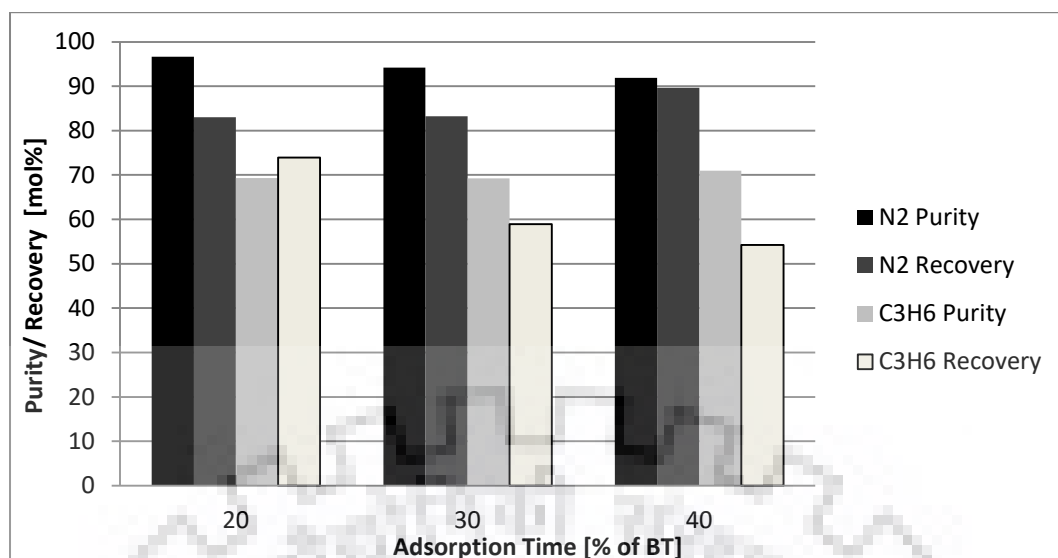


Figure 4.36 Effect of adsorption time on product purities and recoveries at 200 kPa adsorption pressure and adsorption time equal to 40% of BT time (20% propylene in feed, feed rate $400 \times 10^{-3} \text{ dm}^3/\text{min}$)

4.3 PROPYLENE-NITROGEN SEPARATION: ECONOMIC ANALYSIS

The HPCL-Mittal Energy Limited (HMEL), Bathinda refinery in India produces 440 kTPA of propylene. As per the data received from HMEL, the composition of polypropylene reactor purge gas is as follows: nitrogen: 49.80 (mol %), propylene: 51.20 (mol %). The gas is being flared without the recovery of either nitrogen or propylene. It may be noted that impurities in this purge gas also consists of ethane, propane, and pentane. The total amount of these impurities is nominally 2.0 mol%. However, for the following analysis these impurities are treated at propane. The Assumption is reasonable as the adsorbent used for propylene adsorption shall also adsorb these trace impurities.

A preliminary economic analysis of the flaring of nitrogen and propylene vis-à-vis their recovery by the PVSA process reported in this thesis is as follows:

Chapter-4

Table 4.6: Preliminary economical benefit calculations of recovery of nitrogen and propylene by PVSA process

Basis of Calculation	
Stream	Polypropylene reactor purge gas
Molar flow, kmol/h	44.80
Composition (mol %)	
Nitrogen	49.80
Propylene	51.20
Avg. Molecular Weight, kg/kmol	43.00
Nitrogen Recovery by PVSA	
Nitrogen in flared gas, kmol/h	22.31
Nitrogen in flared gas, Nm ³ /h	499.75
Nitrogen in flared gas, Nm ³ /year (Assuming 330/year operation)	3,958,043
Cost of Nitrogen in refinery, INR/ Nm ³	4.0
Value of Nitrogen in flared gas, INR/year	15,832,173
Benefit of implementation of PVSA process	
PVSA Process performance	
Nitrogen Purity, mol%	99.9
Nitrogen Recovery, mol%	70.0
Nitrogen recovered, Nm ³ /year	
	2,770,360
Value of Nitrogen recovered, INR/year	11,082,519
Propylene Recovery by PVSA	
Propylene in flared gas, kmol/h	22.94
Propylene in flared gas, kg/h	963.38
Propylene in flared gas, Tonne/year (Assuming 330/year operation)	7630
Spot price of Propylene in refinery, USD/ tonne (Refinery grade propylene)	900
Value of propylene in flared gas, USD/year	6,867,000
Value of propylene in flared gas, INR/year (@1 USD=INR 70)	480,690,000
Value of propylene in flared gas, Crore INR/year (INR 1 crore = INR 10,000,000)	48.07
Benefit of implementation of PVSA process	
PVSA Process performance	
Propylene Purity, mol%	60
Propylene Recovery, mol%	80
Propylene recovered, tonne/year	
	6104
Value of propylene recovered, INR/year	384,552,000

Chapter-4

It is found that recovery of propylene and nitrogen offer substantial economic benefit. However, a detailed cost-benefit analysis which will also involve considerations into capital and operating costs involved in the setting up and running of the PVSA plant is required. As mentioned earlier, an industrial PVSA plant based on this thesis shall run in multi-column mode and hence the firm capital and operating cost estimation will require further work towards development of a multi-column process.

4.4 CONCLUSION

Selective adsorption and recovery of propylene by (i) Separation of propylene from propane and (ii) Separation of propylene from nitrogen was experimentally tested. Industrially relevant feed compositions such as C_3 splitter bottom, the propane-propylene mixture from steam cracker and FCC off-gases, the propylene-nitrogen mixture from polypropylene off-gas were considered for the study.

The breakthrough curve is significant in the development of an adsorption process. Breakthrough curves under wide operating ranges for temperature, pressure and flow rates were experimentally generated. These breakthrough curves were analyzed minutely and derived data mainly dynamic breakthrough adsorption capacity of propylene was correlated with single component isotherms.

A single adsorber column, six-step PVSA cycle was envisaged and implemented in an automated PVSA unit. The PVSA cycle was extensively tested by key performance indices such as product purity, recovery, and productivity of the adsorbent. Recovery of propylene from a very dilute mixture (12 mol% propylene in propane) is reported here. There are no literature reports for recovery of propylene from such dilute streams. Propylene purity was enhanced from 10-12 mol% to >55 mol%. These are very promising results and a closer scrutiny on the overall feasibility of such adsorptive process is required.

Propylene was recovered from equimolar mixtures of propane and propylene, with purity more than 75 mol% with a productivity value of ~5.0 mol/h/kg which is better than the literature reported values.

Propylene and nitrogen recovery from polypropylene unit purge gas is also an industrially relevant and commercially attractive opportunity. It was experimentally demonstrated that the PVSA process could be utilized to recover high purity nitrogen (>99 mol% and >65 mol%

Chapter-4

recovery) and refinery-grade. The experimental results are comparable with scarcely available experimental data for this adsorptive separation.

A preliminary analysis suggests that the propylene-nitrogen mixture from polypropylene reactor purge gas contains significant amount of propylene and nitrogen recovery of these can lead to significant savings, As per the results obtained in this work nitrogen can be obtained in purity in excess of 99 mol% and this nitrogen can be recycled. Moreover the simultaneous recovery in refinery grade purity (> 60 mol% purity) is possible. The recovered propylene can be sent to the C_3 Splitter or used as a reactant in gasoline alkylation unit as such.



CHAPTER-5 CONCLUSIONS AND RECOMMENDATIONS

5.1 CONCLUSION

Based on the results and discussions presented in chapter 3 and 4 screening of potential adsorbents for selective adsorption of propylene from propylene bearing gaseous streams by pressure swing adsorption and evaluation of the selected adsorbent that is zeolite 13x (Zeochem), the following major conclusions can be drawn:

5.1.1 Synthesis, characterisation and screening of potential adsorbents

- A novel adsorbent, Na-ETS-10 was selected to be synthesised in the laboratory following the literature reported methods
- Na-ETS-10 was successfully synthesised in pure form. The synthesised adsorbent was free from impurities such as quartz and Na-ETS-4
- Among the commercial adsorbents, two equilibrium separation based adsorbents, zeolite 5A (UOP) and zeolite 13X (Zeochem), were chosen to be evaluated based on the findings of the literature survey
- Adsorption equilibrium isotherms of propane, propylene and nitrogen were measured for Na-ETS-10, zeolite 5A (UOP) and zeolite 13X (Zeochem), over the temperature and pressure range of 273- 423 K and 0-300 kPa respectively
- Zeolite 13X (Z10-04, Zeochem) Show the highest capacity for propylene adsorption these adsorbents
- The experimental isotherms were best fitted to a DSL model by non-linear regression using an MS Excel Solver
- To predict the propylene-propane and propylene-nitrogen binary isotherm, IAST model was employed
- An iterative solver for solving the IAST model was developed, and the model was successfully validated to reproduce the literature reported binary and ternary isotherm data. The applicability of the IAST model was established using the Thermodynamics Consistency test (TCT)

- The IAST Binary adsorption equilibrium was predicted for the following four binary mixtures:

Propylene: 50 mol%, balance propane (**Steam cracker off-gas**)

Propylene: 85 mol%, balance propane (**FCC off gas**)

Propylene: 20 mol%, balance propane (**Polymerization Unit off-gas**)

Propylene: 30 mol%, balance propane (**Polymerization Unit off-gas**)

- Among the three adsorbents, zeolite 13x (Z10-04, Zeochem) showed the highest binary adsorption capacity and propylene/propane, propylene/nitrogen ideal adsorption selectivity for all the streams
- Zeolite 13x (Z10-04, Zeochem) was chosen to be evaluated further for experimental investigations for recovery of propylene bearing streams

5.1.2 Propylene separation by pressure swing adsorption

5.1.2.1 Propylene-propane from C3 splitter bottom

- The PSA studies were conducted in a fully automated single column PVSA unit
- The binary breakthrough of the propane-propylene mixture was conducted at the temperature and pressure range of 303-423 K and 200-500 kPa respectively.
- Propylene adsorption capacity at the breakthrough time decreases with increase in temperature for all the feed mixtures, reflecting the reduction of equilibrium adsorption capacity at a higher temperature
- owing to the nature of adsorption isotherms the adsorption capacity and breakthrough increases with pressure which is in congruence with the properly adsorption isotherm at the respective temperature and pressure
- There is a very small change in the breakthrough capacity measured at different flow rates but similar temperature and pressure. This implies that with the introduction of feed majority of propylene is adsorbed very rapidly and the approach to saturation of equilibrium is very slow.

- With feed mixture containing 12% of propylene in propane, the feed stream could be upgraded to refinery-grade propylene (>50% propylene) with over 50% of overall propylene recovery 500 kPa and 303 K.
- With an increase in temperature, the purity remains almost constant however the propylene recovery increases linearly with temperature (from 58% at 303 K to 82% at 348 K)
- Higher propylene productivity values could be obtained, owing to higher equilibrium capacity for propylene.
- These productivity values were not compared with the literature reported data as to best of our knowledge; no literature report has addressed the recovery of propylene from a dilute stream containing 10-12% propylene in propane

5.1.2.2 Propylene recovery from steam cracker off the gas

- for feed containing 50% Propylene (Hydrocracker off-gas), the recovery of propylene decreases, the low recovery of propylene with 50% propylene in feed matches with literature data (Da Silva and Rodrigues, 2001a).
- This was attributed to the very strong adsorption of propylene at low temperature.
- The purity of propylene seems to be independent of adsorption time as mass transfer zone of propylene is progresses rapidly towards the exit of the reactor.
- Productivity is a function of recovery and is observed to be following the trend of recovery values.
- Higher values (~ 8 mol/ hr/kg) from the literature reported that data is attributed to higher propylene recovery values obtained

5.1.2.3 Propylene recovery from polypropylene reactor off- gas

- Propylene and nitrogen recovery from polypropylene reactor off-gas has not been studied with commercial 13X zeolite so far
- The VSA cycle studies appear to be applicable for recovery of both nitrogen and propylene

- Nitrogen is obtained at a very high purity of > 99 mol% with nitrogen recovery ranging from ~60-70 mol%.
- The nitrogen productivity (>20 mol/hr/kg) is very high, as against literature reported data of (2.86 mol/hr/kg) for MOF MIL-Fe-100, as the adsorbent is highly selective for propylene over nitrogen

5.2 RECOMMENDATIONS

Based on the present study, following further studies are recommended for future work

- To optimise the synthesis method for CPO-27-Cu and its testing for propylene adsorption
- To compare the IAST with Real Adsorbed Solution Theory (RAST). RAST takes into account the non-idealities in the adsorbed phase which is assumed to be ideal in IAST
- To calculate the kinetic mass transfer coefficients by the development of appropriate mathematical model and fitting of the breakthrough data to the model
- To study the separation of propylene from C3 bottom splitter and polypropylene off gases in depth, as there is very little data available in the literature
- To simulate experimental PSA/VSA data generated in this thesis for further parameter optimization
- Detailed cost calculation for capital and operating expenses and an cost-benefit analysis needs to be carried out

BIBLIOGRAPHY

1. Aarti, Biswas, N., Nanoti, A., Divekar, S., Gode, N.G., Dasgupta, S., Goswami, A.N., 2011. CO₂ recovery from mixtures with nitrogen in a vacuum swing adsorber using metal organic framework adsorbent: A comparative study. *Int. J. Greenh. Gas Control* 7, 225–229. <https://doi.org/10.1016/j.ijggc.2011.10.007>
2. Adamson, A.W., 1976. *Physical Chemistry of Surfaces*. John Wiley, New York.
3. Ahmed, M.J., Mohammed, A.H.A.K., Kadhum, A.A.H., 2010. Prediction of breakthrough curves for light hydrocarbons adsorption on 4A molecular sieve zeolite. *Korean J. Chem. Eng.* 27, 752–758. <https://doi.org/10.1007/s11814-010-0164-0>
4. Aitani, A.M., 2007. Propylene production. *Encyclopedia Chem. Process.* <https://doi.org/10.1081/E-ECHP-120037901>
5. Al-Baghli, N.A., Loughlin, K.F., 2006. Binary and Ternary Adsorption of Methane, Ethane, and Ethylene on Titanosilicate ETS-10 Zeolite 248–254.
6. Al-Baghli, N.A., Loughlin, K.F., 2005. Adsorption of Methane, Ethane, and Ethylene on Titanosilicate ETS-10 Zeolite. *J. Chem. Eng. Data* 50, 843–848. <https://doi.org/10.1021/je0496793>
7. Albright, L.F., Li, K.W., 1970. Alkylation of Isobutane with Light Olefins Using Sulfuric Acid. Reaction Mechanism and Comparison with HF Alkylation. *Ind. Eng. Chem. Process Des. Dev.* 9, 447–454. <https://doi.org/10.1021/i260035a013>
8. Alvarado, M., 2017. Methanol Industry Overview [WWW Document]. URL https://ngi.stanford.edu/sites/default/files/Alvarado_Stanford_Methanol_Meeting_2017.pdf (accessed 1.1.19).
9. Alvarado, M., 2016. Global Methanol Outlook [WWW Document]. Methanol.Org. URL <http://www.methanol.org/wp-content/uploads/2016/07/Marc-Alvarado-Global-Methanol-February-2016-IMPCA-for-upload-to-website.pdf> (accessed 1.1.19).
10. Anson, A., Wang, Y., Lin, C.C.H., Kuznicki, T.M., Kuznicki, S.M., 2008. Adsorption of ethane and ethylene on modified ETS-10. *Chem. Eng. Sci.* 63, 4171–4175. <https://doi.org/10.1016/j.ces.2008.05.038>
11. Armor, J.N., 1994. Separation Technology, in: Vansant, E.F. (Ed.), *Separation Technology*. Elsevier Inc., Amsterdam, p. 163.
12. Arya, A., Divekar, S., Rawat, R., Gupta, P., Garg, M.O., Dasgupta, S., Nanoti, A., Singh, R., Xiao, P., Webley, P.A., 2015. Upgrading Biogas at Low Pressure by Vacuum Swing Adsorption. *Ind. Eng. Chem. Res.* 54, 404–413. <https://doi.org/10.1021/ie503243f>

Bibliography

13. Ayawei, N., Ebelegi, A.N., Wankasi, D., 2017. Modelling and Interpretation of Adsorption Isotherms. *J. Chem.* 2017, 1–11. <https://doi.org/10.1155/2017/3039817>
14. Bagreev, A., Katikaneni, S., Parab, S., Bandosz, T.J., 2005. Desulfurization of digester gas: prediction of activated carbon bed performance at low concentrations of hydrogen sulfide. *Catal. Today* 99, 329–337. <https://doi.org/10.1016/j.cattod.2004.10.008>
15. Bakken, E., Cobden, P.D., Henriksen, P.P., Håkonsen, S.F., Spjelkavik, A.I., Stange, M., Stensrød, R.E., Vistad, Ø., Blom, R., 2011. Development of CO₂ sorbents for the SEWGS process using high throughput techniques. *Energy Procedia* 4, 1104–1109. <https://doi.org/10.1016/j.egypro.2011.01.161>
16. Bartholomew, C.H., Farrauto, R.J., 2005. Fundamentals of industrial catalytic processes, *Fundamentals of industrial catalytic process*. John Wiley & Sons, Inc., New Jersey.
17. Berlin, N.H., 1966. Method for providing an oxygen-enriched environment.
18. Brunauer, S., Emmett, P.H., Teller, E., 1938. Adsorption of Gases in Multimolecular Layers. *J. Am. Chem. Soc.* 60, 309–319. <https://doi.org/10.1021/ja01269a023>
19. Bryan, P.F., 2004. Removal of Propylene from Fuel-Grade Propane. *Sep. Purif. Rev.* 33, 157–182. <https://doi.org/10.1081/SPM-200042095>
20. Cabrera, A.L., Zehner, J.E., Coe, C.G., Gaffney, T.R., Farris, T.S., Armor, J.N., 1993. Preparation of carbon molecular sieves, I. Two-step hydrocarbon deposition with a single hydrocarbon. *Carbon N. Y.* 31, 969–976. [https://doi.org/10.1016/0008-6223\(93\)90200-T](https://doi.org/10.1016/0008-6223(93)90200-T)
21. Calleja, G., Jimenez, A., Pau, J., Domínguez, L., Pérez, P., 1994. Multicomponent adsorption equilibrium of ethylene, propane, propylene and CO₂ on 13X zeolite. *Gas Sep. Purif.* 8, 247–256. [https://doi.org/http://dx.doi.org/10.1016/0950-4214\(94\)80005-7](https://doi.org/http://dx.doi.org/10.1016/0950-4214(94)80005-7)
22. Campo, M.C., Ribeiro, A.M., Ferreira, A., Santos, J.C., Lutz, C., Loureiro, J.M., Rodrigues, A.E., 2013. New 13X zeolite for propylene/propane separation by vacuum swing adsorption. *Sep. Purif. Technol.* 103, 60–70. <https://doi.org/10.1016/j.seppur.2012.10.009>
23. Cen, P., Yang, R.T., 1985. Separation of a Five-Component Gas Mixture by Pressure Swing Adsorption. *Sep. Sci. Technol.* 20, 725–747. <https://doi.org/10.1080/01496398508060701>
24. Chandrasekhar, V., Mohapatra, C., Banerjee, R., Mallick, A., 2013. Synthesis, Structure, and H₂/CO₂ Adsorption in a Three-Dimensional 4-Connected Triorganotin

Bibliography

- Coordination Polymer with a sqc Topology. *Inorg. Chem.* 52, 3579–3581.
<https://doi.org/10.1021/ic302528b>
25. Chao, S., Han, S., Kim, J., K, C., Choudary, N. V., Kumar, B., 1998. Adsorbents and methods for the separation of ethylene and propylene and/or unsaturated hydrocarbons from mixed gases. US Patent Application US/2002/0005118 A1.
[https://doi.org/10.1016/j.\(73\)](https://doi.org/10.1016/j.(73))
26. Chapin, L.E., Liolios, G.C., Robertson, T.M., 1985. Which alkylation--HF or H₂SO₄. *Hydrocarb. Process.* 64, 67.
27. Chatterjee, S., De, S., 2014. Adsorptive removal of fluoride by activated alumina doped cellulose acetate phthalate (CAP) mixed matrix membrane. *Sep. Purif. Technol.* 125, 223–238. <https://doi.org/https://doi.org/10.1016/j.seppur.2014.01.055>
28. Chatterjee, S., Mondal, S., De, S., 2018. Design and scaling up of fixed bed adsorption columns for lead removal by treated laterite. *J. Clean. Prod.* 177, 760–774.
<https://doi.org/https://doi.org/10.1016/j.jclepro.2017.12.249>
29. Chen, X., Ming, S., Wu, X., Chen, C., Asumana, C., Yu, G., 2013. Cu(I)-Based Ionic Liquids as Potential Absorbents to Separate Propylene and Propane. *Sep. Sci. Technol. (Philadelphia, PA, United States)* 48, 2317–2323.
<https://doi.org/10.1080/01496395.2013.794836>
30. Chen, Y.D., Yang, R.T., Uawithya, P., 1994. Diffusion of oxygen, nitrogen and their mixtures in carbon molecular sieve. *AIChE J.* 40, 577–585.
<https://doi.org/10.1002/aic.690400402>
31. Cheripally, G.S., Mannava, A., Kumar, G., Gupta, R., Saha, P., Mandal, B., Uppaluri, R., Gumma, S., Ghoshal, A.K., 2013. Measurement and Modeling of Adsorption of Lower Hydrocarbons on Activated Carbon. *J. Chem. Eng. Data* 58, 1606–1612.
<https://doi.org/10.1021/je3013217>
32. Choudary, N. V., Kumar, P., Bhat, T.S.G., Cho, S.H., Han, S.S., Kim, J.N., 2002. Adsorption of Light Hydrocarbon Gases on Alkene-Selective Adsorbent. *Ind. Eng. Chem. Res.* 41, 2728–2734. <https://doi.org/10.1021/ie010546+>
33. Chowdhury, P., Bikkina, C., Meister, D., Dreisbach, F., Gumma, S., 2009. Comparison of adsorption isotherms on Cu-BTC metal organic frameworks synthesized from different routes. *Microporous Mesoporous Mater.* 117, 406–413.
<https://doi.org/https://doi.org/10.1016/j.micromeso.2008.07.029>
34. Chowdhury, T., Shi, M., Hashisho, Z., Sawada, J. a., Kuznicki, S.M., 2012. Regeneration of Na-ETS-10 using microwave and conductive heating. *Chem. Eng. Sci.*

Bibliography

- 75, 282–288. <https://doi.org/10.1016/j.ces.2012.03.039>
35. Comito, R.J., Metzger, E.D., Wu, Z., Zhang, G., Hendon, C.H., Miller, J.T., Dincă, M., 2017. Selective Dimerization of Propylene with Ni-MFU-4l. *Organometallics* 36, 1681–1683. <https://doi.org/10.1021/acs.organomet.7b00178>
36. Costa, E., Calleja, G., Jimenez, A., Pau, J., 1991. Adsorption equilibrium of ethylene, propane, propylene, carbon dioxide, and their mixtures on 13X zeolite. *J. Chem. Eng. Data* 36, 218–224. <https://doi.org/10.1021/je00002a020>
37. Da Silva, F.A., Rodrigues, A.E., 2001a. Propylene/Propane Separation by Vacuum Swing Adsorption Using 13X Zeolite. *AIChE J.* 47, 341–357.
38. Da Silva, F.A., Rodrigues, A.E., 2001b. Vacuum Swing Adsorption for Propylene/Propane Separation with 4A Zeolite. *Ind. Eng. Chem. Res.* 40, 5758–5774. <https://doi.org/10.1021/ie0008732>
39. Da Silva, F.A., Rodrigues, A.E., 1999. Adsorption Equilibria and Kinetics for Propylene and Propane over 13X and 4A Zeolite Pellets. *Ind. Eng. Chem. Res.* 38, 2051–2057. <https://doi.org/10.1021/ie980640z>
40. Das, T.K., Chandwadkar, A.J., Budhkar, A.P., Sivasanker, S., 1996. Studies on the synthesis of ETS-10 II. Use of organic templates. *Microporous Mater.* 5, 401–410. [https://doi.org/10.1016/0927-6513\(95\)00075-5](https://doi.org/10.1016/0927-6513(95)00075-5)
41. Dasgupta, S., Divekar, S., Aarti, Spjelkavik, A.I., Didriksen, T., Nanoti, A., Blom, R., 2015. Adsorption properties and performance of CPO-27-Ni/alginate spheres during multicycle pressure-vacuum-swing adsorption (PVSA) CO₂ capture in the presence of moisture. *Chem. Eng. Sci.* 137, 525–531. <https://doi.org/10.1016/j.ces.2015.06.064>
42. Dasgupta, S., Nanoti, A., Gupta, P., Jena, D., Goswami, A.N., Garg, M.O., 2009. Carbon di-oxide removal with mesoporous adsorbents in a single column pressure swing adsorber. *Sep. Sci. Technol.* 44, 3973–3983. <https://doi.org/10.1080/01496390903183170>
43. Dickey, A.N., Yazaydin, A.Ö., Willis, R.R., Snurr, R.Q., 2012. Screening CO₂/N₂ selectivity in metal-organic frameworks using Monte Carlo simulations and ideal adsorbed solution theory. *Can. J. Chem. Eng.* 90, 825–832. <https://doi.org/10.1002/cjce.20700>
44. Dietzel, P.D.C., Johnsen, R.E., Fjellvåg, H., Bordiga, S., Groppo, E., Chavan, S., Blom, R., 2008. Adsorption properties and structure of CO₂ adsorbed on open coordination sites of metal-organic framework Ni₂(dhtp) from gas adsorption, IR spectroscopy and X-ray diffraction. *Chem. Commun.* 5125–5127. <https://doi.org/10.1039/B810574J>

Bibliography

45. Dietzel, P.D.C., Panella, B., Hirscher, M., Blom, R., Fjellvåg, H., 2006. Hydrogen adsorption in a nickel based coordination polymer with open metal sites in the cylindrical cavities of the desolvated framework. *Chem. Commun.* 1, 959–961. <https://doi.org/10.1039/b515434k>
46. Divekar, S., Nanoti, A., Dasgupta, S., Aarti, Chauhan, R., Gupta, P., Garg, M.O., Singh, S.P., Mishra, I.M., 2016. Adsorption equilibria of propylene and propane on zeolites and prediction of their binary adsorption with the ideal adsorbed solution theory. *J. Chem. Eng. Data* 61, 2629–2637. <https://doi.org/10.1021/acs.jced.6b00294>
47. Do, D.D., 1998. *Adsorption Analysis: Equilibria and Kinetics*, Chemical Engineering. Imperial College Press, London. <https://doi.org/10.1142/9781860943829>
48. Eisele, P., Killpack, R., 2012. Propene. *Ullmann's Encycl. Ind. Chem.* https://doi.org/10.1002/14356007.a22_211.pub2
49. Everett, D.H., 1972. Definitions, Terminology and Symbols in Colloid and Surface Chemistry. *Pure Appl. Chem.* 31, 579–638.
50. Ferreira, A., Lin, Z., Anderson, M.W., 1998. Synthesis of microporous titanosilicate ETS-10 from TiCl₄ and TiO₂: a comprehensive study 23, 253–263.
51. Freundlich, H., 1931. Of the adsorption of gases. Section II. Kinetics and energetics of gas adsorption. *Trans. Faraday Soc* 28, 195–201. <https://doi.org/10.1039/TF9322800195>
52. Garci, A., Delgado, A., Uguina, A., Vicente, I.A., 2008. Adsorption and Diffusion Parameters of Methane and Nitrogen on Microwave-Synthesized ETS-4 6107–6115.
53. Ghosh, T.K., Lin, H. Da, Hines, A.L., 1993. Hybrid adsorption-distillation process for separating propane and propylene. *Ind. Eng. Chem. Res.* 32, 2390–2399. <https://doi.org/10.1021/ie00022a024>
54. Ginsberg, J., 1996. Sohio Acrylonitrile Process National Historic Chemical Landmark Brief History of Acrylonitrile [WWW Document]. *Am. Chem. Soc.* URL <https://www.acs.org/content/acs/en/education/whatischemistry/landmarks/acrylonitrile.html> (accessed 1.12.18).
55. Grande, C.A., Blom, R., Andreassen, K.A., Stensrød, R.E., 2017. Experimental Results of Pressure Swing Adsorption (PSA) for Pre-combustion CO₂ Capture with Metal Organic Frameworks. *Energy Procedia* 114, 2265–2270. <https://doi.org/https://doi.org/10.1016/j.egypro.2017.03.1364>
56. Grande, C. A., Cavenati, S., Da Silva, F.A., Rodrigues, A.E., 2005. Carbon molecular sieves for hydrocarbon separations by adsorption. *Ind. Eng. Chem. Res.* 44, 7218–7227.

Bibliography

- <https://doi.org/10.1021/ie050376r>
57. Grande, C. A., Firpo, N., Basaldella, E., E., R.A., 2005. Propane / Propene Separation by SBA-15 and π -Complexated Ag-SBA-15. *Adsorption* 11, 775–780.
58. Grande, C.A., Gascon, J., Kapteijn, F., Rodrigues, A.E., 2010a. Propane/propylene separation with Li-exchanged zeolite 13X. *Chem. Eng. J.* 160, 207–214.
<https://doi.org/10.1016/j.cej.2010.03.044>
59. Grande, C.A., Gigola, C., Irio, A.L., Rodrigues, E., 2003a. Propane – Propylene Binary Adsorption on Zeolite 4A. *Adsorption* 9, 321–329.
60. Grande, C.A., Gigola, C., Rodrigues, A.E., 2002. Adsorption of Propane and Propylene in Pellets and Crystals of 5A Zeolite. *Ind. Eng. Chem. Res.* 41, 85–92.
<https://doi.org/10.1021/ie010494o>
61. Grande, C.A., Poplow, F., Rodrigues, A.E., 2010b. Vacuum pressure swing adsorption to produce polymer-grade propylene. *Sep. Sci. Technol.* 45, 1252–1259.
<https://doi.org/10.1080/01496391003652767>
62. Grande, C.A., Rodrigues, A.E., 2005. Propane/Propylene Separation by Pressure Swing Adsorption Using Zeolite 4A. *Ind. Eng. Chem. Res.* 44, 8815–8829.
<https://doi.org/10.1021/ie050671b>
63. Grande, C.A., Rodrigues, A.E., 2004. Adsorption of Binary Mixtures of Propane–Propylene in Carbon Molecular Sieve 4A. *Ind. Eng. Chem. Res.* 43, 8057–8065. <https://doi.org/10.1021/ie049327p>
64. Grande, C.A., Silva, V.M.T.M., Gigola, C., 2003b. Adsorption of propane and propylene onto carbon molecular sieve. *Carbon N. Y.* 41, 2533–2545.
65. Hanif, A., Dasgupta, S., Divekar, S., Arya, A., Garg, M.O., Nanoti, A., 2014. A study on high temperature CO₂ capture by improved hydrotalcite sorbents. *Chem. Eng. J.* 236, 91–99. <https://doi.org/10.1016/j.cej.2013.09.076>
66. He, Y., Zhou, W., Qian, G., Chen, B., 2014. Methane storage in metal–organic frameworks. *Chem. Soc. Rev.* 43, 5657–5678. <https://doi.org/10.1039/C4CS00032C>
67. Hoffmann, E. De, Stroobant, V., 2007. *Mass Spectrometry Principles and Applications Third Edition, Mass spectrometry reviews.* <https://doi.org/10.1002/mas.20296>
68. Horváth, G., Kawazoe, K., 1983. Method for the calculation of effective pore size distribution in molecular sieve carbon. *J. Chem. Eng. Japan* 16, 470–475.
<https://doi.org/10.1252/jcej.16.470>
69. Houdek, J., Hemler, C., Pittman, R., Upson, L., 2001. Developing a process for the new century. *Pet. Technol. Q.* 6, 141.

Bibliography

70. Hutson, N.D., Yang, R.T., 1997. Theoretical basis for the Dubinin-Radushkevitch (D-R) adsorption isotherm equation. *Adsorption* 3, 189–195.
<https://doi.org/10.1007/BF01650130>
71. Iler, R.K., 1979. *The Chemistry of Silica: Solubility, Polymerization, Colloid and Surface Properties and Biochemistry of Silica*. Wiley, New York.
72. Jahn-Teller Effect [WWW Document], n.d. URL https://en.wikipedia.org/wiki/Jahn-Teller_effect (accessed 3.6.19).
73. Jaroniec, M., Choma, J., Lu, X., 1991. An improved method for evaluating the micropore-size distribution from adsorption isotherm. *Chem. Eng. Sci.* 46, 3299–3301.
[https://doi.org/https://doi.org/10.1016/0009-2509\(91\)85033-T](https://doi.org/https://doi.org/10.1016/0009-2509(91)85033-T)
74. Jarvelin, H., Fair, J.R., 1993. Adsorptive separation of propylene-propane mixtures. *Ind. Eng. Chem. Res.* 32, 2201–2207. <https://doi.org/10.1021/ie00022a001>
75. Jasper, S., El-Halwagi, M., 2015. A Techno-Economic Comparison between Two Methanol-to-Propylene Processes. *Processes* 3, 684–698.
<https://doi.org/10.3390/pr3030684>
76. Jiang, Y., Ling, J., Xiao, P., He, Y., Zhao, Q., Chu, Z., Liu, Y., Li, Z., Webley, P.A., 2018. Simultaneous biogas purification and CO₂ capture by vacuum swing adsorption using zeolite NaUSY. *Chem. Eng. J.* 334, 2593–2602.
<https://doi.org/https://doi.org/10.1016/j.cej.2017.11.090>
77. Joshi, G. V., Patel, H.A., Bajaj, H.C., Jasra, R. V, 2009. Intercalation and controlled release of vitamin B6 from montmorillonite--vitamin B6 hybrid. *Colloid Polym. Sci.* 287, 1071–1076. <https://doi.org/10.1007/s00396-009-2067-3>
78. Kapoor, A., Yang, R.T., 1989. Kinetic separation of methane—carbon dioxide mixture by adsorption on molecular sieve carbon. *Chem. Eng. Sci.* 44, 1723–1733.
[https://doi.org/10.1016/0009-2509\(89\)80014-4](https://doi.org/10.1016/0009-2509(89)80014-4)
79. Kapur, M., Mondal, M.K., 2013. Mass transfer and related phenomena for Cr(VI) adsorption from aqueous solutions onto *Mangifera indica* sawdust. *Chem. Eng. J.* 218, 138–146. <https://doi.org/10.1016/J.CEJ.2012.12.054>
80. Karmakar, S., Roy, D., Janiak, C., De, S., 2019. Insights into multi-component adsorption of reactive dyes on MIL-101-Cr metal organic framework: Experimental and modeling approach. *Sep. Purif. Technol.* 215, 259–275.
<https://doi.org/https://doi.org/10.1016/j.seppur.2019.01.013>
81. Keller, G.E., E., M.A., Verma, S.K., Williamson, K.D., 1992. “Olefin Recovery and Purification via Silver Complexation,” in *Separation and Purification Technology*, 1st

Bibliography

- ed. Marcel Dekker, New York.
82. Khalighi, M., Chen, Y.F., Farooq, S., Karimi, I.A., Jiang, J.W., 2013a. Propylene/Propane Separation Using SiCHA. *Ind. Eng. Chem. Res.* 52, 3877–3892. <https://doi.org/10.1021/ie3026955>
83. Khalighi, M., Chen, Y.F., Farooq, S., Karimi, I.A., Jiang, J.W., 2013b. Propylene / Propane Separation Using SiCHA.
84. Khalighi, M., Karimi, I.A., Farooq, S., 2014. Comparing SiCHA and 4A zeolite for propylene/propane separation using a surrogate-based simulation/optimization approach. *Ind. Eng. Chem. Res.* 53, 16973–16983. <https://doi.org/10.1021/ie404392j>
85. Khashimova, D., Keil, F.J., Kholmatov, K., 2008. Alkanes in Zeolites - Molecular Simulations , Empirical Isotherms, Mixtures. *J. Univ. Chem. Technol. Metall.* 43, 335–344.
86. Kim, W.J., Lee, M.C., Yoo, J.C., Hayhurst, D.T., 2000. Study on the rapid crystallization of ETS-4 and ETS-10. *Microporous Mesoporous Mater* 41, 79–88.
87. Ko, C.H., Han, S.S., Park, J.H., Cho, S.H., Kim, J.N., 2006. Silver nitrate impregnated pellet-type adsorbents for propylene/propane separation. *Ind. Eng. Chem. Res.* 45, 9129–9135. <https://doi.org/10.1021/ie051119p>
88. Kuah, W.C., Effendy, S., Farooq, S., 2018. Industrial Scale Propylene/Propane Separation Using Pressure Vacuum Swing Adsorption. *Ind. Eng. Chem. Res.* 57, 6451–6463. <https://doi.org/10.1021/acs.iecr.8b00289>
89. Kumar, R., 1990. Adsorption process for recovering two high purity gas products from multicomponent gas mixtures. US 4913709. <https://doi.org/10.13140/RG.2.2.22077.92647>
90. Kumar, R., Golden, T.C., White, T.R., Rokicki, A., 1992. Novel Adsorption Distillation Hybrid Scheme for Propane/Propylene Separation. *Sep. Sci. Technol.* 27, 2157–2170. <https://doi.org/10.1080/01496399208019472>
91. Kuznicki, S.M., 1987. Large-pored crystalline titanium molecular sieve zeolites. US4853202A.
92. Lamia, N., Wolff, L., Leflaive, P., Leinekugel-Le-Cocq, D., Gomes, P.S., Grande, C.A., Rodrigues, A.E., 2008. Equilibrium and fixed bed adsorption of 1-butene, propylene and propane over 13X zeolite pellets. *Sep. Sci. Technol.* 43, 1124–1156. <https://doi.org/10.1080/01496390801888136>
93. Langmuir, I., 1916. The constitution and fundamental properties of solids and liquids. *J. Am. Chem. Soc.* 38, 2221–2295.

Bibliography

94. Liu, J., Liu, Y., Kayrak Talay, D., Calverley, E., Brayden, M., Martinez, M., 2015. A new carbon molecular sieve for propylene/propane separations. *Carbon* N. Y. 85. <https://doi.org/10.1016/j.carbon.2014.12.089>
95. Liu, J., Tian, J., Thallapally, P.K., McGrail, B.P., 2012. Selective CO₂ Capture from Flue Gas Using Metal–Organic Frameworks—A Fixed Bed Study. *J. Phys. Chem. C* 116, 9575–9581. <https://doi.org/10.1021/jp300961j>
96. Lowell, S., Shields, J.E., 1984. Adsorption isotherms, in: *Powder Surface Area and Porosity*. Springer Netherlands, Dordrecht, pp. 11–13. https://doi.org/10.1007/978-94-009-5562-2_3
97. Lowell, S., Shields, J.E., Thomas, M.A., Thommes, M., 2004. Characterization of Porous Solids and Powders Surface Area Pore Size and Density. <https://doi.org/10.1007/s13398-014-0173-7.2>
98. Luna-Triguero, A., Vicent-Luna, J.M., Becker, T.M., Vlught, T.J.H., Dubbeldam, D., Gómez-Álvarez, P., Calero, S., 2017. Effective Model for Olefin/Paraffin Separation using (Co, Fe, Mn, Ni)-MOF-74. *ChemistrySelect* 2, 665–672. <https://doi.org/10.1002/slct.201601095>
99. Lv, L., Su, F., Zhao, X.S., 2004. A reinforced study on the synthesis of microporous titanosilicate ETS-10. *Microporous Mesoporous Mater.* 76, 113–122. <https://doi.org/https://doi.org/10.1016/j.micromeso.2004.08.004>
100. Lv, L., Tsoi, G., Zhao, X.S., 2004. Uptake Equilibria and Mechanisms of Heavy Metal Ions on Microporous Titanosilicate ETS-10. *Ind. Eng. Chem. Res.* 43, 7900–7906. <https://doi.org/10.1021/ie0498044>
101. Maghsoudi, H., 2015. Equilibrium adsorption analysis of microporous adsorbents in propene/propane binary mixture separation. *Adsorption* 21, 547–556. <https://doi.org/10.1007/s10450-015-9695-3>
102. Maiti, A., DasGupta, S., Basu, J.K., De, S., 2007. Adsorption of arsenite using natural laterite as adsorbent. *Sep. Purif. Technol.* 55, 350–359. <https://doi.org/https://doi.org/10.1016/j.seppur.2007.01.003>
103. Malek, A., Farooq, S., 1998. Hydrogen purification from refinery fuel gas by pressure swing adsorption. *AIChE J.* 44, 1985–1992. <https://doi.org/10.1002/aic.690440906>
104. Malek, A., Farooq, S., 1996. Comparison of isotherm models for hydrocarbon adsorption on activated carbon. *AIChE J.* 42, 3191–3201. <https://doi.org/10.1002/aic.690421120>
105. Mallick, A., Saha, S., Pachfule, P., Roy, S., Banerjee, R., 2010. Selective CO₂ and H₂

Bibliography

- adsorption in a chiral magnesium-based metal organic framework (Mg-MOF) with open metal sites. *J. Mater. Chem.* 20, 9073–9080. <https://doi.org/10.1039/C0JM01125H>
106. Mallick, A., Schön, E.-M., Panda, T., Sreenivas, K., Díaz, D.D., Banerjee, R., 2012. Fine-tuning the balance between crystallization and gelation and enhancement of CO₂ uptake on functionalized calcium based MOFs and metallogels. *J. Mater. Chem.* 22, 14951–14963. <https://doi.org/10.1039/C2JM30866E>
107. Manu, V., Mody, H.M., Bajaj, H.C., Jasra, R. V, 2009. Adsorption of Cu²⁺ on Amino Functionalized Silica Gel with Different Loading. *Ind. Eng. Chem. Res.* 48, 8954–8960. <https://doi.org/10.1021/ie900273v>
108. Masala, A., Vitillo, J.G., Mondino, G., Grande, C.A., Blom, R., Manzoli, M., Marshall, M., Bordiga, S., 2017. CO₂ Capture in Dry and Wet Conditions in UTSA-16 Metal–Organic Framework. *ACS Appl. Mater. Interfaces* 9, 455–463. <https://doi.org/10.1021/acsami.6b13216>
109. Mason, J.A., Sumida, K., Herm, Z.R., Krishna, R., Long, J.R., 2011. Evaluating metal-organic frameworks for post-combustion carbon dioxide capture via temperature swing adsorption. *Energy Environ. Sci.* 4, 3030–3040. <https://doi.org/10.1039/c1ee01720a>
110. Mathias, P.M., Kumar, R., Moyer, J.D., Schork, J.M., Srinivasan, S.R., Auvil, S.R., Talu, O., 1996. Correlation of multicomponent gas adsorption by the dual-site Langmuir model. Application to nitrogen/oxygen adsorption on 5A-zeolite. *Ind. Eng. Chem. Res.* 35, 2477–2483. <https://doi.org/10.1021/ie950291y>
111. Miltenburg, A., Zhu, W., Kapteijn, F., Moulijn, J.A., 2006. Adsorptive separation of light olefin / paraffin mixtures 350–354. <https://doi.org/10.1205/cherd05021>
112. Mishra, P., Mekala, S., Dreisbach, F., Mandal, B., Gumma, S., 2012. Adsorption of CO₂, CO, CH₄ and N₂ on a zinc based metal organic framework. *Sep. Purif. Technol.* 94, 124–130. <https://doi.org/https://doi.org/10.1016/j.seppur.2011.09.041>
113. Mishra, P., Uppara, H.P., Mandal, B., Gumma, S., 2014. Adsorption and Separation of Carbon Dioxide Using MIL-53(Al) Metal-Organic Framework. *Ind. Eng. Chem. Res.* 53, 19747–19753. <https://doi.org/10.1021/ie5006146>
114. Mofarahi, M., Sadrameli, M., Towfighi, J., 2005. Four-Bed Vacuum Pressure Swing Adsorption Process for Propylene/Propane Separation. *Ind. Eng. Chem. Res.* 44, 1557–1564. <https://doi.org/10.1021/ie034016k>
115. Mofarahi, M., Salehi, S.M., 2012. Pure and binary adsorption isotherms of ethylene and ethane on zeolite 5A. *Adsorption* 19, 101–110. <https://doi.org/10.1007/s10450-012-9423-1>

Bibliography

116. Mofarahi, M., Sayyedi, M., 2009. Pure and Binary Adsorption Isotherms of Nitrogen and Oxygen on Zeolite 5A. *J. Chem. Eng. Data* 6–13. <https://doi.org/10.1021/je8006919>
117. Mohan, S.V., Karthikeyan, J., 1997. Removal of lignin and tannin colour from aqueous solution by adsorption onto activated charcoal. *Environ. Pollut.* 97, 183–187. [https://doi.org/https://doi.org/10.1016/S0269-7491\(97\)00025-0](https://doi.org/https://doi.org/10.1016/S0269-7491(97)00025-0)
118. Mohan, S.V., Ramanaih, S. V, Sarma, P.N., 2008. Biosorption of direct azo dye from aqueous phase onto *Spirogyra* sp. I02: Evaluation of kinetics and mechanistic aspects. *Biochem. Eng. J.* 38, 61–69. <https://doi.org/https://doi.org/10.1016/j.bej.2007.06.014>
119. Mohan, S.V., Rao, N.C., Karthikeyan, J., 2002. Adsorptive removal of direct azo dye from aqueous phase onto coal based sorbents: a kinetic and mechanistic study. *J. Hazard. Mater.* 90, 189–204. [https://doi.org/https://doi.org/10.1016/S0304-3894\(01\)00348-X](https://doi.org/https://doi.org/10.1016/S0304-3894(01)00348-X)
120. Mondal, M. K., 2009. Removal of Pb(II) ions from aqueous solution using activated tea waste: Adsorption on a fixed-bed column. *J. Environ. Manage.* 90, 3266–3271. <https://doi.org/https://doi.org/10.1016/j.jenvman.2009.05.025>
121. Mondal, M.K., 2010. Removal of Pb(II) from aqueous solution by adsorption using activated tea waste. *Korean J. Chem. Eng.* 27, 144–151. <https://doi.org/10.1007/s11814-009-0304-6>
122. Moulijn, J.A., Makkee, M., Van-Diepen, A., 2013. *Chemical Process Technology*, 2nd ed. John Wiley & Sons, Inc., Chichester.
123. Mukherjee, R., De, S., 2016. Preparation, characterization and application of powdered activated carbon-cellulose acetate phthalate mixed matrix membrane for treatment of steel plant effluent. *Polym. Adv. Technol.* 27, 444–459. <https://doi.org/10.1002/pat.3690>
124. Munshieva, M.K., 2001. Propylene dimerization over nickel-ion exchanged zeolites in the liquid phase. *Turkish J. Chem.* 25, 419–423.
125. Myers, A.L., Prausnitz, J.M., 1965. Thermodynamics of mixed-gas adsorption. *AIChE J.* 11, 121–127.
126. Myers, A.L., Valenzuela, D., 1986. Computer algorithm and graphical method for calculating adsorption equilibria of gas mixtures. *J. Chem. Eng. Japan* 19, 392–396. <https://doi.org/10.1252/jcej.19.392>
127. Narayan, R., Meena, R.P., Patel, A.K., Prajapati, A.K., Srivastava, S., Mondal, M.K., 2016. Characterization and application of biomass gasifier waste material for adsorptive removal of Cr (VI) from aqueous solution. *Environ. Prog. Sustain. Energy* 35, 95–102.

Bibliography

- <https://doi.org/10.1002/ep.12205>
128. Narin, G., Ribeiro, A.M., Ferreira, A., Hwang, Y.K., Lee, U.-H., Loureiro, J.M., Chang, J.-S., Rodrigues, A.E., 2014. Propylene/Nitrogen Separation in a By-Stream of the Polypropylene Production: From Pilot Test and Model Validation to Industrial Scale Process Design and Optimization. *Ind. Eng. Chem. Res.* 53, 9199–9213.
<https://doi.org/10.1021/ie4031727>
129. Ntiamoah, A., Ling, J., Xiao, P., Webley, P.A., Zhai, Y., 2016. CO₂ Capture by Temperature Swing Adsorption: Use of Hot CO₂-Rich Gas for Regeneration. *Ind. Eng. Chem. Res.* 55, 703–713. <https://doi.org/10.1021/acs.iecr.5b01384>
130. Ntiamoah, A., Ling, J., Xiao, P., Webley, P.A., Zhai, Y., 2015. CO₂ capture by vacuum swing adsorption: role of multiple pressure equalization steps. *Adsorption* 21, 509–522. <https://doi.org/10.1007/s10450-015-9690-8>
131. Oden, E.C., Burch, W.J., 1949. Alkylation of Isobutane with Propylene - Commercial Production using Sulfuric Acid Catalyst. *Ind. Eng. Chem.* 41, 2524–2530.
<https://doi.org/10.1021/ie50479a034>
132. Padin, J., Yang, R.T., 2000. New sorbents for olefin / paraffin separations by adsorption via π -complexation : synthesis and effects of substrates 55, 2607–2616.
133. Pan, Y., Li, T., Lestari, G., Lai, Z., 2012. Effective separation of propylene/propane binary mixtures by ZIF-8 membranes. *J. Memb. Sci.* 390–391, 93–98.
<https://doi.org/10.1016/j.memsci.2011.11.024>
134. Park, J.-H., Kim, J.-N., Cho, S.-H., 2000. Performance analysis of four-bed H₂ PSA process using layered beds. *AIChE J.* 46, 790–802.
<https://doi.org/10.1002/aic.690460413>
135. Patel, H.A., Somani, R.S., Bajaj, H.C., Jasra, R. V, 2006. Nanoclays for polymer nanocomposites, paints, inks, greases and cosmetics formulations, drug delivery vehicle and waste water treatment. *Bull. Mater. Sci.* 29, 133–145.
<https://doi.org/10.1007/BF02704606>
136. Pawar, R.R., Patel, H.A., Sethia, G., Bajaj, H.C., 2009. Selective adsorption of carbon dioxide over nitrogen on calcined synthetic hectorites with tailor-made porosity. *Appl. Clay Sci.* 46, 109–113. <https://doi.org/https://doi.org/10.1016/j.clay.2009.07.009>
137. PEMRG, 2016. World Plastics Production 1950 – 2015 [WWW Document]. *Plast. Mark. Res. Gr. / Consult. Mark. Ind. GmbH*. URL [https://committee.iso.org/files/live/sites/tc61/files/The Plastic Industry Berlin Aug 2016 - Copy.pdf](https://committee.iso.org/files/live/sites/tc61/files/The%20Plastic%20Industry%20Berlin%20Aug%202016%20-%20Copy.pdf) (accessed 1.20.19).

Bibliography

138. Pires, J., Pinto, M.L., Granadeiro, C.M., Barbosa, A.D.S., Cunha-Silva, L., Balula, S.S., Saini, V.K., 2014a. Effect on selective adsorption of ethane and ethylene of the polyoxometalates impregnation in the metal-organic framework MIL-101. *Adsorption* 20, 533–543. <https://doi.org/10.1007/s10450-013-9592-6>
139. Pires, J., Pinto, M.L., Saini, V.K., 2014b. Ethane Selective IRMOF-8 and Its Significance in Ethane–Ethylene Separation by Adsorption. *ACS Appl. Mater. Interfaces* 6, 12093–12099. <https://doi.org/10.1021/am502686g>
140. Pires, J., Saini, V.K., Pinto, M.L., 2008. Studies on Selective Adsorption of Biogas Components on Pillared Clays: Approach for Biogas Improvement. *Environ. Sci. Technol.* 42, 8727–8732. <https://doi.org/10.1021/es8014666>
141. Plaza, M.G., Ribeiro, A.M., Ferreira, A., Santos, J.C., Lee, U.H., Chang, J.S., Loureiro, J.M., Rodrigues, A.E., 2012. Propylene/propane separation by vacuum swing adsorption using Cu-BTC spheres. *Sep. Purif. Technol.* 90, 109–119. <https://doi.org/10.1016/j.seppur.2012.02.023>
142. Prasanth, K.P., Bajaj, H.C., Chung, H.D., Choo, K.Y., Kim, T.H., Jasra, R. V., 2009. Hydrogen sorption in transition metal modified ETS-10. *Int. J. Hydrogen Energy* 34, 888–896. <https://doi.org/https://doi.org/10.1016/j.ijhydene.2008.10.078>
143. Purkait, M.K., DasGupta, S., De, S., 2005a. Adsorption of eosin dye on activated carbon and its surfactant based desorption. *J. Environ. Manage.* 76, 135–142. <https://doi.org/https://doi.org/10.1016/j.jenvman.2005.01.012>
144. Purkait, M.K., Gusain, D.S., DasGupta, S., De, S., 2005b. Adsorption Behavior of Chrysoidine Dye on Activated Charcoal and Its Regeneration Characteristics by Using Different Surfactants. *Sep. Sci. Technol.* 39, 2419–2440. <https://doi.org/10.1081/SS-120039347>
145. Redlich, O., Peterson, D.L., 1959. A Useful Adsorption Isotherm. *J. Phys. Chem.* 63, 1024. <https://doi.org/10.1021/j150576a611>
146. Rege, S.U., Padin, J., Yang, R.T., 1998. Olefin/paraffin separations by adsorption: π -Complexation vs. kinetic separation. *AIChE J.* 44, 799–809. <https://doi.org/10.1002/aic.690440405>
147. Ribeiro, A.M., Campo, M.C., Narin, G., Santos, J.C., Ferreira, A., Chang, J.-S., Hwang, Y.K., Seo, Y.-K., Lee, U.-H., Loureiro, J.M., Rodrigues, A.E., 2013. Pressure swing adsorption process for the separation of nitrogen and propylene with a MOF adsorbent MIL-100(Fe). *Sep. Purif. Technol.* 110, 101–111. <https://doi.org/10.1016/j.seppur.2013.03.009>

Bibliography

148. Rosson, R., Wampler, J.M., Serkiz, S., Goto, M., Kahn, B., Elliott, W.C., 2007. Freundlich and dual langmuir isotherm models for predicting 137cs binding on savannah river site soils. *Health Phys.* 94, 18–32.
<https://doi.org/10.1097/01.hp.0000278416.04381.31>
149. Ruthven, D.M., 1984. *Principles of Adsorption and Adsorption Processes*. John Wiley & Sons, Inc., New York.
150. Ruthven, D.M., Farooq, S., Knaebel, K.S., 1993. *Pressure Swing Adsorption*. VCH Publishers Inc., New York.
151. Ruthven, D.M., Raghavan, N.S., Hassan, M.M., 1986. Adsorption and diffusion of nitrogen and oxygen in a carbon molecular sieve. *Chem. Eng. Sci.* 41, 1325–1332.
[https://doi.org/https://doi.org/10.1016/0009-2509\(86\)87105-6](https://doi.org/https://doi.org/10.1016/0009-2509(86)87105-6)
152. Ruthven, D.M., Reyes, S.C., 2007. Adsorptive separation of light olefins from paraffins. *Microporous Mesoporous Mater.* 104, 59–66.
<https://doi.org/10.1016/j.micromeso.2007.01.005>
153. Saini, V.K., Pinto, M., Pires, J., 2010. High Pressure Adsorption Studies of Ethane and Ethylene on Clay-Based Adsorbent Materials. *Sep. Sci. Technol.* 46, 137–146.
<https://doi.org/10.1080/01496391003789197>
154. Sanz, R., Martínez, F., Orcajo, G., Wojtas, L., Briones, D., 2013. Synthesis of a honeycomb-like Cu-based metal-organic framework and its carbon dioxide adsorption behaviour. *Dalt. Trans.* 42, 2392–2398. <https://doi.org/10.1039/c2dt32138f>
155. Schell, J., Casas, N., Blom, R., Spjelkavik, A.I., Andersen, A., Cavka, J.H., Mazzotti, M., 2012. MCM-41, MOF and UiO-67/MCM-41 adsorbents for pre-combustion CO₂ capture by PSA: adsorption equilibria. *Adsorption* 18, 213–227.
<https://doi.org/10.1007/s10450-012-9395-1>
156. Seredych, M., Bandosz, T.J., 2010. Adsorption of dibenzothiophenes on activated carbons with copper and iron deposited on their surfaces. *Fuel Process. Technol.* 91, 693–701. <https://doi.org/https://doi.org/10.1016/j.fuproc.2010.01.019>
157. Shi, M., Avila, A.M., Yang, F., Kuznicki, T.M., Kuznicki, S.M., 2011. High pressure adsorptive separation of ethylene and ethane on Na-ETS-10. *Chem. Eng. Sci.* 66, 2817–2822. <https://doi.org/10.1016/j.ces.2011.03.046>
158. Shi, M., Lin, C.C.H., Kuznicki, T.M., Hashisho, Z., Kuznicki, S.M., 2010. Separation of a binary mixture of ethylene and ethane by adsorption on Na-ETS-10. *Chem. Eng. Sci.* 65, 3494–3498. <https://doi.org/10.1016/j.ces.2010.02.048>
159. Sievers, W., Mersmann, A., 1994. *Single and Multicomponent Adsorption Equilibria of*

Bibliography

- Carbon Dioxide, Nitrogen, Carbon Monoxide and Methane in Hydrogen Purification Processes. *Chem. Eng. Technol.* 17, 325–337.
160. Sing, K.S.W., 1994. Physisorption of gases by carbon blacks. *Carbon N. Y.* 32, 1311–1317. [https://doi.org/10.1016/0008-6223\(94\)90117-1](https://doi.org/10.1016/0008-6223(94)90117-1)
161. Sips, R., 1948. On the Structure of a Catalyst Surface. *J. Chem. Phys.* 16, 490–495. <https://doi.org/10.1063/1.1746922>
162. Sircar, S., 1979. Separation of multicomponent gas mixtures. US 4171206.
163. Sivakumar, S. V, Rao, D.P., 2006. A four-bed PSA for clean separation of ethylene-ethane mixture., in: *AIChE Annu. Meet., Conf. Proc. American Institute of Chemical Engineers*, pp. 117e/1-117e/4.
164. Skarstrom, C.W., 1960. Method and apparatus for fractionating gaseous mixtures by adsorption. US 2944627.
165. Spencer, D.H.T., 1967. *Porous Carbon Solids*. Academic Press, New York.
166. Stoeckli, H.F., 1990. Microporous carbons and their characterization: The present state of the art. *Carbon N. Y.* 28, 1–6. [https://doi.org/10.1016/0008-6223\(90\)90086-E](https://doi.org/10.1016/0008-6223(90)90086-E)
167. Stoeckli, H.F., 1977. A generalization of the Dubinin—Radushkevich equation for the filling of heterogeneous micropore systems. *J. Colloid Interface Sci.* 59, 184–185. [https://doi.org/10.1016/0021-9797\(77\)90355-1](https://doi.org/10.1016/0021-9797(77)90355-1)
168. Su, L.L.F., Zhao, X.S., 2006. Synthesis and characterization of microporous titanosilicate ETS-10 with different titanium precursors. *J. Porous Mater.* 13, 263–267. <https://doi.org/10.1007/s10934-006-8014-5>
169. Sun, Y., Webley, P.A., 2010. Preparation of activated carbons from corncob with large specific surface area by a variety of chemical activators and their application in gas storage. *Chem. Eng. J.* 162, 883–892. <https://doi.org/10.1016/j.cej.2010.06.031>
170. Swaidan, R.J., Ghanem, B., Swaidan, R., Litwiller, E., Pinnau, I., 2015. Pure- and mixed-gas propylene/propane permeation properties of spiro- and triptycene-based microporous polyimides. *J. Memb. Sci.* 492, 116–122. <https://doi.org/10.1016/j.memsci.2015.05.044>
171. Tagliabue, M., Millini, R., Blom, R., Zanardi, S., Rizzo, C., Dietzel, P.D.C., 2010. Methane storage on CPO-27-Ni pellets. *J. Porous Mater.* 18, 289–296. <https://doi.org/10.1007/s10934-010-9378-0>
172. Tagliabue, M., Rizzo, C., Millini, R., Dietzel, P.D.C., Blom, R., Zanardi, S., 2011.

Bibliography

- Methane storage on CPO-27-Ni pellets. *J. Porous Mater.* 18, 289–296.
<https://doi.org/10.1007/s10934-010-9378-0>
173. Talu, O., 1998. Needs, status, techniques and problems with binary gas adsorption experiments. *Adv. Colloid Interface Sci.* 76–77, 227–269.
[https://doi.org/10.1016/S0001-8686\(98\)00048-7](https://doi.org/10.1016/S0001-8686(98)00048-7)
174. Tang, X., Ripepi, N., Stadie, N.P., Yu, L., Hall, M.R., 2016. A dual-site Langmuir equation for accurate estimation of high pressure deep shale gas resources. *Fuel* 185, 10–17. <https://doi.org/10.1016/j.fuel.2016.07.088>
175. Taylor, P., Saini, V.K., Pinto, M., Pires, J., 2010. High Pressure Adsorption Studies of Ethane and Ethylene on Clay-Based Adsorbent Materials High Pressure Adsorption Studies of Ethane and Ethylene on Clay-Based Adsorbent Materials. *Sep. Sci. Technol.* 37–41. <https://doi.org/10.1080/01496391003789197>
176. Thinnes, B., 2010. On-purpose propylene production. *Hydrocarb. Process.* 89, 19–21.
177. Thomas, W.J., Crittenden, B., 1998. *Adsorption Technology & Design*. Elsevier Science and Technology Books.
178. Thompson, R.W., 1998. *Recent Advances in the Understanding of Zeolite Synthesis, Synthesis*. Springer Berlin Heidelberg, Berlin, Heidelberg. https://doi.org/10.1007/3-540-69615-6_1
179. Tiscornia, I., Irusta, S., Prádanos, P., Téllez, C., Coronas, J., Santamaría, J., 2007. Preparation and Characterization of Titanosilicate Ag-ETS-10 for Propylene and Propane Adsorption. *J. Phys. Chem. C* 111, 4702–4709.
<https://doi.org/10.1021/jp070044v>
180. Valenzuela, D.P., Myers, A.L., 1989. *Adsorption Equilibrium Data Handbook*. Prentice-Hall, Hemel Hempstead.
181. van Miltenburg, A., Gascon, J., Zhu, W., Kapteijn, F., Moulijn, J. a., 2008. Propylene/propane mixture adsorption on faujasite sorbents. *Adsorption* 14, 309–321.
<https://doi.org/10.1007/s10450-007-9101-x>
182. Vijayaraghavan, K., Padmesh, T.V.N., Palanivelu, K., Velan, M., 2006. Biosorption of nickel(II) ions onto *Sargassum wightii*: Application of two-parameter and three-parameter isotherm models. *J. Hazard. Mater.* 133, 304–308.
<https://doi.org/10.1016/j.jhazmat.2005.10.016>
183. von Gemmingen, U., 1993. A new approach to adsorption isotherms. *Gas Sep. Purif.* 7, 175–181. [https://doi.org/10.1016/0950-4214\(93\)80007-J](https://doi.org/10.1016/0950-4214(93)80007-J)
184. Waghmode, S.B., Thakur, V. V, Sudalai, A., Sivasanker, S., 2001. Efficient liquid

Bibliography

- phase acylation of alcohols over basic ETS-10 molecular sieves. *Tetrahedron Lett.* 42, 3145–3147. [https://doi.org/10.1016/S0040-4039\(01\)00389-6](https://doi.org/10.1016/S0040-4039(01)00389-6)
185. Wattanakarunwong, P., 2015. Propylene Market [WWW Document]. URL <http://irpc.listedcompany.com/misc/PRESN/20150515-propylene-market-analyst.pdf> (accessed 2.26.18).
186. Webley, P.A., Qader, A., Ntiamoah, A., Ling, J., Xiao, P., Zhai, Y., 2017. A New Multi-bed Vacuum Swing Adsorption Cycle for CO₂ Capture from Flue Gas Streams. *Energy Procedia* 114, 2467–2480. <https://doi.org/https://doi.org/10.1016/j.egypro.2017.03.1398>
187. Weston, M.H., Colón, Y.J., Bae, Y.S., Garibay, S.J., Snurr, R.Q., Farha, O.K., Hupp, J.T., Nguyen, S.T., 2014. High propylene/propane adsorption selectivity in a copper(catecholate)-decorated porous organic polymer. *J. Mater. Chem. A* 2, 299. <https://doi.org/10.1039/c3ta12999c>
188. Wu, J., Zhou, L., Sun, Y., Su, W., Zhou, Y., 2007. Measurement and prediction of adsorption equilibrium for a H₂/N₂/CH₄/CO₂ mixture. *AIChE J.* 53, 1178–1191. <https://doi.org/10.1002/aic.11169>
189. Xu, H., Zhang, Y., Navrotsky, A., 2001. Enthalpies of formation of microporous titanosilicates 47, 285–291.
190. Yang, R., 1987. Gas Separation by Adsorption Processes, *Gas Separation & Purification*. [https://doi.org/10.1016/0950-4214\(88\)80042-2](https://doi.org/10.1016/0950-4214(88)80042-2)
191. Yang, R.T., 2003. *Adsorbents: Fundamentals and Applications*. Wiley Interscience.
192. Yang, R.T., 1987. Adsorber Dynamics: Bed Profiles and Breakthrough Curves, in: Yang, R.T. (Ed.), *Gas Separation by Adsorption Processes*. Butterworth-Heinemann, pp. 141–200. <https://doi.org/https://doi.org/10.1016/B978-0-409-90004-0.50008-8>
193. Yu, C., Fan, X., Yu, L., Bandosz, T.J., Zhao, Z., Qiu, J., 2013. Adsorptive Removal of Thiophenic Compounds from Oils by Activated Carbon Modified with Concentrated Nitric Acid. *Energy & Fuels* 27, 1499–1505. <https://doi.org/10.1021/ef400029b>
194. Yun, J.H., Choi, D.K., Kim, S.H., 1999. Equilibria and dynamics for mixed vapors of BTX in an activated carbon bed. *AIChE J.* 45, 751–760. <https://doi.org/10.1002/aic.690450410>
195. Zhao, G.X.S., Lee, J.L., Chia, P.A., 2003. Unusual Adsorption Properties of Microporous Titanosilicate ETS-10 toward Heavy Metal Lead. *Langmuir* 19, 1977–1979. <https://doi.org/10.1021/la026490l>
196. Zito, P.F., Caravella, A., Brunetti, A., Drioli, E., Barbieri, G., 2015. Estimation of

Bibliography

- Langmuir and Sips Models Adsorption Parameters for NaX and NaY FAU Zeolites. J. Chem. Eng. Data 60, 2858–2868. <https://doi.org/10.1021/acs.jced.5b00215>
197. Zwilling, D.P., Golden, T.C., Weist, E. (Jr. . L., Ludwig, K.A., 2003. (12) United States Patent. US 6576043 B2.



PUBLICATION FROM THE THESIS

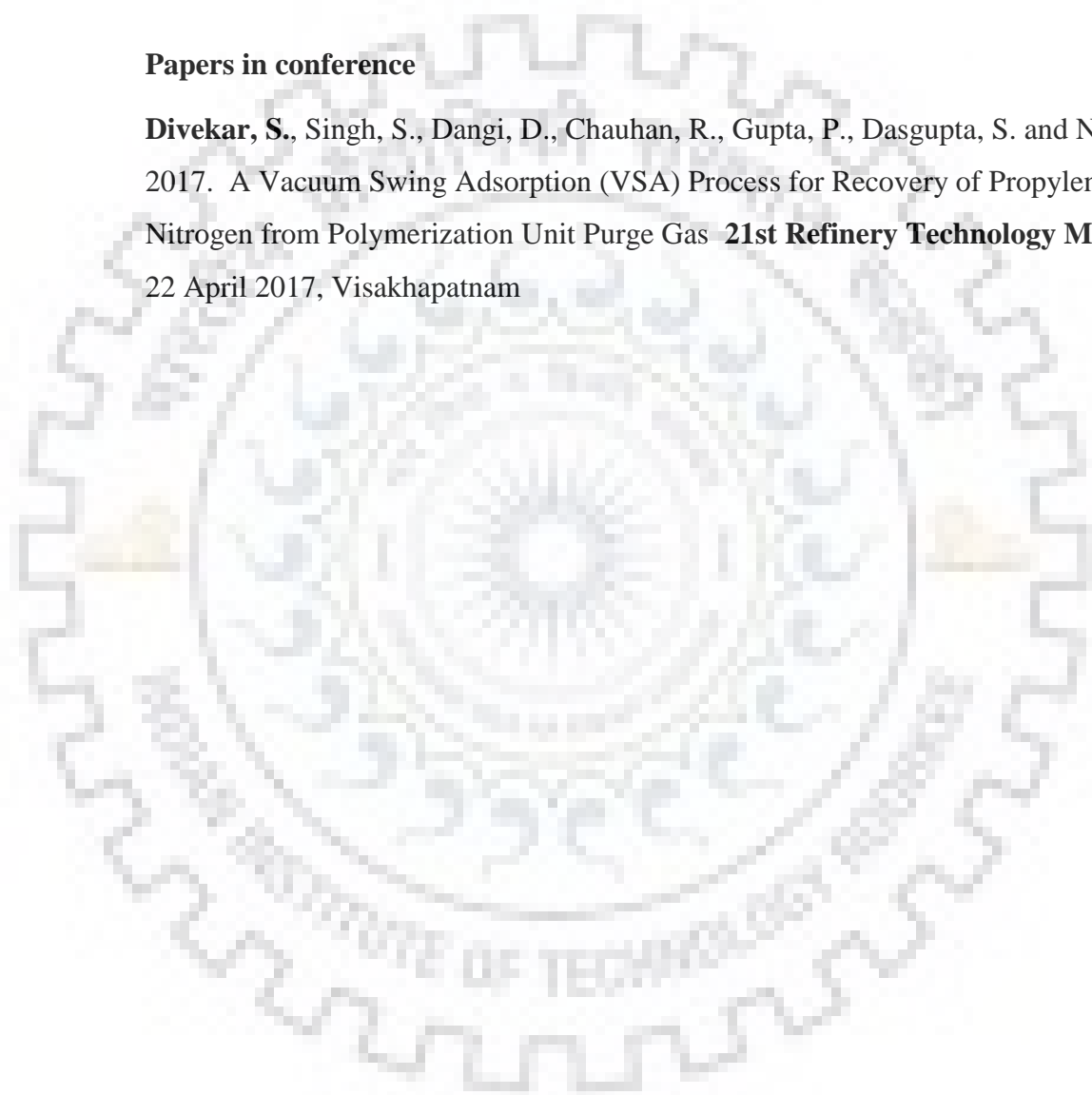
PUBLICATION FROM THE THESIS

Publication in SCI Journals

Divekar, S., Nanoti, A., Dasgupta, S., Aarti, Chauhan, R., Gupta, P., Garg, M.O., Singh, S.P., Mishra, I.M., 2016. Adsorption equilibria of propylene and propane on zeolites and prediction of their binary adsorption with the ideal adsorbed solution theory. J. Chem. Eng. Data 61, 2629–2637. <https://doi.org/10.1021/acs.jced.6b00294>

Papers in conference

Divekar, S., Singh, S., Dangi, D., Chauhan, R., Gupta, P., Dasgupta, S. and Nanoti A. 2017. A Vacuum Swing Adsorption (VSA) Process for Recovery of Propylene and Nitrogen from Polymerization Unit Purge Gas **21st Refinery Technology Meet : 20-22 April 2017, Visakhapatnam**



Annexure-A: Properties of propylene

Annexure-A: Properties of propylene

Physical Properties of Propylene (Eisele and Killpack, 2012)

Molecular Formula	C_3H_6
Molecular Weight, g/mol	42.08
Melting point, °C	-185.25
Boiling Point, °C	-47.70
Critical Temperature, °C	91.76 °C
Critical Pressure, MPa	4.621
Molar Volume, L (STP)	21.976
Density Relative to Air	1.49
The heat of fusion, kJ/kg	71.37
Lower Heating Value, kJ/kg	45.813
Enthalpy of formation ΔH_{298} , kJ/mol	20.43
Lower Explosion Limit (LEL) in Air (at 1 bar, 20 °C) , vol%	2.0
Upper Explosion Limit (HEL) in Air (at 1 bar, 20 °C) , vol%	11.1 vol%